

See discussions, stats, and author profiles for this publication at:
<https://www.researchgate.net/publication/231530427>

Detection of Chiral Disorder in Langmuir Monolayers Undergoing Spontaneous Chiral Segregation

ARTICLE *in* JOURNAL OF THE AMERICAN CHEMICAL SOCIETY · MARCH 1999

Impact Factor: 12.11 · DOI: 10.1021/ja982123d

CITATIONS

20

READS

22

5 AUTHORS, INCLUDING:



Jens Als-Nielsen

University of Copenhagen

45 PUBLICATIONS 1,753 CITATIONS

[SEE PROFILE](#)



Meir Lahav

Weizmann Institute of Science

298 PUBLICATIONS 9,720 CITATIONS

[SEE PROFILE](#)



Leslie Leiserowitz

Weizmann Institute of Science

305 PUBLICATIONS 11,887 CITATIONS

[SEE PROFILE](#)

**Chirality as a Tool for Studying Molecular Self-Organization
in Two- and Three-Dimensional Crystals.
Supramolecular Design in Two Dimensions.**

Thesis for the Degree of Doctor of Philosophy

by

Ivan Kuzmenko

Submitted to the Scientific Council of
the Weizmann Institute of Science,
Rehovot, Israel

April, 1999

UMI Number: DP17839

INFORMATION TO USERS

The quality of this reproduction is dependent upon the quality of the copy submitted. Broken or indistinct print, colored or poor quality illustrations and photographs, print bleed-through, substandard margins, and improper alignment can adversely affect reproduction.

In the unlikely event that the author did not send a complete manuscript and there are missing pages, these will be noted. Also, if unauthorized copyright material had to be removed, a note will indicate the deletion.



UMI Microform DP17839

Copyright 2009 by ProQuest LLC
All rights reserved. This microform edition is protected against
unauthorized copying under Title 17, United States Code.

ProQuest LLC
789 East Eisenhower Parkway
P.O. Box 1346
Ann Arbor, MI 48106-1346

This work had been carried out under the supervision
of Prof. Meir Lahav and Prof. Leslie Leiserowitz
at the Department of Materials and Interfaces,
The Weizmann Institute of Science

"The fetish of today is neither royalty nor religion...
The sacrosanct fetish of today is science.
Why don't you get some of your friends to go for that
wooden-faced panjandrum - eh?"

Joseph Conrad
Secret Agent

6.52 We feel that even when all possible scientific questions have been answered, the problems of our own life remain completely untouched. Of course there are then no questions left, and this itself is the answer.

Ludwig Wittgenstein
Tractatus Logico-Philosophicus

Table of Contents

1. Introduction.....	1
1.1 General overview of the research area.....	1
1.1.1 Molecular chirality and crystallization.....	1
1.1.2 Structure and symmetry of Langmuir monolayers.....	3
1.1.3 Packing modes of long aliphatic chains in Langmuir films.....	5
1.1.4 Spontaneous chiral separation in two and three dimensions.....	6
1.1.5 Molecular recognition and supra-molecular design.....	12
1.1.6 Synchrotron X-ray diffraction.....	14
1.2 Scope of the work.....	15
1.3 References.....	16
2. Published and unpublished research papers related to this thesis.....	20
2.1 Twinned crystals of enantiomorphous morphology of racemic alanine induced by optically resolved α -amino acids; a stereochemical probe for the early stages of crystal nucleation.....	20
2.2 Packing of hydrocarbon chains and symmetry of condensed phases in Langmuir monolayers.....	32
2.3 Aspects of spontaneous separation of enantiomers in two- and three-dimensional crystals.....	40
2.4 Detection of chiral disorder in Langmuir monolayers undergoing spontaneous chiral segregation.....	51
2.5 Formation of chiral interdigitated multilayers at the air-liquid interface through acid-base interactions.....	57
2.6 Design of interdigitated films <i>via</i> amidinium-carboxylate interactions at air-liquid interface; potential replication properties of the system.....	62
2.7 Use of the diastereomeric interactions to probe the in-plane attachment of water-soluble complexes to Langmuir films.....	81
3. Overall summary and conclusions.....	99
Appendix.....	102
Statement of collaboration.....	111

1. Introduction

1.1 General review of the research area

1.1.1 Molecular chirality and crystallization

Chirality, *i.e.* non-identity of an object with its own mirror image, is a fundamental property of molecules associated with life. Indeed, all but one of the 20 biologically occurring amino acids are chiral.¹ Moreover, all of them have the same left form. The reason why only the one chiral form of molecules was chosen in the process of evolution remains a puzzle.

Crystallization of organic matter may be represented as one of the primitive forms of molecular self-assembly, in which a regularly organized object (crystal) is built of the same molecular objects through multiple interactions. A racemic mixture, containing equal amounts of left (*S*) and right (*R*) molecules may either crystallize into a racemic crystal or spontaneously separate into enantiomorphous *R*- and *S*-crystals, that contain molecules of only one handedness. Formation of chiral crystals, constituted by molecules of the same handedness, when grown from racemic mixtures, may be considered as a first step from 'racemic' chemistry towards chiral biology.

Spontaneous separation of a racemic mixture into *R*- and *S*-crystals manifests itself in the chiral crystal habit due to the appearance of hemihedral faces, as was first observed by Pasteur 150 years ago.² In fact, it was the crystal morphology that enabled Pasteur to recognize the right, left and racemic forms of tartaric acids.

The crystal habit is defined by the relative rates of its growth in different directions: the faster the growth in a given direction, the smaller the corresponding face. The thermodynamic shape of a crystal, according to J.W. Gibbs and P. Curie, is defined by the minimum free surface energy.³ G. Wulff had proven that a crystal body of the minimum surface energy always contains a point from which vectors can be drawn normal to the crystal faces and the vector lengths are proportional to the corresponding surface energies. Hartman and Perdok suggested the attachment energy, *i.e.* the energy per molecule that is released after attachment of a new slice in a given crystallographic direction, to be a measure for the corresponding growth rate.⁴ Based on this concept, the theoretical growth form of a crystal can be obtained, but *ab initio* prediction of crystal morphology still remains a generally unsolved problem.

The shape of a crystal grown from solution can be influenced by various factors, in particular, by the solvent that affects the free surface energy (thermodynamic factor) due to specific binding and inhibition of some of the crystal faces. Crystallographic knowledge on molecular packing arrangement of molecular crystals

can be employed in order to design 'tailor-made' auxiliaries, that are similar to the host molecules of the growing crystal, and therefore may stereospecifically bind and control the crystal growth.⁵

Tailor-made auxiliaries may be classified into two categories: inhibitors and promoters. Monolayers of amphiphilic molecules on water may be used to induce and promote the growth of a variety of three-dimensional crystals at the monolayer solution interface by means of structural match, molecular complementarity or electrostatic interactions. For example, long-chain alcohols can induce nucleation of ice due to structural similarity between the monolayer film and the (001) surface structure of epitaxially growing ice-crystals.⁶⁻⁸ Tailor-made inhibitors of crystal growth can be used for a variety of purposes, which include morphological engineering and etching, reduction of crystal symmetry, assignment of absolute structure of chiral molecules and polar crystals, elucidation of the effect of solvent on crystal growth and crystallization of a desired polymorph.^{5,9}

According to generally accepted theories,¹⁰ crystallization proceeds in two stages: formation of crystallization centers (clusters) and their further growth towards the macroscopic crystal. One of the important unsolved problems of crystal growth theories is how matter self-organizes to go from a disordered state in solution (vapor, melt) into ordered crystalline clusters. Until now, all attempts to model the crystallization process failed to describe real system behavior.^{11,12} Direct experimental monitoring of the crystal growth at the very early stages of crystal nucleation is also fraught with difficulties yet *certain information on the critical size and the structure of nuclei can still be obtained through indirect observation.*

In our studies on crystal nucleation we adopted a logical working hypothesis that at the onset of crystallization, nuclei form structures akin to that of the macroscopic crystal. The strength of this simple assumption is that one may utilize known structural information stored in the grown crystal for the design of auxiliary molecules which can be stereospecifically targeted at those nuclei with arrangements similar to that of the mature crystal, and so prevent their eventual growth. This hypothesis has been successfully applied for the resolution of enantiomers which form conglomerates on crystallization,^{13,14} for the induced growth of metastable crystalline polymorphs¹⁵ and for the oriented crystallization of glycine at the air-aqueous solution interface, in the presence of chiral resolved α -amino acids.¹⁶ We shall make use of the above concept in order to glean information on the nucleation process of α -alanine

Racemic (R,S) and chiral (R or S) forms of α -alanine have very similar structures, as was first pointed out by Simpson and Marsh,¹⁷ therefore their lattice energies are close in magnitude. The cell dimensions of the two structures are almost identical and both crystal forms are composed of hydrogen-bonded double strands running along c -axis. In the (S)-form the homochiral double strands are arranged in a

anti-parallel manner. As to the racemic (*R,S*)-form, vectors of (*R*)- or (*S*)-double strands running along the *c*-axis are all collinear, what makes the crystal to be polar. This difference manifest itself in strikingly different crystal morphologies of the chiral and racemic forms of alanine.

Small amounts of chiral-resolved tailor-made additives did not bring about the crystallization of enantiomers of racemic alanine upon crystallization but rather induced growth of unusually twinned racemic crystals (section 2.1). This observation was explained on the assumption that at the nucleation stage the solution contains {*R*}, {*S*} and {*R,S*} nuclei. *R'* inhibitor molecules bind to {*R,S*} and *R* nuclei in solution, but do not bind to the {*S*} nuclei and the latter serve as a template onto which the (*R,S*) crystals nucleate and grow. *X-ray diffraction analysis of the middle part of the twinned crystal provided an estimate of the critical nucleus size of the chiral (*S*)-form.*

1.1.2 Structure and symmetry of Langmuir monolayers

This section contains a general introduction into the structural and symmetry aspects of Langmuir films; more detailed account on the packing aspects of commonly used Langmuir molecules bearing long hydrocarbon chains is given in the next section.

Amphiphilic molecules, namely those that comprise a relatively large hydrophobic moiety and a small hydrophilic headgroup, are able to form monolayers on water, aqueous solutions and on some other liquids. Such monolayers are called Langmuir films.

Despite the fact that Langmuir monolayers are known for more than a century since they were first discovered by Pockels and Lord Rayleigh^{18,19} and then properly characterized and interpreted by Langmuir,²⁰ the molecular structure of the films remained unclear until the recent development of *in-situ* experimental techniques such as grazing incidence X-ray diffraction (GIXD),^{21,22} X-ray (XR) and neutron reflectivity, epifluorescence microscopy (EFM)^{23,24} and Brewster angle microscopy (BAM).^{25,26} GIXD and XR can provide information on the subnanometer scale, whereas EFM and BAM - data on the domain size and shape on the microscopic scale.

Most of the amphiphiles, studied to date in Langmuir monolayers, incorporate one aliphatic chain C_nH_{2n+1} of various lengths ($n=13-31$) and a hydrophilic moiety *X* (*X* = OH, COOH, COOCH₃, NH₂, CH(NH₂)COOH etc.) or may contain two or more chains, as in phospholipids. Langmuir films may exist in various states on liquid surface, depending on the nature of the headgroup and the subphase as well as thermodynamic conditions (surface pressure, temperature); therefore a generic phase diagram of long-chain amphiphiles can hardly be obtained. Phase diagrams of long-chain fatty acids and alcohols, as studied by surface pressure-molecular area (π -*A*)

isotherms, GIXD, EFM and BAM, demonstrate a number of phases. Very briefly, an increase of surface pressure (or decrease of temperature) leads to transition from two dimensional "gas" G (no order), through various partially ordered mesomorphous states (obsolete names are "liquid expanded" and "liquid condensed"), to the 2D crystalline state CS.^{27,28} In many respects mesophases in Langmuir films are two-dimensional analogues of liquid crystals.

Because of the polar nature of amphiphilic molecules they are always oriented in such a way that their headgroups are immersed in the liquid subphase and the symmetry of crystalline Langmuir films is described by four 2D lattice types (triclinic, rectangular, tetragonal, hexagonal) and 17 plane groups.²⁹ Taking into account that most of the studied amphiphiles bear a rod-like aliphatic chain of elliptical cross-section, the choice of the plane group for closely packed 2D crystals without molecular disorder becomes limited to essentially three plane groups $p1$ (oblique lattice), pg (rectangular lattice) and $p3$ (trigonal lattice). Symmetry of Langmuir mesophases of one-dimensional periodicity (2D smectics) belongs to the seven groups of borders.³⁰

Alkyl chain axes are parallel within a layer. (In bulk crystals there are very few examples of criss-crossed packed hydrocarbon chains.³¹) The molecules in a hexagonal cell are aligned vertically relative to the plane of the film, while in the centered rectangular cell (distorted hexagonal) they are tilted along a symmetry direction, and in the oblique cell - along any arbitrary direction. Most of the Langmuir monolayers studied to date by GIXD are two-dimensional powders of randomly ordered 2D crystallites on the water surface (i.e. the film is ordered with respect to the normal to the water surface, but randomly oriented about the vector normal). Thus, the diffraction spectra consist of coinciding Bragg rods of reflections (h,k,q_z) and (\bar{h},\bar{k},q_z) (a description of the method is given in the Appendix), the notation $\{h,k,q_z\}$ designating both reflections.

The hexagonal cell has three equivalent lattice spacings d_{hk} : d_{10} , d_{01} and $d_{1\bar{1}}$, corresponding to the nearest-neighbor molecular surrounding. The GIXD spectrum from these three reflections will appear as a single reflection with all three equivalent Bragg rods peaking at $q_z = 0\text{\AA}^{-1}$ (see the Appendix). The corresponding GIXD spectrum for the centered rectangular (distorted hexagonal) cell will comprise two peaks; one a superimposed doublet arising from the coinciding $\{1,0\}$ and $\{0,1\}$ reflections, and the other the remaining $\{1,\bar{1}\}$. In the oblique cell all the three reflections $\{1,0\}$, $\{0,1\}$ and $\{1,\bar{1}\}$ are resolved. If long-chain molecules are packed in the rectangular or triclinic lattice, the direction and degree of molecular tilt can be easily extracted from the three q_z maxima position of the corresponding Bragg rods. Structure factor calculation can provide even deeper insight into details of molecular packing to almost atomic resolution.

1.1.3 Packing modes of long aliphatic chains in Langmuir films

Since most of the amphiphiles studied on liquid surfaces bear aliphatic tails, the general packing modes of hydrocarbon chains have to be understood. This chapter briefly describes our analysis of packing modes of hydrocarbon chains observed in Langmuir monolayers as compared to bulk crystals.

Most of the ordered non-chiral amphiphilic monolayers studied to date pack in a rectangular unit cell containing two chains related by glide symmetry. The chain axes of these glide-related molecules are always parallel to each other and are either directed normal to the layer plane, or tilted from the layer normal. The symmetry of the rectangular unit cell is preserved, when the chain tilt occurs along one of the two symmetry-permitted short a or long b lattice vectors, corresponding to the nearest-neighbor (NN) and the next-nearest neighbor (NNN) directions, respectively .

The packing of hydrocarbon chains can be classified according to the subcell $a_{\perp} \times b_{\perp} \times c$, in which a_{\perp} and b_{\perp} describe a two-dimensional lattice perpendicular to the chain axis and $c=2.54\text{\AA}$ corresponds to the internal periodicity along the axis of the hydrocarbon zigzag. The 2D lattice, as defined by the a_{\perp} and b_{\perp} axes, is essentially independent of the degree of chain tilt from the layer normal, but does depend on the packing mode, as demonstrated by numerous examples in bulk crystals. Hydrocarbon chains in the overriding majority of known 3D structures of lipids, pack such that the chain axes are all aligned parallel within a layer. The very rare examples of criss-cross packing found in bulk crystals, in which molecular chain axes within a layer are not all parallel, do not have an analogue in Langmuir films studied to-date by GIXD. Such a criss-cross arrangement of the hydrocarbon chains if packed in a rectangular unit cell and glide-plane running along b (criss-crossing may only occur in the NNN direction) would give rise to an intense low-order (1,0) reflection. The fact that the symmetry allowed (1,0) reflection was generally absent or extremely weak in all the GIXD data for non-chiral or racemic monolayers clearly indicated that hydrocarbon chain axes must be parallel.

In order to characterize and compare the packing of long hydrocarbon chains in various monolayers at different temperatures and surface pressures independent of the effect of tilt, a unit cell projected onto a plane perpendicular to the chain axes with dimensions $a_{\perp} \times b_{\perp}$ is to be considered. In a distribution of the cell dimensions a_{\perp} and b_{\perp} of monolayers of non-chiral substances and racemic mixtures for both crystalline phases and mesophases (see Chapter 2.2) two different regions of relatively dense chain packing with 18.6\AA^2 and 19.0\AA^2 correspond to two distinct projected cells. The one unit cell ($a_{\perp} = 5.0\text{\AA}$, $b_{\perp} = 7.5\text{\AA}$) is a fingerprint of the herringbone (HB) packing arrangement, the common packing mode in bulk organic crystals.³¹⁻³³ The noticeable deviation in dimensions of the $4.4 \times 8.7 \text{ \AA}^2$ unit cell from that of the standard HB motif

suggests a different packing arrangement. A search for a possible packing mode that satisfies the $4.4 \times 8.7 \text{ \AA}^2$ cell revealed an arrangement, we labeled as pseudo-herringbone packing mode (PHB), that was described by Kitaigorodskii,³² with a dihedral angle of 40° between the planes of two glide-related hydrocarbon chains. Kitaigorodskii regarded the latter motif as implausible because of a relatively low packing density. Indeed, a search in the Cambridge Structural Database for 3D structures containing closely-packed alkyl chains with the angle between backbone planes differing widely from 0° and 90° yielded only two examples with projected unit cell dimensions $a_{\perp}=4.1\text{--}4.6 \text{ \AA}$, $b_{\perp}=8.0\text{--}8.4 \text{ \AA}$ and the interplane angle of $33\text{--}42^\circ$, close to those of the PHB packing mode.

In Langmuir films, the pseudo-herringbone packing (PHB) appears to be a typically occurring packing motif, unlike the bulk crystals.

We characterized both packing arrangements with use of energy calculations that suggested for Langmuir monolayers with highly tilted hydrocarbon chains the existence of various phases under similar thermodynamic conditions.

1.1.4 Spontaneous chiral separation in two and three dimensions

In this chapter we examine common and disparate features of spontaneous chiral separation of racemic mixtures in two and three dimensions upon crystallization.

In 1848 Louis Pasteur demonstrated that sodium ammonium tartrate tetrahydrate precipitates into crystals of enantiomorphous morphology (related by mirror symmetry), each constituted by only {R}- or {S}-tartrate molecules.²

Despite the considerable body of data available today on molecular crystal structures,³⁴ our present knowledge of intermolecular interactions does not suffice regarding two fundamental aspects of a Pasteur-type experiment. First and foremost, we are still not able to predict with reasonable certainty whether the racemic mixture of a given chiral molecule will crystallize as a conglomerate or form a racemic crystal. The second aspect concerns the presence or absence of crystal hemihedrism, which is part of fundamental problem of prediction of the crystal morphology.⁴ The solution of the first problem belongs to the general field of crystal structure prediction, where the central question to be addressed is how molecules are arranged to build a periodic array. An *ab initio* prediction of possible molecular packing modes leading eventually to the observed crystal structures remains fraught with difficulties although tremendous progress has been made in the development of computational methods.³⁵ A major deficiency lies in the determination of precise atom-atom potential parameters that dictate the conformation and packing of molecules in crystals. Kinetic factors that play a dominant role in the early stages of molecular self-assembly into clusters, which may

lead to the formation of metastable crystalline polymorphs.³⁶ is an additional complication to the problem.

In the event a racemic mixture in solution separates into chiral crystals of opposite handedness, the question whether the crystals develop hemihedrism or not is mostly a consequence of the interaction between crystal surfaces and the environment. In principle, by growing the conglomerates in a chiral environment, the two enantiomorphs may assume different habits. Indeed, a simple way to distinguish between two enantiomorphs is growth in the presence of chiral "tailor-made" additive that will enantioselectively interact with only one of the enantiomorphs.

The interaction between chiral molecular additives and crystal surfaces leads us to chirality in two-dimensional periodic arrays. The question whether racemates of amphiphilic molecules will separate into two-dimensional crystallites of opposite handedness has long been prone to uncertainty.³⁷ Only recently with the application of grazing incidence X-ray diffraction (GIXD), scanning tunneling microscopy (STM) and scanning force microscopy (SFM) for probing surfaces at the subnanometer level, has it become possible to distinguish the molecular packing arrangement of conglomerates and racemic compounds of two-dimensional assemblies.

Empirical and statistical approach In the absence of a general theory of molecular packing in crystals, various rules of thumb have been proposed to rationalize the spontaneous resolution of racemates. In this regard Jacques and his school have deduced some general trends of behavior.³⁸ About 10% of reported racemates undergo spontaneous resolution. This tendency depends upon the shape, symmetry and functional groups of the molecules providing some empirical guidelines in the search for new systems. For example, statistical studies based on five hundred compounds had demonstrated that the frequency of salts that form conglomerates is two to three times higher than that observed amongst molecular crystals.³⁸ Moreover, molecules which possess a two- or three-fold axis such as the dissymmetric helicenes or organo cobalt amines complexes^{39,40} have a greater tendency to crystallize in chiral space groups. In contrast, for molecules such as carboxylic acids and primary amides that tend to form hydrogen-bonded cyclic dimers, the racemates will crystallize in centrosymmetric arrangements where the center of the pair coincides with the crystallographic center of inversion. On the other hand, if the carboxylic acid or amide contains an additional hydrogen bonding group, such as β -hydroxy-acids or β -sulphoxy acids⁴¹ or amides,⁴² the molecules form hydrogen bonds between the carboxy group and the hydroxy or sulphoxy groups of neighboring molecules leading to chiral chains. What determines whether the crystal will be chiral or not depends on the symmetry elements relating the chains to form the complete structure. These

empirical rules were instrumental in the search for non-chiral molecules that crystallize in chiral single crystals for the performance of spontaneous asymmetric synthesis.⁴³

Theoretical approach Spontaneous separation of enantiomers can be driven by thermodynamic or kinetic factors. Wallach proposed an empirical rule that the most thermodynamically stable crystal structures are those that assume the most dense packing arrangements.⁴⁴ He also suggested that, in general, racemic compounds will be more dense than the corresponding enantiomorphs, and therefore will appear more frequently. A recent analysis by Brock, Schweizer and Dunitz, making use of the crystal data set from the Cambridge Structural Database (CSD), had shown that Wallach's rule pertaining to the density of racemic crystals and enantiomorphs does not generally hold.⁴⁵

Kitaigorodskii explained the fact that the limited number of space groups usually observed in crystals, namely $P2_1/c$, $\bar{P}1$, $P2_12_12_1$, $P2_1$, $C2/c$, $Pbca$ and $Pna2_1$ is a consequence of the maximum packing density,^{46,47} implying that the major component of lattice energy is given by the van der Waals interactions. However, there are many systems where the molecular interactions are directed, as in hydrogen bonds, and thus the structure of highest packing density (Wallach's rule) does not necessarily have the minimum lattice energy.

The space group analysis is helpful in order to limit a global search of generated possible crystal structures by *ab initio* methods involving the use of lattice energy computations.³⁵ A standard model for calculating crystal lattice energy is by pairwise summing of atom-atom potential energy terms that involve three distinct contributions. The most important arises from dispersion forces which are non-directional. These forces, which are attractive and assume to have an inverse sixth power dependence, make the overriding contribution to the crystal energy because all atoms of the molecule are involved in them. A second contribution to the energy comes from the exchange-repulsive forces generally taken to have an inverse twelfth power or exponentially decreasing distance dependence. The third contribution is the electrostatic interaction energy arising from the charge distribution in the molecule. Such interactions are long range and direction dependent. The van der Waals energy terms, *i.e.* dispersion and repulsive coefficients, are generally determined by empirical methods.⁴⁸ The Coulomb term may be determined in different ways: by empirical methods, quantum-mechanical calculations or from experimental electron density deformation distributions making use of low-temperature X-ray diffraction data.⁴⁹ The first two methods are prone to error, moreover only net atomic charges have been used. The third method, which is the most accurate since it inherently takes into account the crystal field, yields atomic charges and dipole and quadrupole moments.^{49,50} This method is not commonly used since it involves detailed experimental and computational work.

If the lattice energies of minimum *ab initio* structures for chiral and racemic crystalline phases can be computed, the prediction of the thermodynamically driven chiral separation may be characterized by the chiral discrimination factor Δ_E defined as

$$\Delta_E = \frac{E_{\{R\}} + E_{\{S\}} - E_{\{RS\}}}{E_{\{R\}} + E_{\{S\}} + E_{\{RS\}}}$$

where $E_{\{R\}}$, $E_{\{S\}}$, $E_{\{RS\}}$ are lattice energies for $\{R\}$, $\{S\}$ and $\{RS\}$ crystalline phases, respectively. If $\Delta_E < 0$, which is rarely the case, chiral separation would occur, otherwise when $\Delta_E > 0$ the R and S molecules precipitate into racemic structures.

For achiral molecules, nonchiral space groups are far more frequent than chiral space groups, as given by their distribution in the Cambridge Structural Database. For racemic mixtures, other factors come into play. In systems such as alanine or tyrosine, the solubilities in water of the racemic and enantiomeric forms (total number of dissolved molecules) are about the same, perhaps as a consequence of very similar lattice energies (the same melting points, very similar structural arrangements). In these systems the formation of a racemate has an obvious advantage, reaching supersaturation much before each of the two enantiomorphs. Indeed, all attempts to induce a preferred precipitation of chiral alanine crystals from the racemic mixture grown in the presence of "tailor-made" additives proved to be unsuccessful. The formation of the racemic nuclei appeared to be inhibited and the chiral nuclei were formed, but secondary epitaxial growth on the chiral nuclei eventually gave rise to twinned racemic crystals.⁵¹ All in all, it would appear therefore, that the lattice energy of a pair of enantiomorphs must be decidedly more stable than that of the corresponding racemate, whose structure is generally unknown.

Spontaneous chiral segregation in 2-D Chiral discrimination of molecules in solution and in Langmuir films has been examined theoretically by Andelman and de Gennes considering interactions only within a molecular pair.^{52,53} Their overall conclusion that heterochiral pair interactions should be generally favoured should be relevant to dilute fluid phases, but hardly to crystalline systems, where multiple molecular interactions and crystal symmetry play a dominating role. Therefore, their analysis on chiral discrimination cannot be applied to crystalline Langmuir films. We shall see below that the occurrence of spontaneous resolution in two-dimensional crystals may depend upon subtle differences in molecular structure.

Unlike three-dimensional crystals, the detection of spontaneous resolution in two-dimensions is not straightforward. Early surface pressure-area isotherms measurements on racemic and chiral Langmuir monolayers by Lundquist led her to the conclusion that certain racemates undergo spontaneous resolution in two dimensions.⁵⁴

Similar studies by Arnett suggested that racemic mixtures of myristoyl alanine C₁₇H₃₅CONH(CHOH)COOH, separate into islands of opposite chirality,^{37,55} as was recently established by grazing incidence X-ray diffraction and epifluorescence microscopy.⁵⁶

Separation of enantiomers in racemic Langmuir films was demonstrated recently by SFM and STM. Eckhardt et al⁵⁷ reported the spontaneous separation in Langmuir films of a tetracyclic alcohol transferred onto a mica surface. An SFM image of the film consisted of chiral crystalline domains, related by mirror symmetry. Walba et al⁵⁸ reported on the spontaneous resolution of a liquid crystal of racemic biphenyl deposited onto a freshly cleaved surface of highly oriented graphite and measured by STM.

In principle, the outline of two-dimensional single crystals delineated by straight boundary lines at the air-liquid interface should reflect the plane group symmetry of the crystal and thus may display chiral hemihedral shapes in the event of enantiomorphous crystals. Two-dimensional enantiomorphous domains at the air-liquid interface can be detected by Brewster angle and epifluorescence microscopies. However, observed two-dimensional domains were never single crystals but rather assemblies of crystallites, often assuming dendritic morphologies.^{59,60} Rietz et al⁶¹ reported an example where racemic α -diols assume chiral patterns, as shown by the epifluorescence measurements. However, according to GIXD measurements, the unit cell of the racemic mixture is not oblique as found for the pure enantiomer, but rather rectangular, indicating formation of a true racemate.⁵⁹ In this respect, we note the comments by Selinger and Selinger who pointed out that the formation of spiral defects in two-dimensional aggregates leads to chiral symmetry breaking on the macroscopic length scale, even without any microscopic chiral order.⁶² *Therefore optical methods do not suffice to establish spontaneous separation of enantiomers in two-dimensional crystals.* Moreover, observed chiral patterns on the macroscopic level by epifluorescence microscopy may be caused by an interaction between the monolayer domain with the chiral resolved probe molecules which may act as "tailor-made" inhibitors of crystal growth in specific directions. Consequently, even racemic structures may assume a chiral shape. A three-dimensional analogue of such an effect has been reported recently on racemic alanine that crystallizes in a nonchiral space group but assumes a chiral morphology when crystallized in the presence of small quantities of a resolved α -amino acid, although the internal structure of the crystal remains racemic.⁵¹

Control of spontaneous chiral separation in two-dimensional crystals

The engineering of 3-D crystal structures with desired features have been used for purposes such as pinpointing molecular interactions, and the performance of solid

state reactions. Such an approach has recently been applied for achieving spontaneous separation in two-dimensional crystals.⁶³

The most important symmetry elements by which organic molecules are related in three-dimensional crystals are, of course, translation, center of inversion, twofold screw axis and glide plane. In the two-dimensional counterpart at a liquid surface for amphiphilic molecules that are specifically oriented *vis-a-vis* the water surface, the situation is simpler. The center of inversion, the glide with its plane parallel to the water surface and the corresponding twofold screw symmetry are precluded. The only remaining symmetry elements are translation and a glide whose plane is perpendicular to the water surface. Thus, in principle, it should be easier to bring about spontaneous segregation of chiral molecules in 2-D crystals at the solution interface. In order to induce separation of chiral territories the glide symmetry and the possible formation of solid solutions between the two enantiomers must be prevented.

Oriented crystallization of α -glycine under monolayer of amphiphilic α -amino acids provided evidence, albeit indirect, of two-dimensional ordering of the amphiphiles.⁶⁴ Recently a focus was put on the design of α -amino acid amphiphiles that their racemates would spontaneously separate or form a racemic compound.⁶³ Thus monolayers of amphiphiles of the type $C_nH_{2n+1}CH(NH_3^+)CO_2^-$, labelled C_n -gly, $n=10,12,16$ have been studied by grazing incidence X-ray diffraction (GIXD).

In order to achieve the spontaneous separation in α -amino acid monolayers, it was imperative to induce translational packing of the alkane chains within the layer. Secondary amides have a pronounced tendency to form N-H \cdots O hydrogen bonds by translation. Therefore we focused on monolayer films of N^ϵ -derivatives of lysine $C_nH_{2n+1}-CO-NH-(CH_2)_4-CH(NH_3^+)CO_2^-$, labelled C_n -lys, $n=11,17,21,29$.

The GIXD patterns from the films of the three racemic systems (*R,S*) C_n -lys $n=11,17,21$ and the enantiomerically pure counterparts are similar and indicate an oblique cell containing one independent molecule.

Increasing the length of the hydrocarbon chain of the C_n -lys amphiphile enhances the tendency for packing in the herring-bone motif leading to the formation of racemic two-dimensional crystals, as observed by GIXD for the C_{29} -lys monolayers.

Partial solid solubilities of one enantiomer into the lattice of the other enantiomorph is frequently observed in three-dimensional crystals. *We might expect that such solubilities in two-dimensional crystallites should be even more pronounced.* In the α -amino acids the chiral disorder can occur only via an interchange of the C-H and C-NH $_3^+$ groups around the chiral center, since the hydrocarbon chain must remain in its original position. Hence it seems that such solid solubility is highly improbable, since it will involve the loss of at least one hydrogen bond and a decrease in lattice energy of at least 6 kcal/mole.

Structural and thermodynamic data on diastereomeric mixtures of phenylethylamine mandelates were used in order to achieve spontaneous separation of enantiomers in two-dimensions. Water-soluble phenylethyamine $C_6H_5\text{-CH(CH}_3\text{)}\text{NH}_2$ and mandelic acid $C_6H_5\text{-CH(OH)COOH}$ each have one chiral carbon and form diastereomeric salts of various compositions.⁶⁵ The stability and solubility of the two salts (R,R') and (R,S') are drastically different in favour of the (R,R') salt formation.^{66,67} Both of the molecules were derivatized with alkane chains in the *para*-position of their benzene rings for the Langmuir film studies. 1:1 mixtures of R or S *p*-tetradecylphenylethylamine, $C_{14}H_{29}\text{-C}_6H_4\text{-CH(CH}_3\text{)}\text{NH}_2$, and R' or S' *p*-pentadecylmandelic acid, $C_{15}H_{31}\text{-C}_6H_4\text{-CH(OH)COOH}$, form on water stable highly crystalline monolayer films independent of molecular chirality, according to the GIXD measurements. The unit cells of the (R,R') and (R,S') films are each oblique and contain one diastereomeric pair of molecules. The GIXD pattern of the diastereomeric mixture (R,S') is different from that of (R,R'), whereas the equimolar mixture of the four components gives rise to a diffraction pattern almost identical to that of the (R,R') mixture. Studies on different chiral compositions of the the four-component system proved the formation of chiral domains containing enantiomeric disorder.⁶⁸ A similar kind of disorder of the α -hydroxy group of mandelic acid has been observed in three-dimensional crystals of analogous structures of phenylethylamine mandelate derivatives.

This example shows that the p1 lattice symmetry (one molecule per unit cell) for the crystallites obtained from racemic mixtures cannot provide unambiguous proof of a Pasteur-type separation in two dimensions unless enantiomeric disorder may be excluded based on other considerations, as in the α -amino acid systems.

1.1.5 Molecular recognition and supra-molecular design

In this chapter we show how the ideas of supramolecular design mostly used for 3D crystals can be extended to two-dimensional crystalline films floating on liquid surfaces.

One of the most fundamental unsolved problems in chemistry is predicting, based solely on its molecular structure, how a molecule will pack in the solid state.⁶⁹ The development of a general and applicable theory of the solid state is considered a prerequisite for the design and control of crystal packing arrangements, *i.e.* the "crystal engineering".⁷⁰ Because such a theory is not currently available, chemists have to adopt an empirical approach by making use of collected information, such as in the Cambridge Structural Database (CSD),³⁴ on known structural motifs typical for various kinds of functional groups. Such an approach was sucessfully developed for 3D crystal engeneering.^{5,71,72}

Molecular design can be applied for generation of crystalline 2D films at air-liquid interface, as for example, for the films made up of two complementary molecules, one water-insoluble with a long chain, and the other water-soluble, extracted from the solution subphase. Different architectures may be prepared in this way. *One approach has been to engineer interdigitated films via acid-base interactions between long-chain water-insoluble, and water-soluble, organic molecules.* Another procedure has been to form complexes between long-chain dicarboxylic acids and metal ions, eventually generating nanocrystals of metal sulfides via gas-solid reactions. A third approach involved supramolecular multi-component systems prepared *in-situ* at the air-solution interface. Here we briefly describe the design and characterization of all three approaches.

It is possible to form at the air-solution interface, bilayers composed of interdigitated molecules A and B with acid-base complementarity, where A has a long hydrocarbon chain and B does not. As appropriate bimolecular systems which may form such an interdigitated motif at the air-aqueous solution interface, the 3D crystal structures composed of mandelic acid, $C_6H_5CHOHCO_2H$ (MA), and phenylethylamine, $C_6H_5CHCH_3NH_2$ (PEA), were made use of.^{66,67} The crystal structure containing molecules MA and PEA with the same handedness, *e.g.* *R*-(MA) and *R*-(PEA), labelled (*R,R'*), where either the acid or the amine is modified by attaching a long hydrocarbon chain in the *para* position, is compatible with formation of the interdigitated arrangement, but not the crystal structure containing PEA and MA of opposite handedness, *i.e.* (*R,S'* or *S,R'*).

A film of *R*-($C_{15}H_{31}$ -MA) over a solution of *S'*-(PEA) did not diffract at any point along the compression isotherm. In contrast, replacing the solution by *R'*-(PEA) yielded a GIXD pattern, after high compression. The film structure, determined to near atomic resolution, is an interdigitated crystalline trilayer, whose alkyl chains exposed to air are disordered because of the gaps created by the interleaved PEA units. The lack of an ordered interdigitated structure when the PEA units were of *S'*-configuration was interpreted in terms of an incompatibility between the packing of the chains and the head groups. A model for the process of molecular reorganization as function of film compression, for the (*R,R'*) system was proposed.⁷³

In an analogous manner, crystalline interdigitated films have been formed from a variety of other types of binary acid-base, water-insoluble and water-soluble systems (see section 2.6). All display similar pressure-area isotherms. It appears that the basic requirement for interdigitation is the spontaneous formation first of the mixed monolayer comprising the two complementary acid-base components in proper registry, despite the loss in effective chain packing. Indeed the system will only pack well if the chains are interdigitated.

A monolayer comprised of acid and base, both long-chain substituted, forms ordered mixed system. In studies related to replication of organized molecular systems in solution,⁷⁴ experiments were carried out to induce replication of the ordered acid and base moieties of amphiphilic molecules at the air-solution interface by the formation of a complementary array of water-soluble acid and base molecules in solution. Experiments using benzoic acid and benzamidium as the acid and base components were unsuccessful (see section 2.6).

Organometallic films The formation of the interdigitated two-component systems discussed above led to the idea that water-insoluble and water-soluble components can interact at the air-solution interface to spontaneously form oriented crystalline architectures. The long-chain α,ω dicarboxylic acids, when deposited on water, form crystallites in which the molecules are aligned with their long axes somewhat off the normal to the water surface. A very different organization of these molecules was determined by GIXD on aqueous subphases containing divalent Cd^{2+} and Pb^{2+} ions.⁷⁵ The dicarboxylic acids react with the ions to form the corresponding diacid-salt. The molecules self assemble with their hydrocarbon chains *parallel* to the water surface, forming crystalline films about 50 \AA thick. Within the film the metal ions are arranged in thin layers 33 \AA apart, corresponding to the lattice repeat along the diacid chain.

The crystalline multilayers of the metal α,ω dicarboxylic acid salts on transfer to hydrophobized glass were reacted with H_2S , yielding quantum dots with a moderate homodispersity of diameter ranging from 2 to 4 nm for both the cadmium and the lead salts.⁷⁶

More complex crystalline film architectures could be self-assembled at the air-solution interface. Recently, oriented bilayer crystalline films, composed of 3x3 grids of nine silver ions bound to six ligand molecules were prepared *in-situ* at the air-aqueous solution interface by interaction of the free ligand molecules spread on the aqueous solution, as determined from the GIXD pattern, X-ray reflectivity, scanning force microscopy, and X-ray photoelectron spectroscopy measurements.⁷⁵

1.1.6 Synchrotron X-ray diffraction

Synchrotron radiation that revolutionized scattering experiments in general and in particular X-ray synchrotron radiation which is concentrated in a narrow angular range, polarized and has a wide spectral distribution which may be tunable with appropriate monochromating devices. Crystallography based on radiation from an excited metal source has succeeded to the extent that the determination of moderate-size (down to sub millimeter scale) crystal structures is now an essentially and almost routine analytical technique. Synchrotron radiation extends the field to much smaller systems.

Small amounts of scattering matter at surfaces, in thin films (single to few molecular layers thick) or in microcrystals can be studied. Moreover, use of intense synchrotron X-ray beam has led to the breakthrough in the structure determination of crystal structure of very large molecules with unit cell axis as large as 300Å and beyond.⁷⁷

The intensity measured in a conventional X-ray scattering experiment is proportional to the number of scatterers, *i.e.*, the irradiated sample volume. This, in turn, is proportional to the penetration depth of the radiation in a sample. For X-rays of about 1Å wavelength, this penetration ranges from a few micrometers for very highly absorbing material to a few millimeters for low absorbing materials. In contrast, the depth to which the surface effects persist rarely extends beyond 100Å. Consequently, scattering from the surface region is so weak compared to that from the bulk that it is completely overwhelmed by it. Restricting the penetration depth to the surface region is therefore a prerequisite for all surface diffraction/scattering experiments. This is achieved by using grazing angles of incidence and employing the phenomenon of total external reflection from the surface. At incidence angles smaller than some known critical angle the X-ray refracted wave becomes evanescent travelling along the surface. The amplitude of the evanescent wave decays exponentially with depth (see Appendix). The evanescent wave may therefore be diffracted by crystalline material in a surface layer of that thickness and provide information on its in plane structure. Such diffraction is called grazing incidence X-ray diffraction (GIXD). The principles of GIXD for the study of two-dimensional crystalline films of amphiphilic molecules at the air-liquid interface have been detailed in a review,⁷⁸ further details are given in Appendix.

1.2 Scope of the work

This work is focused on using chirality as a tool to study crystallization process in two and three dimensions. Several aspects have been considered.

Observation of particular twinning of racemic {R,S}-alanine provided some insight into first stages of crystal nucleation. Chiral nuclei of (S)-alanine serve as templates onto which racemic alanine crystals may later grow. The critical size of the chiral nucleus was estimated based on X-ray analysis of the central part of the twinned crystal.

Crystallization in two-dimensions can be considered as a first step towards bulk crystal formation especially relevant to layered structures. Thin films floating on liquid surfaces have an advantage that their growth and development can be *directly* studied *in situ* by surface sensitive techniques (such as GIXD and XR); whereas such monitoring is yet impossible for bulk crystal nucleation in solution.

Spontaneous separation of enantiomers that is one of important aspects of crystallization of chiral molecules since Pasteur's classic experiment. Various aspects of the spontaneous separation has been examined for two and three dimensions. We could demonstrate, by choosing a proper diastereomeric system, that chiral disorder may play a crucial role in two-dimensional films such that the oblique symmetry of the unit cell is not a sufficient proof for spontaneous chiral segregation, as was believed in some previous studies and other arguments have to be involved.

Supramolecular design in two dimensions was given special attention. We were looking for design of interdigitated films on liquid surfaces, constructed from water-insoluble amphiphilic molecules and water soluble species *via* acid-base complementarity. These films were fully structurally characterized by suitable surface-sensitive techniques such as GIXD, XR and AFM. We also suggested a mechanism how a disordered monolayer formed in the first place is transformed upon compression into a crystalline interdigitated multilayer. A study of two diastereomeric systems (*R,R'*) and (*R,S'*) had shown that the process of interdigitation at the interface is remarkably sensitive to the molecular composition and chirality although may occur in various systems involving strong acid-base interactions.

To provide better understanding on symmetry and structure of two-dimensional monolayers we have analysed common hydrocarbon chain packing of aphiphilic molecules in non-chiral and racemic Langmuir monolayers. A new packing mode, that we called pseudo-herringbone (PHB) that does not occur in bulk crystals has been assigned and characterized with lattice energy calculations.

1.3 References

- (1) Branden, C., Tooze, J. *Introduction to the protein structure.*; Garland Publishing, Inc.: New York and London, 1991, pp 302.
- (2) Pasteur, L. *Ann. Phys.* **1848**, 24, 442.
- (3) *Crystal form and structure*; Dowden, Hutchinson & Ross, Inc.: Stroudsburg, Pensilvania, 1977; Vol. 34, pp 368.
- (4) Hartman, P. In *Crystal growth: an introduction*; P. Hartmann, Ed.; North-Holland Publ. Co.: Amsterdam, 1973; pp 367.
- (5) Weissbuch, I.; Popovitz-Biro, R.; Lahav, M., Leiserowitz, L. *Acta Cryst. B* **1995**, 51, 115.
- (6) Majewski, J.; Margulis, L.; Jacquemain, D.; Leveiller, F.; Bohm, C.; Arad, T.; Talmon, Y.; Lahav, M., Leiserowitz, L. *Science* **1993**, 261, 891.
- (7) Majewski, J.; Popovitzbiro, R.; Kjaer, K.; Alsnelsen, J.; Lahav, M., Leiserowitz, L. *J. Phys. Chem.* **1994**, 98, 4087.

- (8) Popovitz-Biro, R.; Wang, J. L.; Majewski, J.; Shavit, E.; Leiserowitz, L.. Lahav, M. *J. Am.Chem.Soc.* **1994**, *116*, 1179.
- (9) Addadi, L.; Berkovitch-Yellin, Z.; Weissbuch, I.; Lahav, M., Leiserowitz, L. In *Topics in Stereochemistry* Wiley: New York, 1986; Vol. 16; pp 1.
- (10) Zhdanov, G. S. *Crystal physics*; 1965, pp 469.
- (11) Gavezzotti, A., Filippini, G. *Chem. Commun.* **1998**, 287.
- (12) Gavezzotti, A. *Crystall. Rev.* **1998**, *7*, 5.
- (13) Addadi, L.; Weinstein, S.; Gati, E.; Weissbuch, I., Lahav, M. *J. Am. Chem. Soc.* **1982**, *104*, 4610.
- (14) Zbaida, D.; Weissbuch, I.; Shavit-gati, E.; Addadi, L.; Leiserowitz, L., Lahav, M. *Reactive Polymers* **1987**, *6*, 241.
- (15) Staab, E.; Addadi, L.; Leiserowitz, L., Lahav, M. *Advanced Materials* **1990**, *2*, 40.
- (16) Weissbuch, I.; Frolow, F.; Addadi, L.; Lahav, M., Leiserowitz, L. *J. Am. Chem. Soc.* **1990**, *112*, 7718.
- (17) Simpson, H. J., Marsh, R. E. *Acta Crystallogr.* **1966**, *1966*, 550.
- (18) Pockels, A. *Nature* **1891**, *43*, 437.
- (19) Rayleigh, L. *Phylos. Mag.* **1899**, *48*, 321.
- (20) Langmuir, J. *J. Am. Chem. Soc.* **1917**, *39*, 1848.
- (21) Kjaer, K.; Als-Nielsen, J.; Helm, C. A.; Laxhuber, L. A., Möhwald, H. *Phys. Rev. Lett.* **1987**, *58*, 2224.
- (22) Dutta, P.; Peng, J. B.; Lin, B.; Ketterson, J. B.; Prakash, M.; Georgopoulos, P., Ehrlich, S. *Phys. Rev. Lett.* **1987**, *58*, 2228.
- (23) Lösche, M., Möhwald, H. *Rev. Sci. Instrum.* **1984**, *55*, 1968.
- (24) Moy, V. T.; Keller, D. J.; Gaub, H. E., McConnel, H. M. *J. Phys. Chem.* **1986**, *90*, 3198.
- (25) Hénon, S., Meunier, J. *Rev. Sci. Instrum.* **1991**, *62*, 936.
- (26) Höning, D., Möbius, D. *J. Phys. Chem.* **1991**, *95*, 4590.
- (27) Kaganer, V. M., Loginov, E. V. *Phys. Rev. E* **1995**, *51*, 2237.
- (28) Peterson, I. R., Kenn, R. M. *Langmuir* **1994**, *10*, 4645.
- (29) *International Tables for X-ray Crystallography*; 2nd ed. ed.; Kynoth Press: Birmingham, U.K., 1965; Vol. 1, pp 58.
- (30) Vainshtein, B. K. *Modern Crystallography*; 2nd Ed. ed.; Berlin, 1994; Vol. 1, pp 107.
- (31) Abrahamsson, S.; Dahlén, B.; Löfgren, H., Pascher, I. In *Prog. Chem. Fats other Lipids* Pergamon Press: 1978; Vol. 16; pp 125.
- (32) Kitaigorodski, A. I. In Consultants Bureau Press: New York: 1961; Vol. Ch. 4; pp 117.
- (33) Segerman, E. *Acta Crystallographica* **1965**, *19*, 789.

- (34) Allen, F. H.; Kennard, O., Taylor, R. *Acc. Chem. Res.* **1983**, *16*, 146.
- (35) *Theoretical aspects and computer modelling of the molecular solid state*; Gavezzotti, A., Ed.; John Wiley & Sons: 1996; Vol. 1, pp 237.
- (36) Dunitz, J., Bernstein, J. *Acc. Chem. Res.* **1995**, *1995*, 193.
- (37) Arnett, E. M., Thompson, O. *J. Am. Chem. Soc.* **1981**, *103*, 968.
- (38) Jacques, J.; Collet, A., Wilen, S. H. *Enantiomers, Racemates and Resolutions*; John Wiley & Sons: New York, 1981.
- (39) Bernal, I. *Inorg. Chim. Acta* **1985**, *96*, 99.
- (40) Bernal, I. *Inorg. Chim. Acta* **1985**, *101*, 175.
- (41) Leiserowitz, L., Weinstein, M. *Acta Crystallogr.* **1975**, *B31*, 1463.
- (42) Weinstein, S.; Leiserowitz, L., Gil-Av, E. *J. Am. Chem. Soc.* **1980**, *102*, 2768.
- (43) Addadi, L., Lahav, M. *Pure & Appl. Chem.* **1979**, *51*, 1269.
- (44) Wallach, O. *Liebigs Ann. Chem.* **1885**, *286*, 90.
- (45) Brock, C. P.; Schweizer, W. B., Dunitz, J. D. *J. Am. Chem. Soc.* **1991**, *113*, 9811.
- (46) Brock, C. P., Dunitz, J. D. *Chemistry of Materials* **1994**, *6*, 1118.
- (47) Belsky, V. K.; Zorkaya, O. N., Zorky, P. M. *Acta Crystallogr.* **1995**, *A51*, 473.
- (48) Hagler, A. T.; Huler, E., Lifson, S. *J. Am. Chem. Soc.* **1974**, *96*, 5319.
- (49) Hirshfeld, F. L. *Theor. Chim. Acta* **1977**, *44*, 129.
- (50) Berkovitch-Yellin, Z., Leiserowitz, L. *J. Am. Chem. Soc.* **1982**, *104*, 4052.
- (51) Weissbuch, I.; Kuzmenko, I.; Vaida, M.; Zait, S.; Leiserowitz, L., Lahav, M. *Chem. Mat.* **1994**, *6*, 1258.
- (52) Andelman, D., de Gennes, P. G. *C. R. Acad. Sci.* **1988**, *307*, 233.
- (53) Andelman, D., Orland, H. *J. Am. Chem. Soc.* **1993**, *115*, 12322.
- (54) Lundquist, M. *Prog. Chem. Fats Other Lipids* **1978**, *16*, 101.
- (55) Stewart, M. V., Arnett, E. M. In *Topics in Stereochemistry* John Wiley & Sons Inc.: New-York, 1982; Vol. 13; pp 195.
- (56) Nassoy, P.; Goldmann, M.; Bouloussa, O., Rondelez, F. *Phys. Rev. Lett.* **1995**, *75*, 457.
- (57) Eckhardt, C. J.; Peachey, N. M.; Swanson, D. R.; Takacs, J. M.; Khan, M. A.; Gong, X.; Kim, J. H.; Wang, J., Uphaus, R. A. *Nature* **1993**, *362*, 614.
- (58) Stevens, F.; Dyer, D. J., Walba, D. M. *Angew. Chem. Int. Ed. Engl.* **1996**, *35*, 900.
- (59) Mohwald, H.; Dietrich, A.; Bohm, C.; Brezesinski, G., Thoma, M. *Molecular Membrane Biology* **1995**, *12*, 29.
- (60) Vollhardt, D. *Adv. Colloid Interface Sci.* **1996**, *64*, 143.

- (61) Rietz, R.; Brezesinski, G., Mohwald, H. *Ber. Bunsen Ges. Phys. Chem.* **1993**, *97*, 1394.
- (62) Selinger, J. V., Selinger, R. L. B. *Phys. Rev. E* **1995**, *51*, R860.
- (63) Weissbuch, I.; Berfeld, M.; Bouwman, W.; Kjaer, K.; Als-Nielsen, J.; Lahav, M., Leiserowitz, L. *J. Am. Chem. Soc.* **1997**, *119*, 933.
- (64) Landau, E. M.; Levanon, M.; Leiserowitz, L.; Lahav, M., Sagiv, J. *Nature* **1985**, *318*, 353.
- (65) Diego, H. L. Thesis, Department of Chemistry, H.C. Ørsted Institute, University of Copenhagen, 1995.
- (66) Briando, M. C.; Leclercq, M., Jacques, J. *Acta Crystallogr.* **1979**, *B35*, 2751.
- (67) Larsen, S., Diego, H. L. *Acta Crystallogr.* **1993**, *B49*, 303.
- (68) Kuzmenko, I.; Kjaer, K.; Als-Nielsen, J.; Lahav, M., Leiserowitz, L. *J. Am. Chem. Soc.* **1996**, *118*, 2657.
- (69) Gavezzotti, A. *Acc. Chem. Res.* **1994**, *27*, 309.
- (70) Schmidt, G. M. T. *Pure Appl. Chem.* **1971**, *27*, 647.
- (71) Etter, M. C. *Acc. Chem. Res.* **1990**, *23*, 120.
- (72) Desiraju, G. R. *Crystal Engineering*; Elsevier: New York, 1989.
- (73) Kuzmenko, I.; Buller, R.; Bouwman, W. G.; Kjaer, K.; Als-Nielsen, J.; Lahav, M., Leiserowitz, L. *Science* **1996**, *274*, 2046.
- (74) Terfort, A., von Kiedrowski, G. *Angew. Chem. Int. Ed. Engl.* **1992**, *31*, 654.
- (75) Weissbuch, I.; Lahav, M.; Leiserowitz, L.; Lederer, K.; Godt, A.; Wegner, G.; Howes, B. P.; Kjaer, K., Als-Nielsen, J. *J. Phys. Chem.* **1998**, *102*, 6313.
- (76) Guo, S.; Popovitz, R.; Weissbuch, I.; Guo, S.; Popovitz, R.; Weissbuch, I.; Cohen, H.; Hodes, G., Lahav, M. **1998**, *10*, 121.
- (77) Swanson, D. R.; Hardy, R. J., Eckhardt, C. J. *J. Chem. Phys.* **1996**, *105*, 673.
- (78) Als-Nielsen, J.; Jacquemain, D.; Kjaer, K.; Leveiller, F.; Lahav, M., Leiserowitz, L. *Phys. Rep.* **1994**, *246*, 251.

2. Published and unpublished research papers related to this thesis

2.1 Twinned crystals of enantiomorphous morphology of racemic alanine induced by optically resolved α -amino acids; a stereochemical probe for the early stages of crystal nucleation

**Isabelle Weissbuch, Ivan Kuzmenko, Madeleine Vaida, Sigal Zait,
Leslie Leiserowitz and Meir Lahav**

Department of Materials and Interfaces, The Weizmann Institute of Science, 76100,
Rehovot, Israel

Twinned Crystals of Enantiomorphous Morphology of Racemic Alanine Induced by Optically Resolved α -Amino Acids; A Stereochemical Probe for the Early Stages of Crystal Nucleation[†]

Isabelle Weissbuch,* Ivan Kuzmenko, Madeleine Vaida, Sigal Zait,
Leslie Leiserowitz,* and Meir Lahav*

*Department of Materials and Interfaces, The Weizmann Institute of Science 76100,
Rehovot, Israel*

Received March 1, 1994. Revised Manuscript Received May 2, 1994*

Crystallization of *R,S*-alanine in the presence of small amounts of other resolved α -amino acids results in the precipitation of the racemic compound as twinned crystals displaying a propeller-like morphology of 222 symmetry, in contrast to needlelike crystals of *mm2* symmetry when grown from pure aqueous solution. This unusual twinning is explained by assuming that the supersaturated solutions contain ordered clusters of structures akin to the mature crystals of (*R,S*)-, (*R*)-, and (*S*)-alanine. The resolved α -amino acid additive, e.g., *R'*, stereospecifically inhibits growth of the *R,S* and *R* nuclei but not of the *S* nuclei. The latter serve as a template onto which the (*R,S*) crystals nucleate and grow. A model which takes into consideration the structural similarity between the racemic and chiral resolved forms of alanine to explain the twinning is presented. An X-ray diffraction analysis of a twinned crystal specimen is in agreement with a gradual change in structure, from a chiral crystal of space group *P2₁2₁2₁* to the racemic compound of space group *Pna2₁*. To substantiate the model, crystals of alanine were grown from optically enriched solutions containing excess of one of the alanine enantiomers, which also induce the twinning phenomenon and an overall reduction in crystal symmetry. The relevance of these observations to the early stages of crystal nucleation is discussed.

Introduction

Crystal nucleation plays a paramount role in determining the physical and chemical properties of materials. Yet understanding and controlling the dynamics of the early stages of self-aggregation of molecules *en route* to crystal formation are still at a rudimentary stage. In the absence, to date, of general analytical tools to monitor, *in situ*, the structural changes of the embryonic species, indirect methods have still to be applied.

We adopt a logical working hypothesis that at the onset of crystallization nuclei form structures akin to that of the mature crystal. The strength of this simple assumption is that one may utilize known structural information stored in the grown crystal for the design of auxiliary molecules which can be stereospecifically targeted at those nuclei with arrangements similar to that of the mature crystal, and so prevent their eventual growth. This hypothesis has been successfully applied for the resolution of enantiomers which form conglomerates on crystallization,^{1,2} for the induced growth of metastable crystalline poly-

morphs,³ and for the oriented crystallization of glycine at the air-aqueous solution interface, in the presence of chiral resolved α -amino acids.⁴

The same procedure may be applied for the resolution of enantiomers that prefer to precipitate as racemic crystals provided there is not too large an energy gap and difference in solubility between the two phases. The auxiliary molecules must inhibit nucleation of the racemic as well as one of the enantiomorphous crystals. For such systems, the general approach for the crystallization of a particular phase, can be represented as follows. In a supersaturated solution containing a racemic mixture of *R*- and *S*-molecules one may anticipate the formation of a variety of nuclei among which are those with structures akin to the corresponding mature crystalline phases of the racemic compound (*R,S*), and the enantiomorphous (*R*) and (*S*) forms (Scheme 1). A chiral auxiliary, say *R'*, is designed such that on addition to the solution it will enantioselectively bind to {*R,S*} and {*R*} nuclei but not to the {*S*} nuclei. While adsorbed on the surfaces of those nuclei, the additive will prevent their further growth. Since we may expect that the *R'* additives do not stereospecifically bind to the {*S*} nuclei, the latter will grow unperturbed and eventually precipitate.

This methodology was successfully applied for the induced optical resolution of (*R,S*)-histidine-HCl.⁵ Ap-

* The paper is dedicated to the memory of Peggy Etter, whose untimely death has deprived the community of solid-state chemists of one of its leading figures. We present a piece of work that embodies elements that were close to her scientific interests on crystal nucleation and hydrogen bonding.

† Abstract published in *Advance ACS Abstracts*, August 15, 1994.

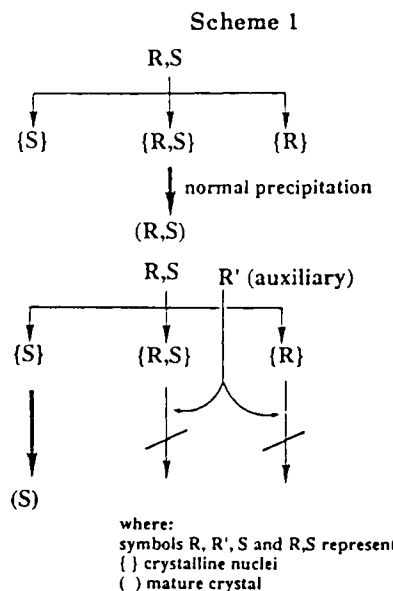
(1) Addadi, L.; Weinstein, S.; Gati, E.; Weissbuch, I.; Lahav, M. *J. Am. Chem. Soc.* 1982, 104, 4610.

(2) Zbaida, D.; Weissbuch, I.; Shavit-Gati, E.; Addadi, L.; Leiserowitz, L.; Lahav, M. *React. Polym.* 1987, 6, 241.

(3) Staab, E.; Addadi, L.; Leiserowitz, L.; Lahav, M. *Adv. Mater.* 1990, 2, 40.

(4) Weissbuch, I.; Frolow, F.; Addadi, L.; Lahav, M.; Leiserowitz, L. *J. Am. Chem. Soc.* 1990, 112, 7718.

(5) Weissbuch, I.; Zbaida, D.; Addadi, L.; Lahav, M.; Leiserowitz, L. *J. Am. Chem. Soc.* 1987, 109, 1869.



plying this approach for (R,S) -alanine resulted, however, in an unusual twinning⁶⁻⁸ of the racemic compound displaying a propeller morphology, instead of precipitation of the chiral enantiomorph.

Here we describe a model that explains the formation of these twinned crystals by taking into account the similarity in structure of racemic and chiral alanine coupled with the enantioselective role played by the chiral additives. Furthermore, the twinning process also provided information on the structure of the molecular aggregate involved in the nucleation process.

Experimental Section

All α -amino acids were commercial analytical grade materials and they were used without further purification.

Crystallization Experiments. (R,S) -Alanine crystals were grown by slow evaporation of racemic aqueous solutions of concentration 25 g/100 mL, either pure or in the presence of 1–5 wt % optically pure or racemic α -amino acid additives such as phenylalanine, threonine, leucine. Series of crystals were grown from supersaturated solutions containing $R:S$ (or $S:R$) alanine ratios varying from 40:60 to 0:100. In general the crystals were collected after 1–2 days. The crystals grown in the presence of additive or from solutions of 40:60 ($R:S$ or $S:R$) alanine composition always displayed twinning.

Scanning Electron Microscopy. Crystals were first coated with gold and then mounted into the scanning electron microscope (SEM).

X-ray Diffraction Measurements. Crystallographic measurements were performed on a four-circle Rigaku single-crystal diffractometer using Cu K α radiation from an 18-kW rotating anode X-ray generator. The X-ray beam was filtered with a graphite monochromator. The structure was refined using SHELXL-92 software.

Gas Chromatography. Enantiomeric composition of various alanine crystals was determined using a Hewlett-Packard 5890 gas chromatograph equipped with a 25-mm fused silica Chirasil-S-valine capillary column (purchased from Compact) at 95 °C, and 10 psi column head pressure with carrier gas (He) and FID detection. To get a volatile material, alanine crystals were derivatized as the *N*-(trifluoroacetyl)alanine isopropyl ester.⁹

(6) Cahn, R. W. *Adv. Phys. Q. Suppl. Philos. Mag.* 1954, 3, 12.

(7) Gay, P. *The Crystalline State, An Introduction*; Oliver and Boyd: Edinburgh, 1972.

(8) Klapper, H. *Prog. Cryst. Growth Charact.* 1987, 14, 367.

(9) Konig, W. A. *The Practice of Enantiomer Separation by Capillary Gas Chromatography*; Huthig: Heidelberg, 1987; p 20.

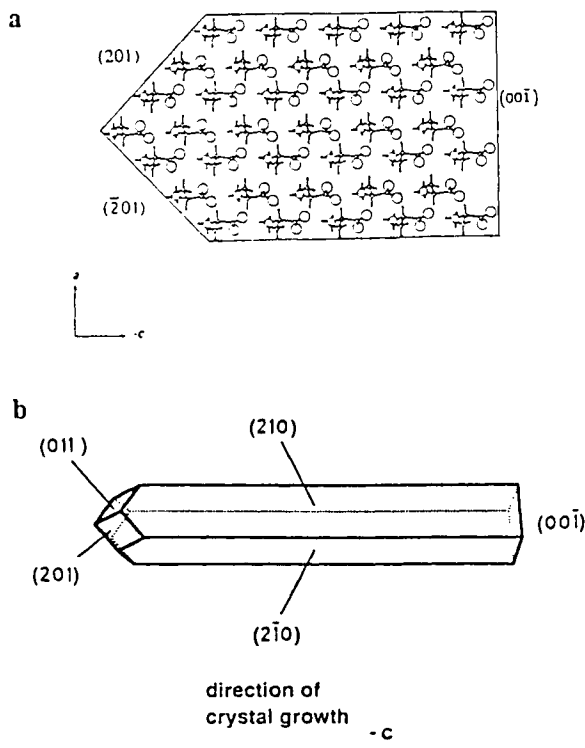


Figure 1. (a) Packing arrangement of (R,S) -alanine viewed along the *b* direction as delineated by the crystal faces. Note that the top and bottom horizontal lines are the intersections between the (210) and $(\bar{2}10)$ and $(2\bar{1}0)$ and $(\bar{2}\bar{1}0)$ planes. (b) Computer-drawn morphology of the (R,S) -alanine crystals. Note that in some crystals $\{101\}$ capped faces were observed instead of $\{201\}$.

Results and Discussion

Crystallization of (R,S) -Alanine. (R,S) -Alanine crystallizes from water in the orthorhombic polar space group $Pna2_1$ ($a = 12.06 \text{ \AA}$, $b = 6.05 \text{ \AA}$, $c = 5.82 \text{ \AA}$).¹⁰ The crystals, which are needlelike in the *c* direction, are delineated by four symmetry-related side faces $\{210\}$, a “flat face” at one end of the polar *c* axis and “capped faces” at the opposite end (Figure 1). Thus the crystals exhibit morphological symmetry $mm2$, in keeping with the space group $Pna2_1$. The absolute structure of the crystal *vis-a-vis* its polar morphology was assigned using two independent methods. We performed experiments in the presence of additives that selectively inhibited growth at each of the two opposite poles of the crystal¹¹ and enantioselectively etched the $\{210\}$ side faces of the crystal during initial stages of dissolution.¹² By these means we found that the molecules are arranged such that the NH_3^+ groups emerge at the “capped end” of the crystal and so the CO_2^- groups at the end terminated by a “flat face”. The direction from the “capped end” to the “flat face” was arbitrarily denoted as $-c$, and so the “flat face” was indexed $(00\bar{1})$ (Figure 1). We had also shown that in aqueous solutions pure (R,S) -alanine crystals grow unidirectionally, via a “relay” type mechanism, along the polar axis at the $(00\bar{1})$ face which exposes the carboxylate groups.¹³ The crystals barely grow in the opposite $+c$ direction at which end the amino groups

(10) Donohue, J. *J. Am. Chem. Soc.* 1950, 72, 949.

(11) Wolf, J. M.Sc. Thesis, Feinberg Graduate School, 1986.

(12) Shimon, L. J. W.; Wireko, F. C.; Wolf, J.; Weissbuch, I.; Addadi, L.; Berkovitch-Yellin, Z.; Lahav, M.; Leiserowitz, L. *Mol. Cryst. Liq. Cryst.* 1986, 137, 67.

(13) Shimon, L. J. W.; Vaida, M.; Addadi, L.; Lahav, M.; Leiserowitz, L. *J. Am. Chem. Soc.* 1990, 112, 6215.

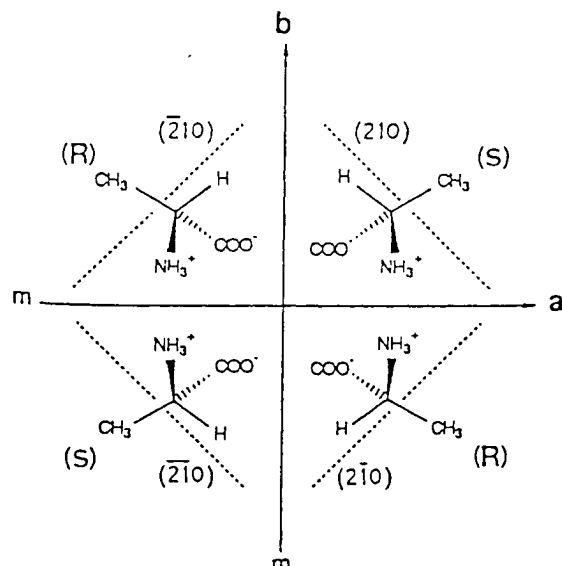
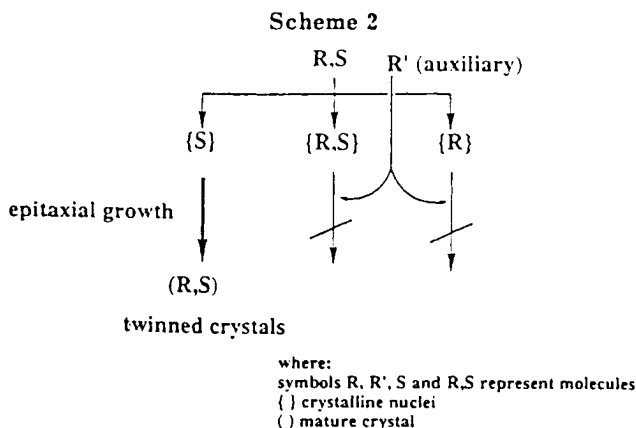


Figure 2. Illustrative representation of the molecular orientations vis-à-vis the four $\{210\}$ faces in the (R,S) -alanine crystal as viewed down the c axis. At each face only one of the four symmetry-related molecules is oriented such that its $C-\text{CH}_3$ group emerges from the face.

are exposed. Given the absolute sense of the crystal polarity with respect to the c axis, the orientation of the R and S molecules as viewed along the c axis are shown in Figure 2. The orientation of the two enantiomeric molecules can be described in terms of their $C-\text{CH}_3$ groups emerging from the $\{210\}$ side faces. The $C-\text{CH}_3$ groups of the S molecules emerge from the $\{210\}$ and $\{\bar{2}\bar{1}0\}$ faces, while the methyl groups of the R molecules emerge from the $(\bar{2}10)$ and $(2\bar{1}0)$ faces. Thus S' - α -amino acid additives can be adsorbed on the $\{210\}$ and $\{\bar{2}\bar{1}0\}$ faces and affect their growth, whereas R' - α -amino acid additives can be adsorbed and affect the growth of the $(\bar{2}10)$ and $(2\bar{1}0)$ faces.

Induced Twinning of (R,S) -Alanine Crystals by Optically Resolved α -Amino Acid Additives. In an attempt to obtain induced spontaneous resolution of racemic alanine following the procedure described in Scheme 1, we have grown these crystals in the presence of optically pure α -amino acids threonine or phenylalanine, say of S configuration. Instead of resolving the compound as was found in the case of (R,S) -histidine-HCl, the precipitated crystals proved to be (R,S) -alanine, assuming a propeller-like shape with the long axis of the propeller parallel to the c axis (Figure 3). These crystals exhibit an enantiomorphous morphological symmetry 222 which differs from the $mm2$ achiral morphological symmetry of the pure crystal. On symmetry principles we might have expected the affected crystals to exhibit morphological point symmetry 112, being grown in the presence of the chiral α -amino additive.

One way to account for the 222 morphology of the crystals grown in the presence of optically resolved additives is to assume that the two halves are twinned about the central ab plane of the crystal. This would also be in accordance with the fast crystal growth with equal rates at the two opposite ends of the propeller, which is only possible if both ends expose COO^- groups. Here we remind ourselves that in the absence of additive the crystals grow unidirectionally along the polar axis, only at the COO^- end. Close inspection of the crystals showed that the twin



parts appear to be stitched together across the middle of the crystal, and are surprisingly attached at "faces" exposing the positively charged NH_3^+ groups. When (R,S) -alanine was grown in the presence of the α -amino acid additive of opposite handedness, in this case (R) -threonine or phenylalanine, the twinned crystals assumed the enantiomorphous morphology. The propeller shape is made manifest not only by the twinned nature of the crystal about its center, but also by the shape of the affected side faces, which are no longer parallel to the c axis as they are in the pure form, corresponding to $\{210\}$. The affected faces at each side of the crystal were indexed as $(21-0.1)$ and $(\bar{2}1-0.1)$ when the additive is an S' - α -amino acid, and in case the additive is an R' - α -amino acid they are $(\bar{2}1-0.1)$ and $(2\bar{1}-0.1)$. This assignment of the affected faces is understood in terms of the twinning model, where each end of the crystal grows along the $-c$ carboxylate end, and the enantioselective binding of the chiral additives to the $\{210\}$ faces, as described in the previous section. The chiral nature of the propeller arises macroscopically from the fact that the affected pair of side faces, say $(21-\Delta l)$ and $(\bar{2}1-\Delta l)$ ¹⁴ and the unaffected pair, $(\bar{2}10)$ and $(2\bar{1}0)$, have different areas and slopes. Moreover a cross-sectional (001) cut through each crystal half describes a parallelogram. Had the affected faces remained unchanged of the type $\{210\}$, the twinning would not have been immediately obvious.

Mechanism of Twinning. To explain this unusual twinning, we propose the following mechanism (Scheme 2). Let us return to the assumption that supersaturated solutions of R,S -alanine contain a variety of clusters which resemble the corresponding crystals of the (R,S) and resolved (R) - and (S) -alanine. The R' - α -amino acid additive present in the solution will stereospecifically inhibit growth or even formation of clusters of $\{R,S\}$ and $\{R\}$ forms of alanine. Following this hypothesis, the R' additive will bind to a lesser extent, if at all, to the $\{S\}$ nuclei, and so should not prevent their growth. We rationalize the formation of (R,S) twins by assuming that the $\{S\}$ nuclei serve as templates for epitaxial nucleation and growth of (R,S) crystals by virtue of a particular similarity between the racemic and chiral crystal forms, a fact pointed out by Simpson and Marsh.¹⁵ Following this mechanism, twinning should be avoided when the crystals of alanine are grown in the presence of racemic α -amino acids, as was indeed experimentally observed.

(14) The gentle slope of the affected side faces of the twinned crystals indicates Miller indices $\{21-\Delta l\}$, where Δl is very low and found to vary from 0.05 to 0.1, depending on crystallization conditions.

(15) Simpson, H. J.; Marsh, R. E. *Acta Crystallogr.* 1966, 20, 550.

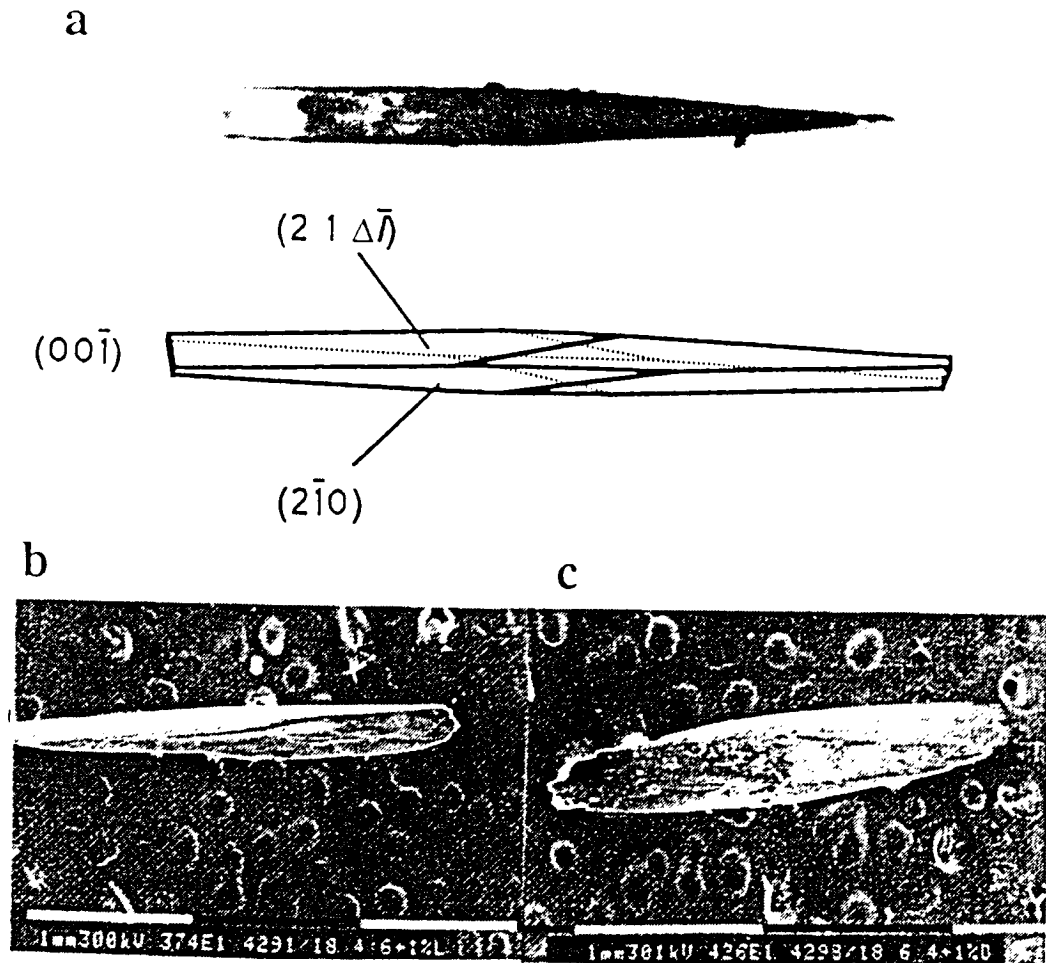


Figure 3. (a) Photograph and computer drawn morphology of (R,S) -alanine twin crystals grown in the presence of 1% S-threonine or S-phenylalanine additive. (b) Photograph of twinned alanine crystal grown from solution containing 40:60 R:S mixture in the presence of 1% S-phenylalanine. (c) Photograph of the crystal enantiomorphous to (b) obtained from a 60:40 R:S mixture grown in the presence of 1% R-phenylalanine.

Figure 4 shows the crystalline packing arrangement of (S) -alanine¹⁵⁻¹⁷ which belongs to the orthorhombic space group $P2_12_12_1$, with axial dimensions¹⁸ $a = 12.32 \text{ \AA}$, $b = 6.03 \text{ \AA}$, $c = 5.78 \text{ \AA}$, which are almost identical to that of (R,S) -alanine. The crystal is composed of hydrogen-bonded chains running parallel to the c axis. These chains are interlinked by N-H...O hydrogen bonds about a 2-fold screw axis parallel to the c axis yielding a polar double strand, as in (R,S) -alanine. These double strands are further interconnected by N-H...O bonds in (S) -alanine, generated by 2_1 axes along a (or along b) to yield antiparallel double strands along the c direction. In the (R,S) form the corresponding hydrogen bonds are generated by n (and so a) glide symmetry so that all double polar strands are parallel along the polar c axis.

As already mentioned the twinned crystals expose CO₂⁻ groups at the two opposite ends. Thus we focus only on the corresponding epitaxial attachment of the polar crystals of (R,S) -alanine to the two opposite (001) and $(00\bar{1})$ faces of the chiral (S) -alanine nucleus,¹⁹ as depicted in Figure 5. All the hydrogen bonded chains of S -alanine molecules parallel to the c axis that emerge from the $\{001\}$

face of the $\{S\}$ nucleus with their CO₂⁻ groups exposed at the face maintain the same structure on "conversion" to the racemic crystal. But all those S -alanine chains, which are antiparallel to the above and so emerge from the same $\{001\}$ face with their NH₃⁺ groups exposed, must, beyond the interface, be replaced by R molecules oppositely oriented vis-à-vis the c axis. Thus across the $\{001\}$ interface the NH₃⁺ groups of the S and R molecules are directed at each other and separated by about 5 Å as seen in Figure 5.

The S chains, which are "converted" into R chains at the (001) and $(00\bar{1})$ interfaces of (S) -alanine, are related by 2_1 symmetry along the a or b axes in view of the $P2_12_12_1$ symmetry of the chiral crystal. The transformation from the chiral to the racemic phase does not have to occur abruptly at the interface. It may take place gradually along the c axis provided the transformation occurs within each double hydrogen-bonded polar strand whose structure has been described above. In such a way all hydrogen bonds are maintained, except at those points where S chains are replaced by R chains, and the changes in the van der Waals contacts are minor (Figures 5 and 6). As shall be discussed later, the observed crystals of (S) -alanine

(16) Dunitz, J. D.; Ryan, R. R. *Acta Crystallogr.* 1966, **21**, 617.

(17) Destro, R.; Marsh, R. E.; Bianchi, R. *J. Phys. Chem.* 1988, **92**, 966.

(18) We have interchanged the a and b axes specified by Simpson and Marsh¹⁵ in order that they be compatible with those of (R,S) -alanine.

(19) For stereochemical reasons we may expect that (R,S) -alanine may bind to the $\{001\}$ faces of (S) -alanine such that the ends of the attached (R,S) crystals would expose NH₃⁺ groups, but for kinetic reasons such twinned crystals do not form.

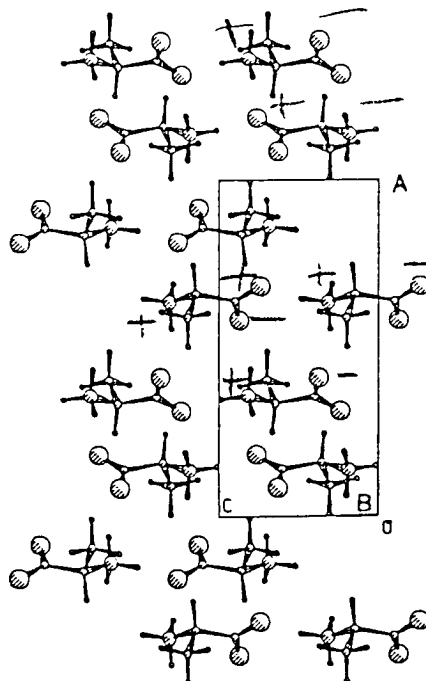


Figure 4. Packing arrangement of (S)-alanine viewed along the *b* axis.

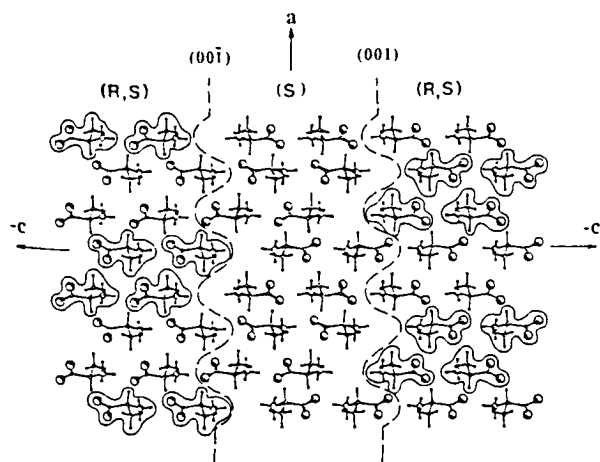


Figure 5. Proposed molecular arrangement of the complex "nucleus" composed of a central {S} "nucleus" onto whose (001) and (001) "faces" {R,S}-nuclei have been epitaxially grown. *R* molecules are encircled for clarity. Note that the two {R,S} "nuclei" are related by 2-fold screw symmetry about the *a* axis of (S)-alanine.

do not exhibit {001} faces, at the opposite ends along the *c* axis but rather {101} faces. Nevertheless these faces make an angle sufficiently shallow with respect to the (001) plane that the arguments given in terms of epitaxy at this interface hold. A preliminary test of the feasibility of such an epitaxy was undertaken by growing (R,S)-alanine at the opposite faces of seed crystals of (S) or (R)-alanine as shown in Figure 7.

To obtain further insight on the twinning phenomenon, we tried to probe the structure of the twinned parts by a variety of techniques. All attempts made to detect the presence of enantiomeric excess of S-alanine from the twinned zone of the crystals grown in the presence of *R'*- α -amino acid additives, were unsuccessful. We were unable to detect circular dichroism of the copper complex of alanine or obtain any enantiomeric excess, using gas

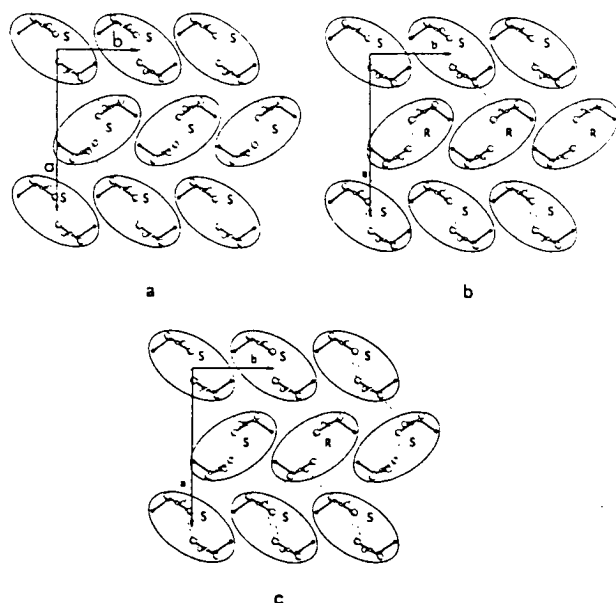


Figure 6. Packing arrangements of alanine viewed along the *c* axis: (a) (S)-alanine; (b) (R,S)-alanine; (c) proposed arrangement of the transitional phase in which one double hydrogen-bonded strand of *S* molecules is replaced by a double *R* strand. The double hydrogen-bonded polar strands along *c*, each enclosed by an ellipse for clarity, describe the two molecular chains interlinked by a 2_1 axis where the molecules in each chain are hydrogen-bonded along *c*.



Figure 7. Photograph of crystals of (R,S)-alanine epitaxially grown at the opposite sides of an (S)-alanine seed.

chromatography (GC) on a capillary chiral column. On the other hand, structural information suggestive of a chiral nucleus embedded within the twinned zone could be obtained by X-ray diffraction measurements, from the reflections which are symmetry forbidden in the pure (R,S) crystal, as shall be described.

Characterization of the Twinned Crystals by Electron Microscopy. Various twinned crystals were examined by scanning electron microscopy (SEM). Each of the specimens showed a narrow crack along the perimeter in the middle of the twinned crystal, separating the two propeller halves. These cracks formed a zigzag pattern approximately perpendicular to the polar *c* axis (Figure 8). Assuming the proposed mechanism of epitaxial growth, we may reasonably deduce that the starting nucleus is located somewhere inside this crack. The approximate width of the crack was $1.5 \mu\text{m}$. Assuming a cube-shaped "nucleus" of this dimension, would lead to a volume of $4 \times 10^{-9} \text{ mm}^3$ compared with the typical volume of the crystal of $\sim 0.3 \times 0.3 \times 3 \text{ mm} = 0.3 \text{ mm}^3$. Thus the volume of this deduced "nucleus", located in the crack, is 8 orders of magnitude smaller than the mature crystal.

The structural source of the perturbation leading to the formation of these cracks is not completely clear. We know from X-ray diffraction measurements on some twinned specimens (see below), that the two propeller halves are not completely aligned; there is a shear angle of about 0.7° between their *ab* planes. Whether the distortion arises



Figure 8. SEM photograph of the crack in a twinned (*R,S*) crystal. The *c* axis of the crystal is indicated.

from a mismatch between the cell dimensions of the chiral nucleus and the racemic crystal or because of repulsion between the exposed NH₃ groups of the two epitaxially grown halves at their (001) "faces" as they eventually "meet", is not clear.

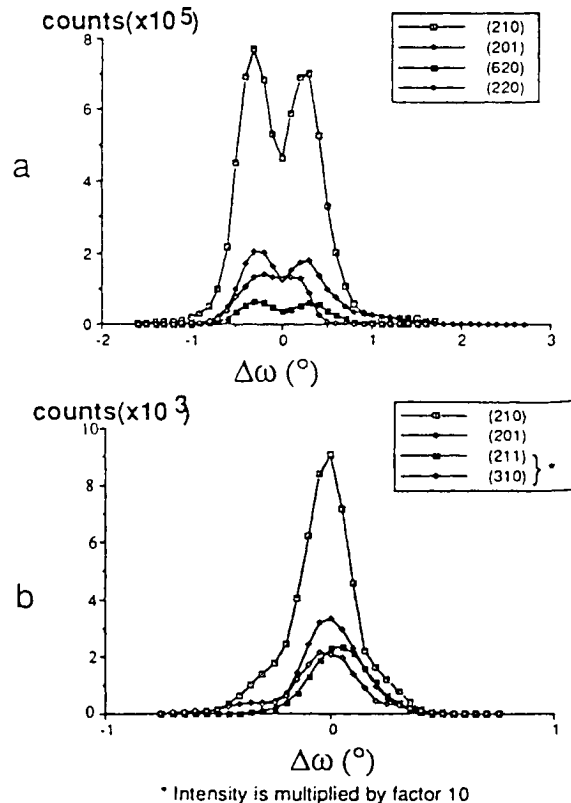
X-ray Diffraction Analysis of Twinned Crystals. The deduction that the twinned crystals of (*R,S*)-alanine consist of a central nucleus of one of the enantiomorphs, from which two ends the two halves of the (*R,S*) crystal grew, is supported by X-ray diffraction measurements.

A propeller-shaped crystal specimen of dimensions 0.1 × 0.1 × 0.8 mm was mounted on the diffractometer along the *c* axis, the direction of crystal elongation. Several reflections measured with a standard collimator,²⁰ of diameter 1 mm, so that the whole crystal was bathed in the X-ray beam, yielded split diffraction profiles indicating two crystal halves (Figure 9a). Adjustment of the height of the crystal so that only each of its two crystal halves were separately irradiated, yielded regular diffraction profiles corresponding to a single crystal (Figure 9b). The precise orientation of each of the two halves was determined. Misalignment between the two halves occurs primarily in the *ab* plane with a "twist" angle of about 0.7° whereas the misalignment angle along the propeller *c* axis is about 0.3°. This result is in keeping with the observation that the two crystal halves appear stitched together across the central plane (Figure 8).

A "nucleus" with a crystal structure similar to that of (*R*)- or (*S*)-alanine in space group *P*2₁2₁ implies that only X-ray reflections of the type *h*00, 0*k*0, 00*l*, *h,k,l* = 2*n* + 1 should be absent on symmetry grounds. On the other hand, the symmetry-forbidden reflections for the two crystal halves of space group *Pna*2₁ are 0*k*0, *k* + *l* = 2*n* + 1 and *h*0*l*, *h* = 2*n* + 1. Making use of a narrow X-ray beam collimator²¹ of diameter 0.1 mm, the symmetry-forbidden reflections were measured from the twinned crystal separately irradiated at its center and two ends. Only two reflections, the (012) and (001), coming only from the crystal center, had significant net intensities. To preclude

(20) The cross-sectional diameter of the beam illuminating the crystals was about 1 mm for the 1-mm collimator. Here we note that a graphite crystal was used as a monochromator for the X-ray beam.

(21) We did not measure the cross-sectional diameter of the beam illuminating the crystal but, since the diameter of the beam with the wide collimator was approximately 1 mm, we could deduce that the beam was considerably reduced in intensity. Note that the ratio of intensities of the (210) reflection measured with the wide and narrow colimators was in the range 100, in keeping with the relative areas of the two collimators (see Figure 9).



* Intensity is multiplied by factor 10

Figure 9. ω -scans measured for some general reflections of a twinned (*R,S*)-alanine crystal specimen: (a) scans taken from the whole crystal using a wide collimator; (b) scans taken from a tip of the crystal using a narrow collimator. Note that in an ω -scan the X-ray detector is kept at the Bragg 2θ angle, and the crystal is rotated around its diffracting position.

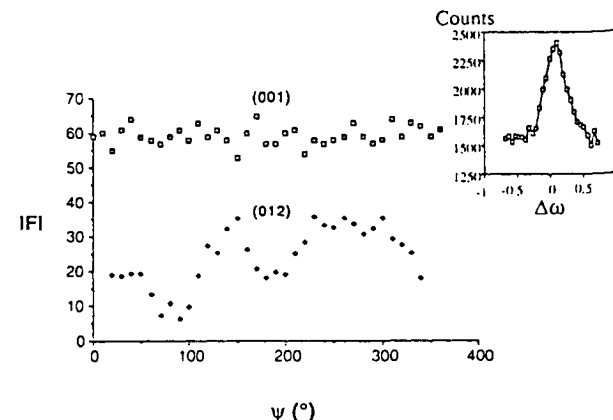


Figure 10. ψ -scans for the (001) and (012) reflections. Note that in a ψ -scan the X-ray detector is kept at the Bragg 2θ angle, the crystal is always in diffraction position and is rotated around its diffracting vector $d_{(hkl)}$; in this case (*hkl*) being (001) or (012). Note that $|F|$ corresponds to the magnitude of the observed structure factor $|F| = K(I - B)^{1/2}$, where *I* is the integrated intensity of the reflection, *B* is the background, and *K* a geometrical factor. The insert shows an ω scan of the (001) reflection for a particular value of ψ , indicating a definite diffraction peak.

the possibility of multiple X-ray diffraction ψ scans were measured for these two reflections (Figure 10). Moreover ω -scans were made for the (012) reflection at 12 different ψ values (Figure 11). From these results there can hardly be any doubt as to the presence of the two reflections. Table 1 lists the strongest calculated structure-factor $|F(hkl)|$ values for the crystal structures of (*R,S*)-alanine

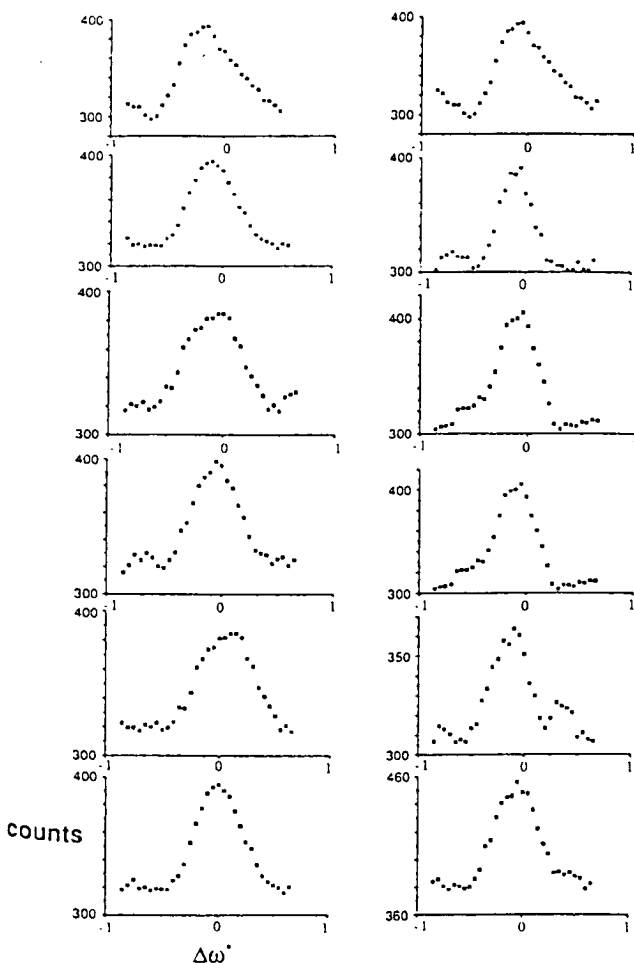


Figure 11. ω -scans measured for the (012) reflection at 12 different ψ -orientations of the crystal ranging from 0 to 360° in steps of 30° .

Table 1. Strongest Calculated Structure Factors for the Crystal Structures of (*R,S*)-Alanine and (*S*)-Alanine

<i>(R,S)</i> -alanine		<i>(S)</i> -alanine	
<i>hkl</i>	<i>F</i>	<i>hkl</i>	<i>F</i>
210	100	210	101
400	93	400	91
002	68	002	65
201	55	012 ^a	64
410	52	410	49
112	51	620	49
620	48	220	48
220	46	311	42
311	39	101 ^a	41
011	32	412	39
402	30	301 ^a	36

^a Reflections which are symmetry forbidden in (*R,S*)-alanine.

and (*S*)-alanine. The (012) reflection, which is symmetry-forbidden for (*R,S*) alanine, has one of the highest $|F(hkl)|$ values in the list for (*S*)-alanine. Therefore, on the basis that the measured intensity of the (012) reflection comes from a $P_{2_1}2_12_1$ nucleus of chiral alanine we have been able to derive its crystal volume. For this purpose we made use of the measured volume of the twinned crystal, coupled with a knowledge of the relative diffraction intensities from the two crystalline phases of alanine. Assuming the crystal nucleus of alanine is cubic in dimension, the calculated length²² of each side is 5 μm . To obtain significant intensities from such a small "crystal", advantage was taken of the high X-ray flux from the 18-kW

Table 2. Crystal Form and Composition Obtained by Crystallization from Supersaturated Solutions of Various *R:S* Compositions

solution composition (<i>R:S</i>)-alanine	crystal form	crystal composition ^a		remarks
		% <i>R</i>	% <i>S</i>	
50:50	<i>R,S</i> needles	50	50	
40:60	<i>R,S</i> twinned	48	52	middle part 45:55
60:40	<i>R,S</i> twinned	51	49	
35:65	<i>R,S</i> twinned	47	53	
65:35	<i>R,S</i> twinned	51	49	
30:70	<i>S + R,S</i> polycrystals	36	64	
25:75	<i>S + R,S</i> polycrystals	28	72	middle part 30:70 end parts 26:74
22:78	<i>S + R,S</i> polycrystals			
20:80	<i>S + R,S</i> polycrystals	10	90	
17:83	<i>S + R,S</i> polycrystals	8	92	middle part 5:95 end parts 10:90
15:85	affected <i>S</i> crystals	0.7	99.3	

^a Estimated error in composition is about 1%.

rotating anode X-ray generator as well as long measuring times. The length of 5 μm is of the same order of magnitude as the width of the "stitched" crack across the center of the specimen crystal measured by electron scanning microscopy (Figure 8).

There remains, however, the problem of accounting for the presence of the (001) reflection which is symmetry forbidden for the space groups of both (*R,S*)-alanine (*Pna*2₁) and chiral alanine (*P*2₁2₁2₁). The presence of the (001) reflection indicates a loss of the 2-fold screw axis along the *c* axis. A simple way to rationalize the loss of this symmetry element is to assume that the structural transition from *P*2₁2₁2₁ to *Pna*2₁ is gradual as described above. We had postulated that the transition from (*S*)-alanine to (*R,S*)-alanine involves a random replacement of *S*-alanine hydrogen-bonded double strands parallel to *c*, by the corresponding *R*-double strands (see Figure 6). In this way, the 2-fold screw symmetry along *c* would be partially lost for the intermediate disordered region. We cannot, however, make a qualitative estimate of the effect of such disorder on the intensity of the (001) reflection.

Induced Twinning of (*R,S*)-Alanine Crystals Grown from Chiral Nonracemic Mixtures of Alanine. Additional support for the proposed twinning mechanism was provided by growth of single crystals of (*R,S*)-alanine from enantiomerically enriched solutions. The presence of say excess *R*-alanine will generate higher concentrations of {*R*} nuclei as templates for the growth of the twinned crystals. Indeed, when crystals were grown from supersaturated solutions of enantiomeric *R:S* ratios in the range from 45:55 to 35:65, twinned crystals with propeller-like shape were obtained. The enantiomeric composition of these crystals was determined by GC, and the results showed an *R:S* ratio for all the specimens, fluctuating around a value of 50:50.

The composition of the middle zone of the twinned crystals was also examined by GC. Crystals grown from supersaturated solutions of a 40:60 *R:S* ratio contained a 45:55 *R:S* composition of alanine in the middle zone (Table 2). The presence of an excess of the *S* enantiomer, in the twinned zone supports our proposed mechanism that the nucleus of the twinned crystals must be *S*-like.

(22) An (*S*)-alanine "nucleus" of volume $\sim 100 \mu\text{m}^3$ which is approximately 10^{-10} g would not be detectable by GC, being overwhelmed by the amount of material of $\sim 0.1 - 1 \text{ mg}$ cut from the *R,S* crystal. Regarding the CD measurements, the estimated amount of material from the nucleus is well below the threshold detection limit of the instrument used.

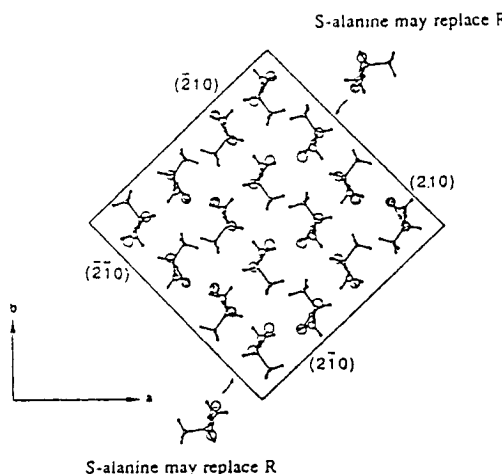


Figure 12. Packing arrangement of (R,S) -alanine viewed down the c axis, delineated by the (210) and $(\bar{2}10)$ faces, showing where adsorbed (S) -alanine molecules may replace R -molecules. Note that at each face only one of the four symmetry related molecules has its C(chiral)-H bond emerging from the face. The dark molecules are S -alanine. The N(amino) atom has a larger circle than the C(methyl) atom.

The 40:60 $R:S$ alanine mixture in solution gave the same enantiomorphous propeller-shape of the twinned crystals as a 50:50 mixture in the presence of S -phenylalanine additive. This result can be understood in terms of two consecutive growth mechanisms: The first involves twinning starting from a chiral nucleus arising from a local excess of S -alanine followed by epitaxial growth of (R,S) -alanine. The second involves formation of the propeller shape which can be understood in terms of replacement of R molecules by S -alanine molecules at the (210) and $(\bar{2}10)$ faces, as shown in Figure 12. This replacement can take place because of an interchange of a hydrogen atom by an CH_3 group (Figure 12). Note that the S -phenylalanine additive replaces an S -alanine molecule on the same face as S -alanine replaces R -alanine. Crystallization from solutions containing a combination of 40:60 $R:S$ mixture and 1% S -phenylalanine yielded the regular propeller-shape crystals (Figure 3b). An enantiomorphous morphology (Figure 3c) was obtained with the 60:40 $R:S$ and 1% R -phenylalanine. But 1% R -phenylalanine addition to the solution containing 40:60 $R:S$ mixture resulted in almost powder-like crystals where all side faces were affected.

Crystals were also grown from supersaturated solutions containing the $R:S$ -alanine ratios varying from 35:65 to 0:100 (Figure 13 and Table 2). Supersaturated solutions with a $R:S$ ratio of 35:65 yielded (R,S) twinned crystals of composition close to 50:50, and a solution composition of 15:85 gave affected (S) -alanine crystals (Figure 13) containing minor amounts of R -alanine. Solutions with $R:S$ ratios 30:70, 25:75, and 20:80 yielded polycrystals displaying an unusual morphology incorporating both the shape of the (R,S) twin form and that of the (S) -alanine (Figure 13). The pure (S) -alanine crystals exhibit well-developed faces of type $\{210\}$, $\{110\}$, and, at the opposite ends along the c axis, $\{101\}$ faces (Figure 13e). These crystals become elongated in c on growth in the presence of the opposite enantiomer (Figure 13d).²³

(23) We note that Simpson and Marsh¹⁵ reported needlelike crystals of (S) -alanine exposing $\{110\}$ side faces when grown from aqueous solution.

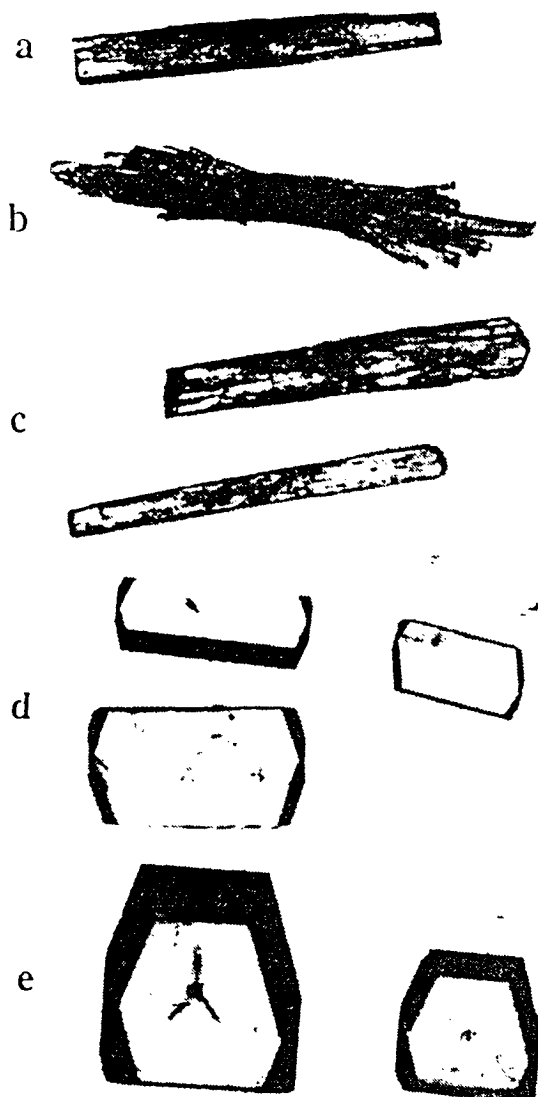


Figure 13. Photographs of crystals grown from supersaturated solutions containing alanine of various enantiomeric $R:S$ ratios: (a) 35:65; (b) 25:75; (c) 20:80; (d) 15:85; (e) 0:100.

Solutions containing 17:83 $R:S$ mixtures yielded polycrystalline material of racemic and chiral forms. Optical resolution was nevertheless achieved by addition of 1% R -phenylalanine to these solutions. This result indicates that the growth of both $\{R\}$ and $\{R,S\}$ nuclei into stable crystals are inhibited. Furthermore, the result is similar to the optical resolution of R,S histidine-HCl,⁵ in the sense that the chiral additive inhibited formation of both the racemic as well as the chiral form homomeric to the additive.

X-ray Diffraction Analysis of a Twinned Crystal Grown from a 40:60 R,S Mixture. A twinned propeller-shaped crystal of alanine grown from a 40:60 $R:S$ mixture of dimensions $0.6 \times 0.1 \times 1.1$ mm was explored by X-ray diffraction. When the whole crystal was bathed in the X-ray beam, it yielded observable intensities for many of the reflections forbidden by space group $Pna2_1$. The same behavior was observed when only the crystal center or its ends were irradiated using a narrow X-ray beam. These results pointed to a pronounced reduction in symmetry throughout the whole crystal.²⁴⁻²⁸

Table 3. Crystallographic Data for (R,S)-Alanine Twinned Crystals

	crystal grown from 50:50 R:S and 1% S-phenylalanine	(R,S)-alanine grown from a 40:60 R:S mixture	
temperature/K	290	290	100
space group	$Pna2_1$	$P1$	$P1$
formula	$C_3H_8NO_2$	$C_3H_8NO_2$	$C_3H_8NO_2$
$a/\text{\AA}$	12.025(3)	12.019(3)	11.895(2)
$b/\text{\AA}$	6.041(2)	6.032(2)	5.964(1)
$c/\text{\AA}$	5.829(2)	5.828(2)	5.826(2)
α/deg	90.00(3)	90.01(3)	89.98(2)
β/deg	90.02(3)	90.03(2)	90.04(2)
γ/deg	89.99(3)	89.76(2)	89.67(1)
$V/\text{\AA}^3$	423.5	422.5	413.9
z	4	4	4
X-radiation	$Cu K\alpha$ (1.5418 Å)	$Cu K\alpha$ (1.5418 Å)	$Cu K\alpha$ (1.5418 Å)
crystal size $\times 10$ (mm)	1 \times 1 \times 8	6 \times 1 \times 6	6 \times 1 \times 6
no. of reflections*			2675

* Intensities of X-ray reflections forbidden for $Pna2_1$ space group were measured at speeds 8 times slower than the "normal" reflections.

Table 4

(a) Laue Symmetry	2/m2/m2/m	2/m11	12/m1	112/m
$R_m(F^2)_g$	0.068	0.090	0.089	0.046
no. of "independent reflections" ^b	399	654	685	685
(b) space group	$Pna2_1$	$Pn11$	$P1a1$	$P112_1$
no. of observed	184	58	126	6
"symmetry-forbidden" reflections ($F/\sigma(F)$) ^c	3.2	4.3	2.8	7.0

^a $R_m(F^2) = \sum |F^2 - F_{\bar{i}}^2| / \sum F_i^2$, where F^2 is the average of the set of observed symmetry-related structure factors and F_i^2 is the i th individual observed structure factor. ^b Note that the number of "independent" reflections depends upon the Laue symmetry assignment. ^c $(F/\sigma(F))$ is the average value of the ratio of F_{obs} divided by $\sigma(F_{\text{obs}})$.

To determine the crystal structure by X-ray diffraction, measurements were made on only one-half of the propeller ($0.6 \times 0.1 \times 0.6$ mm) which was cut from the specimen crystal. In this way we avoided a masking of the reduction in lattice symmetry that would have been imposed by crystal twinning about the central ab plane. The specimen crystal was cooled to a temperature of ~ 100 K for the X-ray diffraction measurements in order to facilitate structure determination. Cell dimensions and information on X-ray diffraction data collection are given in Table 3.

Evidence in favor of crystal symmetry lowering was obtained from the following results. The unit-cell dimensions (Table 3) indicates a monoclinic cell, with c as the unique axis since the angle γ deviates significantly from 90° , unlike the α and β values. This effect cannot be due to the reduction in crystal temperature, since the unit-cell angles at room temperature followed the same pattern.

Reflections within a hemisphere of reciprocal space out to $\sin \theta/\lambda$ of 0.56, were measured (Table 3). The agreement factor, $R_m(F^2)$, between the intensities of symmetry-related reflections assuming crystal point symmetries 2/m2/m2/m, 2/m11, 12/m1, and 112/m (Table 4a) favors 112/m, indicating monoclinic symmetry with c as the unique axis.

(24) Vaida, M.; Shimon, L. J. W.; Weissinger-Lewin, Y.; Frolow, F.; Lahav, M.; Leiserowitz, L.; McMullan, R. K. *Science* 1988, 241, 1475.

(25) Gopalan, P.; Peterson, M. L.; Crundwell, G.; Kahr, B. *J. Am. Chem. Soc.* 1993, 115, 3366.

(26) McBride, J. M.; Bertman, S. B. *Angew. Chem., Int. Ed. Engl.* 1989, 28, 330.

(27) Allen, F. M.; Buseck, P. R. *Am. Mineral.* 1988, 73, 568.

(28) Shimon, L. J. W.; Vaida, M.; Frolow, F.; Lahav, M.; Leiserowitz, L.; Weissinger-Lewin, Y.; McMullan, R. K. *Faraday Discuss.* 1993, 95, 307.

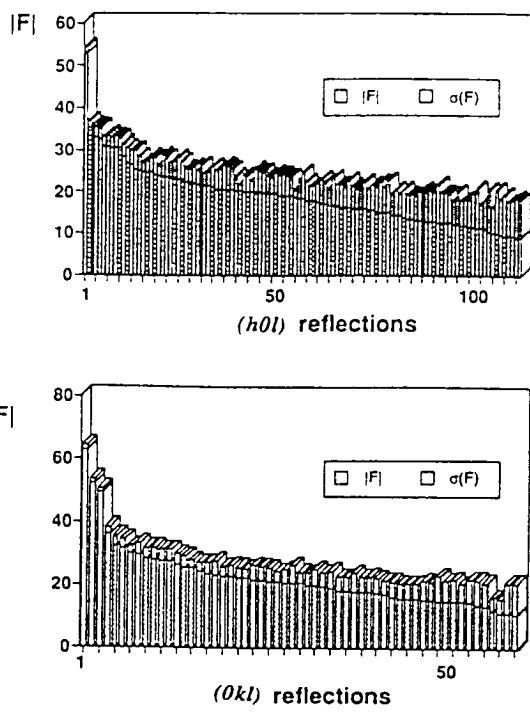


Figure 14. Observed structure factor $|F_{(hkl)}$ values of symmetry-forbidden (for space group $Pna2_1$) reflections for the (R,S)-alanine crystal grown from 40:60 R:S mixture; (a) $(h0l)$ reflections, $h = 2n + 1$; (b) $(0kl)$ reflections, $k + l = 2n + 1$.

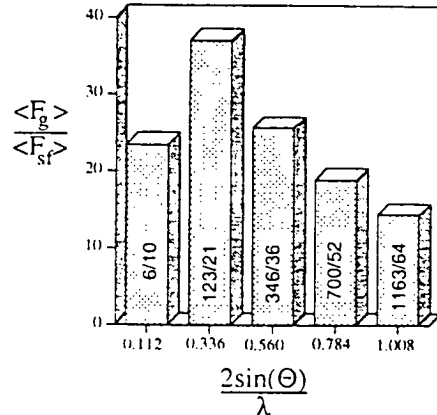


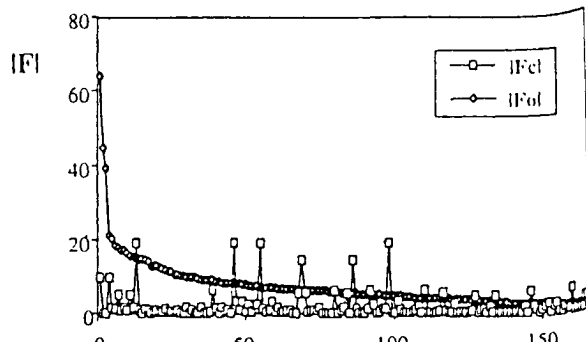
Figure 15. Ratio of the average values of F_{obs} for general $\langle F_g \rangle$ and "symmetry-forbidden" reflections $\langle F_{sf} \rangle$ in shells of reciprocal space $(2 \sin \theta)/\lambda$. Also given are the number of general hkl reflections vs the number of "symmetry-forbidden" reflections.

This result is in agreement with the unit cell dimensions. Furthermore the n and a glide planes, that appear in pure (R,S)-alanine, are lost since the X-ray reflections forbidden by these two symmetry elements are indeed observed (Figure 14 and Table 4b). The intensities of these "symmetry-forbidden" reflections were much weaker than the general reflections hkl , according to the histogram given in Figure 15. The loss of the n and a glide planes does not however negate the presence of a 2-fold screw axis along the c direction. The loss of the 2_1 axis along c is evident from the presence of the weak X-ray reflections $00l$, $l = 2n + 1$ (see Table 4b). At this point we stress that the twinned crystal of (R,S)-alanine grown from a racemic solution but in the presence of the additive S-phenylalanine, described in the previous section, did not show the presence of symmetry-forbidden reflections, but for (001) and (012) only in the middle zone of the crystal. This

crystal and the specimen grown from a solution containing 40:60 R:S mixture were of approximately the same size. The diffraction data of the specimen crystal grown from the 40:60 R:S mixture still leave, however, for an ambiguity in pinpointing the space group of the structure.

We may resolve this question in the following way. We try to rationalize the reduction in symmetry in terms of the affected crystal morphology and given the fact that the crystals grown from a 40:60 R:S solution contain only 1–2% excess of occluded S enantiomer, according to GC analysis. The two affected side faces of the cut prismatic crystal were of the type $(21-\Delta l)$ and $(\bar{2}\bar{1}-\Delta l)$; the other two faces $(2\bar{1}0)$ and $(\bar{2}10)$ remained unchanged, as in pure (R,S)-alanine. This morphology is compatible with the adsorption of S-alanine molecules at particular R type sites on the affected faces (Figure 12). An S-alanine molecule can only occupy an R type surface site on the affected faces without incurring repulsive intermolecular contacts if the C–CH₃ group emerges from the face. Consequently only one of the four crystallographically different surface sites on the affected $[21-\Delta l]$ faces may be partially occupied by S-alanine molecules replacing regular R molecules. Occlusion of such S molecules would lead to a reduction in crystal symmetry to P1. The two structures, resulting from occlusion through the $(21-\Delta l)$ and $(\bar{2}\bar{1}-\Delta l)$ faces are not identical but rather related by 2-fold screw symmetry, in keeping with the fact that the affected sites on the $(21-\Delta l)$ and $(\bar{2}\bar{1}-\Delta l)$ faces are related by 2_1 symmetry. Since the crystal may be regarded as composed of mosaic blocks diffracting independently, the X-ray intensity contribution to each (hkl) reflection comes from two crystal structures, each of symmetry P1, but related to each other by 2-fold symmetry about the c axis. Thus the prismatic crystal may be regarded as composed of two P1 sectors, related by 2-fold point symmetry, coherently intertwined about the central (210) plane that intersects the two halves of the prism. In this way we may account for the monoclinic character with c as the unique axis of the cut prismatic crystal.

The crystal structure was first refined assuming the space group $Pna2_1$ with anisotropic temperature factors for the C, N, and O atoms. The H atoms were located by difference Fourier syntheses in their expected positions. Further refinement with fixed H-atoms positions, and a common isotropic temperature factor for all H-atoms yielded a reliability index $R(F) = 0.035$ for all the symmetry permitted reflections averaged according to the Laue point symmetry mmm . The $R(F)$ factor calculated for Laue point symmetry $\bar{1}$ (namely, without averaging the symmetry-related reflections) was 0.065. Including the symmetry-forbidden reflections $(0kl, k + l = 2n + 1; h0l, h = 2n + 1)$ had a minor effect on this agreement factor. The $R(F)$ index of 0.035 is low and would, at first sight, indicate that the $Pna2_1$ assignment of the space group is correct. But all the observed data and analysis described above rules out this possibility unambiguously. Thus we searched in the difference Fourier synthesis for evidence of enantiomeric disorder in the crystal. The four strongest peaks in the resulting Fourier difference map were close to the oxygen atoms, in the region where lone pair density is expected to be. The fifth strongest peak lay in the direction of the C(chiral)–H vector at a distance of about 1.5 Å from the C(chiral) atom position. This peak corresponds to a methyl carbon atom at an enantiomerically disordered molecular site, in terms of the arguments on molecular



(0kl) and (h0l) reflections

Figure 16. Observed (\diamond) and calculated (\square) structure factors F_{hkl} for the "symmetry-forbidden" reflections $0kl, k + l = 2n + 1$ and $h0l, h = 2n + 1$.

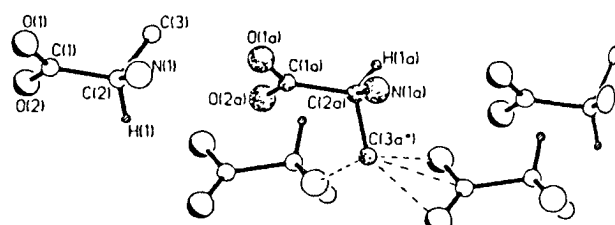


Figure 17. Short intermolecular contacts about a disordered site in the crystal. The dark molecule represents a S-alanine occupying a crystallographic R site. The short $C(3a')\cdots N(1)$, $C(3a')\cdots O(2)$, $C(3a')\cdots C(1)$ and $C(3a')\cdots O(1)$ distances are 2.7, 2.8, 2.6, and 2.2 Å respectively.

adsorption outlined above. Therefore we constructed a crystal structure in which the unit cell was composed of two ordered S-type sites, one ordered R-type site and the remaining R-type site occupied by a composite molecule consisting of primarily R mixed with an S molecule.²⁹ We naturally assumed that the conformation of the S molecule was such that its CO₂⁻ and NH₃⁺ groups coincided with that of the dominant R species. The space group of this structure is P1. We took care of the crystal "twinning" about the central (210) plane by combining the calculated intensity contributions of the (hkl) and $(\bar{h}\bar{k}\bar{l})$ reflections. Refinement which involved only the linked occupancy of the CH₃ and H groups at the disordered sites, as a parameter, yielded for the S molecules an occupancy of 0.020(4). Only the symmetry-forbidden reflections were used to determine the occupancy, whose value corresponds to an average of 50.5% S molecules in the overall crystal. The final $R(F)$ index was 0.43. The match between the observed and calculated $|F|$ values for all these "symmetry-forbidden" reflections is shown in Figure 16. Clearly, the model, in which the H and CH₃ groups are interchanged for the composite molecule at the site of occlusion, does not yield a good fit between the F_{obs} and F_{calc} for the "symmetry-forbidden" reflections. We did not take into account a concerted rearrangement of the molecules in the vicinity of the site of disordered occlusion arising from very short intermolecular contacts (Figure 17). Indeed we propose that this rearrangement must be a regular feature at the occlusion sites within the diffracting domains, in order to account for the presence of the

(29) This assumption is in keeping with the observed change in crystal morphology of chiral resolved N-cinnamoylalanine grown in the presence of its enantiomer (Berkovitch-Yellin, Z.; Addadi, L.; Idelson, M.; Leiserowitz, L.; Lahav, M. *Nature* 1982, 256, 27).

symmetry-forbidden reflections and the observed Laue symmetry. Moreover, this model implies that the enantiomeric disorder occurs within the crystal bulk³⁰ rather than on the surfaces of mosaic blocks. This system, of reduced crystal symmetry, differs from two host-additive organic systems with reduced crystal symmetry studied by X-ray and neutron diffraction³¹ in two main respects: the latter contained relatively high amounts of occluded additive (>8%) which caused only minor perturbation of the normal intermolecular contacts.

Conclusion

We have provided information on the structure of nuclei formed at very early stages of the crystallization process. The unusual shape of the enantiomorphous twins of (R,S)-alanine induced by the chiral α -amino acid additives is *prima facie* evidence that the clusters, at very early stages of their formation, assume structures akin to their mature crystalline phases. In systems where more than one crystalline phase can be formed, additive molecules designed on the structural basis of the mature crystal can be targeted stereospecifically to particular nuclei resulting in a prevention of their growth into macroscopic crystals. The present results demonstrate that the "tailor-made" additive is a far more efficient inhibitor during the stage of crystal nucleation than during the later stage of crystal growth. But once the nuclei of the phase unaffected by the additive reached a certain size, it acted as a template for the epitaxial crystallization of the thermodynamically

more stable form, leading to unusual twinning of the crystal of (R,S)-alanine. The "tailor-made" auxiliary can reduce the speed of growth of the faces it interacts with and modify the morphology of the crystal, but hardly can prevent the crystal formation. The X-ray intensity diffraction pattern of a twinned crystal of (R,S)-alanine grown from 40:60 R:S alanine solutions indicated symmetry lowering as a result of enantiomeric disorder.

The present studies also have bearing on theoretical aspects of crystal nucleation. The existence of structured clusters in supersaturated solutions prior to crystal nucleation invokes again the central role played by the anisotropy in intermolecular forces in the organization of molecules and raises the question whether the importance of interfacial effects have not been overstated in classical theories.^{33,34}

Recent studies have been made on the self-organization of amphiphilic and bolaamphiphilic molecules at air-solution interfaces into crystalline monolayers and multilayers^{35,36} of three-to-five layers thick. The ability to observe their structure and follow their dynamics as affected by "tailor-made" additives by modern methods such as grazing incidence X-ray diffraction, complemented by atomic force microscopy and cryo-transmission electron microscopy, should provide a more direct entry in the understanding of the mechanism of growth, dissolution and microtwinning of clusters at the early stages of crystal nucleation.

Acknowledgment. We acknowledge the help of Eli Friedman. We thank the Israel Academy of Basic Sciences and Humanities for financial support.

(30) The diffraction results obtained on the specimen crystal grown from 40:60 R:S mixture in solution raises the question whether occasional enantiomeric disorder does not occur by the same mechanism of adsorption and occlusion in the case of a crystal grown from racemic solution. As already mentioned, the X-ray diffraction results obtained from the twinned crystal of (R,S)-alanine grown from a 50:50 mixture but in the presence of 1% S-phenylalanine did not show the presence of symmetry-forbidden reflections beside the (001) and (012) in the middle zone of the crystal.

(31) The two host-additive systems studied were asparagine-aspartic acid²² and cinnamamide-thienylacrylamide.^{24,28}

(32) Weissinger-Lewin, Y.; Frolow, F.; McMullan, R. K.; Koetzle, T. F.; Lahav, M.; Leiserowitz, L. *J. Am. Chem. Soc.* 1989, 111, 1035.

(33) Larsen, M. A. In *Advances in Industrial Crystallization*, Butterworth-Heinemann Ltd.: London, 1991, p 20.

(34) Peters, G. H.; Eggebrecht J.; Larsen, M. A. *Proceedings of the 11th Symposium on Industrial Crystallization*; Mersmann, A., Ed., Garmisch, Germany, 1990; p 883.

(35) Popovitz-Biro, R.; Majewski, J.; Margulis, L.; Cohen, S.; Leiserowitz, L.; Lahav, M. *J. Phys. Chem.* 1994, 98, 4970.

(36) Weinbach, S.; Kjaer, K.; Grüber, G.; Legrand, J.-F.; Als-Nielsen, J.; Lahav, M.; Leiserowitz, L. *Science* 1994, 264, 1566.

2.2 Packing of hydrocarbon chains and symmetry of condensed phases in Langmuir monolayers

Ivan Kuzmenko,* Vladimir M. Kaganer^Y and Leslie Leiserowitz*

*Department of Materials and Interfaces, The Weizmann Institute of Science, 76100,
Rehovot, Israel

^YInstitute of Crystallography, Russian Academy of Sciences, 117333 Moscow, Russia,
and Max Planck Institute of Colloids and Interfaces D-12489 Berlin, Germany

Packing of Hydrocarbon Chains and Symmetry of Condensed Phases in Langmuir Monolayers

Ivan Kuzmenko,[†] Vladimir M. Kaganer,^{*,‡,§} and Leslie Leiserowitz[†]

Department of Materials and Interfaces, The Weizmann Institute of Science, 76100 Rehovot, Israel. Institute of Crystallography, Russian Academy of Sciences, 117333 Moscow, Russia, and Max Planck Institute of Colloids and Interfaces, D-12489 Berlin, Germany

Received July 21, 1997. In Final Form: March 17, 1998

We compare the packing characteristics of alkyl chains in Langmuir monolayers of nonchiral and racemic compounds as determined from available grazing incidence X-ray diffraction data. The analysis demonstrates a gradual change of the projected unit cell dimensions from those of a hexagonal packing of hydrocarbon chains, characteristic of high-temperature monolayer phases, to one of two more dense rectangular packing modes with the projected unit cell dimensions $5.0 \times 7.5 \text{ \AA}^2$ and $4.4 \times 8.7 \text{ \AA}^2$, characteristic of low-temperature phases. The $5.0 \times 7.5 \text{ \AA}^2$ unit cell incorporates the well-known herringbone arrangement, with an ideally 90° dihedral angle between the planes of carbon backbone chains. The $4.4 \times 8.7 \text{ \AA}^2$ cell, almost never observed in 3D structures, is characterized by a 40° dihedral angle. We characterize the packing modes by lattice energy calculations. The distribution of the projected unit cell dimensions for the various Langmuir monolayers reveals no discontinuity in the local molecular order between crystalline phases and mesophases. The local symmetry of the molecular packing, as determined from the X-ray data, is compared with the symmetry deduced from the Landau theory of phase transitions. The symmetry of the local order in the mesophases is not maintained on the long-range length scale. We show that two phases of the same local molecular arrangement, a herringbone-ordered two-dimensional crystal and the corresponding one-dimensional mesophase, possess mutually orthogonal directions of glide symmetry.

Introduction

The first clear-cut evidence for the in-plane regular structure in the condensed phases of Langmuir monolayers was found with the use of grazing-incidence X-ray diffraction (GIXD) ten years ago.^{1,2} Since then a large number of X-ray structural studies of monolayers of different substances have been performed. Most of them were devoted to partially ordered^{3–17} and 2D crystalline^{18–29} phases of simple amphiphiles—fatty acids, alcohols, and

their derivatives. At least eight structurally distinct condensed phases were revealed for nonchiral substances. Structures of low-temperature crystalline phases correspond to one of the dense packing modes of hydrocarbon chains in three-dimensional organic crystals. The higher-temperature phases are mesophases, possessing partial orientational and translational disorder. We refer hereafter to low-temperature phases as those corresponding to the crystalline state of the monolayer and to high-

* Corresponding author.

[†] The Weizmann Institute of Science.

[‡] Permanent Address: Russian Academy of Sciences.

[§] Max Planck Institute of Colloids and Interfaces. Alexander von Humboldt Research Fellow.

(1) Kjaer, K.; Als-Nielsen, J.; Helm, C. A.; Laxhuber, L. A.; Möhwald, H. *Phys. Rev. Lett.* **1987**, *58*, 2224.

(2) Dutta, P.; Peng, J. B.; Lin, B.; Ketterson, J. B.; Prakash, M.; Georgopoulos, P.; Ehrlich, S. *Phys. Rev. Lett.* **1987**, *58*, 2228.

(3) Barton, S. W.; Thomas, B. N.; Flom, E. B.; Rice, S. A.; Lin, B.; Peng, J. B.; Ketterson, J. B.; Dutta, P. *J. Chem. Phys.* **1988**, *89*, 2257.

(4) Kjaer, K.; Als-Nielsen, J.; Helm, C. A.; Tippmann-Krayer, P.; Möhwald, H. *J. Phys. Chem.* **1989**, *93*, 3200.

(5) Lin, B.; Shih, M. C.; Bohanon, T. M.; Ice, G. E.; Dutta, P. *Phys. Rev. Lett.* **1990**, *65*, 191.

(6) Bohanon, T.; Lin, B.; Shih, M.; Ice, G.; Dutta, P. *Phys. Rev. B* **1990**, *41*, 4846.

(7) Kenn, R. M.; Böhm, C.; Bibo, A. M.; Peterson, I. R.; Möhwald, H.; Als-Nielsen, J.; Kjaer, K. *J. Phys. Chem.* **1991**, *95*, 2092.

(8) Tippmann-Krayer, P.; Möhwald, H. *Langmuir* **1991**, *7*, 2303.

(9) Schlossman, M. L.; Schwartz, D. K.; Pershan, P. S.; Kawamoto, E. H.; Kellogg, G. J.; Lee, S. *Phys. Rev. Lett.* **1991**, *66*, 1599.

(10) Shih, M. C.; Bohanon, T. M.; Mikrut, J. M.; Zschack, P.; Dutta, P. *J. Chem. Phys.* **1992**, *96*, 1556.

(11) Shih, M. C.; Bohanon, T. M.; Mikrut, J. M.; Zschack, P.; Dutta, P. *Phys. Rev. A* **1992**, *45*, 5734.

(12) Shih, M. C.; Bohanon, T. M.; Mikrut, J. M.; Zschack, P.; Dutta, P. *J. Chem. Phys.* **1992**, *97*, 4485.

(13) Durbin, M.; Malik, A.; Ghaskadvi, R.; Zschack, P.; Dutta, P. *J. Phys. Chem.* **1994**, *98*, 1753.

(14) Shih, M. C.; Durbin, M. K.; Malik, A.; Zschack, P.; Dutta, P. *J. Chem. Phys.* **1994**, *101*, 9132.

(15) Kaganer, V. M.; Peterson, I. R.; Kenn, R. M.; Shih, M. C.; Durbin, M.; Dutta, P. *J. Chem. Phys.* **1995**, *102*, 9412.

(16) Brezesinski, G.; Scalas, E.; Struth, B.; Möhwald, H.; Bringezu, F.; Gehlert, U.; Weidemann, G.; Vollhardt, D. *J. Phys. Chem.* **1995**, *99*, 8758.

(17) Scalas, E.; Brezesinski, G.; Möhwald, H.; Kaganer, V. M.; Bouwman, W. G.; Kjaer, K. *Thin Solid Films* **1996**, *284*, 56.

(18) Jacquemain, D.; Leveiller, F.; Weinbach, S. P.; Lahav, M.; Leiserowitz, L.; Kjaer, K.; Als-Nielsen, J. *J. Am. Chem. Soc.* **1991**, *113*, 7684.

(19) Leveiller, F.; Jacquemain, D.; Leiserowitz, L.; Kjaer, K.; Als-Nielsen, J. *J. Phys. Chem.* **1992**, *96*, 10380.

(20) Weinbach, S. P.; Jacquemain, D.; Leveiller, F.; Kjaer, K.; Als-Nielsen, J.; Leiserowitz, L. *J. Am. Chem. Soc.* **1993**, *115*, 11110.

(21) Weinbach, S. P.; Kjaer, K.; Als-Nielsen, J.; Lahav, M.; Leiserowitz, L. *J. Phys. Chem.* **1993**, *97*, 5200.

(22) Weissbuch, I.; Majewski, J.; Kjaer, K.; Als-Nielsen, J.; Lahav, M.; Leiserowitz, L. *J. Phys. Chem.* **1993**, *97*, 12848.

(23) Weissbuch, I.; Leveiller, F.; Jacquemain, D.; Kjaer, K.; Als-Nielsen, J.; Leiserowitz, L. *J. Phys. Chem.* **1993**, *97*, 12858.

(24) Leveiller, F.; Böhm, C.; Jacquemain, D.; Möhwald, H.; Leiserowitz, L.; Kjaer, K.; Als-Nielsen, J. *Langmuir* **1994**, *10*, 819.

(25) Wang, J.-L.; Leveiller, F.; Jacquemain, D.; Kjaer, K.; Als-Nielsen, J.; Lahav, M.; Leiserowitz, L. *J. Am. Chem. Soc.* **1994**, *116*, 1192.

(26) Böhm, C.; Leveiller, F.; Jacquemain, D.; Möhwald, H.; Kjaer, K.; Als-Nielsen, J.; Weissbuch, I.; Leiserowitz, L. *Langmuir* **1994**, *10*, 830.

(27) Majewski, J.; Popovitz-Biro, R.; Bouwman, W. G.; Kjaer, K.; Als-Nielsen, J.; Lahav, M.; Leiserowitz, L. *Chem. Eur. J.* **1995**, *35*, 304.

(28) Weissbuch, I.; Berkovic, G.; Yam, R.; Als-Nielsen, J.; Kjaer, K.; Lahav, M.; Leiserowitz, L. *J. Phys. Chem.* **1995**, *99*, 6036.

(29) Weissbuch, I.; Berfeld, M.; Bouwman, W.; Kjaer, K.; Als-Nielsen, J.; Lahav, M.; Leiserowitz, L. *J. Am. Chem. Soc.* **1997**, *119*, 933.

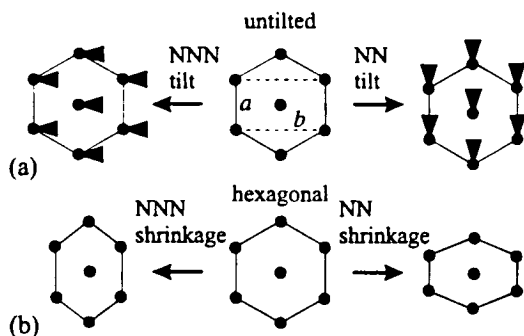


Figure 1. (a) Directions of tilt toward nearest neighbor (NN) and next-nearest neighbor (NNN) of long hydrocarbon chains in a hexagonal representation of the rectangular unit cell. The equidistant hexagon is used for convenience to show the six neighbors surrounding the central molecule. (b) Distortion (shrinkage) of the hexagonal cell in the NN and NNN directions, as given by projection onto the plane perpendicular to molecular axis.

temperature phases as those close to the temperature of the liquid expanded–liquid condensed phase transition. The actual temperature of the transition depends on the substance and the chain length, increasing by 5–10 °C per each additional CH_2 group.³⁰

In three-dimensional crystals of various long-chain amphiphiles the hydrocarbon chains appear in a limited number of packing modes, originally described by Kitagorodskii³¹ and Segerman³² on the basis of the geometrical principle of close packing. It is plausible that molecules in Langmuir monolayers adopt one of the energetically favorable packing motifs, since the packing density is very close to that in bulk crystals. The aim of the present paper is to analyze packing of hydrocarbon chains in Langmuir monolayers on the basis of available GIXD data.

Distribution of Projected Unit Cell Dimensions

Most of the ordered nonchiral amphiphilic monolayers studied to date pack in a rectangular unit cell containing two chains related by glide symmetry. The chain axes of these glide-related molecules are always parallel to each other and are either directed normal to the layer plane or tilted from the layer normal. The symmetry of the rectangular unit cell is preserved, when tilt occurs along one of the two symmetry-permitted short a_1 or long b_1 lattice vectors, corresponding to the nearest neighbor (NN) and the next-nearest neighbor (NNN) directions, respectively (Figure 1a).

The packing of hydrocarbon chains can be classified according to the subcell $a_1 \times b_1 \times c$, in which a_1 and b_1 describe a two-dimensional lattice perpendicular to the chain axis and $c = 2.54 \text{ \AA}$ corresponds to internal periodicity along the axis of hydrocarbon zigzag.^{31–33} The 2D lattice, as defined by the a_1 and b_1 axes, is essentially independent of the degree of chain tilt from the layer normal but does depend on the packing mode, as demonstrated by numerous examples in bulk crystals.^{33,34} Hydrocarbon chains in the overriding majority of known 3D structures of lipids pack such that the chain axes are

all aligned parallel within a layer. The very rare examples of crisscross packing found in bulk crystals, in which molecular chain axes within a layer are not all parallel, do not have an analogue in Langmuir films studied to date by GIXD. Such a crisscross arrangement of the hydrocarbon chains if packed in a rectangular unit cell and glide-plane running along b (crisscrossing may only occur in the NNN direction) would give rise to an intense low-order (1,0) reflection. The fact that the (1,0) reflection was generally absent or extremely weak in all the known GIXD data for nonchiral or racemic monolayers indicated clearly that two hydrocarbon chains, one in the origin and one in the center of the rectangular unit cell, are related by pseudotranslation and therefore the chain axes must be parallel.

In order to characterize and compare the packing of long hydrocarbon chains in various monolayers at different temperatures and surface pressures independent of the effect of tilt, we consider a unit cell projected onto a plane perpendicular to the chain axes with dimensions $a_1 \times b_1$. A distribution of the cell dimensions a_1 and b_1 , of monolayers of nonchiral substances and racemic mixtures for both crystalline phases and mesophases^{3–29,35–37} is shown in Figure 2a. A plot analogous to that in Figure 2a was originally proposed by Steitz et al.,³⁸ who compared lattice spacings of monolayers deposited on solid substrates with that of the monolayers on the water surface. In Figure 2b and c the data for fatty acids and the remaining amphiphiles are shown separately to better resolve the points from different data sets.

In most of the monolayers under consideration here, such as fatty acids, alcohols, or amides, the headgroup size does not exceed the cross-sectional area of the hydrocarbon chain. In some monolayers, such as glycerols^{16,17} or phospholipids,³⁷ the headgroups are more bulky and molecules tilt in order to preserve close contacts between their tails. Nevertheless, hydrocarbon chains in these substances adopt the same packing modes as those of the amphiphiles whose headgroup size is compatible with the cross-sectional area of the chain (Figure 2).

All data points of Figure 2a lie, with some scatter, on a large arc. The central part of the arc corresponds to nearly hexagonal packing of orientationally-disordered molecules at high temperatures. Such disorder requires a relatively large area per molecule ($20\text{--}21 \text{ \AA}^2$). Lowering of the temperature is accompanied by a reduction in the area per molecule and a concomitant lattice distortion from the hexagonal to a rectangular unit cell. A distribution curve as obtained for an amphiphile compound under various thermodynamical conditions (as for the acid $\text{C}_{20}\text{H}_{41}\text{COOH}$, Figure 2b) displays no discontinuity between mesophases and crystalline phases. Moreover, a particular data point in the general distribution arc (Figure 2a) may represent either a crystalline or a mesomorphic state of a monolayer for different substances. The two ends of the arc correspond to relatively dense chain packings, with cross-sectional areas of 18.6 and 19.0 \AA^2 . The average dimensions of the projected rectangular unit cell $a_1 \times b_1$ containing two molecules are 5.0×7.5 and 4.4×8.7 , respectively. Both cells can be considered as distorted from the hexagonal cell of the monolayer

(30) Bibo, A. M.; Peterson, I. R. *Adv. Mater.* **1990**, *2*, 309.

(31) Kitagorodskii, A. I. *Organic Chemical Crystallography*; Consultants Bureau: New York, 1961.

(32) Segerman, E. *Acta Crystallogr.* **1965**, *19*, 789.

(33) Abrahamsson, S.; Dahlén, B.; Löfgren, H.; Pascher, I. *Prog. Chem. Fats Other Lipids* **1978**, *16*, 125.

(34) Small, D. M. *Handbook of Lipid Research*; Plenum Press: New York and London, 1986; Vol. 4, Chapters 2, 5, and 8.

(35) Böhm, C.; Möhwald, H.; Leiserowitz, L.; Als-Nielsen, J.; Kjaer, K. *Biophys. J.* **1993**, *64*, 553.

(36) Brezesinski, G.; Dietrich, A.; Dobner, B.; Möhwald, H. *Prog. Colloid Polym. Sci.* **1995**, *98*, 255.

(37) Bringezi, F.; Brezesinski, G.; Nuhn, P.; Möhwald, H. *Biophys. J.* **1996**, *70*, 1789.

(38) Steitz, R.; Mitchell, E. E.; Peterson, I. R. *Thin Solid Films* **1991**, *205*, 124.

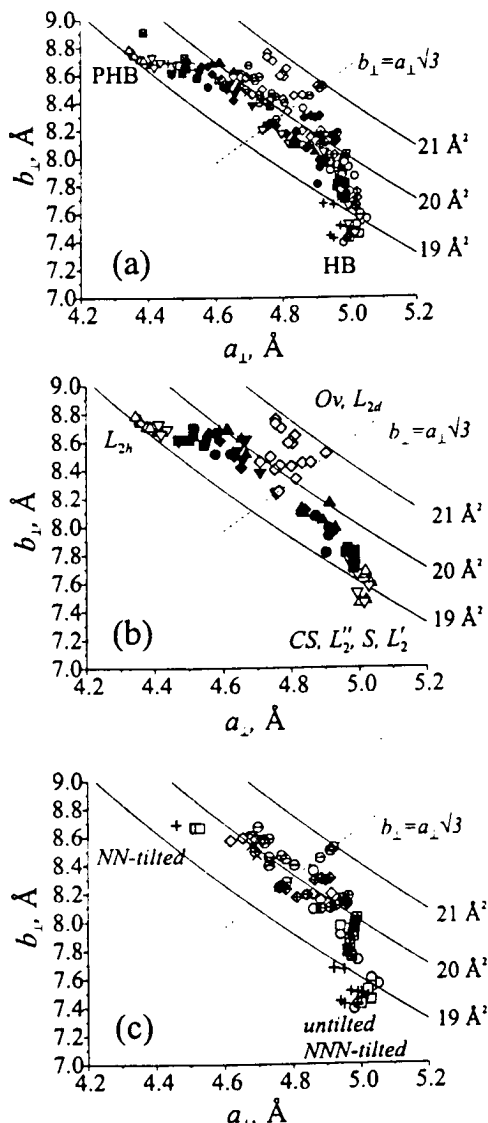
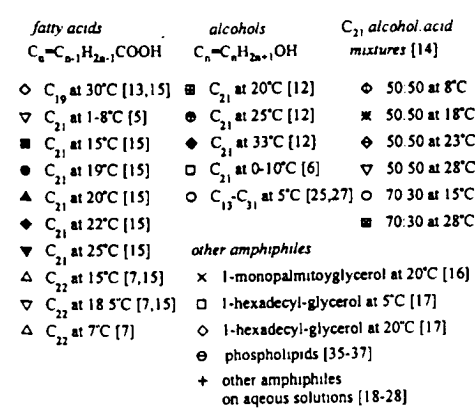


Figure 2. Distribution of projected unit cell parameters (a_1 , b_1) extracted from GIXD data of various nonchiral and racemic Langmuir monolayers. Parallel solid lines correspond to specified values of constant cross-sectional area $A = a_1 b_1 / 2$ occupied by a single hydrocarbon chain. The dashed line corresponds to the hexagonal projected unit cell with $b_1 = a_1 \sqrt{3}$. (a) Data for all substances. Labels HB and PHB denote (a_1, b_1) regions characteristic for herringbone and pseudo-herringbone packing modes, respectively. (b) Data for long-chain fatty acids. The labels of the phases CS , S , L''_2 , L'_{2d} , and Ov specify the regions of their corresponding data points. (c) Data for various amphiphiles, excluding the data for fatty acids.

containing orientationally disordered chains with lattice spacings of approximately 5.1 Å and the area per molecule 22 Å². This hexagonal lattice can be expressed as centered rectangular with the unit cell dimensions 5.1 × 8.7 Å². The two dense packing modes can be obtained by shrinking the hexagonal cell either along the a - or b -direction, corresponding to an NN or NNN shrinkage, respectively (Figure 1b). The directions of chain tilt and of distortion in the projected unit cell are correlated in most of the monolayers studied: the projected unit cells of NN-tilted phases most often shrink in the a_1 -direction, whereas the projected unit cells in NNN-tilted phases and untilted phases shrink along b_1 . In several cases, including the phase L''_2 of fatty acids, however, the NN tilt is accompanied by the shrinkage of the projected unit cell along b_1 .^{5,19,25,28}

For fatty acids (Figure 2b), the data points obtained along the surface pressure–molecular area isotherm of a given substance contribute to both the left and right wings of the arc arising from two tilted phases: the low-pressure NN-tilted phase L_2 and the higher-pressure NNN-tilted phase L'_2 , respectively. The observed NNN-tilted phases of the long-chain alcohols contribute data points only to the right wing of the arc. The left part of the arc in Figure 2b and c corresponds mostly to the NN-tilted phases. Figure 2 does not include the data for the acid $C_{20}H_{41}-COOH$ on the aqueous subphase containing calcium ions at pH = 10.9,¹⁰ since the corresponding rectangular unit cell of dimensions 4.1 × 9.1 Å² largely deviates from the universal arc. Such a distortion is possibly caused by strong ionic interactions between the calcium cations and the negatively charged carboxylate groups.

Packing of the Chains by Lattice Energy Calculations

The dense molecular packing characterized by the 5.0 × 7.5 Å² unit cell is a fingerprint of the herringbone (HB) arrangement, the common packing mode of hydrocarbon chains in bulk organic crystals.^{31,33,34} The noticeable deviation of the 4.4 × 8.7 Å² unit cell dimensions from those of the standard HB motif suggests a different packing arrangement. A search for a possible packing mode that satisfies the 4.4 × 8.7 Å² cell revealed an arrangement described by Kitaigorodskii (ref 31, Figure 130b), who regarded it as implausible because of a relatively low packing density. This arrangement, which we label as the pseudo-herringbone packing mode (PHB), is shown in Figure 3 together with the regular HB motif. The PHB mode, as characterized by Kitaigorodskii on the basis of the van der Waals radii of the carbon and hydrogen atoms, should have a dihedral angle of 40° between the backbone planes of the chains. The projected cell parameters of the PHB arrangement as estimated by Kitaigorodskii are $a_1 = 4.2$ Å and $b_1 = 9.0$ Å. Figure 3 represents slightly different values derived from an energy minimization procedure described below, which are in better agreement with the experimental data of Figure 2. A search in the Cambridge Structural Database³⁹ for 3D structures containing closely-packed alkyl chains with the angle between backbone planes differing widely from 0° and 90° yielded two examples with projected unit cell dimensions $a = 4.1-4.6$ Å and $b = 8.0-8.4$ Å and the interplane angle 33–42°, close to those of the PHB packing mode.^{40,41}

(39) Allen, F. H.; Kennard, O.; Taylor, R. *Acc. Chem. Res.* 1983, 16, 146.

(40) Bocelli, G.; Grenier-Loustalot, M.-F. *Acta Crystallogr. C* 1987, 43, 1223.

(41) Lang, J.; Zhu, H.; Xin, X.; Chen, M. *Chem. J. Chin. Univ.* 1992, 13, 18.

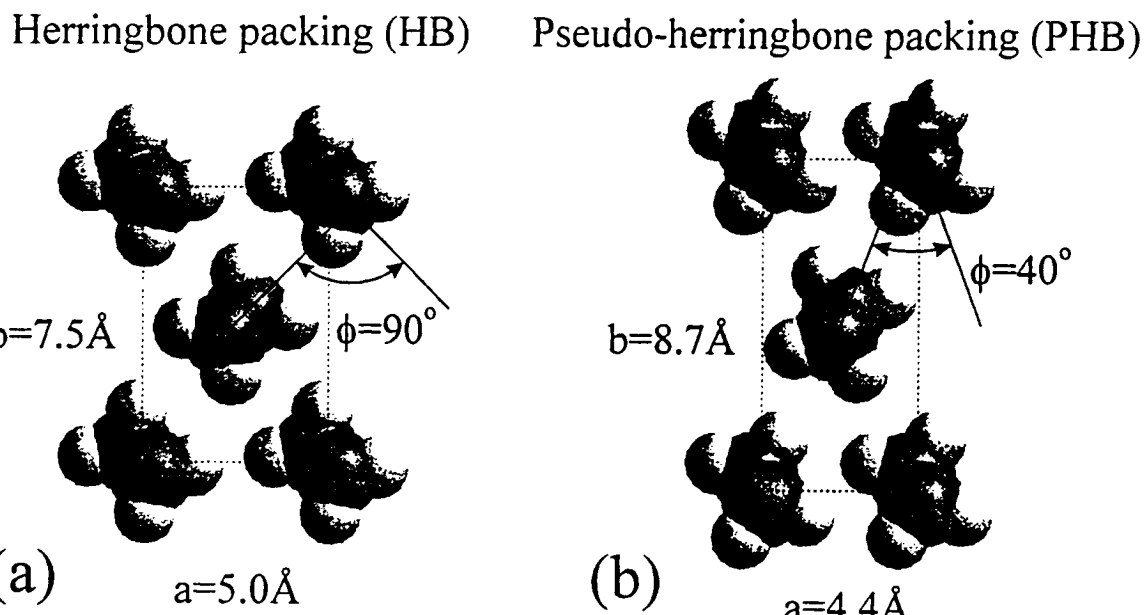


Figure 3. (a) Herringbone (HB) and (b) pseudo-herringbone (PHB) packing modes of hydrocarbon chains.

We carried out the lattice energy calculations on the herringbone and pseudo-herringbone motifs in order to glean information on their relative energies. Monolayers of various substances in different phases, crystalline and mesomorphic, have similar unit cell dimensions, which point to the dominant role of the interaction energy between neighboring hydrocarbon chains. The lattice energy calculations neglect thermal motion of the molecules and their interaction with the water subphase. Such effects can in principle be taken into account in molecular dynamics simulations. However, the simulations performed to date (see e.g. refs 42–47 and references therein) could not reveal the herringbone or pseudo-herringbone packing of the hydrocarbon chains, because of the fixed shape and limited size of the simulation cell, together with periodic boundary conditions. These factors impose hexagonal arrangement of the molecules during the simulations, although the molecules were allowed to move.

The simple lattice energy calculations presented below have the advantage that the optimized unit cell dimensions can be obtained easily from the energy minimization procedure while other parameters such as the tilt angle, the angle between backbone planes, and symmetry constraints are kept fixed. These calculations did not model any real monolayer system whose state is greatly influenced by the nature of hydrophilic headgroups, by their interactions between each other and with the water subphase, and by thermal molecular motion. We rather used the lattice energy calculations as a qualitative tool for studying the energy of hydrocarbon chain packing, limiting our search of energy minima by symmetry constraints justified within the scope of the known data.

In the following calculations we simplified our search of the energy minima on the basis of the following assumptions. One independent molecule in a general position in a rectangular unit cell with a glide symmetry along either a or b was always assumed. The calculations

were done in two steps. First, keeping the chain axes aligned normal to the layer plane, relative energies of different packing modes, as defined by the dihedral angle ϕ between backbone planes of the glide-related molecules, were examined. Then for a fixed ϕ we inspected the effect of the chain tilt θ from the layer normal on the layer energy.

The lattice energy calculations were performed with use of the Cerius^{2.0} software package (BIOSYM/Molecular Simulations). A C₂₃H₄₈ chain and Dreiding force field involving 6–12 Lennard–Jones atomic potentials⁴⁸ were chosen for energy calculations, and zero charges were set on all atoms. Minimization was done using the modified Newton algorithm,⁴⁹ convergence accelerating smearing,⁵⁰ and the nonbond cutoff distance 7 Å. The arithmetic mean of the atomic radii was used for the well depth radius between nonequivalent atoms in the Lennard–Jones 6–12 potentials, and the geometric mean was used for the well depth.

Figure 4 presents the energy of a two-dimensional lattice of the alkane molecules with chain axes aligned normal to the layer plane. The lattice has a rectangular cell with either a - or b -glide symmetry constraints. At every fixed value of angle ϕ between backbone planes of vertically oriented alkyl chains, the cell dimensions were varied in order to minimize the lattice energy.

The calculations for b -glide symmetry reveal three minima. The minimum at $\phi = 90^\circ$ with the calculated cell parameters $5.1 \times 7.4 \text{ \AA}^2$ refers to the standard HB packing (O_{\perp}). Another minimum at $\phi = 40^\circ$ with the cell parameters $4.4 \times 8.7 \text{ \AA}^2$ corresponds to the PHB motif. A third minimum at $\phi = 180^\circ$ with calculated cell dimensions $4.5 \times 8.2 \text{ \AA}^2$, that has not yet been observed in Langmuir monolayers, corresponds to the packing mode O_{\parallel} , that occurs but rarely in the three-dimensional crystals with the reported average cell dimensions $4.7 \times 7.9 \text{ \AA}^2$.³³

Three energy minima were also obtained for a rectangular cell with a -glide symmetry (Figure 4). The minimum

- (42) Hautman, J.; Klein, M. L. *J. Chem. Phys.* **1990**, *93*, 7483.
- (43) Bareman, J. P.; Klein, M. L. *J. Phys. Chem.* **1990**, *94*, 5202.
- (44) Collazo, N.; Rice, S. A. *Langmuir* **1991**, *7*, 3144.
- (45) Moller, M. A.; Tildesley, D. J.; Kim, K. S.; Quirke, N. *J. Chem. Phys.* **1991**, *94*, 8390.
- (46) Karaborni, S.; Toxvaerd, S. *J. Chem. Phys.* **1992**, *97*, 5876.
- (47) Karaborni, S. *Langmuir* **1993**, *9*, 1334.

- (48) Mayo, S. L.; Olafson, B. D.; Goddard, W. A. *J. Phys. Chem.* **1990**, *94*, 8897.

- (49) Gill, P. E.; Murray, W.; Wright, M. H. *Practical Optimization*; Academic Press: London, 1981; Chapter 4.

- (50) Pertsin, A. J.; Kitagorodsky, A. I. *The Atom–Atom Potential Method*; Springer-Verlag: Berlin, 1987.

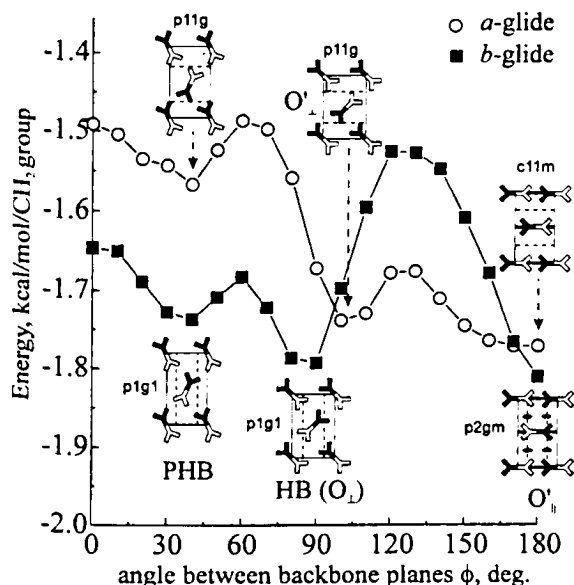


Figure 4. Lattice energy (per CH₂ group) of C₂₃H₄₈ alkane chains, aligned normal to the layer and packed in a 2D rectangular unit cell, as a function of the variation of dihedral angle between neighboring backbone planes of glide-related molecules. The two energy curves correspond to the two principal directions of glide, either along *a* or *b*. The insets schematically show projected packing arrangements with their 2D symmetry notations corresponding to the energy minima.

at $\phi = 100^\circ$, cell dimensions 5.2 \times 7.3 Å², reflects an alternative of the standard HB packing. This packing mode, labeled O' in the literature,³³ is energetically less favorable than the standard HB (O₁) packing and has just a few examples in bulk crystals. The dihedral angle between the neighboring chains usually exceeds 90° and can be as large as 120°.³³ A shallow minimum at $\phi = 40^\circ$ corresponds to a mode, that was neither considered theoretically nor observed in 3D crystals. The minimum at $\phi = 180^\circ$ corresponds to the packing arrangement which is constrained by the *a*-glide symmetry. If the *a*-glide constraint is released, the structure should relax to a triclinic or monoclinic packing in which all chains have their backbone planes parallel. The parallel packing of chains has rarely been encountered for Langmuir monolayers composed of nonchiral molecules,⁵¹ although it should be more frequent for chiral-resolved amphiphiles.²⁹

Thus, energy calculations support the existence of both HB and PHB packing modes and also prove the former should be more favorable for close-packed untilted amphiphilic molecules. The lattice energy curves describing the relative stability of hydrocarbon chain packing can only be considered as semiquantitative. More precise values can be obtained with use of more accurate van der Waals potentials and the Coulomb energy contribution.

The glide symmetry imposes a rectangular 2D lattice with the glide direction either along *a* or *b*. For tilted molecules, the direction of the glide coincides with that of the chain tilt and thus is determined unambiguously. As shown by many examples of 3D structures of long-chain amphiphiles, the cross-sectional subcell of hydrocarbon chains does not depend on the degree of the molecular tilt within a layer. Therefore the angle ϕ between backbone planes of two glide-related molecules, which defines the packing mode, and the tilt angle θ from

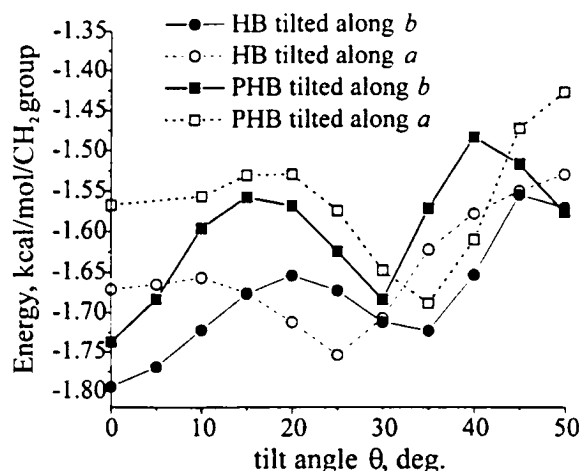


Figure 5. Lattice energy (per CH₂ group) of the C₂₃H₄₈ alkane chains packed in a 2D rectangular unit cell as a function of chain tilt angle from the normal to the layer plane. Two possible tilt directions (either along *a* or *b*) combined with two fixed values of the dihedral angle ($\phi = 90^\circ$ for HB and $\phi = 40^\circ$ for PHB) give rise to four energy curves.

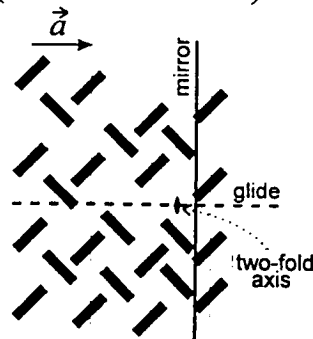
the layer normal can be considered as two independent parameters. On the basis of the results of the first set of lattice energy calculations, we kept the angle between the backbone planes fixed at $\phi = 90^\circ$ for the HB and $\phi = 40^\circ$ for the PHB packing modes. Figure 5 gives the lattice energies as a function of the tilt angle θ for four combinations involving two possible tilt directions of the chains and the two fixed values of the dihedral angle between the chains. At each tilt angle θ the cell dimensions *a* and *b* were optimized in order to minimize the lattice energy. According to the calculations (Figure 5), the HB motif in which the chains are aligned normal to the layer plane ($\theta = 0$) with the glide parallel to the *b* axis yielded the lowest energy. We may anticipate this packing mode to be dominant in the dense untilted monolayer phases. As the tilt angle θ is increased, the energies of the different states converge at $\theta \approx 30^\circ$ which means that the structure of the film is no longer determined by the relative stability of the different hydrocarbon packing motifs but rather by other factors, such as the interactions involving the headgroups and the subphase, as well as by thermal effects. These factors should, for highly tilted hydrocarbon chains, permit the existence of various phases under similar thermodynamic conditions and transitions between them. One example is provided by a transition from the HB phase L'' to the PHB phase L_{2h} in fatty acid monolayers with a preserved molecular tilt azimuth in the NN-direction. Another transition involves "swiveling" of the molecules from the HB phase L', in which the molecules are tilted toward the next-nearest neighbors, to the PHB phase L_{2h}, in which the molecules are tilted toward nearest neighbors.

Symmetry of Crystalline Phases and Mesophases

Figure 2 presents the data sets for both crystalline phases and mesophases. The data sets overlap, reflecting similar intermolecular distances in the crystalline and partially disordered states. These two states can be distinguished in the diffraction experiments by the widths of the diffraction peaks. The resolution-limited peaks designate the translational order on a scale of at least 1000 Å for crystalline phases, while the mesophases are usually characterized by relatively short correlation lengths. The continuous variation in cross-sectional cell

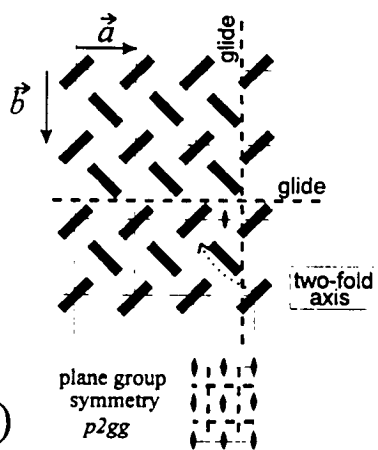
(51) Garnaes, J.; Larsen, N. B.; Bjornholm, T.; Jorgensen, M.; Kjaer, K.; Als-Nielsen, J.; Jorgensen, J. F.; Zasadzinski, J. A. *Science* 1994, 264, 1301.

S (chains untilted)

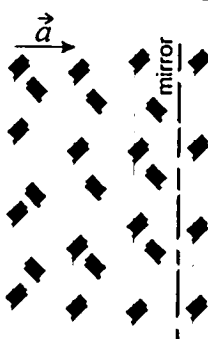


(a) border group symmetry $t : 2 \cdot a$

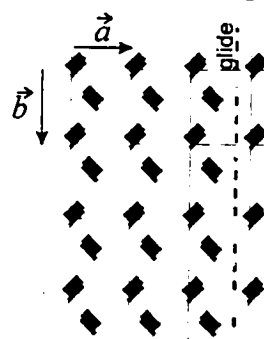
CS (chains untilted)



(c) plane group symmetry $p2gg$

 L'_2 (tilted along b)

(b) border group symmetry $t : m$

HB (tilted along b)

(d) plane group symmetry $p1gl$

Figure 6. Symmetry of monolayer phases with one-dimensional and two-dimensional periodicity: (a) a one-dimensional crystal with vertically aligned hydrocarbon chains possessing twofold molecular disorder and translational disorder in the b direction; (b) a one-dimensional crystal with NNN-tilted hydrocarbon chains, translationally disordered along b ; (c) a two-dimensional crystal with vertically aligned hydrocarbon chains possessing twofold disorder; (d) an ordered crystal with hydrocarbon chains arranged in the herringbone motif and tilted along b .

dimensions from mesophases to crystalline phases in Langmuir monolayers, as given by the distribution in Figure 2a, indicates minor variations in the local packing of the hydrocarbon chains. However, in mesophases the symmetry of the local packing does not maintain itself over long distances. The average molecular distribution in mesophases has a symmetry intermediate between that of a crystal and that of an isotropic liquid. The discrete translational order, characteristic of true crystals, can be lost completely or preserved in some directions. The well-known three-dimensional mesophases are liquid crystals, such as nematics (anisotropic liquids, possessing only orientational molecular order), or smectics, which have periodicity of the layers and are liquid-like within each layer.

The symmetry of the mesophases in Langmuir monolayers cannot be determined from diffraction data only; complementary data from thermodynamic and optical studies have to be employed. The symmetry of the phases as well as its changes can be described in a framework of

the Landau theory of phase transitions.⁵² Here we discuss the symmetry relationships between mesophases and crystalline phases in Langmuir monolayers of the long-chain fatty acids. Their phase diagram contains at least six structurally distinct mesophases, which can be related to the rotator phases of bulk alkanes.^{53,54}

The intermediate temperature range from low-temperature crystalline to high-temperature disordered phases comprises three mesophases in which chains are tilted toward nearest neighbors (NN), tilted toward next-nearest neighbors (NNN), and untilted (labeled as L_{2h} , L'_2 , and S , respectively), in the sequence of increasing surface pressure. These three phases were assigned as mesophases with one-dimensional periodicity.⁵² The symmetry for the S and L'_2 phases is shown in Figure 6 a and b. The hydrocarbon chains are depicted by their backbone planes. The representation in Figure 6a–c implies twofold rota-

(52) Kaganer, V. M.; Loginov, E. B. *Phys. Rev. E* 1995, 51, 2237.

(53) Peterson, I. R.; Kenn, R. M. *Langmuir* 1994, 10, 4645.

(54) Sirota, E. *Langmuir* 1997, 13, 3849.

tional disorder of the chains about their long axes. Equidistantly spaced thin solid lines along the molecular rows represent one-dimensional periodicity in the *a*-direction. The symmetry of the mesophases with one-dimensional periodicity obeys one of the seven groups G_1^2 of borders,⁵⁵ whereas the symmetry of the two-dimensional crystalline phases belongs to one of 17 plane groups^{55,56} G_2^2 .

The untilted mesophase *S*, periodic in the *a*-direction, exhibits the symmetry of borders $t\cdot 2\cdot a$ (Figure 6a). Molecules within a row do not have long-range discrete translational order. Every two neighboring rows of molecules are related by the *a*-glide symmetry in the NN direction. The NNN-tilted phase L'_2 with symmetry of borders $t\cdot m$ (Figure 6b) is obtained from the *S* phase by decreasing the surface pressure. The tilt of the molecules along *b* breaks the original *a*-glide symmetry and the twofold symmetry. Therefore the two orientations of the backbones related by the twofold rotation about the long molecular axis are no longer equivalent. Tilting of the molecules during the phase transition from *S* to the L'_2 phase is a dominant effect in response to a decrease of the surface pressure, while the twofold ordering of the chains occurs as a consequence of symmetry reduction.

Figure 6c presents the symmetry of a 2D crystalline phase *CS*, plane group symmetry $p2gg$, that can be derived from the phase *S* by acquiring additional periodicity in the *b*-direction. The phase preserves the twofold orientational disorder of the hydrocarbon chains, as in the *S* phase. The plane symmetry of this phase incorporates two glide planes along both the *a*- and *b*-directions and generated twofold axes perpendicular to the layer plane. This phase represents a two-dimensional analogue of the *B* modification of bulk alkanes.⁵⁷

Figure 6d depicts the symmetry of the HB crystalline phase (plane group $p1gl$). The HB phase does not possess the *a*-glide symmetry, as compared with the *S* or *CS* phases. Therefore, the tilt of the molecules along *b* is not forbidden by the symmetry of the HB phase even in a compressed state, as a result of the twofold ordering of the backbone planes of the chains, which decreases the entropy of the system and lowers the symmetry. Small values of molecular tilt (less than 5°) were actually revealed by fitting the experimental Bragg rods for highly crystalline monolayer phases.²⁶

Let us consider phase transitions between the above-described phases to show their interrelations in the known phase diagram. The transition from the phase *S* with one-dimensional periodicity (Figure 6a) to the crystalline HB phase (Figure 6d) involves two independent steps of ordering. In other words, the representation of the symmetry group which governs the transition *S*–HB can be reduced into two irreducible representations. One of them describes translational ordering in the *b*-direction; the other represents the twofold ordering of the hydrocarbon chains and their tilt ordering. The phases *CS* and L'_2 (Figure 6b and c) are the intermediate phases that correspond to two possible paths of subsequent ordering from *S* to HB. The symmetry for the experimentally observed phase *CS*,^{6,7} with local herringbone order, cannot be identified with the true crystalline HB phase (Figure 6d), because the transition from the HB phase with NNN-tilted molecules toward the phase L''_2 with NN-tilted

molecules has to be accompanied by a change in the glide plane direction from *b* to *a* and must be first order (discontinuous). That would contradict the experimental observations demonstrating the continuous character of the *CS*– L''_2 phase transition.

The HB phase shown in Figure 6d, with hydrocarbon chains aligned almost perpendicular to the water surface (very small tilt along *b*), which may potentially exist at high surface pressure, cannot be identified with any of the observed phases of long-chain fatty acids or alcohols but may exist in highly crystalline Langmuir monolayers of other substances. For the former compounds this phase can probably be obtained from the phase *CS* by decreasing temperature or increasing the surface pressure. An HB phase of the same symmetry $p1gl$ but with a substantial molecular tilt could be derived on cooling from the phase L'_2 .

Analogous symmetry changes upon a transition from the one-dimensional crystal with periodicity along *b* to its NN-tilted state (L_{2h} phase) and farther to the NN-tilted crystal with pseudo herringbone order are not considered here, since the phase L_{2h} is the only phase in the phase diagram of fatty acids which possesses the PHB local packing. All other backbone-ordered phases of fatty acids with a noticeable tilt of hydrocarbon tails from the layer normal have the regular HB motif, and the transitions from L_{2h} to any of them are first order. The NN-tilted phases of glycerols,^{16,17} arachidamide,²⁰ and some mixed monolayers²² are similar to the phase L_{2h} of fatty acids.

Conclusions

The increase of order in the condensed phases of Langmuir monolayers of various substances is accompanied by a continuous change from a hexagonal packing motif of orientationally-disordered hydrocarbon chains to one of the two closely-packed states. One of them is commonly assigned as the herringbone. The other arrangement, which we designated as the pseudo herringbone motif, is rarely observed in three-dimensional organic crystals but occurs regularly in Langmuir monolayers. Both motifs were characterized by lattice energy calculations. These calculations suggest for Langmuir monolayers with highly tilted hydrocarbon chains the existence of various phases under similar thermodynamic conditions. A gradual drift in lattice spacings going from crystalline phases to mesophases indicates minor changes in local packing of the molecules in the corresponding phase transitions.

Symmetry transformations from mesophases to the herringbone-ordered crystalline phases have been discussed. We deduce that an increase in molecular thermal motion does not simply destroy some symmetry elements of the crystalline phases on transition to the mesophases but also gives rise to new symmetry elements. In particular, the herringbone-ordered 2D crystal and the corresponding higher-temperature 1D periodic phase possess mutually orthogonal directions of glide symmetry.

Acknowledgment. One of us (V.M.K.) thanks I. Peterson for helpful discussions, P. Dutta, M. Durbin, R. Kenn, I. Peterson, and G. Brezesinski for providing the data files of their experimental results, and S. Safran and M. Lahav for their hospitality at the Weizmann Institute. V.M.K. was supported by the Russian Foundation for Basic Research (Grant 96-02-16667) in the initial stage and by the Alexander von Humboldt Foundation in the final stage.

LA970819Z

(55) Vainshtein, B. K. *Modern Crystallography*, 2nd ed.; Springer: Berlin, 1994; Vol. 1, pp 107–111.

(56) *International Tables for X-ray Crystallography*, 2nd ed.; Kynoth Press: Birmingham, U.K., 1965; Vol. 1, pp 58–72.

(57) Ewen, B.; Strobl, G. R.; Richter, D. *Faraday Discuss. Chem. Soc.* 1980, 69, 19.

2.3 Aspects of spontaneous separation of enantiomers in two- and three-dimensional crystals

Ivan Kuzmenko, Isabelle Weissbuch, Eugine Gurovitz, Leslie Leiserowitz and Meir Lahav

Department of Materials and Interfaces, The Weizmann Institute of Science, 76100, Rehovot, Israel

Aspects of Spontaneous Separation of Enantiomers in Two- and Three-Dimensional Crystals

IVAN KUZMENKO, ISABELLE WEISSBUCH, EUGENE GUROVICH, LESLIE LEISEROWITZ,* AND MEIR LAHAV*

Department of Materials and Interfaces, The Weizmann Institute of Science, Rehovot, Israel

ABSTRACT Spontaneous separation of enantiomers in two- and three-dimensional crystals is driven by the same thermodynamic and kinetic factors. However, amphiphilic crystalline monolayers at an interface cannot possess a center of inversion, the most common symmetry element in bulk crystals. This fact should, in principle, lead to better chances for spontaneous separation in the Langmuir or Langmuir-Blodgett monomolecular films. On the other hand, the monolayers of most amphiphiles studied to date incorporate long aliphatic chains that have an intrinsic tendency to pack in a herringbone motif requiring glide plane symmetry, thus creating a bias towards racemate formation. Moreover, 2-D crystals supposedly have a much higher degree of molecular and therefore enantiomeric disorder compared to bulk crystals. All these factors necessitate a careful choice of molecules to guarantee enantiomeric separation in two dimensions. Unambiguous detection of spontaneous resolution in 2-D appears to require atomic resolution of molecular packing arrangement, which can in principle be obtained by grazing incidence X-ray diffraction or atomic force microscopy, whereas in bulk solids spontaneous resolution can be easily detected by various macroscopic methods. This short review provides analogies between spontaneous separation in 3-D and recent examples in 2-D, showing that spontaneous separation generally depends upon subtle differences in molecular structure. *Chirality* 10:415–424, 1998. © 1998 Wiley-Liss, Inc.

KEY WORDS: chiral separation; two- and three-dimensional crystals; grazing incidence X-ray diffraction; atomic force microscopy

Recently, with the advent of modern techniques, it has become possible to study, at the molecular level, spontaneous segregation of racemic mixtures into two-dimensional aggregates of opposite chirality. Here we summarize such findings in terms of molecular organization, the thread common to two- and three-dimensional crystals.

The milestone experiment of Louis Pasteur on the manual separation of the enantiomorphous crystals of sodium ammonium tartrate tetrahydrate, by taking advantage of the hemihedral faces that these crystals express (Fig. 1a), laid the foundations for modern stereochemistry.^{1,2}

Despite the considerable body of data available today on molecular crystal structures,³ our present knowledge of intermolecular interactions does not suffice regarding two fundamental aspects of a Pasteur-type experiment. First and foremost, we are still not able to predict with reasonable certainty whether a given chiral molecule will crystallize as a conglomerate or form a racemic crystal. The second aspect concerns the presence or absence of crystal hemihedrism, which is part of the fundamental problem of prediction of the crystal morphology.⁴ The solution of the first problem belongs to the general field of crystal structure prediction, where the central question to be addressed is how molecules are arranged to build a periodic array. An ab initio prediction of possible molecular packing modes leading eventually to the observed crystal structures re-

mains fraught with difficulties although tremendous progress has been made in the development of computational methods.⁵ A major deficiency lies in the determination of precise atom-atom potential parameters that dictate the conformation and packing of molecules in crystals. Kinetic factors that play a dominant role in the early stages of molecular self-assembly into clusters, which may lead to the formation of metastable crystalline polymorphs,⁶ are an additional complication to the problem.

In the event a racemic mixture in solution separates into chiral crystals of opposite handedness, the question whether the crystals develop hemihedrism or not is mostly a consequence of the interaction between crystal surfaces and the environment. In principle, by growing the conglomerates in a chiral environment, the two enantiomorphs may assume different habits. Indeed, a simple way to distinguish between two enantiomorphs is growth in the presence of chiral “tailor-made” additive that will enantioselec-

This manuscript is respectfully dedicated to the memory of Professor E. Gil-Av, who performed pioneering studies in the field of resolution of enantiomers by gas chromatography.

Contract grant sponsor: Minerva Foundation, Munich, Germany.

*Correspondence to: Leslie Leiserowitz or Meir Lahav, Dept. of Materials and Interfaces, The Weizmann Institute of Science, 76100 Rehovot, Israel. Received for publication 9 May 1997; Accepted 31 July 1997

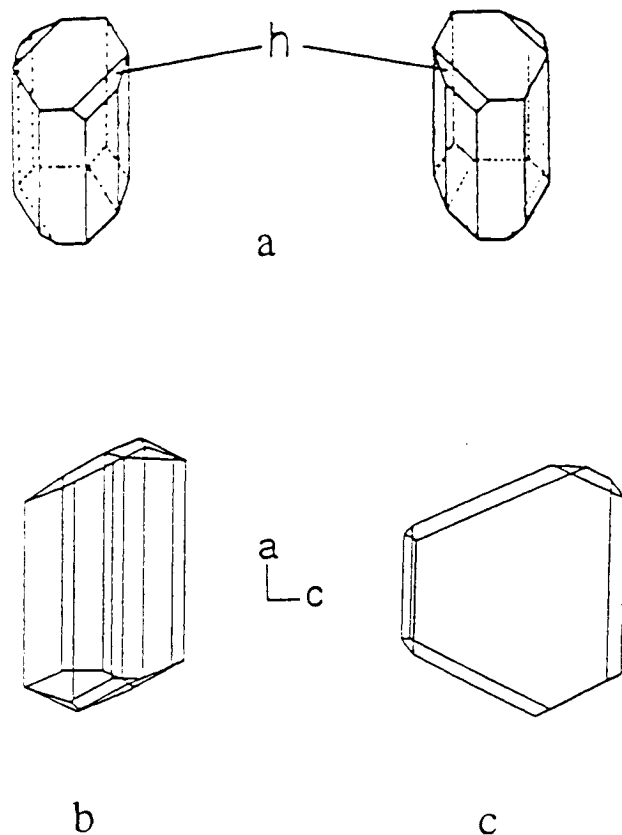


Fig. 1. a: Dextro- and laevo-rotatory sodium ammonium tartrate crystals as described by Pasteur. b,c: Asparagine monohydrate crystals of the (S) form: (b) grown from pure racemic solution, (c) grown from racemic solution containing (S) aspartic acid additive.

tively interact with only one of the enantiomorphs. As an example we present asparagine monohydrate.⁷ Pure aqueous solution yields two enantiomorphs that can barely be distinguished; crystals of the S-enantiomer are shown in Figure 1b. On the other hand, when grown in the presence of S-aspartic acid, the S-crystals became platelike as in Figure 1c and the R-crystals retain the unaffected morphology (as in Fig. 1b). Another simple way of distinguishing between enantiomorphs is by enantioselective etching of the pure crystals in the presence of minor amounts of "tailor-made" enantiomerically pure additives.⁸ Such methods involving crystal morphology changes have become instrumental for the direct assignment of the absolute configuration of chiral molecules,⁹ as an alternative to the Bijvoet technique.¹⁰

The interaction between chiral molecular additives and crystal surfaces leads us to chirality in two-dimensional periodic arrays. The question whether racemates of amphotophilic molecules will separate into two-dimensional crystallites of opposite handedness has long been a puzzle.¹¹ Only recently with the application of grazing incidence X-ray diffraction (GID), scanning tunneling microscopy (STM), and scanning force microscopy (SFM) for probing surfaces at the subnanometer level, has it become possible to distinguish the molecular packing arrangement of conglomer-

ates and racemic compounds of two-dimensional assemblies.

EMPIRICAL AND STATISTICAL STUDIES

In the absence of a general theory of molecular packing in crystals, various rules of thumb have been proposed to rationalize the spontaneous resolution of racemates. In this regard Jacques and his school have deduced some general trends of behavior.¹² About 10% of reported racemates undergo spontaneous resolution. This tendency depends upon the shape, symmetry, and functional groups of the molecules providing some empirical guidelines in the search for new systems. For example, statistical studies based on 500 compounds had demonstrated that the frequency of salts that form conglomerates is two to three times higher than that observed amongst molecular crystals.¹² Moreover, molecules that possess a two- or threefold axis such as the dissymmetric helicenes or organo cobalt amines complexes^{13,14} have a greater tendency to crystallize in chiral space groups. In contrast, for molecules such as carboxylic acids and primary amides that tend to form hydrogen-bonded cyclic dimers, the racemates will crystallize in centrosymmetric arrangements where the center of the pair coincides with the crystallographic center of inversion. On the other hand, if the carboxylic acid or amide contains an additional hydrogen bonding group, such as β -hydroxy-acids or β -sulphoxy acids¹⁵ or amides,¹⁶ the molecules form hydrogen bonds between the carboxy group and the hydroxy or sulphoxy groups of neighboring molecules leading to chiral chains. What determines whether the crystal will be chiral or not depends on the symmetry elements relating the chains to form the complete structure. These empirical rules were instrumental in the search for non-chiral molecules that crystallize in chiral single crystals for the performance of spontaneous asymmetric synthesis.¹⁷

THEORETICAL APPROACH

Spontaneous separation of enantiomers can be driven by thermodynamic or kinetic factors. Wallach proposed an empirical rule that the most thermodynamically stable crystal structures are those that assume the most dense packing arrangements.¹⁸ He also suggested that, in general, racemic compounds will be more dense than the corresponding enantiomorphs, and therefore will appear more frequently. A recent analysis by Brock et al. making use of the crystal data set from the Cambridge Structural Database (CSD), had shown that Wallach's rule pertaining to the density of racemic crystals and enantiomorphs does not generally hold.¹⁹

Kitaigorodskii explained the fact that the limited number of space groups usually observed in crystals, namely $P2_1/c$, $\bar{P}1$, $P2_12_12_1$, $P2_1$, $C2/c$, $Pbca$, and $Pna2_1$ is a consequence of the maximum packing density,^{20,21} implying that the major component of lattice energy is given by the van der Waals interactions. However, there are many systems where the molecular interactions are directed, as in hydrogen bonds, and thus the structure of highest packing density (Wallach's rule) does not necessarily have the minimum lattice energy.

The space group analysis is helpful in order to limit a global search of generated possible crystal structures by ab initio methods involving the use of lattice energy computations.⁵ A standard model for calculating crystal lattice energy is by pairwise summing of atom-atom potential energy terms that involve three distinct contributions. The most important arises from dispersion forces which are non-directional. These forces, which are attractive and assume to have an inverse sixth power dependence, make the overriding contribution to the crystal energy because all atoms of the molecule are involved in them. A second contribution to the energy comes from the exchange-repulsive forces generally taken to have an inverse twelfth power or exponentially decreasing distance dependence. The third contribution is the electrostatic interaction energy arising from the charge distribution in the molecule. Such interactions are long range and direction dependent. The van der Waals energy terms, i.e., dispersion and repulsive coefficients, are generally determined by empirical methods.²² The Coulomb term may be determined in different ways: by empirical methods, quantum-mechanical calculations, or from experimental electron density deformation distributions making use of low-temperature X-ray diffraction data.²³ The first two methods are prone to error, moreover only net atomic charges have been used. The third method, which is the most accurate since it inherently takes into account the crystal field, yields atomic charges and dipole and quadrupole moments.^{23,24} This method is not commonly used since it involves detailed experimental and computational work.

If the minimum lattice energies of ab initio structures for chiral and racemic crystalline phases can be computed, the prediction of the thermodynamically driven chiral separation may be characterized by the chiral discrimination factor Δ_E defined as

$$\Delta_E = \frac{E_{\{R\}} + E_{\{S\}} - E_{\{RS\}}}{E_{\{R\}} + E_{\{S\}} + E_{\{RS\}}}$$

where $E_{\{R\}}$, $E_{\{S\}}$, $E_{\{RS\}}$ are lattice energies for $\{R\}$, $\{S\}$, and $\{RS\}$ crystalline phases, respectively. If $\Delta_E > 0$, which is rarely the case, chiral separation would occur, otherwise when $\Delta_E < 0$ the R and S molecules precipitate into racemic structures.

For achiral molecules, nonchiral space groups are far more frequent than chiral space groups, as given by their distribution in the Cambridge Structural Database. For racemic mixtures, other factors come into play. In systems such as alanine or tyrosine, the solubilities in water of the racemic and enantiomeric forms (total number of dissolved molecules) are about the same, perhaps as a consequence of very similar lattice energies (the same melting points, very similar structural arrangements). In these systems the formation of a racemate has an obvious advantage, reaching supersaturation much before each of the two enantiomorphs. Indeed, all attempts to induce a preferred precipitation of chiral alanine crystals from the racemic mixture grown in the presence of "tailor-made" additives proved to be unsuccessful. The formation of the racemic nuclei appeared to be inhibited and the chiral nuclei were

formed, but secondary epitaxial growth on the chiral nuclei eventually gave rise to twinned racemic crystals.²⁵ All in all, it would appear, therefore, that the lattice energy of a pair of enantiomorphs must be significantly lower than that of the corresponding racemate for spontaneous separation of enantiomers to occur.

TRANSFORMATION OF CENTROSYMMETRIC CRYSTALS INTO ENANTIOMORPHOUS MIXED CRYSTALS

All crystals are delineated by surfaces generally with symmetry lower than the bulk. Thus a racemic mixture of guest molecules occluded via chiral surfaces in a centrosymmetric host crystal may bring about a separation of guest enantiomers inside the mixed crystal, yielding enantiomorphous sectors. The handedness of the sector is determined by the face through which the chiral guest molecules were occluded. We illustrate this concept with the host-guest system glycine/ α -amino acids.²⁶ The host molecules crystallize in a centrosymmetric arrangement (Fig. 2a). These molecules form hydrogen-bonded layers in the *ac* plane, that are interlinked by hydrogen bonds on one side to form centrosymmetric bilayers. In the presence of racemic α -amino acids, the glycine crystals grow as $\{010\}$ plates (Fig. 2b). The S-amino acids are occluded through the $(\bar{0}10)$ face, while the R-amino acids are occluded via the (010) face resulting in the separation of chiral territories. In the event one of the enantiotopic $\{010\}$ faces is blocked by an interface, namely glass or air-solution,²⁷ only one guest enantiomer will be occluded, leading to mixed chiral crystals (Fig. 2c).

The same concept of transforming centrosymmetric crystals into enantiomorphous mixed crystals is valid even if both the host and guest molecules are nonchiral. This concept was taken advantage of to perform asymmetric synthesis within enantiomorphous mixed crystals of cinnamide/cinnamic acid²⁸ and cinnamide/ β -thienylacrylamide,²⁹ via solid-state dimerization³⁰ between host and guest molecules, yielding chiral cyclobutane products.

SPONTANEOUS SEPARATION OF ENANTIOMERS IN TWO DIMENSIONS

Chiral discrimination of molecules in solution and in Langmuir films has been examined theoretically by Andelman, de Gennes and coworkers considering interactions only within a molecular pair.^{31,32} Their overall conclusion that heterochiral pair interactions should be generally favoured should be relevant to dilute fluid phases, but hardly to crystalline systems, where multiple molecular interactions and crystal symmetry play a dominating role. Therefore, their analysis on chiral discrimination cannot be applied to crystalline Langmuir films. We shall see below that the occurrence of spontaneous resolution in two-dimensional crystals may depend upon subtle differences in molecular structure.

Unlike three-dimensional crystals, the detection of spontaneous resolution in two-dimensions is not straightforward. Early surface pressure-area isotherm measurements on racemic and chiral Langmuir monolayers by Lundquist led her to the conclusion that certain racemates undergo

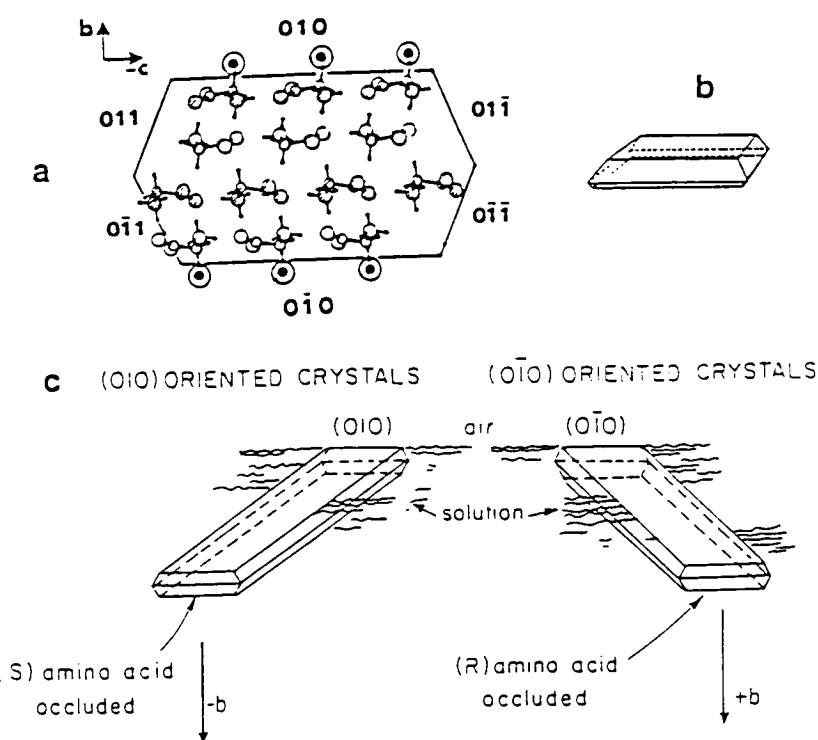


Fig. 2. a: Packing arrangement of α -glycine viewed along the α -axis and delineated by its crystal phases. b: Crystal morphology of α -glycine when grown in the presence of racemic α -amino acid additives. c: Oriented floating crystals of α -glycine grown on solutions of racemic hydrophobic α -amino acids.

spontaneous resolution in two dimensions.³³ Similar studies by Arnett and colleagues suggested that racemic mixtures of myristoyl alanine $C_{17}H_{35}CONH(CHOH)COOH$, separate into islands of opposite chirality,^{11,34} as was recently established by grazing incidence X-ray diffraction and epifluorescence microscopy.³⁵

Separation of enantiomers in racemic Langmuir films was demonstrated recently by SFM and STM. Eckhardt et al.³⁶ reported the spontaneous separation in Langmuir films of a tetracyclic alcohol transferred onto a mica surface. An SFM image of the film consisted of chiral crystalline domains, related by mirror symmetry. Stevens et al.³⁷ reported on the spontaneous resolution of a liquid crystal of racemic biphenyl deposited onto a freshly cleaved surface of highly oriented graphite and measured by STM.

In principle, the outline of two-dimensional single crystals delineated by straight boundary lines at the air-liquid interface should reflect the plane group symmetry of the crystal and thus may display chiral hemihedral shapes in the event of enantiomorphous crystals. Two-dimensional enantiomorphous domains at the air-liquid interface can be detected by Brewster angle and epifluorescence microscopies. However, observed two-dimensional domains were never single crystals but rather assemblies of crystallites, often assuming dendritic morphologies.^{38,39} Rietz et al.⁴⁰ reported an example where racemic α -diols assume chiral patterns, as shown by the epifluorescence measurements. However, according to GID measurements, the unit cell of the racemic mixture is not oblique as found for the pure enantiomer, but rather rectangular, indicating formation of

a true racemate.³⁸ In this respect, we note the comments by Selinger and Selinger who pointed out that the formation of spiral defects in two-dimensional aggregates leads to chiral symmetry breaking on the macroscopic length scale, even without any microscopic chiral order.⁴¹ Therefore, optical methods do not suffice to establish spontaneous separation of enantiomers in two-dimensional crystals. Moreover, observed chiral patterns on the macroscopic level by epifluorescence microscopy may be caused by an interaction between the monolayer domain with the chiral resolved probe molecules, which may act as "tailor-made" inhibitors of crystal growth in specific directions. Consequently, even racemic structures may assume a chiral shape. A three-dimensional analog of such an effect has been reported recently on racemic alanine that crystallizes in a nonchiral space group but assumes a chiral morphology when crystallized in the presence of small quantities of a resolved α -amino acid, although the internal structure of the crystal remains racemic.²⁵

CONTROL OF SPONTANEOUS SEPARATION IN TWO-DIMENSIONAL CRYSTALS

The engineering of 3-D crystal structures with desired features has been used for purposes such as pinpointing molecular interactions, and the performance of solid state reactions. Such an approach has recently been applied for achieving spontaneous separation in two-dimensional crystals.⁴²

The most important symmetry elements by which organic molecules are related in three-dimensional crystals

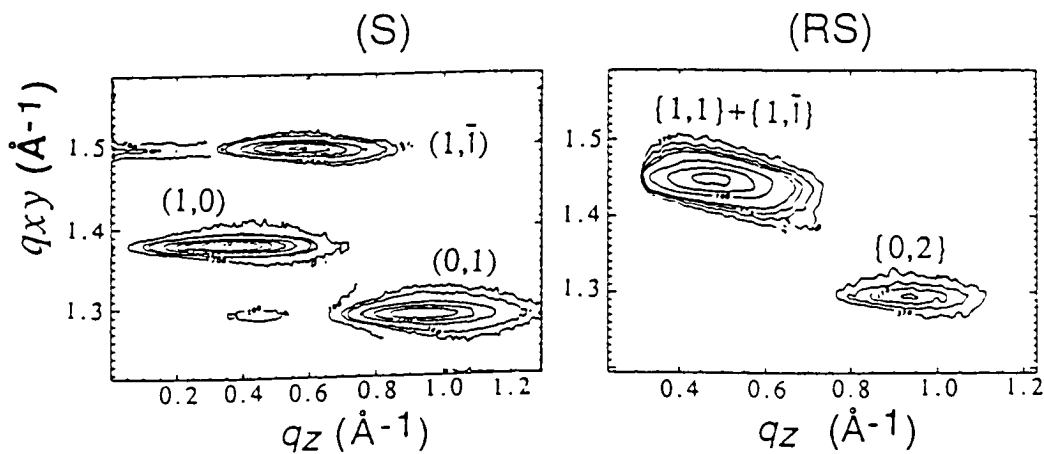


Fig. 3. GID patterns for the monolayers of the optically pure and racemic amphiphiles $C_{16}\text{-gly}$, shown as two-dimensional intensity contour plots $I(q_x, q_y)$, along the horizontal q_x and vertical q_z components.

are, of course, translation, center of inversion, twofold screw axis, and glide plane. In the two-dimensional counterpart at a liquid surface for amphiphilic molecules that are specifically oriented vis-à-vis the water surface, the situ-

ation is simpler. The center of inversion, the glide with its plane parallel to the water surface, and the corresponding twofold screw symmetry are precluded. The only remaining symmetry elements are translation and a glide whose

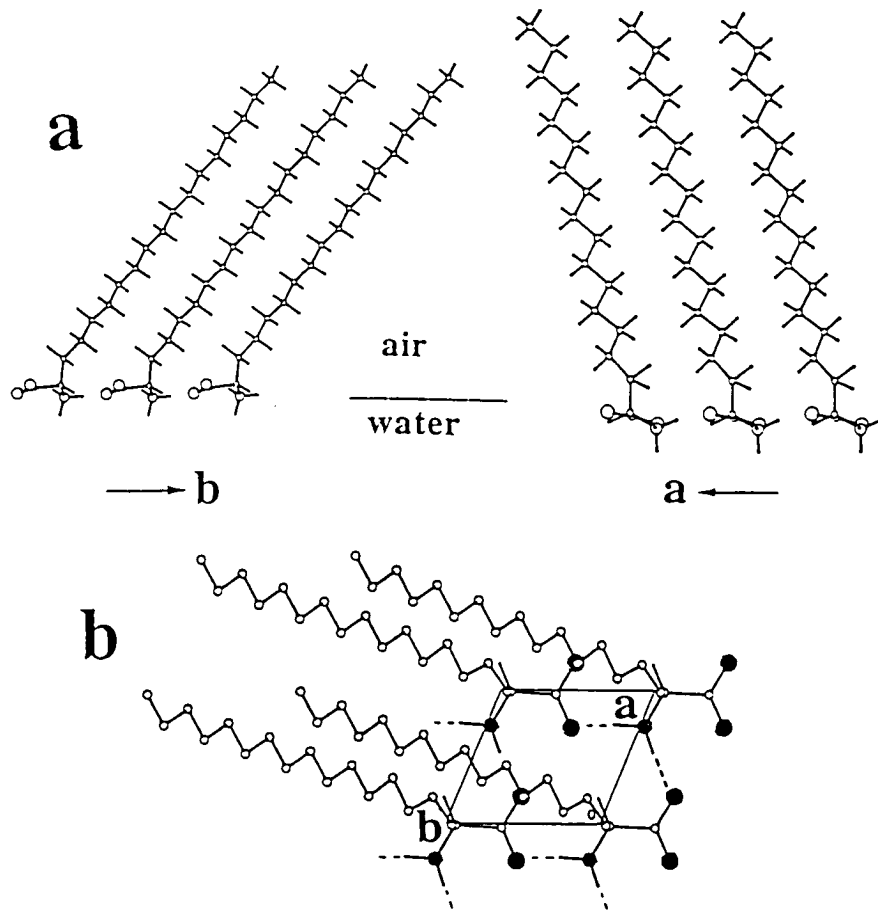


Fig. 4. The 2-D crystalline packing arrangement of the (S)- $C_{16}\text{-gly}$ monolayer on water surface. Views parallel (a) and perpendicular (b) to the water surface. For clarity the N and O atoms of the head groups in b are filled and the H atoms of the n -alkyl chains are omitted.

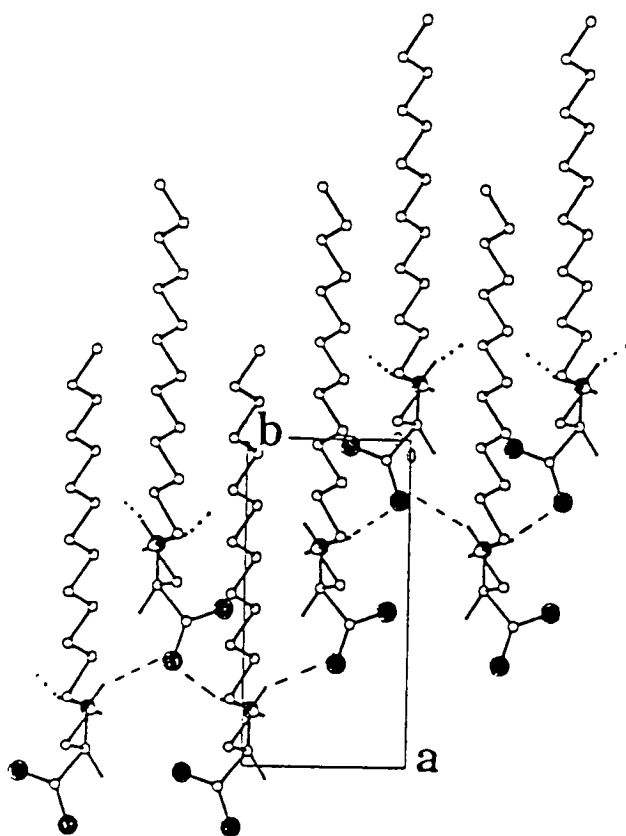


Fig. 5. The 2-D crystalline packing arrangement of the heterochiral domains of the (R,S)-C₁₆-gly monolayer on the water subphase, viewed perpendicular to the layer. For clarity the N and O atoms of the head groups are filled and the H atoms of the n-alkyl chains are omitted.

plane is perpendicular to the water surface. Thus, in principle, it should be easier to bring about spontaneous segregation of chiral molecules in 2-D crystals at the solution interface. In order to induce separation of chiral territories,

the glide symmetry and the possible formation of solid solutions between the two enantiomers must be prevented.

Oriented crystallization of α -glycine under monolayer of amphiphilic α -amino acids provided evidence, albeit indirect, of two-dimensional ordering of the amphiphiles.⁴³ Recently a focus was put on the design of α -amino acid amphiphiles, that their racemates would spontaneously separate or form a racemic compound.⁴² Thus monolayers of amphiphiles of the type C_nH_{2n+1}CH(NH₃₊)CO₂⁻, labelled C_n-gly, n = 10,12,16, have been studied by grazing incidence X-ray diffraction (GID) (Fig. 3).

The enantiomerically pure amphiphile crystallizes in an oblique cell, of dimensions $a = 4.91\text{\AA}$, $b = 5.25\text{\AA}$, $\gamma = 112^\circ$, are compatible with the plane group p1 in which the molecules of a single chirality are related by translation symmetry only. The packing arrangement is shown in Figure 4 and X-ray structure factor calculations yielded a good fit to the GID data. In contrast, the GID patterns from the various racemic amphiphiles C_n-gly n = 10,12,16 (Fig. 3, right) yielded a rectangular unit cell of dimensions $a = 4.80\text{\AA}$, $b = 9.67\text{\AA}$. The molecules in the monolayers are related by glide symmetry in the herring-bone motif, in the plane group p1g1 whose glide plane is parallel to the b axis. The packing arrangement is shown in Figure 5.

In order to achieve the spontaneous separation in α -amino acid monolayers, it was imperative to induce translational packing of the alkane chains within the layer. Secondary amides have a pronounced tendency to form N-H . . . O hydrogen bonds by translation. Therefore we focused on monolayer films of N⁺-derivatives of lysine C_nH_{2n+1}CO-NH-(CH₂)₄-CH(NH₃₊)CO₂⁻, labelled C_n-lys, n = 11,17,21,29.

The GID patterns from the films of the three racemic systems (R,S) C_n-lys n = 11,17,21 and the enantiomerically pure counterparts are similar (shown for C₁₇-lys in Fig. 6), and indicate an oblique cell containing one independent molecule. The packing arrangement is shown in Figure 7, as deduced from the GID data.

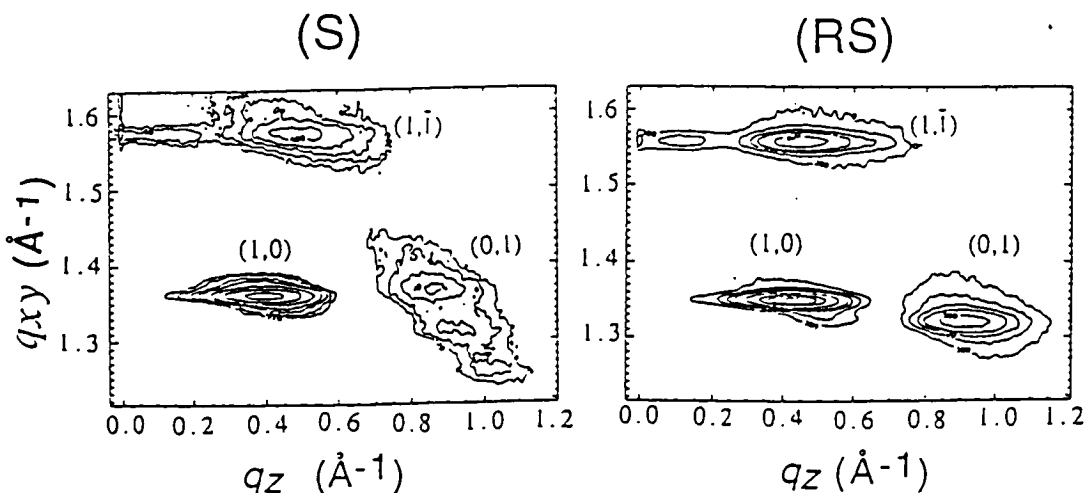


Fig. 6. GID patterns for the monolayers of the optically pure and racemic amphiphiles C₁₇-lys, shown as two-dimensional intensity contour plots I(q_x, q_z), along the horizontal q_x and vertical q_z components.

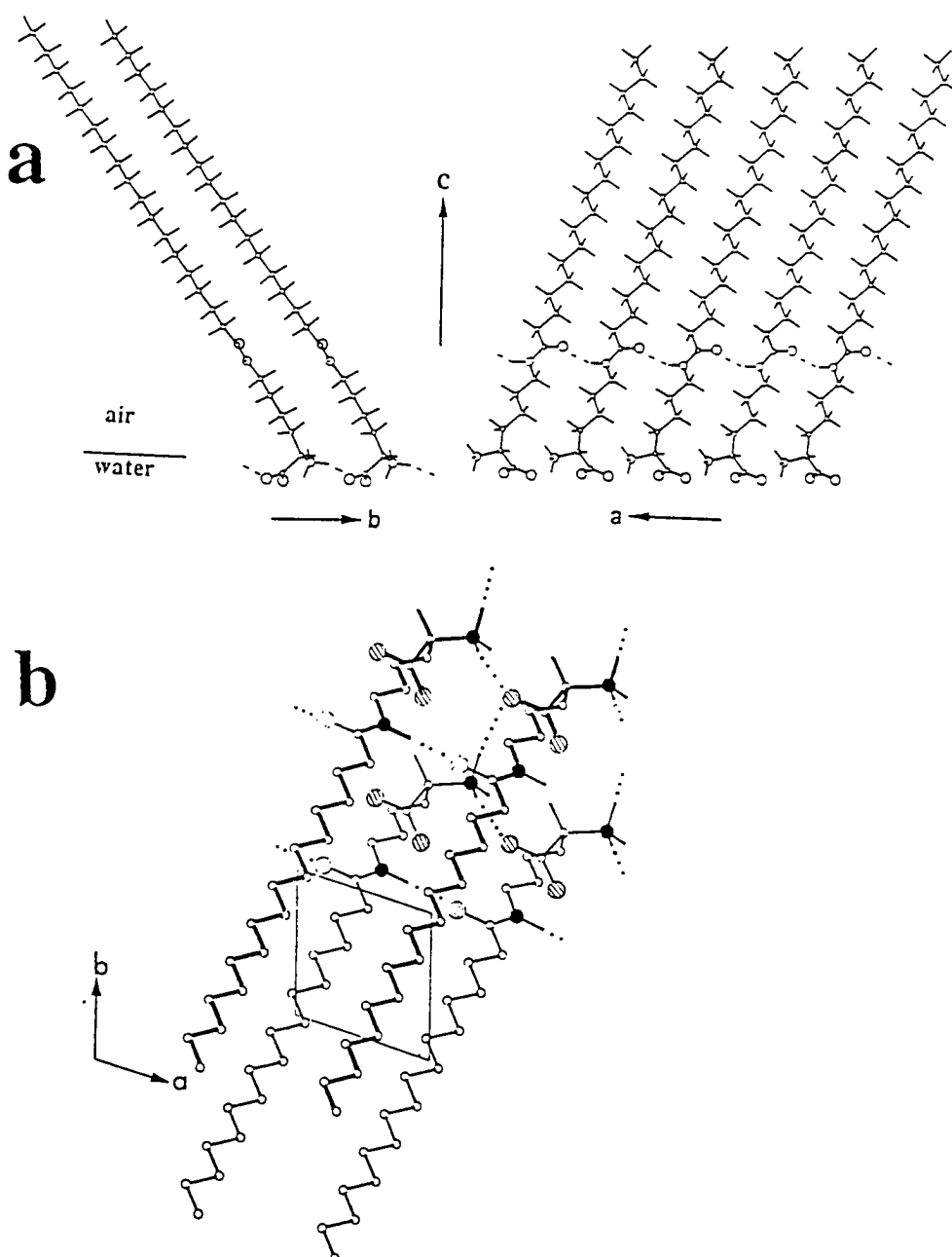


Fig. 7. The 2-D crystalline model packing arrangement of the chiral domains, shown for molecules of (R)-configuration, of the (R,S) C_{17} -lys monolayer on the water surface. Views are parallel (a) and perpendicular (b) to the water surface. For clarity the N and O atoms of the head groups in b are filled and the H atoms of the n-alkyl chains are omitted.

Increasing the length of the hydrocarbon chain of the C_{n} -lys amphiphile enhances the tendency for packing in the herring-bone motif, leading to the formation of racemic two-dimensional crystals, as observed by GID for the C_{29} -lys monolayers.

Partial solid solubilities of one enantiomer into the lattice of the other enantiomorph is frequently observed in three-dimensional crystals. We might expect that such solubilities in two-dimensional crystallites should be even more pronounced. In the α -amino acids, the chiral disorder can

occur only via an interchange of the C-H and $C-NH_3^+$ groups around the chiral center, since the hydrocarbon chain must remain in its original position. Hence, it seems that such solid solubility is highly improbable, since it will involve the loss of at least one hydrogen bond and a decrease in lattice energy of at least 6 kcal/mol.

The various α -amino acid amphiphiles, when deposited on aqueous solutions of copper acetate, form crystalline monolayers of the copper complex.⁴⁴ In contrast to the monolayers spread on water, the copper complex of the

two types of amphiphiles C_n-gly and C_n-lys forms two-dimensional racemic crystals, according to the GID data. Thus, a subtle interplay between the nature of the polar head groups and the hydrocarbon chains determines the overall packing mode.

Structural and thermodynamic data on diastereomeric mixtures of phenylethyamine mandelates were used in order to achieve spontaneous separation of enantiomers in two dimensions. Water-soluble phenylethyamine C₆H₅-CH(CH₃)NH₂ and mandelic acid C₆H₅-CH(OH)COOH each have one chiral carbon and form diastereomeric salts of various compositions.⁴⁵ The stability and solubility of the two salts (R,R') and (R,S') are drastically different in favour of the (R,R') salt formation.^{46,47} Both of the molecules were derivatized with alkane chains in the *para*-position of their benzene rings for the Langmuir film studies. 1:1 mixtures of R or S *p*-tetradecylphenylethyamine, C₁₄H₂₉-C₆H₄-CH(CH₃)NH₂, and R' or S' *p*-pentadecylmandelic acid, C₁₅H₃₁-C₆H₄-CH(OH)COOH, form on water-stable highly crystalline monolayer films independent of molecular chirality, according to the GID measurements (Fig. 8). The unit cells of the (R,R') and (R,S') films are each oblique and contain one diastereomeric pair of molecules. The GID pattern of the diastereomeric mixture (R,S') is different from that of (R,R'), whereas the equimolar mixture of the four components gives rise to a diffraction pattern almost identical to that of the (R,R') mixture. Studies on different chiral compositions of the four-component system proved the formation of chiral domains containing enantiomeric disorder.⁴⁸ A similar kind of disorder of the α -hydroxy group of mandelic acid has been observed in three-dimensional crystals of analogous structures of phenylethyamine mandelate derivatives. This example shows that $\mathbf{p} \cdot \mathbf{l}$ lattice symmetry (one molecule per unit cell) for the crystallites obtained from racemic mixtures cannot provide unambiguous proof of a Pasteur-type separation in two dimensions unless enantiomeric disorder may be excluded as in the α -amino acid systems.

SELF-ORGANIZATION OF SUPRAMOLECULAR HELICAL ARCHITECTURES

We have shown how periodic order in three- and two-dimensional crystalline systems induces spontaneous sepa-

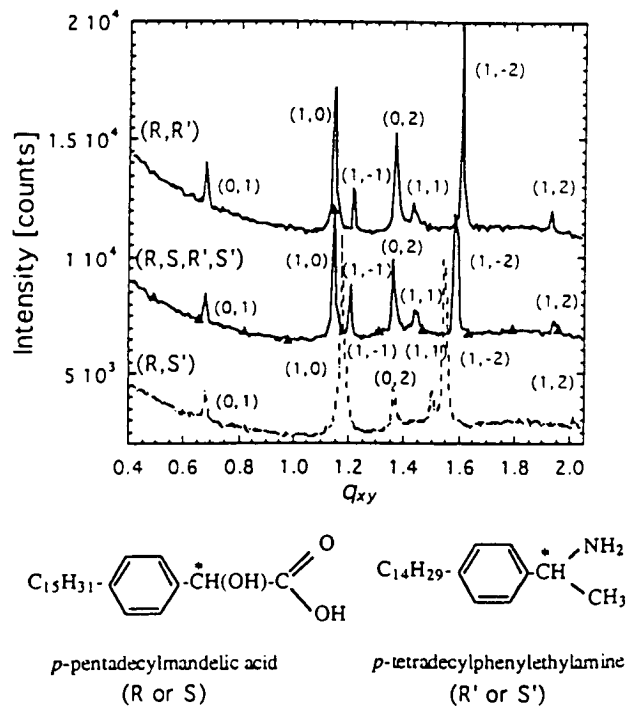
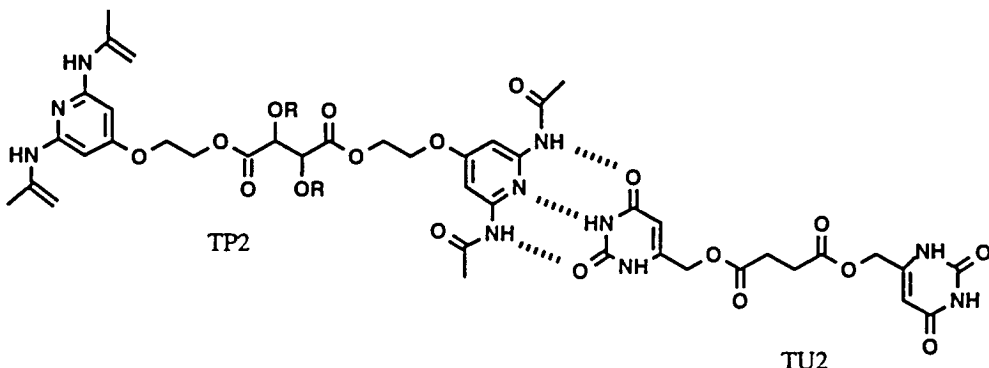


Fig. 8. GID Bragg peaks with assigned (h,k) indices for three diastereomeric 1:1 mixtures of C₁₄H₂₉-C₆H₄-CH(CH₃)NH₂ and C₁₅H₃₁-C₆H₄-CH(OH)COOH. q_{xy} (\AA^{-1}) is the in-plane component of the wave vector q .

ration of enantiomers. Self-organization into helical architectures may also bring about a separation of chiral territories.

The formation of helical ribbons has been reported for chiral molecules as diverse as N-octyl-D-galactonamide,⁴⁹ a double-chain glutamic acid ester with tetraalkylammonium head group,⁵⁰ and a double-chain phospholipid with a nucleotide head group.⁵¹ More recently, Lehn et al.^{52,53} described the self-assembly of supramolecular liquid crystalline polymers from complementary chiral units TP₂ and TU₂ via hydrogen bonding [T represents L, D-, or *meso*(M)-tartaric acid derivatives covalently linked to 2,6-diaminopyridine (P) or uracil (U)] (Scheme 1).

A mixture of the enantiomerically pure components L-P₂



Scheme 1.

plus L-U₂ and D-P₂ plus D-U₂ yielded helical textures of opposite handedness, as observed by electron microscopy, whereas no helicity was found for the *meso*- mixtures. The racemic mixtures of all four components yielded long superhelices of opposite handedness in the same sample, as observed by electron microscopy.

OUTLOOK

The concepts associated with spontaneous separation of enantiomers in two- and three-dimensional crystals have many features in common. However, structural characterization of two-dimensional assemblies on the molecular level is still fraught with difficulties. The monitoring from inception of spontaneous separation of enantiomers in two-dimensional systems at the nanometer level may provide a better understanding of diastereomeric interactions.

Spontaneous resolution in two-dimensions should be of relevance to scientists interested in the origin of chirality. In principle, the molecular requirements for inducing spontaneous separation in two-dimensional crystals at interfaces are easier than in the three-dimensional counterparts. Thus, one may anticipate that such two-dimensional chiral aggregates might have played a pivotal role as templates for spontaneous asymmetric transformations, which drive racemic mixtures into enantiomerically pure systems that could have occurred at prebiotic times.

ACKNOWLEDGMENTS

The GID experiments were conducted together with J. Als-Nielsen and K. Kjaer. We thank M. Berfeld whose work contributed to the studies on chiral and racemic amphiphilic amino acids. We acknowledge financial support from the Minerva Foundation, Munich, Germany, and we thank HASYLAB, Desy, Hamburg, for synchrotron beam time.

LITERATURE CITED

- Pasteur, L. Ann. Phys. 24:442, 1848.
- Eliel, E.L., Wilen, S.H. Stereochemistry of Organic Compounds. New York: Wiley-Interscience, 1994.
- Allen, F.H., Kennard, O., Taylor, R. Systematic analysis of structural data as a research technique in organic chemistry. Acc. Chem. Res. 16:146-153, 1983.
- Hartmann, P. Structure and morphology. In: Crystal Growth: An Introduction, Vol. 1. Amsterdam: North-Holland Publ. Co., 1973:367-402.
- Gavezzotti, A. Theoretical Aspects and Computer Modelling of the Molecular Solid State. New York: John Wiley & Sons, 1996:237.
- Dunitz, J., Bernstein, J. Disappearing polymorphs. Acc. Chem. Res. 28:193-200, 1995.
- Addadi, L., Berkovitch-Yellin, Z., Domb, N., Gati, E., Lahav, M., Leiserowitz, L. Resolution of enantiomers by stereospecific habit modifications. Nature 296:21-26, 1982.
- Shimon, L.J.W., Lahav, M., Leiserowitz, L. Design of stereoselective etchants for organic crystals. Application for the sorting of enantiomorphs and direct assignment of absolute configuration of chiral molecules. J. Am. Chem. Soc. 107:3375-3378, 1985.
- Addadi, L., Berkovitch-Yellin, Z., Weissbuch, I., Lahav, M., Leiserowitz, L. A link between macroscopic phenomena and molecular chirality: Crystals as probes for the direct assignment of absolute configuration of chiral molecules. In: Topics in Stereochemistry, Vol. 16. New York: John Wiley & Sons Inc., 1986:1-85.
- Bijvoet, J.M., Peerdeman, A.F., van Bommel, A.J. Determination of the absolute configuration of optically active compounds by means of X-rays. Nature 168:271-272, 1951.
- Arnett, E.M., Thompson, O. Chiral aggregation phenomena. 2. Evidence for practical "two-dimensional resolution" in a chiral monolayer. J. Am. Chem. Soc. 103:968-970, 1981.
- Jacques, J., Collet, A., Wilen, S.H. Enantiomers. Racemates and Resolutions. New York: John Wiley & Sons, 1981.
- Bernal, J. The phenomenon of conglomerate crystallization. III. Spontaneous resolution in coordination compounds. III. The structures and absolute configuration of $\Lambda(\delta\lambda\delta)[(-)_{589}-cis-\alpha-(triethylenetetraamine)Co(NO_2)_2Cl \cdot H_2O$ (I). $\Lambda(\delta\lambda\delta)[(-)_{589}-cis-bis-ethylenediamine Co(NO_2)_2Cl \cdot (II)$ - stereomers displaying CLAVIC dissymmetry. Inorg. Chim. Acta 96:99-110, 1985.
- Bernal, J. The phenomenon of conglomerate crystallization. IV. The structure and absolute configuration of $\Lambda(\delta\lambda\delta)[(-)_{589}-cis-Co(en)_2(NO_2)_2\{trans-Co(NH_3)(NO_2)_4\}$, a substance containing Clavie dyssymmetric cations and anions. Inorg. Chim. Acta 101:175-184, 1985.
- Leiserowitz, L., Weinstein, M. Studies in crystal chirality. 1. Chiral hydrogen-bonded structures. Acta Crystallogr. B31:1463-1466, 1975.
- Weinstein, S., Leiserowitz, L., Gil-Av, E. Chiral secondary amides. 2. Molecular packing and chiral recognition. J. Am. Chem. Soc. 102:2768-2772, 1980.
- Addadi, L., Lahav, M. Towards the planning and execution of an "absolute" asymmetric synthesis of chiral dimers and polymers with quantitative enantiomeric yield. Pure Appl. Chem. 51:1269-1284, 1979.
- Wallach, O. Liebigs Ann. Chem. 286:90-143, 1885.
- Brock, C.P., Schweizer, W.B., Dunitz, J.D. On the validity of Wallach's rule: On the density and stability of racemic crystals compared with their chiral counterparts. J. Am. Chem. Soc. 113:9811-9820, 1991.
- Brock, C.P., Dunitz, J.D. Towards a grammar of crystal packing. Chem. Mater. 6:1118-1127, 1994.
- Belsky, V.K., Zorkaya, O.N., Zorky, P.M. Structural classes and space groups of organic homomolecular crystals: New statistical data. Acta Crystallogr. A51:473-481, 1995.
- Hagler, A.T., Huler, E., Lifson, S. Energy functions for peptides and proteins. I. Derivation of a consistent force field including the hydrogen bond from amide crystals. J. Am. Chem. Soc. 96:5319-5327, 1974.
- Hirshfeld, F.L. Bonded-atom fragments for describing molecular charge densities. Theor. Chim. Acta 44:129, 1977.
- Berkovitch-Yellin, Z., Leiserowitz, L. Atom-atom potential analysis of the packing characteristics of carboxylic acids. A study based on experimental electron density distributions. J. Am. Chem. Soc. 104:4052-4064, 1982.
- Weissbuch, I., Kuzmenko, I., Vaida, M., Zait, S., Leiserowitz, L., Lahav, M. Twinned crystals of enantiomorphous morphology of racemic alanine induced by optically resolved α -amino acids: a stereochemical probe for the early stages of crystal nucleation. Chem. Mater. 6:1258-1268, 1994.
- Weissbuch, I., Addadi, L., Berkovitch-Yellin, Z., Gati, E., Weinstein, S., Lahav, M., Leiserowitz, L. Centrosymmetric crystals for the direct assignment of the absolute configuration of chiral molecules. Application to the α -amino acids by their effect on glycine crystals. J. Am. Chem. Soc. 105:6615-6621, 1983.
- Weissbuch, I., Addadi, L., Berkovitch-Yellin, Z., Gati, E., Lahav, M., Leiserowitz, L. Spontaneous generation and amplification of optical activity in α -amino acids by enantioselective occlusion into centrosymmetric crystals of glycine. Nature 310:161, 1984.
- Vaida, M., Shimon, L.J.W., van Mil, J., Ernst-Cabrera, K., Addadi, L., Leiserowitz, L., Lahav, M. Absolute asymmetric photochemistry using centrosymmetric crystals. The host/guest system (E)-Cinnamamide/(E)-Cinnamic acid. J. Am. Chem. Soc. 111:1029-1034, 1985.
- Vaida, M., Shimon, L.J.W., Weissinger-Lewin, Y., Frolow, F., Lahav, M., Leiserowitz, L., McMullan, R. The structure and symmetry of crystalline solid solutions: A general revision. Science 241:1475-1479, 1988.
- Schmidt, G.M.J. Topochemistry. Part III. The crystal chemistry of some *trans*-cinnamic acids. J. Chem. Soc. 2014-2020, 1964.
- Andelman, D., de Gennes, P.G. Chiral discrimination in a Langmuir monolayer. C.R. Acad. Sci. 307:233, 1988.
- Andelman, D., Orland, H. Chiral discrimination in solutions and in Langmuir monolayers. J. Am. Chem. Soc. 115:12322-12329, 1993.

33. Lundquist, M. Molecular arrangement in condensed monolayer phases. *Prog. Chem. Fats Other Lipids* 16:101–124, 1978.
34. Stewart, M.V., Arnett, E.M. Chiral monolayers at the air-water interface. In: *Topics in Stereochemistry*, Vol. 13. New York: John Wiley & Sons Inc., 1982:195–262.
35. Nassoy, P., Goldmann, M., Bouloffa, O., Rondelez, F. Spontaneous chiral segregation in bidimensional films. *Phys. Rev. Lett.* 75:457–460, 1995.
36. Eckhardt, C.J., Peachey, N.M., Swanson, D.R., Takacs, J.M., Khan, M.A., Gong, X., Kim, J.H., Wang, J., Uphaus, R.A. Separation of chiral phases in monolayer crystals of racemic amphiphiles. *Nature* 362:614–616, 1993.
37. Stevens, F., Dyer, D.J., Walba, D.M. Direct observation of enantiomorphous monolayer crystals from enantiomers by scanning-tunneling microscopy. *Angew. Chem. Int. Ed. Engl.* 35:900–901, 1996.
38. Mohwald, H., Dietrich, A., Bohm, C., Brezesinski, G., Thoma, M. Domain formation in monolayers. *Mol. Membr. Biol.* 12:29–38, 1995.
39. Vollhardt, D. Morphology and phase-behavior of monolayers. *Adv. Colloid Interface Sci.* 64:143–171, 1996.
40. Rietz, R., Brezesinski, G., Mohwald, H. Separation of enantiomers in a monolayer of racemic 3-hexadecyl-oxy-propane-1,2-diol. *Ber. Bunsen Ges. Phys. Chem.* 97:1394–1399, 1993.
41. Selinger, J.V., Selinger, R.L.B. Theory of chiral defects in Langmuir monolayers. *Phys. Rev. E* 51:R860–R863, 1995.
42. Weissbuch, I., Berfeld, M., Bouwman, W., Kjaer, K., Als-Nielsen, J., Lahav, M., Leiserowitz, L. Separation of enantiomers and racemate formation in two-dimensional crystals at the water-surface from racemic α -amino acid amphiphiles: Design and structure. *J. Am. Chem. Soc.* 119:933–942, 1997.
43. Landau, E.M., Levanon, M., Leiserowitz, L., Lahav, M., Sagiv, J. Transfer of structural information from Langmuir monolayers to three-dimensional growing crystals. *Nature* 318:353–356, 1985.
44. Berfeld, M., Weissbuch, I., Leiserowitz, L., Lahav, M. Work in progress.
45. Diego, H.L. Thesis, Department of Chemistry, H.C. Ørsted Institute, University of Copenhagen, 1995.
46. Briano, M.C., Leclercq, M., Jacques, J. Mandelate de Phényl-1 Ethylamine. *Acta Crystallogr.* B35:2751, 1979.
47. Larsen, S., Diego, H.L. A study of two polymorphic modifications of (S)-1-phenylethylammonium (S)-mandelate and the structural features of diastereomeric mandelate salts. *Acta Crystallogr.* B49:303, 1993.
48. Kuzmenko, I., Lahav, M., Leiserowitz, L., Kjaer, K., Als-Nielsen, J. Chiral separation of diastereomeric monolayers at the air/water interface. *HASYLAB Annu. Rep.* 1996.
49. Fuhrhop, J.H., Helfrich, W. Fluid and solid fibers made of lipid molecular bilayers. *Chem. Rev.* 93:1565–1582, 1993.
50. Nakashima, N., Asukuma, S., Kim, J.M., Kunitake, T. Helical superstructures are formed from chiral ammonium bilayers. *Chem. Lett.* 1709–1712, 1984.
51. Yanagawa, H., Ogawa, Y., Furuta, H., Tsuno, K. Spontaneous formation of superhelical strands. *J. Am. Chem. Soc.* 111:4567–4570, 1989.
52. Lehn, J.-M. *Supramolecular Chemistry. Concepts and Perspectives*. Weinheim: VCH, 1995.
53. Gulik-Krzywicki, T., Fouquey, C., Lehn, J.-M. Electron-microscopic study of supramolecular liquid-crystalline polymers formed by molecular-recognition-directed self-assembly from complementary chiral components. *Proc. Natl. Acad. Sci. U.S.A.* 90:163–167, 1993.

2.4 Detection of chiral disorder in Langmuir monolayers undergoing spontaneous chiral segregation

Ivan Kuzmenko,* Kristian Kjaer[§], Jens Als-Nielsen,[#] Meir Lahav* and Leslie Leiserowitz*

*Department of Materials and Interfaces, the Weizmann Institute of Science, Rehovot 76100, Israel

[§]Department of Solid State Physics, Risø National Laboratory, DK-4000 Roskilde, Denmark

[#]Jens Als-Nielsen, Niels Bohr Institute, H.C. Ørsted Laboratory, Copenhagen, Denmark

Detection of Chiral Disorder in Langmuir Monolayers Undergoing Spontaneous Chiral Segregation

Ivan Kuzmenko,^{*†} Kristian Kjaer,[‡] Jens Als-Nielsen,[§] Meir Lahav,[†] and Leslie Leiserowitz^{*†}

Contribution from the Department of Materials and Interfaces, The Weizmann Institute of Science, 76100 Rehovot, Israel, Department of Solid State Physics, Risø National Laboratory DK-4000, Roskilde, Denmark, and H. C. Ørsted Laboratory, Niels Bohr Institute, DK-2100 Copenhagen, Denmark

Received June 18, 1998. Revised Manuscript Received December 18, 1998

Abstract: Acid–base interactions between two different chiral amphiphilic molecules (*p*-pentadecylmandelic acid and *p*-tetradecylphenylethylamine) are used in order to achieve spontaneous chiral segregation from a racemic mixture at the air–water interface, as shown by grazing incidence X-ray diffraction. The extent of possible chiral disorder for both acid and base components is examined. We show that an oblique lattice symmetry is insufficient to guarantee spontaneous segregation of chiral molecules in two-dimensional crystals because of possible chiral disorder.

Introduction

Spontaneous separation of chiral molecules from a racemic mixture into two-dimensional crystals of opposite handedness echoes Pasteur's famous experiment with sodium ammonium tartrate tetrahydrate crystals performed 150 years ago.¹ Definitive evidence on spontaneous separation in bulk crystals can be easily obtained by common experimental tools such as optical rotation measurements, chromatography on chiral columns, phase diagrams, or X-ray structure analysis. Determination of chiral separation in monolayer films is far less straightforward.² Early surface pressure–molecular area (π – A) isotherm measurements provided indirect evidence for spontaneous resolution of some racemates in two dimensions.^{3–5} Much more direct observation of spontaneous separation of enantiomers became possible only with the advent of modern techniques such as grazing incidence X-ray diffraction (GIXD) and atomic force (AFM), scanning tunneling (STM), Brewster angle (BAM), and epifluorescence microscopies. The latter two methods are optical and provide information on the shape of monolayer domains at least a few micrometers in size. Observations of asymmetric shapes of the polycrystalline monolayer domains in racemic mixtures were ascribed to the separation into crystalline clusters of opposite handedness.⁶ A comparative GIXD and epifluorescence microscopy study of racemic diol monolayers on water showed, however, that such a correlation does not necessarily hold.⁷

In this work, we have made use of known acid–base interactions involving two different chiral molecules to induce

chiral separation in two dimensions. Moreover, the use of this acid–base binary system has allowed us to probe the extent of possible chiral disorder.

Experimental Section

General Procedures. ¹H NMR spectra were recorded on a Bruker spectrometer (270 MHz) in CDCl₃ using OTS as internal standard. Multiplicities in ¹H NMR are reported as broad (br), singlet (s), doublet (d), triplet (t), double doublet (dd), quartet (q), double quartet (dq), and multiplet (m). Thin-layer chromatography (TLC) was performed on Merck silica gel plates. Column chromatography was performed on silica gel columns.

***p*-Tetradecylacetophenone (1).** A chloroform solution containing tetradecylbenzene (15.4 g, 56.2 mmol) and acetyl chloride (11.7 g, 0.169 M) was slowly dripped into a chloroform solution of AlCl₃. The mixture was stirred for 1 h while the temperature was kept below 10 °C and then stirred for another hour at 25 °C. The solution was poured into ice. The chloroform layer was separated from the aqueous solution and the latter washed several times with ether. The ether extracts were collected and combined with the chloroform fraction, treated with sodium bicarbonate, and dried with MgSO₄. The organic solvent was evaporated and the solid residue was recrystallized from ethyl acetate/hexane/methanol to yield white solid 1 (13.8 g, 80% yield), mp 54–55 °C. ¹H NMR (CDCl₃) δ 7.88 and 7.23 (dd, 4H, aromatic A₂B₂ system), 2.66 (t, 2H, PhCH₂), 1.60 (s, 3H, COCH₃), 1.28 (m, 24H, aliphatic CH₂), 0.90 (t, 3H, CH₂CH₃).

(R,S)-*p*-Tetradecylphenylethylamine (2). Compound 1 (12.5 g, 41.4 mmol), ammonium acetate (31 g, 378 mmol), and NaBH₄CN (1.76 g, 0.279 M) were dissolved in absolute methanol (20 mL) in an inert N₂ atmosphere. The solution was stirred for 3 days at 60 °C until the reaction was complete. The mixture was acidified with concentrated HCl to pH 2.1. Methanol was evaporated, and the remaining aqueous solution was washed with CH₂Cl₂. The hydrochloride salt of 2 was reacted in water with KOH to release the free amine that was extracted with CH₂Cl₂ and dried to yield 2 (8.0 g, 60% yield), mp 68–69 °C. ¹H NMR (CDCl₃) δ 7.24 (dd, 4H, aromatic A₂B₂ system), 4.08 (q, 1H, NCH), 2.58 (q, 2H, PhCH₂), 1.37 (d, 3H, NCCH₃), 1.25 (m, 24H, aliphatic H), 0.88 (t, 3H, CH₂CH₃).

(R)-(or S)-*p*-Tetradecylphenylethamine (3). Racemic 2 was optically resolved via cocrystallization with optically pure (R)- or (S)-mandelic acid. Racemic 2 (23.5 g, 11 mmol) and R(–)-mandelic acid (1.5 g, 10 mmol) were dissolved in ethyl acetate (250 mL) at 60 °C.

^{*} The Weizmann Institute of Science.

[†] Risø National Laboratory.

[‡] Niels Bohr Institute.

(1) Pasteur, L. *Ann. Phys.* 1848, 24, 442.

(2) Kuzmenko, I.; Weissbuch, I.; Gurovich, E.; Leiserowitz, L.; Lahav, M. *Chirality* 1998, 10, 415.

(3) Lundquist, M. *Prog. Chem. Fats Other Lipids* 1978, 16, 101.

(4) Arnett, E.; Thompson, O. *J. Am. Chem. Soc.* 1981, 103, 968.

(5) Stewart, M.; Arnett, E. *Top. Stereochem.* 1982, 13, 489.

(6) Brezesinski, G.; Rietz, R.; Kjaer, K.; Bouwman, W.; Möhwald, H. *Nuovo Cimento* 1994, 16D, 1487.

(7) Möhwald, H.; Dietrich, A.; Böhm, C.; Brezesinski, G.; Thoma, M. *Mol. Membr. Biol.* 1995, 12, 29.

Thin crystalline plates precipitated upon cooling. The salt was recrystallized several times. The free amine was released in 10% aqueous solution of KOH, extracted with pure CH_2Cl_2 , and washed repeatedly with water, until all the mandelic acid was removed as indicated by TLC (CH_2Cl_2 /ethanol 2:1 solution on silica plates). The solution was dried with MgSO_4 to yield (R)-3 with an optical rotation of $[\alpha]_{D}^{25} = +12.95^\circ$ ($c = 2, \text{CH}_2\text{Cl}_2$). The ^1H NMR spectrum is identical to that of racemic 2. The S-enantiomer of 2 was obtained analogously using (S)-(+)mandelic acid, $[\alpha]_{D}^{25} = -12.77^\circ$ ($c = 2, \text{CH}_2\text{Cl}_2$).

α -Keto- β -(*p*-pentadecylphenyl)ethyl Propionate (4). AlCl_3 (6.86 g, 51.5 mmol) dissolved in chloroform (14 mL) was placed in a three-neck flask in an inert dry N_2 atmosphere. A solution of pentadecylbenzene (10 g, 34.2 mmol) and ethyl oxalyl chloride (7.03 g, 51.5 mmol) in chloroform (7 mL) was slowly added from a dropping funnel at 0–5 °C. During the exothermic reaction, the yellow reaction mixture turned dark brown. The reaction was then stirred in the ice bath for 1 h and then for 3 h at ambient temperature. The reaction mixture was poured into ice, and organic components were extracted three times with ether. The organic fractions were combined and washed with an aqueous solution of sodium bicarbonate and dried with MgSO_4 , and the solvent was evaporated. The yellow oil was chromatographed on a silica column with CH_2Cl_2 /hexane (1:1) to yield 4 (12 g, 91%), mp 129–131 °C. ^1H NMR (CDCl_3) δ 7.16 and 7.30 (dd, 4H aromatic A_2B_2 system), 5.12 (s, 1H, CH), 4.20 (dq, 2H, COOCH_2), 2.59 (t, 2H, ArCH_2), 1.73 (b, 1H, OH), 1.59 (t, 3H, OCH_2CH_3), 1.25 (m, 26H, aliphatic CH_2), 0.87 (t, 3H, CH_2CH_3).

(R)-*p*-Pentadecylmandelic Acid (5). An asymmetric reduction of 4 was performed in the following steps. NaBH_4 (1.47 g, 38.7 mmol) and (R,R)-tartaric acid (5.55 g, 38.0 mmol) were dissolved in THF (130 mL) in a three-necked flask and heated in an inert dry N_2 atmosphere at 70 °C for 3 h. The resulting white suspension was cooled to –20 °C. Compound 4 (9 g, 0.023 M) in THF (10 mL) was added dropwise (exothermic reaction) and the reaction mixture was stirred for 15 h at ~20 °C. Ethyl acetate (60 mL) and 1 M HCl (30 mL) were slowly added to the mixture at 0 °C. After adding water (50 mL), the organic layer was separated, washed several times with an aqueous solution of sodium bicarbonate, and dried with MgSO_4 . The organic solvent was evaporated to yield an oil that was chromatographed on a silica column with ethyl acetate/hexane mixture (1:6). The solvent was evaporated to yield white crystalline ethyl ester of *p*-pentadecylmandelic acid (7.5 g, 87%).

The ester (6.1 g, 15.3 mmol) was added in 5 M KOH/methanol solution (55 mL) with a few drops of water and stirred for 2.5 h at ambient temperature. White crystals of the salt started precipitating after several minutes. After 2 h, the solution with crystals was acidified with HCl and the white crystalline substance was filtered and washed with water and hexane. The solid was recrystallized from THF to yield 5 (3.0 g, 56%), $[\alpha]_{D}^{25} = -63.21$ ($c = 1.01, \text{THF}$). The acid was further optically purified via crystallization with (R)-(+)phenylethylamine for several times until reaching the constant rotation value of $[\alpha]_{D}^{25} = -83.11$ ($c = 0.965, \text{THF}$), mp 119–121 °C. ^1H NMR (CDCl_3) δ 7.08 and 7.27 (dd, 4H, aromatic A_2B_2 system), 5.06 (s, 1H, CH), 2.49 (t, 2H, ArCH_2), 1.16 (m, 26H, aliphatic CH_2), 0.78 (t, 3H, CH_2CH_3).

(R,S)-*p*-Pentadecylmandelic Acid (6). NaBH_4 (0.44 g, 11.61 mmol) was suspended with THF (40 mL) in a three-neck flask in an inert N_2 atmosphere. The mixture was cooled to 0 °C, and 4 (2.84 g, 7.73 mmol) was added in THF (5 mL) dropwise. The reaction mixture was left to stir in the bath for 1 h at 0 °C and overnight at ambient temperature. Ethyl acetate (20 mL) and 1 M HCl (10 mL) were slowly added to the mixture at 0 °C. Water was added and the organic layer separated, washed with sodium bicarbonate, dried with MgSO_4 , and recrystallized in THF to yield the racemic ethyl ester of *p*-pentadecylmandelic acid (1.06 g, 90%). Hydrolysis of the ester was done in the same way as for (R)-5. ^1H NMR of the final product demonstrated the same spectrum as for 5 and zero optical rotation.

X-ray Crystal Structure Determination. A platelike needle of $\{(xR, (1-x)S)\text{-C}_{15}\text{-MA.S-PEA}\}$ (x was found in the refinement) of dimensions $0.2 \times 0.4 \times 0.8 \text{ mm}^3$ was grown by slow cooling of equimolar mixture of (R)-*p*-pentadecylmandelic acid (95% ee) and commercial (S)-PEA from Aldrich (99% ee) dissolved in tetrahydrofuran. Crystallographic measurements were performed at ambient

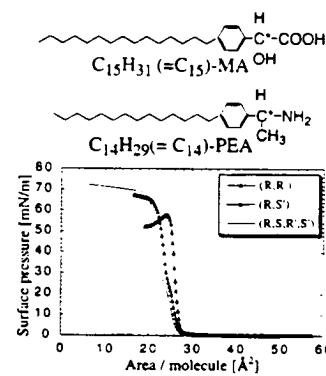


Figure 1. (Top) Structural formulas of the $\text{C}_{15}\text{-MA}$ and $\text{C}_{14}\text{-PEA}$ molecules. The asterisk marks the chiral carbon center. (Bottom) Surface pressure–molecular area (π – A) isotherms at 5 °C for $R\text{.}R'$, $R\text{.}S'$, and $R\text{.}S\text{.}R'\text{.}S'$ diastereomeric films formed by $\text{C}_{15}\text{-MA}$ and $\text{C}_{14}\text{-PEA}$ molecules in a 1:1 molar ratio. The molecular area A was calculated per one amphiphilic molecule, disregarding the difference between MA and PEA.

temperature (17 °C) on a four-circle Rigaku single-crystal diffractometer with a 18-kW rotating anode generator. The intensity data of 4015 reflections ($0 \leq h \leq 67, -10 \leq k \leq 0, 0 \leq l \leq 8$) were measured. After merging equivalent reflections, 1066 observed reflections remained with $I \geq 2\sigma(I)$. The structure was solved with SHELXS97⁸ and refined isotropically with use of SHELXTL97 programs.⁹ Hydrogen atoms at C and N atoms were positioned in calculated positions and refined as riding on the corresponding nonhydrogen atoms with fixed $U = 0.08$. The α -hydroxy oxygen atom was found to be disordered over two sites (xR and yS in the above formula) was close to 1 and constrained in the further refinement ($y = (1 - x)$) while the U factor variable was common for both the oxygen sites. The final refinement resulted in $= 0.45$: empirical formula $\text{C}_{31}\text{H}_{44}\text{O}_3\text{N}$, $M_r = 481.70$ g, orthorhombic, $P2_12_12_1$, $a = 52.140(10)$ Å, $b = 8.450(2)$ Å, $c = 6.8040(10)$ Å, $V = 2997.7(10)$ Å 3 , $Z = 4$, $D_c = 1.067 \text{ g/cm}^3$, Mo $\text{K}\alpha$ (0.710 – 73 Å), $2\theta_{\max} = 55^\circ$, $F(000) = 1056$, $R = 0.139$, and $S = 0.884$.

Grazing Incidence X-ray Diffraction. The GIXD measurements were conducted on the liquid surface diffractometer at the undulator beam line BW1 in HASYLAB at Deutsches Elektronen-Synchrotron (DESY). The synchrotron radiation beam monochromated to wavelengths of 1.336 and 1.452 Å that were used in two synchrotron sessions. The incident angle was adjusted to $\alpha_i = 0.85\alpha_c$, where $\alpha_c \approx 0.14^\circ$. A detailed explanation of the method and experimental setup is given elsewhere.^{10,11} The diastereomeric mixtures were prepared by dropwise spreading of chloroform solutions at ambient temperature in a Langmuir trough and then cooled to 5 °C.

Results and Discussion

Mandelic acid (MA) and phenylethylamine (PEA), each with one chiral center (Figure 1, top), can be used for mutual chiral resolution of their racemic *R,S* mixtures. All the reported (MA, PEA) three-dimensional crystal structures with various chiral composition have a bilayer arrangement with one crystallographically independent (MA,PEA) unit in each layer.^{12–15} The

(8) Sheldrick, G. M. *Acta Crystallogr.* 1990, **A46**, 467.

(9) Sheldrick, G. M. *SHELXL97 Program for the Refinement of Crystal Structures*; University of Göttingen, Germany, 1997.

(10) Als-Nielsen, J.; Jacquemain, D.; Kjaer, K.; Leveiller, F.; Lahav, M.; Leiserowitz, L. *Phys. Rep.* 1994, **246**, 251.

(11) Majewski, J.; Popovitz-Biro, R.; Bouwman, W.; Kjaer, K.; Als-Nielsen, J.; Lahav, M.; Leiserowitz, L. *Chem. Eur. J.* 1995, **1**, 304.

(12) Briango, M.; Leclercq, M.; Jacques, J. *Acta Crystallogr.* 1979, **B35**, 2751.

(13) Larsen, S.; Diego, H. *Acta Crystallogr.* 1993, **B49**, 303.

(14) Diego, H. *Acta Chem. Scand.* 1994, **48**, 306.

(15) Diego, H. I-Phenylethylammonium, mandelates, a structural and physico-chemical investigation of a complicated system of diastereomers. Department of Chemistry, H. C. Ørsted Institute, University of Copenhagen, 1995.

molecules are interconnected by multiple hydrogen bonds within a two-dimensional network. It is important to note that, in all these crystal structures, the MA (or PEA) molecules within a layer have the same absolute configuration. The same structural feature is also preserved in the 3D structures of the MA salts with substituted PEA all assuming very similar packing arrangements.¹⁶ Thermodynamic properties and crystal structures of various PEA-MA compositions demonstrated a higher stability of diastereomeric crystals, in which MA and PEA are of the same absolute configuration. This structural feature should, in principle, be preserved in analogous long-chain compounds which can be used for monolayer studies. Thus, for 1:1 mixtures of racemic long-chain amphiphiles bearing mandelic acid and phenylethylamine head groups, we may expect the monolayer to be separated into crystalline islands composed of (MA,PEA) units of the same absolute configuration, i.e., *R,R'* or *S,S'* rather than their diastereomeric¹⁷ pairs *R,S'* or *S,R'*, where *R* and *S* denote the absolute chiral configuration of MA and *R'* and *S'* that of PEA.

Para-substituted analogues of PEA and MA bearing long hydrocarbon chains C_nH_{2n+1} (labeled C_n) were synthesized to form racemic and chiral resolved amphiphilic compounds $C_{14}\text{-PEA}$ and $C_{15}\text{-MA}$ (Figure 1, top). Surface pressure-molecular area ($\pi-A$) isotherms of three different mixtures ((*R*)- $C_{15}\text{-MA}$, (*R*)- $C_{14}\text{-PEA}$, ((*R*)- $C_{15}\text{-MA}$, (*S*)- $C_{14}\text{-PEA}$), and ((*R,S*)- $C_{15}\text{-MA}$, (*R,S*)- $C_{14}\text{-PEA}$) on Millipore water indicate formation of stable monolayers with a limiting area per molecule of $25-28 \text{ \AA}^2$ (Figure 1). All three isotherms have similar shapes. The GIXD spectra for the three compositions were measured at a surface pressure $\pi = 1 \text{ mN/m}$. All the three measured GIXD patterns display seven narrow Bragg peaks (Figure 2a-c, left) as is evident from their full width at half-maximums (average fwhm in Table 1). These diffraction patterns were fully indexed yielding cell dimensions (Table 1). Each unit cell of area $\sim 51 \text{ \AA}^2$ contains two symmetry-independent long-chain molecular units corresponding to one acid and one amine molecule. The GIXD patterns for the *R,R'* and *R,S'* mixtures are clearly different both in terms of positions of the Bragg peaks, their integrated intensities (Figure 2a,c, left) and, in particular, the shapes of the corresponding Bragg rods (Figure 2d), whereas the mixture *R,S,R',S'* (Figure 2b, left) displays a diffraction pattern almost identical to that of the *R,R'* monolayer. Since the oblique unit cell for *R,S,R',S'* contains only two independent molecules and the monolayer is highly crystalline in view of the narrow Bragg peaks, it is highly plausible that the *R,S,R',S'* mixture segregates into *R,R'* and *S,S'* crystalline islands of opposite handedness. The crystallization process for the three systems is schematically shown in Figure 2a-c (right).

Racemic mixtures of amphiphilic molecules bearing a long hydrocarbon chain and a chiral hydrophilic head group would seem, when compared with their water-soluble analogues in the bulk, to have a lower tendency to separate in two dimensions since hydrocarbon chains readily pack in a herringbone motif in which *R* (right-hand) and *S* (left-hand) molecules are related by glide symmetry. Most of the examples of chiral separation in two dimensions, based on GIXD^{18,19} and in other reports by AFM²⁰ and STM,²¹ have rested primarily upon the finding of an oblique lattice with one amphiphilic molecule per unit cell

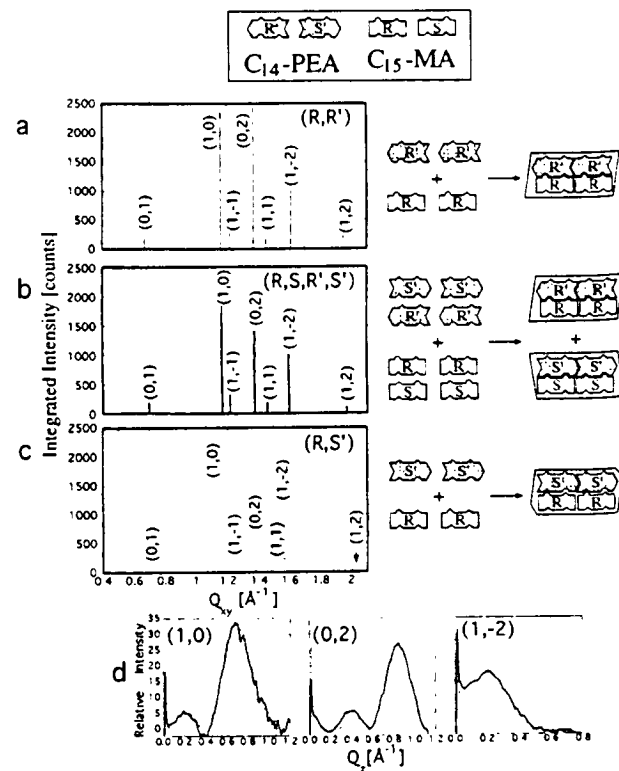


Figure 2. GIXD patterns for the three diastereomeric films *R,R'* (thin line), *R,S'* (dotted line), and *R,S,R',S'* (thick line) measured at 5°C and surface pressure $\pi = 1 \text{ mN/m}$. (a-c, left) The observed Bragg peaks represented by lines of corresponding integrated intensities with assigned (*h,k*) indices. (d) Comparison of Bragg rods of the three diastereomeric systems corresponding to the most intense (1, 0), (0, 2), and (1, -2) reflections, where the type of line corresponds to that as in (a-c, left). (a-c, right) Schematic views of the molecular assembly into crystals corresponding to the three diffraction patterns.

Table 1. Crystallographic Data for the Monolayers

parameters	<i>R,R'</i>	<i>R,S'</i>	$0.5(R,S)-R'$	<i>R,S,R',S'</i>
lattice spacings (\AA)				
d_{01}	9.26	9.25	9.25	9.28
d_{10}	5.48	5.38	5.46	5.47
d_{11}	5.19	5.28	5.25	5.24
d_{02}	4.61	4.62	4.62	4.63
d_{11}	4.37	4.20	4.31	4.35
d_{12}	3.94	4.05	3.99	3.98
d_{12}	3.25	3.13	3.22	3.22
av fwhm ^a (\AA^{-1})	0.0124	0.0197	0.0142	0.0143
av coherence length ^b (\AA)	560	320	480	470
unit cell dimens				
a (\AA)	5.59	5.56	5.60	5.60
b (\AA)	9.40	9.55	9.47	9.48
γ (deg)	101.5	104.8	102.8	102.4
tilt angle (deg)	40	39	41	40
tilt azimuth ^c (deg)	42	49	43	42
unit cell area, A_{v} (\AA^2)	51.5	51.3	51.7	51.8
chain cross-section area	19.7	20.0	19.5	19.9
A_{\perp} (\AA^2)				

^a fwhm, full width at half-maximum of the Bragg peak in Q_{α} units.

^b The coherence length L has been calculated using the standard Scherrer equation:²² $L = (0.9 \times 2\pi)/(fwhm^2 - \Delta^2)^{1/2}$, where the resolution of the Soller colimator, $\Delta = 0.0081 \text{ \AA}^{-1}$ (in Q_{α} units). ^c The angle between the projection of the hydrocarbon chain vector onto the xy plane and the reciprocal vector a^* as determined from the positions of the maximums q_z of the three Bragg rods corresponding to (1, 0), (0, 2), and (1, -2) reflections.¹⁰

leading to an assumption that all molecules are related by translation symmetry and, therefore, of the same handedness.

(16) Kinbara, K.; Sakai, K.; Hashimoto, Y.; Nohiro, H.; Saigo, K. *J. Chem. Soc., Perkin Trans. 2* 1996, 12, 2615.

(17) The term "diastereomeric" refers to optical isomers that are not mirror images of each other.

(18) Nassoy, P.; Goldmann, M.; Bouloussa, O.; Rondelez, F. *Phys. Rev. Lett.* 1995, 75, 457.

(19) Weissbuch, I.; Berfeld, M.; Bouwman, W.; Kjaer, K.; Als-Nielsen, J.; Lahav, M.; Leiserowitz, L. *J. Am. Chem. Soc.* 1997, 119, 933-942.

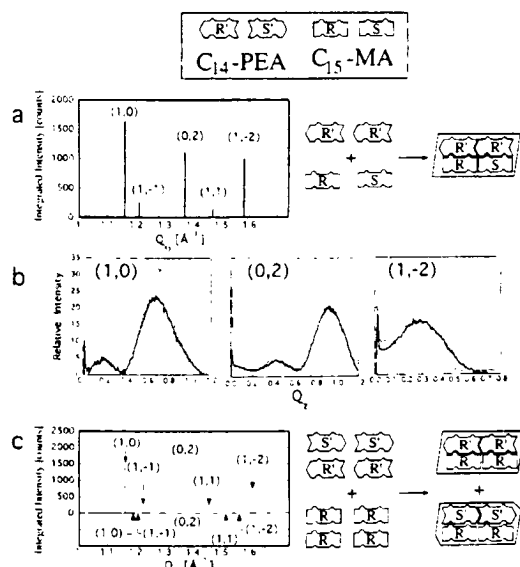


Figure 3. GIXD Bragg peaks (lines) for the two diastereomeric mixtures: (a, left) 0.5(*R,S*)-*R'* and (c, left) *R*-0.5(*R',S'*). where the diffraction pattern for *R*-0.5(*R',S'*) is a combination of the *R,R'* and *R,S'* phases with the *h,k* indices denoted above for *R,R'* and below for *R,S'*. (b) Bragg rod profiles of the 0.5(*R,S*)-*R'* mixture (solid bold line) vs the corresponding Bragg rods of the *R,R'* composition (thin solid line), originally shown in Figure 2d. (a,c, right) Schematic views of the molecular assembly into crystals corresponding to the two diffraction patterns.

Such an assumption neglects potentially high molecular disorder in monolayer films that are often mesophases rather than crystalline aggregates. Thus we may envisage, in the ultimate, a racemic 2D crystal (*R:S* = 1:1) with the *R* and *S* chiral head groups randomly distributed, although the long hydrocarbon tails pack in an oblique unit cell by translation symmetry only.

In order to help evaluate the extent of chiral molecular disorder for both the acid and amine moieties, two chiral compositions *R*-0.5(*R',S'*) and 0.5(*R,S*)-*R'* with a 1:1 acid to amine molar ratio were inspected. Both mixtures display π - A isotherms similar to those previously described. The GIXD measurements gave two qualitatively different results. The mixture 0.5(*R,S*)-*R'* composed of the acid molecules of both handedness and the amine molecules of single handedness gave rise to a diffraction pattern (Table 1 and Figure 3a, left, and b) very similar to that of the *R,R'* system. Since there is only one crystalline phase and the corresponding diffraction pattern has approximately the same intensity distribution as for *R,R'*, we deduce that the 0.5(*R,S*)-*R'* phase is isomorphous with *R,R'*, but where half the *R* sites are randomly occupied by *S* molecules, as schematically shown in Figure 3a (right).

The diffraction spectrum for the *R*-0.5(*R',S'*) mixture, composed of an acid of single chirality and amine molecules of both handedness, combines two overlapping GIXD patterns, characteristic of the *R,R'* and *R,S'* crystalline phases (Figure 3c, left). The relative amount of crystalline material of these two phases is approximately 1.5:1 according to the intensity ratio of the corresponding diffraction patterns.

The diffraction results for the 1:1 mixtures *R*-0.5(*R',S'*) and 0.5(*R,S*)-*R'* suggest that *R,S,R',S'* separates into enantiomor-

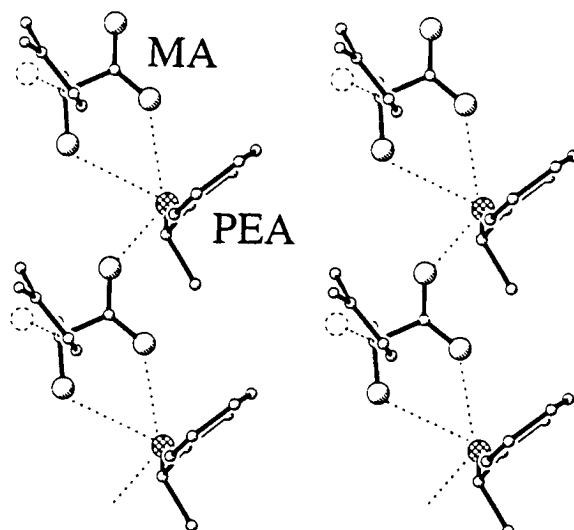


Figure 4. Layer packing of MA and PEA moieties in the observed 3D crystal structure of ((0.5*R*,0.5*S*)-C₁₅-MA,(*R*)-PEA) with the observed chiral disorder of the OH group. All hydrogen atoms and hydrocarbon chains are omitted.

phous domains of composition $((1-x)R, xS)$, R' and $((1-x)S, xR)$, S' , where x is a fraction of "foreign" C₁₅-MA molecules within the *R,R'* and *S,S'* domains. For the three compositions *R,R'*, *R,S,R',S'*, and 0.5(*R,S*)-*R'* there is no significant difference in the Q_{xy} positions of the corresponding Bragg peaks. Nonetheless, comparison of the sensitive (1,-2) Bragg rod of these three mixtures suggests that the *R,S,R',S'* is much closer to *R,R'* than to 0.5(*R,S*)-*R'* (cf. Figure 2d and Figure 3b).

Strong support for the possibility of chiral disorder for the MA moiety may be drawn from the reported 3D structure of ((*R*)-MA,(*S*)-C₁-PEA) with intralayer cell dimensions of $a = 6.0 \text{ \AA}$, $b = 9.1 \text{ \AA}$, and $\gamma = 90^\circ$,¹⁶ which compares with those of the diastereomeric monolayers (Table 1). The interchange of the OH group and the hydrogen atom at the chiral carbon center with the concomitant switch in chirality leads to formation of an extra hydrogen bond and does not impair van der Waals contacts. Experimental proof for such a type of chiral disorder is provided by observed chiral disorder in the 3D crystal structure ((0.45*R*,0.55*S*)-C₁₅-MA,(*R*)-PEA), grown from tetrahydrofuran solution with a large excess of (*S*)-C₁₅-MA molecules (*R:S* = 5:95) and enantiomerically pure (*R*)-PEA. The structure refinement revealed ~50% chiral disorder for the OH group (Figure 4). This structure is therefore a 3D analogue of the Langmuir phase with the 0.5(*R,S*)-*R'* chiral composition.

Conclusions

Diastereomeric interactions between two different chiral molecules were used for the first time to achieve two-dimensional spontaneous chiral separation into crystalline islands of opposite handedness at the air–water interface. The extent of chiral disorder, as assessed from the GIXD pattern analysis, was shown to be always low for the amine component and in some cases high (up to 50%) for the acid component. The results show that an oblique lattice symmetry, even for highly crystalline monolayers, is insufficient proof for spontaneous separation of chiral molecules in two dimensions. One way to ascertain whether such a separation occurred would require a determination of the monolayer crystal structure making use of the Bragg rod diffraction data, complemented by lattice energy calculations.

(20) Eckhardt, C.; Peachey, N.; Swanson, D.; Takacs, J.; Khan, M.; Gong, X.; Kim, J.; Wang, J.; Uphaus, R. *Nature* 1993, 362, 614.

(21) Stevens, F.; Dyer, D.; Walba, D. *Angew. Chem. Int. Ed. Engl.* 1996, 35, 900.

(22) Guinier, A. *X-ray Diffraction*; Freeman: San Francisco, 1968.

Acknowledgment. We thank Ronith Buller and Edna Shavit for synthesis of the chiral amphiphilic molecules, Paul B. Howes for assistance in GIXD measurements, and HASYLAB, DESY, Hamburg, Germany, for synchrotron beamtime. This research was supported by the Israel Science Foundation (ISF) and G. M. J. Schmidt Minerva Center for Supramolecular Architectures and the Danish Foundation for Natural Sciences.

Supporting Information Available: Tables of crystal data, atomic coordinates, bond lengths and angles, isotropic displacement parameters for $((xR,(1-x)S)-C_{15}-MA,(S)-PEA)$ ($x = 0.45$) (PDF). This material is available free of charge via the Internet at <http://pubs.acs.org>.

JA982123D

2.5 Formation of chiral interdigitated multilayers at the air-liquid interface through acid-base interactions

**Ivan Kuzmenko,* Ronith Buller,* Wim G. Bouwman,§ Kristian Kjær,§
Jens Als-Nielsen,# Meir Lahav,* Leslie Leiserowitz***

*Department of Materials and Interfaces, the Weizmann Institute of Science, Rehovot
76100, Israel

§Department of Solid State Physics, Risø National Laboratory, DK-4000 Roskilde,
Denmark

#Jens Als-Nielsen, Niels Bohr Institute, H.C. Ørsted Laboratory, Copenhagen,
Denmark

Formation of Chiral Interdigitated Multilayers at the Air-Liquid Interface Through Acid-Base Interactions

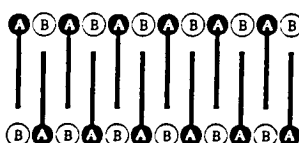
Ivan Kuzmenko, Ronith Buller, Wim G. Bouwman, Kristian Kjær, Jens Als-Nielsen, Meir Lahav, Leslie Leiserowitz*

Thin interdigitated films composed of a long-chain, water-insoluble chiral acid (*p*-pentadecylmandelic acid of absolute configuration *R*) and a water-soluble chiral base (phenylethylamine, *R'*) were constructed at the air-solution interface. The (*R*, *R'*) structure was characterized to near-atomic resolution by grazing-incidence x-ray diffraction (GIXD). The two diastereomeric systems, (*R*, *R'*) and (*R*, *S'*), demonstrate similar surface pressure–molecular area isotherms, but their structures are completely different on the molecular level, as monitored by GIXD. Complementary data on these two architectures were provided by atomic force microscopy.

An important goal of supramolecular chemistry is to find methods to control and stabilize the assembly of molecules into larger structures. One approach is to use the air-solution interface to regulate the assembly process by incorporating strong directional interactions for the generation of ultrathin films. The formation of multilayer films from long-chain molecules with polar head groups by the Langmuir-Blodgett (LB) method is straightforward, but the films must be transferred to a substrate and are not especially stable even after transfer. Such a formation process is governed by relatively weak hydrophobic and hydrophilic interactions.

We have considered the effect of using stronger acid-base interactions to control assembly and have constructed an interdigitated film at the air-solution interface akin to that of a natural membrane (1). We did this by spreading a water-insoluble, long-chain acid on an aqueous solution containing the complementary amine. Compression of the film causes alternating acid-base groups to emerge at either side of the membrane, whereas the central part contains the interdigitated hydrophobic groups of the acid in space-filling contact across a central

plane (Scheme 1). Both the acidic (A) and



Scheme 1.

basic (B) head groups are attached to a chiral carbon center, and the layering and ordering in these films differ greatly between acids and bases of the same handedness (*R*, *R'*) versus opposite handedness (*R*,

S'). The major tool applied for structure elucidation was grazing-incidence x-ray diffraction (GIXD), which allowed us to probe the molecular packing arrangements of the crystalline film to near-atomic resolution.

In a search for an appropriate bimolecular system that satisfied the above criteria, we came across the crystal structures of diastereomeric phenylethylamine mandelates (2, 3). The structure composed of phenylethylamine (PEA) and mandelic acid (MA) molecules of the same handedness, either (*R*, *R'*) or (*S*, *S'*), is characterized by rigid hydrogen-bonded bilayers (Fig. 1A). The phenyl rings within each layer are oriented and positioned in a way that is compatible with the formation of an interdigitated arrangement as in Scheme 1, where only the phenyl ring of the mandelic acid is modified by attaching a long hydrocarbon chain in the para position.

The surface pressure–molecular area (π - A) isotherms of (*R*)-pentadecylmandelic acid [*p*-C₁₅H₃₁-C₆H₄-CH(OH)COOH (C₁₅-MA) (4)] were measured on Millipore-filtered water and on aqueous 0.008 M solutions of (*R*)- and of (*S*)-PEA (C₆H₅-CHCH₃NH₂) (Fig. 2A). The isotherm on water demonstrated regular behavior with an extrapolated A of 24 to 25 Å². The isotherms for the solutions of two PEA enantiomers have peculiar but similar shapes. Both isotherms are expanded and reach a plateau at $A \sim 40$ Å² and $\pi = 42$ to 43

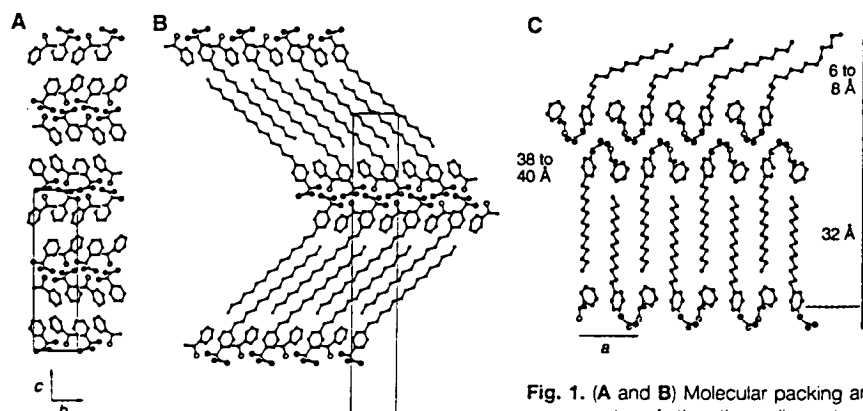


Fig. 1. (A and B) Molecular packing arrangements of the three-dimensional crystals of (*R*-MA, *R*-PEA) (A) and (*R*-C₁₅-MA, *R*-PEA) (B) viewed along the *a* axis. (C) Packing arrangement of the interdigitated (*R*-C₁₅-MA, *R*-PEA) trilayer viewed along the *b* axis. The amorphous and crystalline parts are indicated by the upper and lower arrows at the right; the dashed line represents the air-water interface.

I. Kuzmenko, R. Buller, M. Lahav, L. Leiserowitz, Department of Materials and Interfaces, Weizmann Institute of Science, Rehovot 76100, Israel.
W. G. Bouwman and K. Kjær, Department of Solid State Physics, Risø National Laboratory, DK-4000 Roskilde, Denmark.
J. Als-Nielsen, Niels Bohr Institute, H. C. Ørsted Laboratory, DK-2100 Copenhagen, Denmark.

* To whom correspondence should be addressed.

mN/m (5). The kink preceding the plateau region appears to be sharper for the amphiphile and solute molecules of the same handedness. A pronounced difference exists between the two isotherms in the region of low A . The isotherm for the (R, R') system displays a second rise in the $\pi-A$ curve at $A \approx 13 \text{ \AA}^2$, whereas the plateau for the (R, S') system extends to the end of the isotherm measured.

No GIXD peaks were observed for both diastereomeric systems (6) at two points along their isotherms, $A = 60$ and 50 \AA^2 , corresponding to the expanded region before the plateau. Further compression to $A = 30 \text{ \AA}^2$, corresponding to a point on the plateau, gave rise to a strong diffraction signal only for the (R, R') system (Fig. 2B). Five observed reflections were indexed for a rectangular cell with $a = 8.32 \text{ \AA}$ and $b = 6.82 \text{ \AA}$. From the width of the Bragg rods (7, 8) we estimated the thickness of the crystalline layer to be 32 to 35 \AA (Fig. 2, C to G). The (R, S') system did not diffract at the same point of the isotherm ($A = 30$

\AA^2), nor did it diffract on further compression to a molecular area of $A = 20 \text{ \AA}^2$.

Complementary information on the thickness of the (R, R') and (R, S') films was obtained by atomic force microscopy (AFM) (Fig. 3, A and C, respectively) (9). The films were transferred in a compressed state at $A = 20 \text{ \AA}^2$ onto mica by the LB technique (10). The (R, R') film consisted of patches with two typical heights, $15(2)$ and $38(4) \text{ \AA}$ (numbers in parentheses are standard errors in the last digit). Friction-type measurements had shown that the surfaces at both heights are hydrophobic (they have the same friction coefficient, which is smaller than that of mica) (Fig. 3B) (11). The (R, S') sample consisted of layers with two typical heights, $16(2)$ and $32(4) \text{ \AA}$. According to the friction-type measurements, the surface at $16(2) \text{ \AA}$ appears to be hydrophobic, whereas the surface at $32(4) \text{ \AA}$ demonstrates friction values almost as high as for mica, indicating a hydrophilic character (Fig. 3D).

The GIXD and AFM data suggested the formation of an interdigitated molecular ar-

rangement for the (R, R') film at the air-liquid interface. We thus anticipated a similar motif for the corresponding macroscopic crystal. A single crystal of $(R\text{-C}_{15}\text{-MA}, R\text{-PEA})$, grown from tetrahydrofuran solution, was subjected to an x-ray structure analysis (12). The crystal has orthorhombic symmetry [space group $P2_12_12_1$, $a = 8.347(1) \text{ \AA}$, $b = 6.864(2) \text{ \AA}$, $c = 51.84(1) \text{ \AA}$, Z (number of formula units per cell) = 4] (Fig. 1B). The head groups $[-\text{C}_6\text{H}_4-\text{CH}(\text{OH})\text{COO}^-$ and $\text{C}_6\text{H}_5-\text{CH}(\text{CH}_3)\text{NH}_3^+$] form hydrogen-bonded bilayers, as in the analogous crystalline complex $(R\text{-MA}, R\text{-PEA})$. The packing incompatibility between alternating $\text{C}_{15}\text{-MA}$ and unsubstituted PEA molecular ions within a layer is compensated by interdigitation of the hydrocarbon chains from neighboring bilayers related by twofold screw symmetry along the a axis.

The match in lattice dimensions of the crystalline thin films of $(R\text{-C}_{15}\text{-MA}, S\text{-PEA})$ on the liquid surface to those of the corresponding three-dimensional (3D) crystal structure and the thickness of the crys-

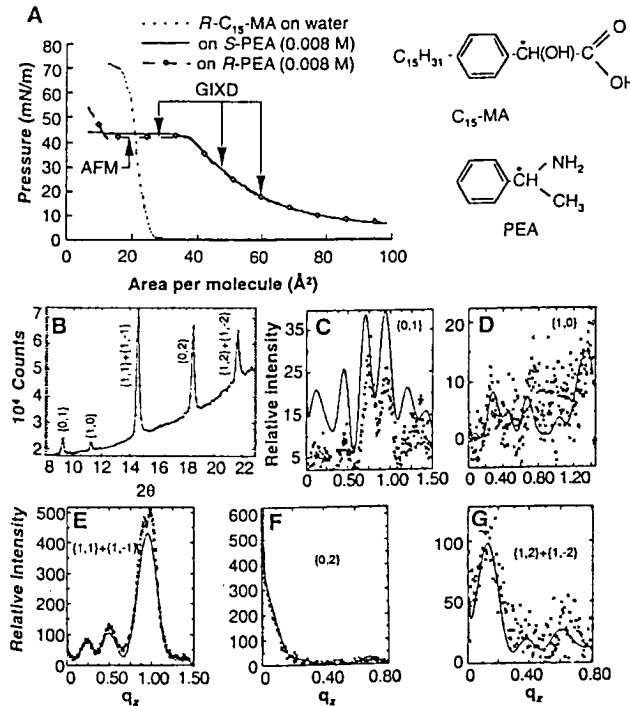
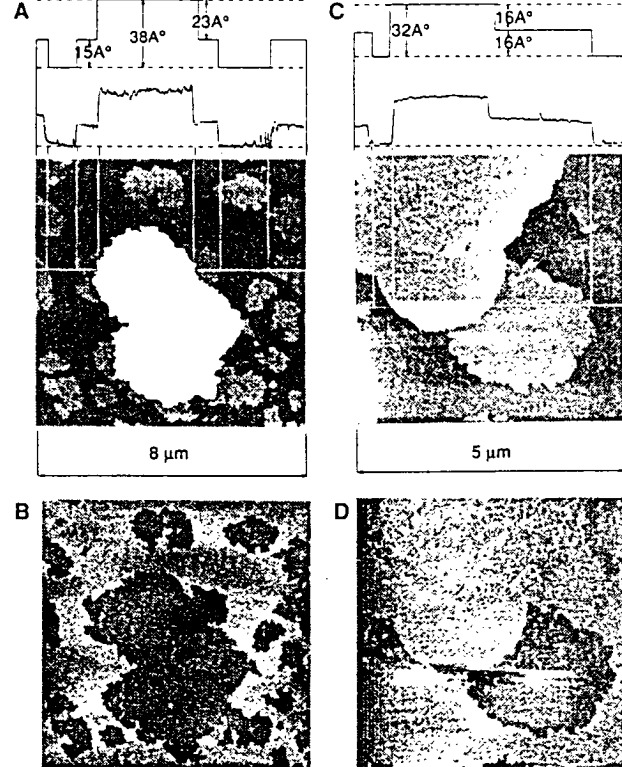


Fig. 2 (left). (A) Surface pressure-area ($\pi-A$) isotherms of $R\text{-C}_{15}\text{-MA}$ on Millipore water and PEA aqueous solutions. The arrows show the states at which GIXD patterns were recorded and AFM measurements for the corresponding LB films were performed. (B through G) The GIXD pattern of $R\text{-C}_{15}\text{-MA}$ spread over 0.008 M aqueous solution of $R\text{-PEA}$ and compressed to an area $A = 30 \text{ \AA}^2$ per molecule at a temperature of 5°C . Shown in (B) are the observed GIXD Bragg peaks with assigned (h,k) indices, where 2θ corresponds to the q_{xy} in-plane component of the wave vector q (wavelength $\lambda = 1.339 \text{ \AA}$). The corresponding measured (crosses) and calculated (solid line) Bragg rod intensity profiles in (C) through (G) are based on the molecular model described in the text; q_z is the out-of-plane



component of the wave vector q in units of \AA^{-1} . Fig. 3 (right). AFM images and the corresponding height profiles of the $(R\text{-C}_{15}\text{-MA}, R\text{-PEA})$ and $(R\text{-C}_{15}\text{-MA}, S\text{-PEA})$ films transferred onto mica by the LB technique at a molecular area $A = 30 \text{ \AA}^2$ per molecule and surface pressure $\pi \approx 40 \text{ mN/m}$: topography (A) and friction-force map (B) for $(R\text{-C}_{15}\text{-MA}, R\text{-PEA})$; topography (C) and friction-force map (D) for $(R\text{-C}_{15}\text{-MA}, S\text{-PEA})$. The vertical lines are a guide for the eye.

talline part of the films, as determined from the Bragg rod widths together with AFM height and friction analysis, indicated formation of a composite trilayer in the plateau region of the isotherm (Fig. 1C). This film consists of a crystalline interdigitated bilayer as in the corresponding 3D crystal structure and a partially disordered monolayer on the top. This monolayer is crystalline at the level of the MA and PEA units by virtue of the hydrogen-bonding bilayer network and is disordered on the top level of the alkyl chains because of the gaps created by the interleaved PEA units (13). This molecular model (14) proved to be most satisfactory, fitting the observed GIXD data well (Fig. 2, C to G). The one noticeable misfit in scale between the observed and calculated (0,1) Bragg rods arises from beam damage of the sample during the GIXD measurements (15).

In terms of molecular reorganization, the absence of diffraction in the first part of the π -A isotherm before the plateau can be attributed to incompatibility between the C_{15} -MA and PEA molecules: when the latter are incorporated in the monolayer, they create gaps between C_{15} -hydrocarbon chains. This alternating juxtaposition does not permit close packing and crystalline organization of

the monolayer. The plateau region of the isotherm at $13 \text{ \AA}^2 < A < 40 \text{ \AA}^2$ per molecule for $(R-C_{15}\text{-MA})$ spread on R-PEA solution reflects a phase transition corresponding to the gradual transformation of the amorphous monolayer into the composite interdigitated trilayer. The second rise of the surface pressure at 13 \AA^2 per molecule reflects a higher compressibility of the trilayer phase that should completely cover the liquid surface at this area (this estimate is based on the cell dimensions of the crystalline film). In Scheme 2A we suggest a simple mechanism for the formation of such a trilayer. We assume that the crystallization starts at the folding stage by virtue of the formation of a stable hydrogen-bonded bilayer, which is maintained upon further compression, leading to an interdigitated trilayer.

The process of molecular reorganization along the isotherm for the (R, S') system is less well understood. Our explanation relies primarily on the AFM analysis and the absence of diffraction in the GIXD measurements. The two typical heights of $16(2) \text{ \AA}$ (hydrophobic surface) and $32(3) \text{ \AA}$ (hydrophilic surface) suggest that, after the kink at $\sim 40 \text{ \AA}^2$ per molecule, the disordered monolayer transforms into an amorphous bilayer. We speculate how it may be generated in

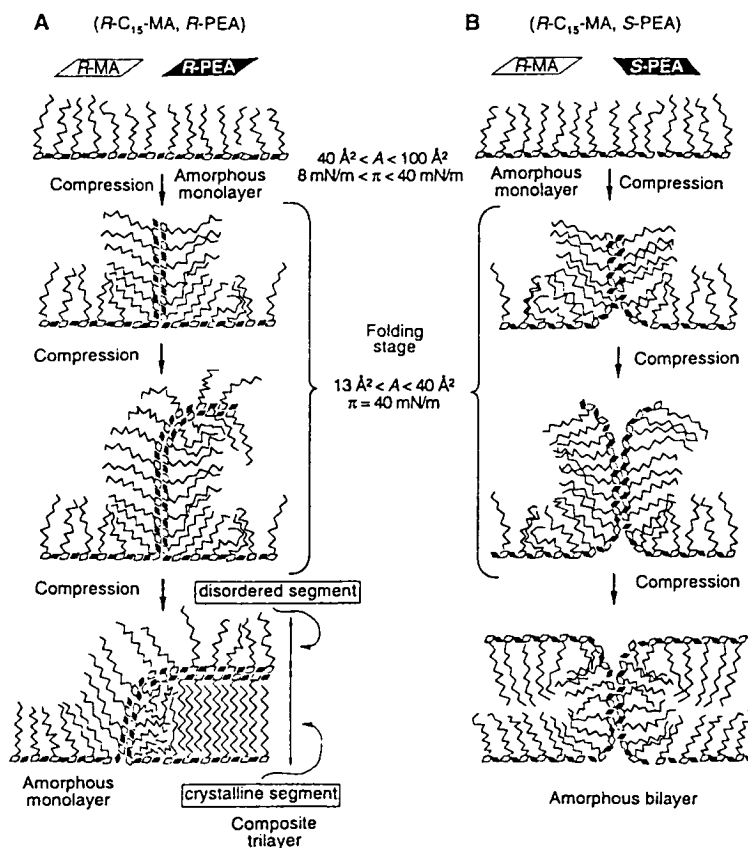
Scheme 2B, assuming that the bilayer at the folding stage is much less stable and is presumably disrupted upon further compression. We propose that the contrast in structural rearrangements of the $(R-C_{15}\text{-MA}, R\text{-PEA})$ and $(R-C_{15}\text{-MA}, S\text{-PEA})$ films on compression arises from the different energies of the hydrophilic bilayer of the head groups at the folding stage as in Scheme 2, and we believe that this contrast correlates with the drastic differences in solubility, crystallization behavior, and heats of fusion (12.4 and 6.6 kcal/mol) (16) of their two water-soluble diastereomeric analogs, $(R\text{-MA}, R\text{-PEA})$ and $(R\text{-MA}, S\text{-PEA})$, respectively. Although for both diastereomeric crystals the overall hydrogen-bonding arrangements are similar (3, 17), the orientations and positions of the phenyl rings within a layer in the $(R\text{-MA}, S\text{-PEA})$ salt are not compatible with the formation of an interdigitated structure (18).

GIXD experiments with chiral $R-C_{15}\text{-MA}$ on a racemic solution of PEA yielded a diffraction pattern similar to that obtained for the $(R-C_{15}\text{-MA}, R\text{-PEA})$ system, but with Bragg peaks of reduced intensity and increased width, showing formation of fewer trilayer crystallites of smaller size. This result arises from the chiral discrimination involving a separation of (R) and (S) enantiomers of PEA at the solution interface. On the other hand, GIXD experiments on a racemic $C_{15}\text{-MA}$ monolayer, which demonstrated a π -A isotherm similar to that obtained for the (R, S') system over a chiral or racemic PEA solution, did not yield diffraction signals, suggesting that the long-chain amphiphilic molecules did not separate into islands of opposite chirality.

We believe that the proposed approach for the molecular design of thin interdigitated films can be extended to other two-component systems composed of a water-insoluble amphiphile and a water-soluble counterpart. Moreover, the ability of such systems to form stable bilayers at the air-liquid interface, and thus to be amenable to characterization at the near-atomic level, may enable us to probe the mechanism of ion transport that occurs in natural membranes.

REFERENCES AND NOTES

- J. L. Slater and C. H. Huang, *Prog. Lipid Res.* **27**, 325 (1988).
- M. C. Brianco, M. Leclercq, J. Jacques, *Acta Crystallogr. B* **35**, 2751 (1979).
- S. Larsen and H. L. Diego, *ibid.* **B49**, 303 (1993).
- We synthesized $(R)\text{-}\rho$ -pentadecylmandelic acid by the Friedel-Craft reaction of pentadecyl benzene with oxalyl chloride in chloroform at 0° to 5°C to yield the α -keto acid [O. Itoh et al., *Bull. Chem. Soc. Jpn.* **57**, 810 (1984)]. The latter was esterified to the corresponding methoxy ester and subsequently reduced by the NaBH_4 (R)-tartrate acid complex according to the method of H. Iwagami et al. [*ibid.* **64**, 175 (1991)] to yield $(R)\text{-}\rho$ -pentadecyl methyl mandelate with an enantiomeric excess (ee) of 57%. We determined this value by nuclear magnetic resonance



Scheme 2.

- (NMR) analysis, using the *tris*(3-(trifluoromethylhydroxymethylene)-(+)-camphorato)europium(III) complex. The compound was hydrolyzed to the corresponding acid and then the optical purity was enhanced up to 97% ee by cocrystallization with commercially available *R*-PEA. The optical purity was checked by NMR and circular dichroism spectra: $[\alpha]_D^{25} = -63.2$ ($C = 1.01$ g/liter tetrahydrofuran).
5. The isotherms were measured from $A = 100$ to 5 \AA^2 per molecule.
 6. The GIXD measurements were conducted on a liquid surface diffractometer at the undulator beamline BW1 at HASYLAB, Deutsches Elektronen-Synchrotron (DESY). The synchrotron radiation beam was monochromated to a wavelength of 1.339 \AA . The incident angle was adjusted to $\alpha_i = 0.85\alpha_c$, where $\alpha_c = 0.14^\circ$. A detailed explanation of the method and experimental setup are given in (7) and (8), respectively. The amphiphile *R*-C₁₅-MA was spread at room temperature in a Langmuir trough and then cooled to 5°C .
 7. J. Als-Nielsen et al., *Phys. Rep.* **246**, 251 (1994).
 8. J. Majewski, *Chem. Eur. J.* **1**, 304 (1995).
 9. We implied, although we have not proven, that no significant changes occurred on deposition of the films on a solid support. The AFM measurements were performed with Nanoscope III FM (Digital Instruments, Goleta, CA) at ambient temperature with a commercial silicon nitride tip, attached to a cantilever with a spring constant of 0.38 N/m .
 10. Film depositions were done on a NIMA trough (NIMA Technology, Coventry, UK) at 20°C and at a surface pressure of $\sim 40 \text{ mN/m}$. Film was transferred onto mica at a constant speed of 10 mm/min .
 11. For the silicon nitride tip used in the AFM studies, the lateral friction coefficient is qualitatively proportional to the hydrophilicity of the surface. A detailed analysis of different factors influencing the lateral friction for self-assembled monolayers on mica is given in Y. Liu et al. [*Langmuir* **12**, 1235 (1996)].
 12. Crystallographic measurements were performed on a four-circle Rigaku single-crystal diffractometer with Cu K_α radiation from a 18-kW rotating anode generator. The structure was solved and refined with the use of SHELXL-91 software. The coordinates have been submitted to the Cambridge Crystallographic Database.
 13. Subtraction of a 25 \AA thickness of the crystalline bilayer as in the 3D structure from the $38(4) \text{ \AA}$ trilayer thickness obtained by AFM leaves $13(4) \text{ \AA}$, which is compatible within a standard deviation with the $16(2) \text{ \AA}$ monolayer thickness.
 14. Comparison of the observed and calculated Bragg rods (the latter obtained by x-ray structure factor computations) showed that the alkyl chains on the top level of the trilayer are disordered and there is no ordered binding of PEA from the subphase.
 15. Beam damage had in fact occurred, but we lacked the quantitative data to introduce a proper correction.
 16. S. P. Zingg, E. M. Arnett, A. T. McPhail, A. A. Bothner-By, W. R. Gilkerson, *J. Am. Chem. Soc.* **110**, 1565 (1988).
 17. H. L. Diego, *Acta Chem. Scand.* **48**, 306 (1994).
 18. In the complex (*R*-MA, *R*-PEA) the phenyl rings within a layer are uniformly tilted in a manner compatible with close packing of the hydrocarbon chains; in the (*R*-MA, S-PEA) salt the phenyl rings are not uniformly tilted.
 19. We thank S. Matis for performing the AFM measurements. Supported by the Minerva Foundation, the German Israeli Foundation (GIF), the Danish Foundation for Natural Sciences, and HASYLAB, DESY, Hamburg, Germany (beam time).

15 July 1996; accepted 8 October 1996

2.6 Design of interdigitated films *via* amidinium-carboxylate interactions at the air-liquid interface; potential replication properties of the system

Ivan Kuzmenko,* Maik Kindermann,† Kristian Kjaer§, Jens Als-Nielsen,# Leslie Leiserowitz*, Genrich von Kiedrowski,† M. Lahav*

*Department of Materials and Interfaces, the Weizmann Institute of Science, Rehovot 76100, Israel

Organische Chemie, Ruhr-Universitaet Bochum, D-44780 Bochum, Germany

§Department of Solid State Physics, Risø National Laboratory, DK-4000 Roskilde, Denmark

#Jens Als-Nielsen, Niels Bohr Institute, H.C. Ørsted Laboratory, Copenhagen, Denmark

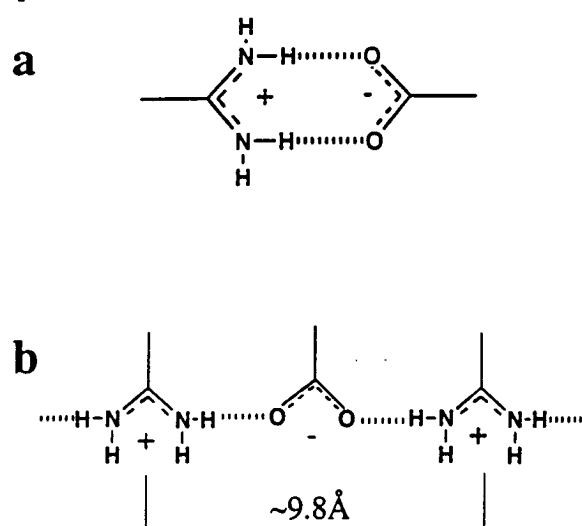
Abstract

Previously we had shown that chiral long-chain amiphilic molecules when spread on the solution containing a suitable chiral water-soluble counterpart may incorporate the water-soluble component and form amorphous monolayers. Such monolayers can be then transformed, upon compression, into crystalline interdigitated films and characterized in detail by grazing-incidence X-ray diffraction (GIXD).¹ Here we expand our approach towards non-chiral systems with strong acid-base interactions between amidinium ($-C(NH_2)_2^+$) and carboxylic ($-C(CO_2)_2^-$) chemical functions that were broadly studied before as building blocks in artificial self-replicating systems and also appeared appropriate for the molecular interactions at the air/liquid interface. As we demonstrate, using GIXD and X-ray reflectivity, amidinium-carboxylate interactions do suffice for the interdigitation process, but are hardly suitable for molecular replication between water-soluble species of aqueous solutions containing water-soluble species with amidinium and carboxylic functions and the analogous headgroups of the mixed monolayer.

Introduction

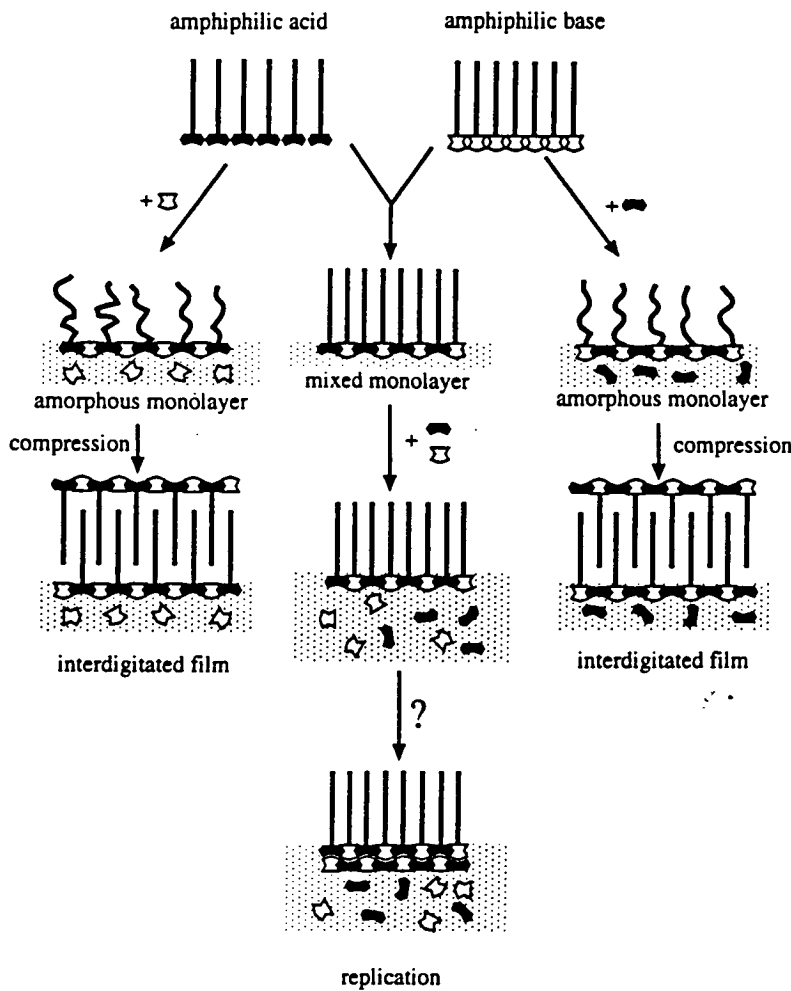
As was shown recently,¹ long-chain amphiphilic acid molecules (pentadecylmandelic acid) when spread on aqueous solutions containing water soluble amine molecules (phenylethylamine) are able to form interdigitated films akin to those found in natural membranes.² The process of interdigitation at the interface was found to be remarkably sensitive to the molecular composition although may occur in various systems involving strong acid-base interactions between the building components and therefore suggests further elaboration.

Specific interactions between the amidinium and the carboxylic acid functions (Scheme 1) are of importance in enzymes containing arginine active sites.³⁻⁷



Scheme 1

The analogous simple chemical systems were extensively studied in aqueous and non-aqueous solutions.⁸⁻¹³ The strong hydrogen bonds of the N-H···O-C type between amidinium (or guanidinium) and carboxylic moieties existing in non-polar solutions were employed both in supramolecular design of 3D architectures^{14,15} and in artificial self-replicating systems¹⁶ that mimic the natural molecular self-replication and may possibly shed light on the origin of evolution of living systems.¹⁷ In this study we have concentrated on two major aspects of using amidinium-carboxylate interactions at the air-water interface. The first aspect of the study was linked to the two-dimensional design of interdigitated films. Strong carboxylate-amidinium interactions appear as suitable to guarantee the formation of a mixed amorphous monolayer of the ...A-B-A-B-A-B... type, where A is the amphiphilic acid moiety and B is the water-soluble base. Upon compression such a monolayer is to be transformed into an interdigitated film as shown in Scheme 2(*right and left*), suggested previously.¹ In the present study we experimentally verify the proposed model of the amorphous self-assembled monolayer, a template that is to be further transformed into an interdigitated film upon compression.



Scheme 2

Our second goal was to study potential replicating properties of the system at the air-water interface, namely in the ability of the water-soluble amidinium and carboxylic components to bind to the pre-formed mixed monolayer containing the same chemical functions as depicted in Scheme 2(*middle*). Water-soluble molecules bearing carboxylic and amidinium functions that bind at the mixed monolayer interface may further participate in chemical reactions between each other in a manner akin to self-replicating systems in bulk solutions.¹⁶

Results and discussion

π -A Isotherms

π -A isotherms of several amphiphilic systems involving carboxylic acid and amidinium chemical functions were studied at the air-water (or air-aqueous solution) interface. *p*-Pentadecylbenzoic acid, C₁₅H₃₁-C₆H₄-CO₂H (labeled C₁₅-benzoic acid), and *p*-heptadecylbenzamidinium C₁₇H₃₅-C₆H₄-CN₂H₃·HPF₄ (labeled C₁₇-benzamidinium) were used as amphiphilic surfactants and benzamidinium, C₆H₅-CN₂H₃, *p*-methylbenzamidinium, CH₃-C₆H₄-CN₂H₃, potassium benzoate, C₆H₅-CO₂K as the water-soluble components.

The surface pressure-molecular area isotherms of amphiphilic C₁₅-benzoic acid, spread on Millipore water at 5° and 20°C, suggest spontaneous formation of a multilayer (3-6 layers), as estimated from the limiting area per molecule of 5-7Å², which is 3-6 times smaller than the area of 20-30Å² usually occupied by amphiphilic molecules bearing a single hydrocarbon chain (Fig.1a, solid line). Such a behavior of the C₁₅-benzoic acid is in contrast with regular fatty acids that always form monolayer films on water for a broad range of hydrocarbon chain lengths C₁₄-C₂₉ (find references in ¹⁸⁻²³). An addition of small amounts of KOH into the water subphase (1.8mM) promotes formation of a stable monolayer of potassium C₁₅-benzoate with a limiting area per molecule of 21-22Å². (Fig.1a, long-dashed line).

C₁₇-benzamidinium forms a monolayer film on the water surface, according to the π -A isotherm measurements (Fig.1b, solid line), with a limiting area per molecule of 23-24Å².

When C₁₅-benzoic acid is spread on solutions containing water-soluble C₆H₅-CN₂H or CH₃-C₆H₄-CN₂H, the isotherm curve becomes expanded with a large kink at A~30Å² preceding the plateau region and a second increase of the surface pressure at ~10Å² (Fig.1a, short-dashed line). The shape of the isotherm by and large resembles that found in the system of long-chain mandelic acid and phenylethylamine.¹ C₁₇-benzamidinium, spread on the aqueous subphase containing C₆H₅-CO₂K, gives rise to the isotherm curve of a similar shape with more expanded plateau region and smaller

pressure kink preceding it (Fig.1b, dashed line). The π - A isotherms for all these systems suggest the same mechanism of the monolayer transformation, as depicted in Scheme 2.

For C_{17} -amidinium spread on aqueous subphase containing $C_6H_5CO_2K$ we studied also the influence of the concentration of the water-soluble species on the degree of expansion of the π - A isotherm before the plateau region ($40\text{\AA}^2 < A < 100\text{\AA}^2$). The experiments demonstrate no observable dependence over the broad concentration range ($3 \cdot 10^{-5}$ - $8 \cdot 10^{-3}$ M), suggesting that the water-soluble and water-insoluble components always form a 1:1 complex at the air-solution interface (Fig.1c).

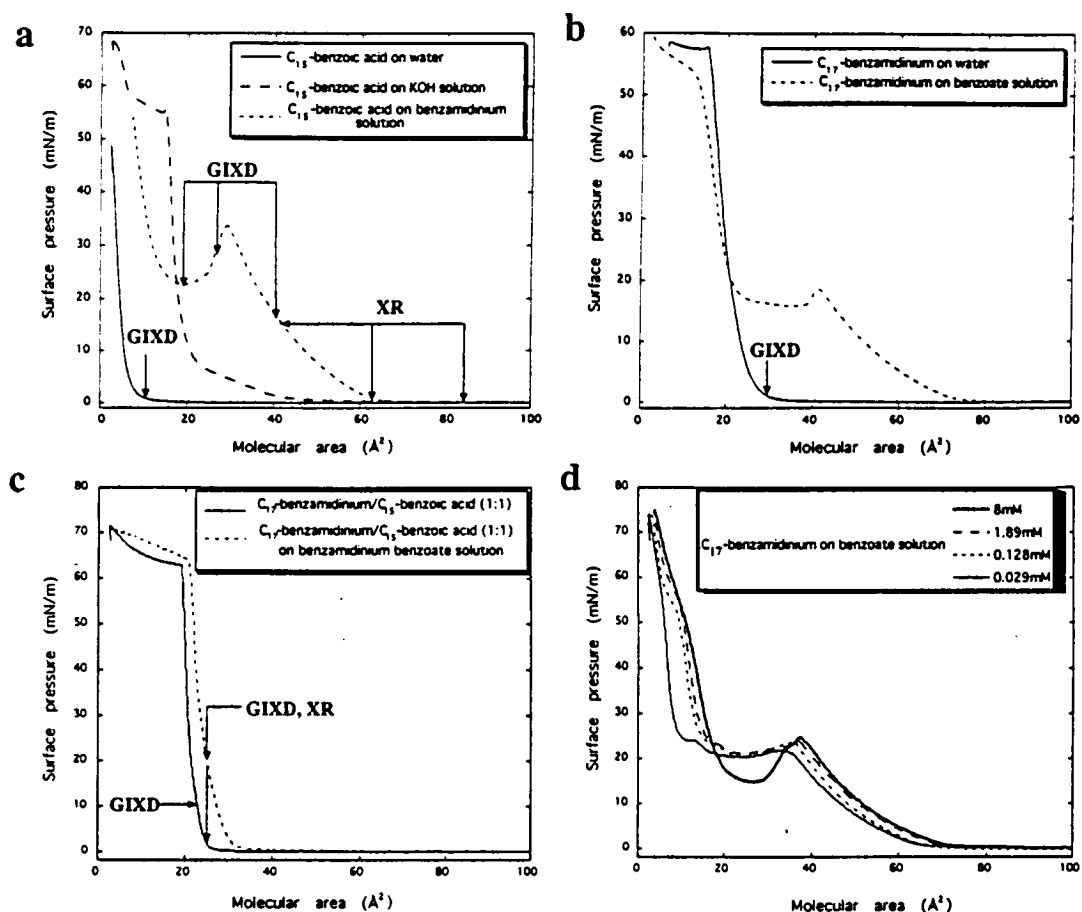


Fig.1 Surface pressure -molecular area isotherms of various systems involving interactions between benzamidinium and benzoate moieties, as described in the inset of each graph and in the text. GIXD and XR measurements were performed in the points marked by arrows.

The 1:1 mixture of C₁₅-benzoic acid and C₁₇-benzamidinium spread on Millipore water forms a stable monolayer, according to the π -A isotherm measurements, with a limiting area per molecule of 24 Å² (Fig.1d, solid line). On the aqueous solutions of benzamidinium (or methyl-benzamidinium) benzoate the isotherm is generally more expanded than on water and the degree of expansion depends on the concentration of the water-soluble components (Fig.1d, dashed line).

Grazing incidence X-ray diffraction (GIXD) measurements

Diluted chloroform solutions of the amphiphilic compounds were spread on Millipore water or on aqueous solutions containing the water-soluble components at ~15°C and then cooled down to the temperature of 5°C, at which the GIXD and X-ray reflectivity measurements were performed.

C₁₅-benzoic acid on pure water

C₁₅-benzoic acid was spread on Millipore water at ambient temperature for a calculated area/molecule of 25 Å², and cooled down to 5°C. The GIXD pattern contains three reflections with strongly modulated Bragg rods, corresponding to a multilayer with the oblique in-plane cell dimensions $a = 6.3\text{ \AA}$, $b = 5.6\text{ \AA}$, $\gamma = 100^\circ$, $A_{xy} = 34.7\text{ \AA}^2$ (Fig.2a).

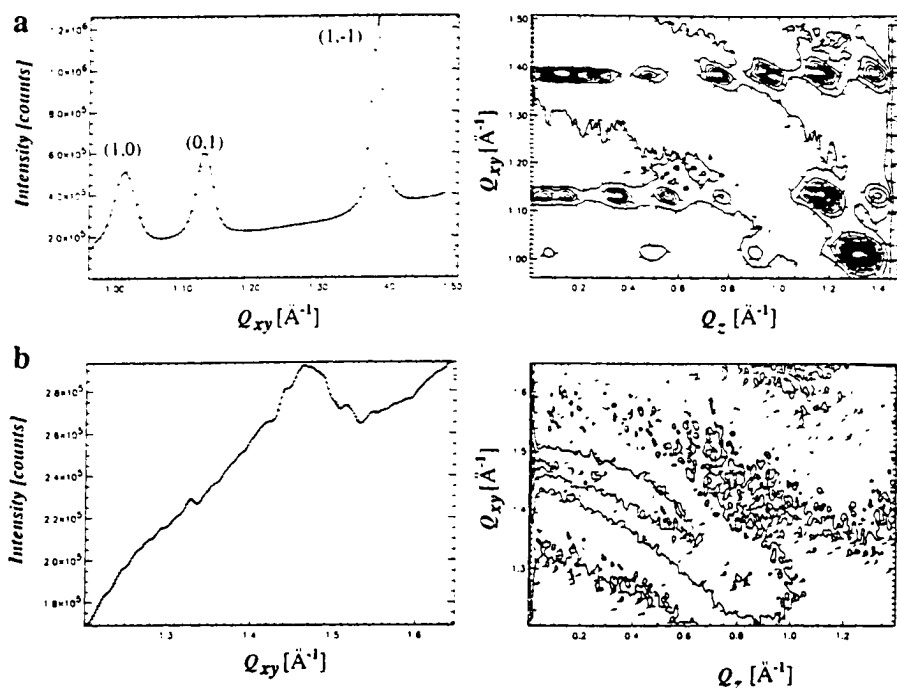


Fig.2 GIXD patterns of (a) C₁₅-benzoic acid and (b) of C₁₇-benzamidinium both on pure Millipore water.

The thickness of the film T is $\sim 90\text{\AA}$ as estimated from the average full width at half maxima (FWHM), $\Delta q_z = 0.06\text{\AA}^{-1}$, of the Bragg rod modulations ($T=0.9 \cdot 2\pi/\Delta q_z$). The total number of the layers (bilayers) constituting the film is equal to 3, given the interlayer spacing is 30.5\AA as calculated from an average Δq_z difference between the maxima of the Bragg rod modulations. From an estimated van-der Waals length of centrosymmetric molecular dimer of C₁₅-benzoic acid, $L_m \sim 52\text{\AA}$, and the bilayer thickness, $T = 30.5\text{\AA}$, the molecular tilt t from the layer normal [$t = \arccos(T/L_m)$] is equal to $\sim 54^\circ$, corresponding to cross-sectional area $A_o = A_{xy} \cdot \cos t = 20.3\text{\AA}^2$. About the same total number of layers is suggested by the ratio between the extrapolated area/molecule from the π - A isotherm (5.7\AA^2) and the unit cell area $A_{xy} \sim 35\text{\AA}^2$. The packing motif of C₁₅-benzoic acid at the air-water interface is not similar to the 3D structure of analogous *p*-heptylbenzoic acid C₇H₁₅-C₆H₄-CO₂H, that has an interdigitated packing motif and completely different intra-layer a, b unit cell dimensions ($a = 4.848\text{\AA}$, $b = 11.79\text{\AA}$, $\gamma = 84.2^\circ$, $A_{xy} = 56.9\text{\AA}^2$)²⁴. The multilayer formation of C₁₅-benzoic acid at the air-water interface, as was alluded to before, is in contrast with monolayer formation of regular fatty acids as well as of similar compound 4-(octadecyloxy)-benzoic acid (C₁₆H₃₃-O-C₆H₄-CO₂H).²⁵ The multilayer formation might be driven by kinetics of the surface crystallization. The ratio between the rate of in-plane (2D) crystallization compared to the growth in the perpendicular out-of-plane direction correlates with the hydrocarbon chain length in accordance with the accepted crystal growth theories.²⁶ Therefore, multilayer formation is plausible for relatively short-chain amphiphiles. Such a spontaneous multilayer formation has been observed for short-chain α -amino acids²⁷ and for simple alkanes crystallized at the air/water interface.²⁸

C₁₇-benzamidinium on pure water

C₁₇-benzamidinium was spread on Millipore water at ambient temperature for a calculated area/molecule of 35\AA^2 , cooled down to 5°C and compressed along the isotherm up to the rise of surface pressure ($\pi = 1\text{mN/m}$, $A = 25\text{\AA}^2$). The GIXD pattern contains a very broad peak (Fig.2b) reflecting a high degree of molecular disorder. We attribute the lack of crystalline order as arising from repulsive interactions between positively charged head groups.

Pentadecylbenzoic acid on aqueous solution containing *p*-methylbenzylamidinium

C₁₅-benzoic acid was spread on aqueous solution containing *p*-methylbenzamidinium (0.008M) prepared by neutralizing *p*-methylbenzamidinium chloride with an equimolar amount of potassium hydroxide. The diffraction patterns

were measured in three points along the π -A isotherm: one - before the kink at the beginning of the plateau region and two others - along the plateau, as marked by arrows in Fig.1a. In the region before the kink, the monolayer is amorphous since it displays no Bragg peaks according to GIXD. The compression to the plateau region gave rise to a diffraction signal. The diffraction pattern measured at 30\AA^2 and 20\AA^2 consists of seven reflections (Fig.3).

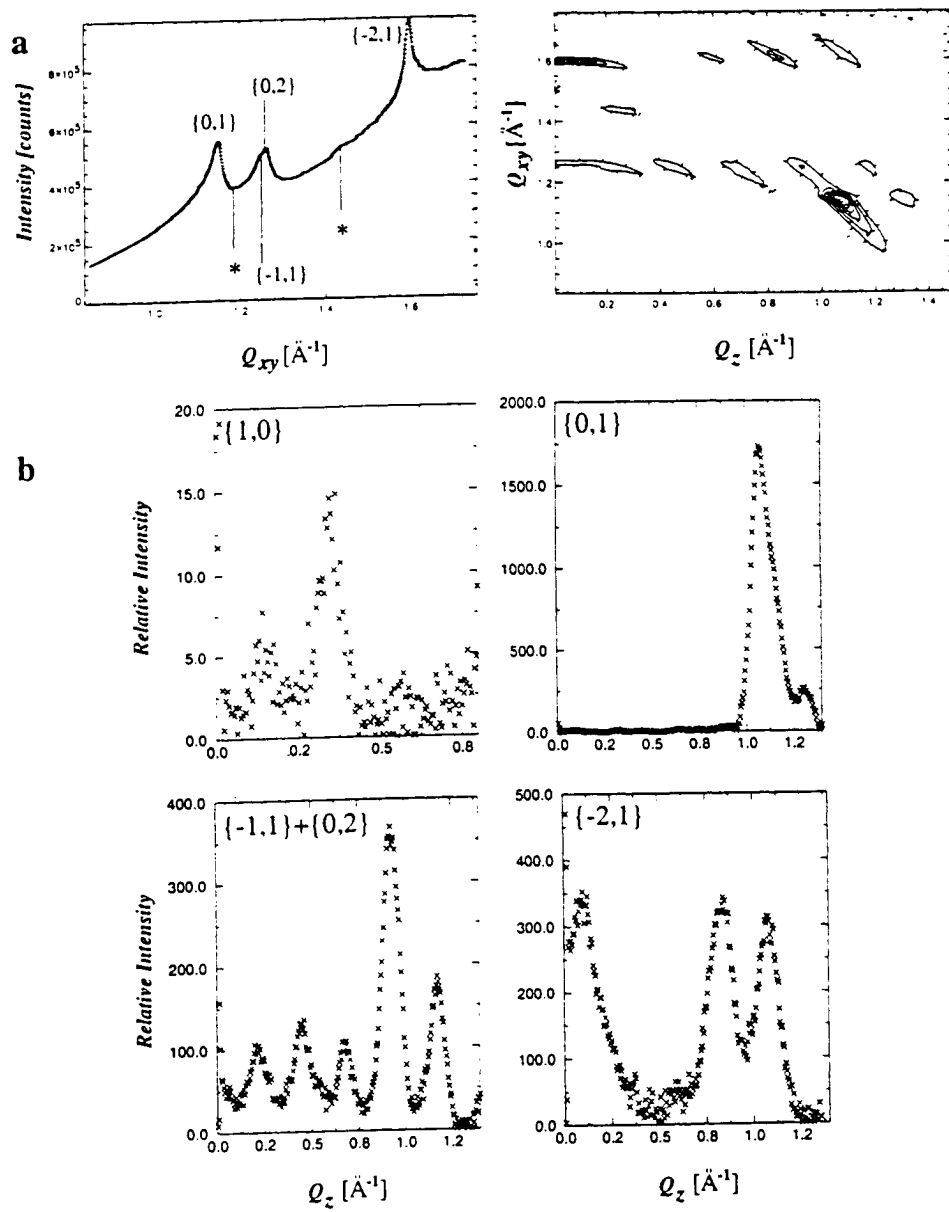
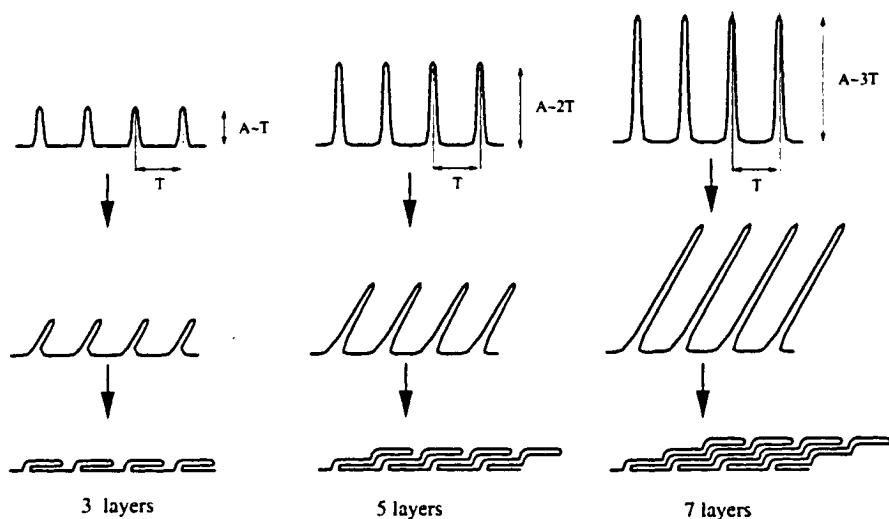


Fig. 3 GIXD pattern for C₁₅-benzoic acid spread on *p*-methylbenzamidine (0.008M), measured at $\sim 20\text{\AA}^2$

Five of them, of relatively strong intensity, could be indexed with an oblique unit cell $a = 10.06\text{\AA}$, $b = 5.50\text{\AA}$, $\gamma = 83.2^\circ$, $A_{xy} = 54.9\text{\AA}^2$. The two remaining peaks (at $q_{xy} = 1.19\text{\AA}$ and $q_{xy} = 1.44\text{\AA}$) of near threshold intensity belong to another crystalline phase, because all the seven peaks cannot be expressed in terms of the same lattice. The minor crystalline phase will not be further discussed. The unit cell dimensions of the major phase almost match the in-layer cell dimensions of the 3D structure of the same composition ($a = 9.58\text{\AA}$, $b = 5.73\text{\AA}$, $\gamma = 90^\circ$, $A_{xy} = 54.9\text{\AA}^2$, *vide infra*), and therefore should have similar packing motif. The inter-layer distance d in the film is equal to 26.4\AA as calculated from the average Δq_z difference of the Bragg rod modulations. The unit cell volume in the film ($d \cdot a \cdot b \cdot \sin\gamma$) is equal to 1449\AA^3 that fits well to the corresponding unit cell volume of the 3D crystal structure ($(a \cdot b \cdot c)/2 = 1438\text{\AA}^3$). The full thickness of the film $T \sim 80\text{\AA}$ as extracted from the FWHM of the Bragg rods is compatible with 6+ layers, where plus sign reflects partially crystalline top layer as depicted in Fig.4c. This thickness is three times of that observed for *R*-pentadecylmandelic acid on *R*-phenylethylamine (Scheme 3).¹



Scheme 3

This difference in behavior might be accounted for by the difference in elastic properties of the amorphous monolayer prior to collapse into the crystalline multilayer, that regulates the average distance between maxima and minima and the amplitude of the corrugated (buckled) monolayer in the compressed state.²⁹

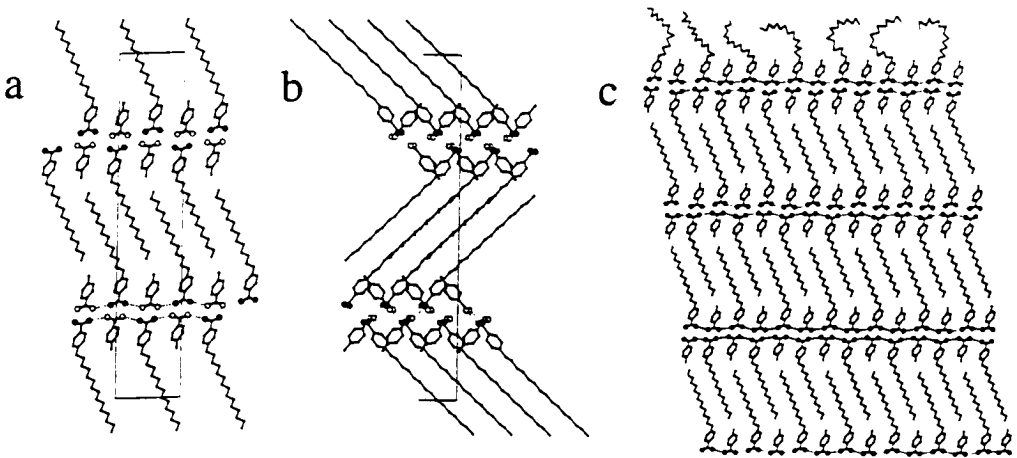


Fig.4 (a,b) Two views (along *a* and *b*) of the 3D structure of *p*-methylbenzamidinium C₁₅-benzoate, (c) Proposed model packing arrangement of the interdigitated film as formed at the air-solution interface, according to the GIXD data.

Heptadecylbenzamidinium and pentadecylbenzoic acid 1:1 mixture on pure water and on solution containing *p*-methylbenzamidinium benzoate

The 1:1 mixture of two amphiphiles was spread on both Millipore water and on a solution of *p*-methylbenzamidinium benzoate (saturated at 5°C) at ambient temperature and then cooled down to 5°C. The monolayer film on pure water was measured at two points along the isotherm: at 24 Å², $\pi = 1\text{mN/m}$, and at 22 Å², $\pi = 10\text{mN/m}$. On saturated solution the GIXD scans were made at 24 Å² ($\pi = 20\text{mN/m}$). The diffraction pattern in each case consists of two peaks corresponding to a rectangular crystalline lattice of *p1g1* symmetry (Table 1, Fig.5a). The hydrocarbon chain axes are tilted from the vertical along the *b*-axis. A linear hydrogen bonding array (Scheme 1b) is typical of the crystal structures involving amidinium and carboxylic functional groups. On water at 24 Å² the rectangular unit cell dimensions are $a = 4.93\text{\AA}$, $b = 9.42\text{\AA}$. The molecular chains are tilted from the layer normal by 29°. The structure factor calculations with a refined molecular model yielded Bragg rod intensity profiles that fitted well the observed data (Fig.5c,d). On saturated solution $a = 4.90\text{\AA}$, $b = 9.06\text{\AA}$, molecules are tilted by 24° from the layer normal. The decrease in the molecular tilt (29° vs. 24°), reflected also in the 2D lattice parameters (see Table 1), can be explained by the

difference in the surface pressure due to the presence of surface active *p*-methylbenzamidinium benzoate. A GIXD pattern of the monolayer film on pure water studied at $\pi = 10\text{mN/m}$ had indicated the molecular tilt and lattice cell dimensions akin to those found on the saturated solution (Table 1, Fig.5b).

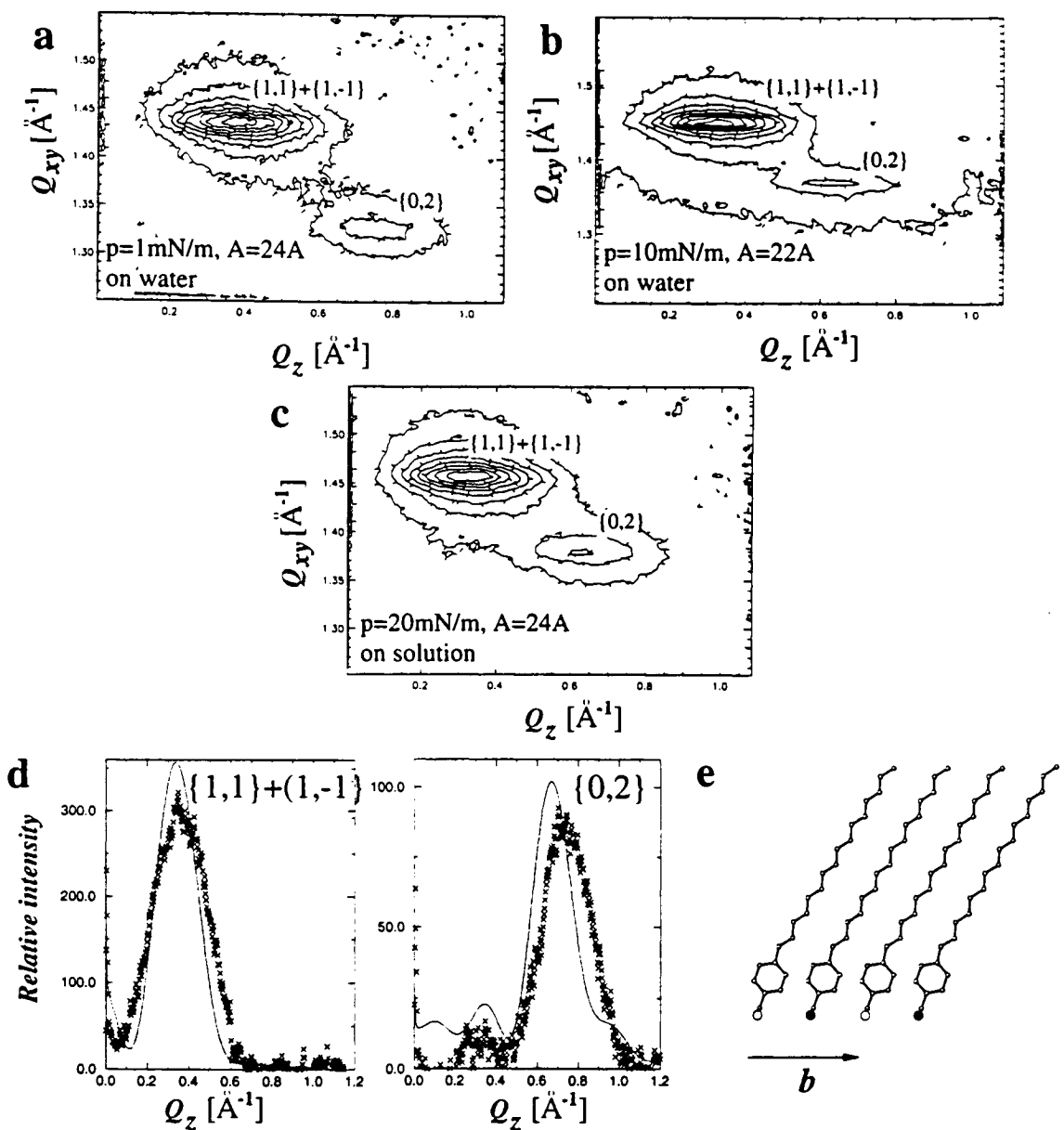


Fig. 5 (a-c) GIXD patterns (contourplots) of the mixed monolayer C₁₇-benzamidinium C₁₅-benzoate on water and on solution containing water soluble benzamidinium benzoate; (d) Observed and calculated intensity distribution along the Bragg rods; (e) Model packing arrangement corresponding to the calculated curves, presented in (d)

Table 1: 2D crystallographic data for the C₁₇-benzamidinium C₁₅-pentadecylbenzoate (1:1) mixed monolayer as obtained by GIXD on water and on saturated solution of *p*-methylbenzamidinium benzoate

A_m^a	π	$I_{(0,2)}/I_{(1,1)}^b$	a	b	t	A_{xy}	a_\perp	b_\perp	$A_o, \text{\AA}^2$
<u>water:</u>									
24	1	0.37	4.93	9.42	29.7	23.2	4.93	8.18	20.1
	10	0.48	4.91	9.11	24.0	22.4	4.91	8.32	20.4
<u>solution:</u>									
24	20	0.48	4.90	9.06	24.1	22.2	4.90	8.27	20.3

^aNominal area per molecule A_m , lattice area A_{xy} , cross-sectional area A_o in \AA^2 , intensity ratio $I_{(0,2)}/I_{(1,1)}$, lattice dimensions a, b and cross-sectional lattice dimensions a_\perp, b_\perp in \AA , molecular tilt t in degrees

The translational repeat along the hydrogen-bonding array (Scheme 1b), which is equal to $\sim 9.8\text{\AA}$ (*vide infra*), is twice the a -length repeat of the monolayer phase and suggests the arrays be running in the a -direction. This array cannot be parallel to the b -axis or run along the diagonal, since the b axis reduces in length upon compression ($9.4\text{--}9.0\text{\AA}$) while the a -axis remains unchanged and is half of the hydrogen-bonding repeat distance. We therefore propose that the hydrogen bonding array is parallel to the a -axis. These molecular rows along b can be stacked in a random manner due to the absence of hydrogen bonding or any other specific interactions between them, such that the x -coordinate of each row might be arbitrarily shifted by the $\pm a/2$ vector (Fig.6). The stacking faults along b , smear out the difference between the acid and the amine molecules in the diffraction pattern and half the real repeat distance along a . The molecular disorder is also expressed in the relatively low density of hydrocarbon chains packing: the cross-sectional average cell dimensions $a_\perp = 4.9\text{\AA}$, $b_\perp = 8.2\text{\AA}$, $A_o = 20.2\text{\AA}^2$, as compared to $A_o = 18.7\text{\AA}^2$ of the standard herringbone packing, signify mesomorphic state of the monolayer.

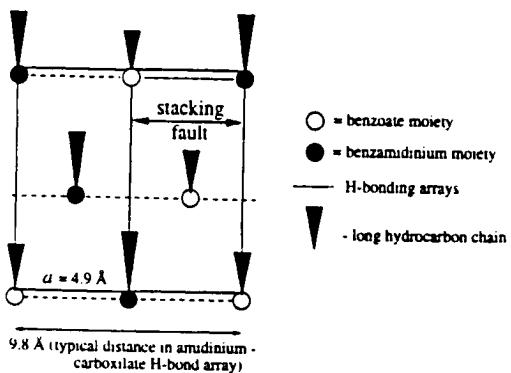


Fig. 6 Schematic representation of the molecular disorder in of the mixed monolayer C₁₇-benzamidinium C₁₅-benzoate on water and on solution containing water soluble benzamidinium benzoate

Specular X-ray Reflectivity Measurements

Pentadecylbenzoic acid on aqueous subphase containing *p*-methylbenzamidinium

The proposed model of the interdigitation process as depicted in Scheme 1 implies as a prerequisite an amorphous mixed monolayer composed of long-chain amphiphilic acid or base molecules and their water-soluble counterparts. This model agrees with the isotherm behavior as well as with the GIXD data (no diffraction before the plateau region) but calls for a direct proof. Specular X-ray reflectivity measurements provide an experimental evidence for the correctness of the proposed model.

The X-ray curves of C₁₅-benzoic acid deposited on aqueous 0.008M solution of *p*-methylbenzamidinium were measured at four points along the π -*A* isotherm before the plateau region, indicated in Fig.1a. The results of the reflectivity measurements and their treatment are summarized in Table 2 and Fig.7(A-D). To fit the experimental curves a three-box model was used with a fixed number of electrons in every box and the molecular area. The model tested incorporates 1:1 complex of C₁₅-benzoic acid and *p*-methylbenzamidinium. Only the dimensions of the three boxes and the surface roughness parameter were refined. The results of the fitting support our interpretation of the expanded region of the π -*A* in which the molecular chains are highly tilted and disordered due to the difference in the cross-sectional area between a hydrocarbon chain (18-20 Å) and two headgroups (~40 Å²) as shown in Fig.7(*top, left*). The cross-sectional area per hydrocarbon chain, as derived from the analysis is 24-27 Å² that suggests very

loose packing and accounts for the difference of diffraction signal before the plateau region.

Table 2: Fitted parameters for the pentadecylbenzoic acid on *p*-methylbenzamidinium aqueous solution (0.08M) in a three-box model

A_m^a	π	N_1	L_1	N_2	L_2	N_3	L_3	σ	$t^\circ b$	A_0^c
85	1	50	1.3	97	1.8	113	5.8	3.5	72	26
64	9	50	1.5	97	2.7	113	7.8	3.4	65	27
55	12	50	2.0	97	2.9	113	8.9	3.5	61	27
44	20 ^d	50	2.4	97	4.0	113	10.0	3.8	57	24

^aNominal area per molecule A_m and cross-sectional area in \AA^2 , N_i in electron units, L_i in \AA , the surface roughness σ parameter in \AA^2 , molecular tilt t in degrees

^b Parameter t corresponds to the degree of the C₁₅-hydrocarbon chain tilt, assuming the chain is stretched and its length is equal to 18.5 \AA^2 , as shown in Fig.7(*left*)

^c Cross-sectional area occupied by one hydrocarbon chain is calculated based on the molecular tilt t and the corresponding A_{xy}

^d This value corresponds to the maximum value right after the monolayer compression. The pressure was slowly decreasing along the reflectivity measurement due to monolayer relaxation reaching 12 mN/m

According to the reflectivity analysis, the molecular tilt gradually decreased upon compression with a corresponding increase of the film thickness. The estimated cross-sectional area per hydrocarbon chain of 24-27 \AA^2 is by 15-30% larger than the maximum cross-sectional area observed in mesomorphic monolayer phases.²³ Such a loose packing accounts for the absence of the diffraction signal before the plateau region. Once the minimum possible area occupied by the two headgroups is reached (~40 \AA^2), further compression forces the monolayer to buckle and the interdigitation to occur.

1:1 mixture of heptadecylbenzamidinium and pentadecylbenzoic acid on pure water and on saturated aqueous solution of *p*-methylbenzamidinium benzoate

The X-ray reflectivity measurements were performed under the same conditions as the corresponding GIXD studies. A three box model was used to fit the observed

specular reflectivity curves. The results of the curve fitting are summarized in Table 3 and depicted in Fig. 7(e,f).

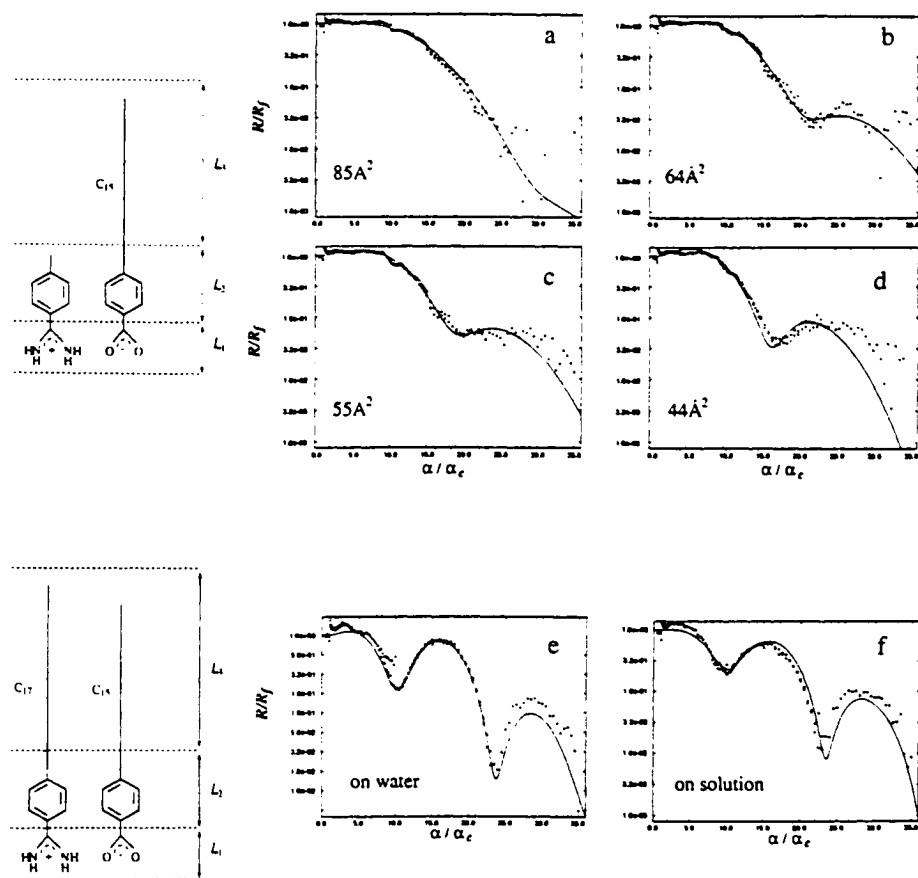


Fig. 7 X-ray reflectivity measured and calculated intensity profiles for:
 (a-d) C_{15} -benzoate on p -methylamidine solution at different compression ratios and for (e,f) C_{17} -benzamidinium C_{15} -benzoate on pure water and on saturated solution of benzamidinium benzoate

Table 3: Fitted parameters for the pentadecylbenzoic acid on 0.008M p -methylbenzamidinium aqueous solution in a three-box model

A_m^a	cov	π	N_1	L_1	N_2	L_2	N_3	L_3	σ
<u>water:</u>									
23	100	1	23	2.3	40	4.1	129	18.0	2.8
<u>solution:</u>									
23	95	20	23	3.1	40	4.0	113	19.5	3.0

^a A_m is in \AA^2 , coverage in percents, surface pressure π in mN/m, N_i in electron units, L in \AA , the surface roughness parameter in \AA^2 .

The overall result of the model calculations suggests no detectable binding of *p*-methylbenzamidinium benzoate layer underneath the preformed monolayer, as was depicted in Scheme 3, since the observed specular reflectivity can be reasonably fitted with the same 3 box model as was used on pure water which implies no binding. This result suggests, that the binding constant of the water-soluble species to the mixed monolayer is too small to assure the bilayer formation. We note that this result is in keeping with experiments which suggested no binding between benzoic acid and benzamidinium in bulk aqueous solutions.

Single Crystal X-ray Diffraction Studies

Pentadecylbenzoate *p*-methylbenzylamidinium

Sodium salt of pentadecylbenzoic acid and methylbenzylamidinium chloride (1:1 ratio) were dissolved in analytical Merck ethanol and NaCl precipitate was filtered off. The flat crystalline needles were obtained by slow cooling of the saturated solution. A suitable single crystal was mounted on an AFC5 Rigaku diffractometer equipped with the rotating anode and the intensity data were measured at ambient temperature (17°C). The crystal structure was solved by direct methods and refined with use of SHELX-97 software.³⁰ The experimental X-ray data are summarized in Table 4.

The structure consists of interdigitated bilayers (Fig.4a,b) and in this respect is very much akin to the 3D crystal structure of *R*-phenylethylamine *R*-pentadecylmandelate. The structure of pentadecylbenzoate *p*-methylbenzylamidinium displays features, characteristic of two reported crystal structures that incorporate only amidinium and carboxylic donor and acceptor functional groups (see also the following section).^{31,32} In these structures amidinium and carboxylic moiety form heterocyclic hydrogen-bonded dimers (Scheme 1a) interlinked by N-H···O bonds (2.8 Å) to form continuous arrays (Scheme 1b). Translational repeat along the array is therefore fixed and equal to 9.6-9.9 Å. This repeat in the structure of pentadecylbenzoate *p*-methylbenzylamidinium coincides with the *a*-axis (9.58 Å). The carboxylic and amidinium moieties belonging to the same hydrogen bonding row form hydrogen bonding dimers with two neighboring raws along the *b*-axis (Fig.4B) leading to a two-dimensional hydrogen bonding bilayer network in the *a*-*b* plane. The dihedral angle between the planes of carboxilate and amidinium neighboring species within a row is close to 90°. An analogous motif has been observed in the crystal structure of primary amides defined as 'shallow' glide motif.

p-methylbenzamidinium benzoate

Needle-like crystals of *p*-methylbenzamidinium benzoate were grown from water solution by slow evaporation.

The hydrogen-bonding arrangement involves the same two types of N-H \cdots O interactions (Scheme 1), as described in the previous section. However, the amidinium and carboxilic moieties form a channel like structure rather than bilayer arrangement, as for *p*-methylbenzamidinium C₁₅-benzoate. The channel incorporates crystallographic two-fold symmetry and distorted non-crystallographic 4₂ symmetry (Fig.8). Each four-side channel is constructed from two symmetry independent cyclic hydrogen-bonded dimers and two more dimers generated by the two-fold symmetry axis. The dimers, stitched by hydrogen bonding, are stacked in infinite wells along the *c*-axis. The outer surface of the channel is hydrophobic; benzene rings of each channel interdigitate with those of four neighboring channels.

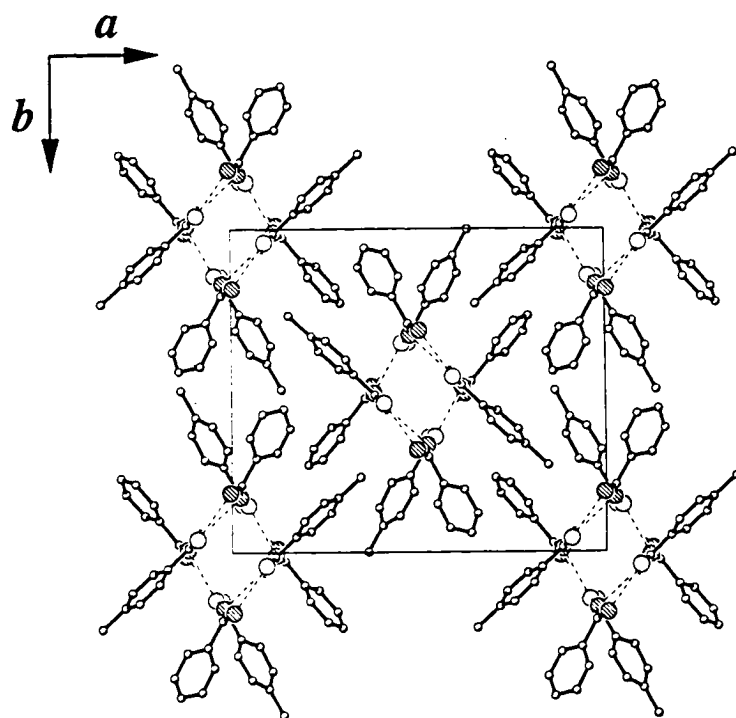


Fig. 8 3D packing arrangement of *p*-methylbenzamidinium benzoate viewed along *c*-axis

References

- (1) Kuzmenko, I.; Buller, R.; Bouwman, W. G.; Kjaer, K.; Als-Nielsen, J.; Lahav, M., Leiserowitz, L. *Science* **1996**, *274*, 2046.
- (2) Slater, J. L., Huang, C. H. *Prog. Lipid. Res.* **1988**, *27*, 325.
- (3) Adams, J. M.; Buehner, M.; Chandrasekhar, K.; Ford, G. C.; Hackert, M. L.; Liljas, A.; Rossman, M. G.; Smiley, J. E.; Allison, W. S.; Everse, J.; Kaplan, N. O., Taylor, S. S. *Proc. Natl. Acad. Sci. U.S.A.* **1973**, *70*, 1968.
- (4) Eventoff, W.; Rossmann, M. G.; Taylor, S. S.; Torff, H. J.; Meyer, H.; Keil, W., Kiltz, H. H. *Proc. Natl. Acad. Sci. U.S.A.* **1977**, *74*, 2677.
- (5) Christianson, D. W., Lipscomb, W. N. *Proc. Natl. Acad. Sci. U.S.A.* **1986**, *83*, 7568.
- (6) Roderick, S. L., Banszak, L. J. *J. Biol. Chem.* **1986**, *261*, 9461.
- (7) Andres, J.; Moliner, V.; Krechl, J., Silla, E. *J. Chem. Soc. Perk. Trans. 2* **1995**, 1551.
- (8) Krechl, J.; Smrckova, S.; Pavlikova, F., Kuthan, J. *Collect. Czech. Chem. Commun.* **1989**, *54*, 2415.
- (9) Krechl, J.; Bohm, S.; Smrckova, S., Kuthan, J. *Collect. Czech. Chem. Comm.* **1989**, *54*, 673.
- (10) Krechl, J.; Bohm, S.; Smrckova, S., Kuthan, J. *Collect. Czech. Chem. Commun.* **1989**, *54*, 673.
- (11) Krechl, J.; Smrckova, S., Kuthan, J. *Collect. Czech. Chem. Commun.* **1990**, *55*, 460.
- (12) Krechl, J.; Smrckova, S.; Ludwig, M., Kuthan, J. *Collect. Czech. Chem. Commun.* **1990**, *55*, 469.
- (13) Krechl, J., Smrckova, S. *Collect. Czech. Chem. Commun.* **1989**, *30*, 5315.
- (14) Echaverren, A.; Galan, A.; Lehn, J.-M., de Mendoza, J. *J. Am. Chem. Soc.* **1989**, *111*, 4994.
- (15) Mueller, G.; Riede, J., Schmidtchen, F. P. *Angew. Chem. Int. Ed. Engl.* **1988**, *27*, 1516.
- (16) Terfort, A., von Kiedrowski, G. *Angew. Chem. Int. Ed. Engl.* **1992**, *31*, 654.
- (17) Hoffmann, S. *Angew. Chem. Int. Ed. Engl.* **1992**, *31*, 1013.
- (18) Peterson, I. R. *Buns. Gessel. Phys. Chemie* **1991**, *95*, 1417.
- (19) Riviere, S.; Henon, S.; Meunier, J.; Schwartz, D. K.; Tsao, M. W., Knobler, C. M. *J. Chem. Phys.* **1994**, *101*, 10045.
- (20) Peterson, I. R., Kenn, R. M. *Langmuir* **1994**, *10*, 4645.
- (21) Kaganer, V. M.; Peterson, I. R.; Kenn, R. M.; Shih, M. C.; Durbin, M., Dutta, P. *J. Chem. Phys.* **1995**, *102*, 9412.

- (22) Luty, T., Eckhardt, C. *J. J. Phys. Chem.* **1996**, *100*, 6793.
- (23) Kuzmenko, I.; Kaganer, V. M., Leiserowitz, L. *Langmuir* **1998**, *14*, 3882.
- (24) Blake, A. J.; Fallis, I. A.; Parsons, S.; Schroder, M., Bruce, D. W. *Acta Crystallogr., C* **1995**, *51*, 2666.
- (25) Weissbuch, I.; Berkovic, G.; Yam, R.; Alsnielsen, J.; Kjaer, K.; Lahav, M., Leiserowitz, L. *J. Phys. Chem.* **1995**, *99*, 6036.
- (26) Hartman, P. In *Crystal growth: an introduction*; P. Hartmann, Ed.; North-Holland Publ. Co.: Amsterdam, 1973; pp 367.
- (27) Weissbuch, I.; Berfeld, M.; Bouwman, W.; Kjaer, K.; Als-Nielsen, J.; Lahav, M., Leiserowitz, L. *J. Am. Chem. Soc.* **1997**, *119*, 933.
- (28) Weinbach, S. P.; Weissbuch, I.; Kjaer, K.; Bouwman, W. G.; Nielsen, J. A.; Lahav, M., Leiserowitz, L. *Adv. Mat.* **1995**, *7*, 857.
- (29) Hu, J. G., Granek, R. *J. Phys. II, France* **1996**, *6*, 999.
- (30) Sheldrick, G. M. *Acta Crystallogr.* **1990**, *A46*, 467.
- (31) Kratochvil, B.; Ondracek, J.; Krechl, J., Hasek, J. *Acta Crystallogr., C* **1987**, *43*, 2182.
- (32) Kratochvil, B.; Ondracek, J.; Maly, K., Csordas, L. *Collect. Czech. Chem. Commun.* **1988**, *53*, 294.

2.7 Use of the diastereomeric interactions to probe the in-plane attachment of water-soluble complexes to Langmuir films

**Maria Berfeld[#], Ivan Kuzmenko[#], Isabelle Weissbuch[#], Hagai Cohen[#],
Paul B. Howes^{##}, Kristian Kjaer^{##}, Jens Als-Nielsen^{###}, Leslie
Leiserowitz[#] and Meir Lahav[#]**

[#]Department of Materials & Interfaces, The Weizmann Institute of Science, 76100 Rehovot, Israel

^{##}Department of Solid State Physics, Risø National Laboratory, DK 4000, Roskilde, Denmark

^{###}Niels Bohr Institute, H.C. Ørsted Laboratory, DK 2100, Copenhagen, Denmark

Abstract

Langmuir monolayers of the copper complexes $S\text{-Cu-}S'$ and $S\text{-Cu-}R'$ [where S represents (S)-palmitoyl-lysine, and S' and R' represent chiral(S) and (R) forms of alanine, serine or valine], were generated *in situ* at the air-solution interface. This formation was accomplished by spreading the amphiphilic α -amino acid on aqueous solution of copper acetate followed by injection of the water-soluble α -amino acid into the subphase. The surface pressure-molecular area isotherms of the Langmuir monolayers $S\text{-Cu-}S'$ and $S\text{-Cu-}R'$ were interpreted in terms of diastereoselective interactions of the water-soluble chiral complexes with structured clusters of the polar head groups of the monolayer and their structures examined by grazing incidence X-ray diffraction (GIXD). In contrast, optically pure α -amino stearic acid forms a multilayer at the air-copper acetate solution interface. These films were transferred onto a solid support and their structures probed by scanning force microscopy (SFM) and X-ray photoelectron spectroscopy (XPS). The relevance of the proposed stereospecific interactions between the crystalline monolayers $S\text{-Cu-}S'$ and $S\text{-Cu-}R'$ and water-soluble chiral complexes are discussed in terms of the role played by in the early stages of crystal nucleation.

Introduction

The ability to monitor structural organization of chiral molecules during the early stages of crystal nucleation is of importance in pure and applied sciences. Clusters formed in supersaturated solutions had been shown to play an ubiquitous role in crystallization processes. Recently we proposed that among these structured clusters there are those that resemble the structure of the macroscopic three-dimensional (3-D) crystalline phase. By applying this working hypothesis it became possible to design auxiliary molecules that can be stereospecifically and enantioselectively targeted at the surfaces of some of these clusters and inhibit their growth¹. This methodology was successfully applied for the control of crystal polymorphism²⁻⁴, inducing⁵ and preventing⁶ crystal twinning and the optical resolution of enantiomers by kinetic crystallization^{7,8}.

Several years ago Harada *et al*⁹ demonstrated that crystallization of copper complexes of racemic aspartic acid in the presence of the optically pure α -amino acid, e.g. S -glutamic acid, results in the precipitation of crystalline copper R,R - aspartate. In order to explain this induction we proposed that the copper complexes of S -glutamic acid interact enantioselectively and inhibit the nucleation of the clusters of S -aspartate and prevent their conversion to the 3-D crystals¹⁰. This mechanism appears to be of general applicability as demonstrated for a large number of systems¹¹.

One way to obtain information on interactions between clusters and chiral molecules is by studies on the oriented growth of crystals at the air-solution interface induced by amphiphilic chiral-resolved molecules. For example, crystals of the centrosymmetric α -form of glycine, grown underneath a Langmuir film of an optically pure water-insoluble α -amino acid, were found to be attached to the monolayer *via* one of the two enantiotopic (010) or (0 $\bar{1}$ 0) faces, depending on the absolute configuration of the monolayer molecules^{12,13}. Such observations led to the conclusion that the water-insoluble α -amino acids at the air-solution interface spontaneously form crystalline domains whose polar head groups serve as a template for an 'epitaxial' nucleation of 3-D crystals.

Here we present studies on the interactions between the amphiphilic diastereomeric copper- α -amino acid complexes at the air-solution interface and water-soluble complexes of the environment. We made use of Cu²⁺ ions since they can bind both with a glycine head group of the amphiphile and water-soluble α -amino acid¹⁴ molecule from the aqueous subphase. Langmuir films of optically-resolved *S* or *R* and racemic (*R,S*) α -amino acids C₁₆H₃₃-CH(NH₃⁺)-COO⁻ (C₁₆-gly) and C₁₅H₃₁-CONH-(CH₂)₄-CH(NH₃⁺)-COO⁻ (C₁₅-lys) were investigated on pure copper acetate solution and in the presence of the optically-resolved *S*- or *R*- alanine, serine and valine (hereafter labeled *R'* or *S'*). The structures of the thin films at the air-solution interface were studied by surface pressure *vs.* molecular area (π -A) isotherms, grazing-incidence X-ray diffraction (GIXD), and by scanning force microscopy (SFM) and X-ray photoelectron spectroscopy (XPS) after deposition onto a solid support.

Experimental section

Materials. The compounds used in this study are:

1 - (*S*) and (*R,S*) α -aminostearic acid were prepared according to a known procedure,¹⁵
2 - Palmitoyl-N ϵ -lysine C₁₅H₃₁-CO ϵ NH-(CH₂)₄-CH(NH₃⁺)CO₂⁻, as the α -amino acids bearing an amide functional group within the chain. The racemic and optically pure long-chain α -amino acids have been synthesized and their purity assessed according to procedures described previously.¹⁶ Serine, valine, alanine and copper acetate were purchased from Sigma and used with no further purification.

(π -A) isotherms. The surface pressure - molecular area isotherms of the films of enantiomerically pure and racemic amphiphiles were measured on an automatic Lauda film balance both on pure water and copper acetate solution ($c = 10^{-3} M$). Enantiomerically pure and racemic aqueous solutions of serine, valine and alanine were injected after monolayer formation on the surface of copper acetate solution. The concentration and amount of the α -amino acid solutions were calculated for a 100 times excess over concentration of Cu²⁺ ions.

GIXD experiments. Grazing incidence X-ray diffraction experiments were carried out on the liquid surface diffractometer at the synchrotron beamline BW1,

Hasylab, Desy, Hamburg. The films on liquid surfaces were prepared by spreading ~0.5mM solutions of the amphiphiles in 98:2 mixture of chloroform-trifluoroacetic acid. Copper acetate aqueous solutions (10^{-3} M) were used as a subphase. After monolayer deposition and evaporation of the solvent the film was compressed to a nominal areas per molecule 36\AA^2 and 25\AA^2 and cooled down to 5°C.

X-ray powder diffraction. Crystals of racemic and chiral-resolved serine copper complexes were grown from water-ethanol mixtures. X-ray powder diffraction spectra (40kV,120mA) of the grown crystals obtained on Rigaku Rotaflex RU-200B diffractometer were in agreement with the reported single crystal structures^{17,18}.

XPS studies. X-ray photoelectron spectroscopy spectra were obtained using a Kratos AXIS-HS spectrometer with a monochromatic Al (K α) radiation source (1486.6 eV). The shift of the spectral lines due to the effect of charging was compensated by a flood gun, while a fine correction for the energy scale calibration was done with respect to the substrate Si 2p3/2 line at 103.3 eV. Because of observed damage of the samples each scan was performed on a fresh spot, such that the overall exposure was kept minimal. The experimental precision of energy line positions is -0.025eV , statistical signal-to-noise ratio for the weakest lines is 4-4.5. The samples were prepared by depositing the floating films of amphiphilic complexes on a glass support by Langmuir-Blodgett technique using a Nima (NIMA Technology, Coventry, UK) trough at target pressure $25\text{ mN}/\text{\AA}^2$ and room temperature. The typical transfer ratios were 85-90%.

SFM studies. A scanning force microscope (Nanoscope III, Digital Instruments) in a contact mode was used to image the films transferred on atomically smooth mica. The floating monolayer films were transferred onto freshly cleaved mica pieces ($1\times 1\text{cm}$) in a specially constructed Teflon trough (surface area 20cm^2) by draining the subphase solution with a motor-driven syringe. The calculated surface coverage was equal to 90%, assuming the formation of a monomolecular film.

Results and discussion

Assembly of Amphiphilic α -Amino Acids on Copper Acetate Solution. α -Amino alkanoic acid. The formation and the structure of stable monolayers of both optically-resolved (*S*) and racemic (*R,S*) α -aminostearic acid (C₁₆-gly) on water were reported recently¹³. On a copper acetate solution the monolayer of (*S*)-C₁₆-gly displayed π -A isotherm with a limiting surface area 18\AA^2 , compared to 25\AA^2 on pure water (Fig. 1A). The racemate behaves differently, with a limiting area of 34\AA^2 on copper acetate (Fig. 1B). After a transfer onto atomically smooth mica the films were examined by SFM (Fig. 2). Such a measurement of (*S*)-C₁₆-gly yielded two typical heights of 17\AA and 51\AA ; the film of (*R,S*)-C₁₆-gly, on the other hand, had an average thickness of $9\text{-}10\text{\AA}$.

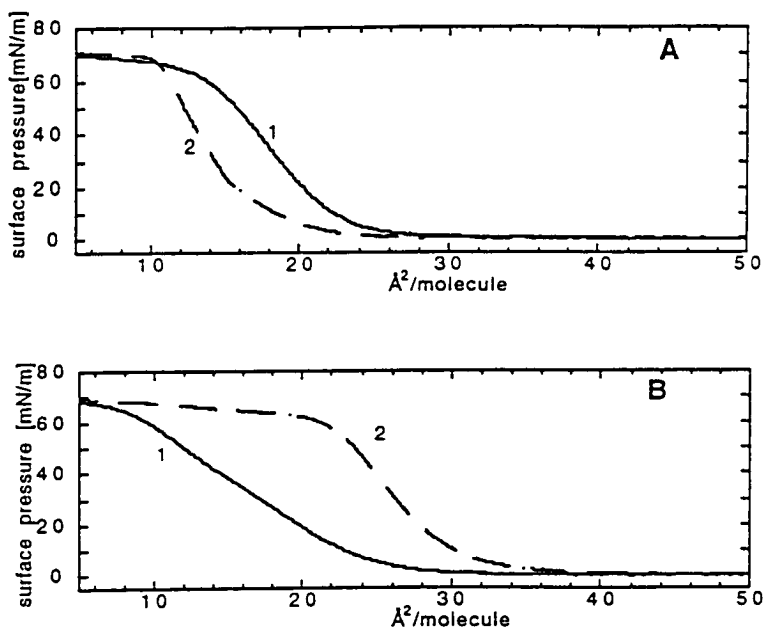


Fig. 1 Surface pressure-molecular area isotherms of C₁₆-gly on pure water (solid line) and copper acetate (broken line) solution:
A - chiral resolved (S)-C₁₆-gly, B - racemic (R,S)-C₁₆-gly

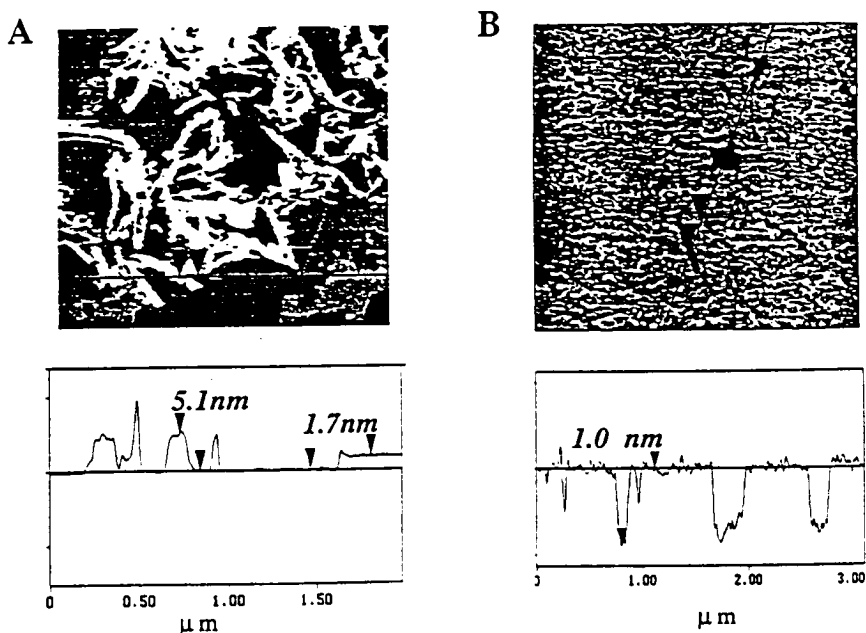


Fig. 2 Scanning force microscopy images of chiral-resolved (A) and racemic (B) C₁₆-gly after transfer from a copper acetate subphase onto atomically smooth mica.

The films of chiral (S)- and (R,S) -C₁₆-gly on copper acetate solution were studied by GIXD¹⁹. The (S)- and (R,S)- systems gave rise to two different diffraction patterns that did not change upon compression from 36 \AA^2 to 25 \AA^2 per molecule. These GIXD patterns were different from those observed on pure water¹³, therefore suggesting binding of Cu ions to the amphiphilic molecules.

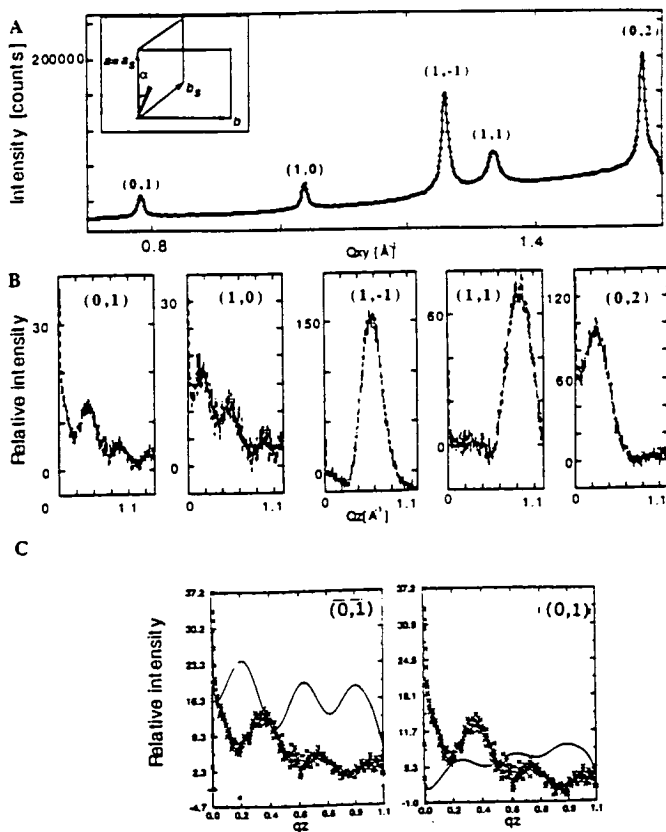


Fig. 3 Grazing incidence X-ray diffraction pattern of racemic C₁₆-gly spread on a copper acetate solution:

A - Bragg peaks with the assigned (*h,k*) indices. Inset shows the two-dimensional unit cell, and the subcell corresponding to the hydrocarbon chain packing. The angle between the projection of the tilted chain (indicated as a wedge) onto the *ab* plane and the *a* axis is $\alpha = 15^\circ$.

B - Bragg rods corresponding to the measured Bragg peaks shown in A;

C - observed (xxx) and calculated (----) (0,1) Bragg rod with two independent molecules at the unit cell and 4 Å separation along the *z* direction between them, ($\Delta z \sim 2.5\text{ \AA}$); *i* - corresponds to the model of the racemic α -aminostearic acid with Cu²⁺ ions bound to it; *ii* - corresponds to the simplified model of the monolayer molecules without contribution of the head groups ($\Delta z \sim 2.5\text{ \AA}$); *iii* - corresponds to two hydrocarbon chains at the same level ($\Delta z = 0$). The inserts show the simplified monolayer structures used for Bragg rod calculation.

The GIXD pattern of (*R,S*)-C₁₆-gly on copper acetate solution was indexed in terms of a pseudo-rectangular cell, $a = 6.10\text{ \AA}$, $b = 8.06\text{ \AA}$, $\gamma = 92.01^\circ$, $A = 49.2\text{ \AA}^2$, consistent with two symmetry-independent amphiphilic molecules in the unit cell (Fig. 3A). The Bragg rod of each of the three reflections (1,1), (1,1̄) and (0,2) has one strong intensity modulation with a full width at half maximum (FWHM) = 0.32 \AA^{-1} ,

corresponding to a monolayer 19.6 Å thick. By contrast, the Bragg rods of the low order (1,0) and (0,1) reflections demonstrate modulations with a FWHM~0.15 Å⁻¹ (Fig. 3C,i). We can attribute the presence of these sharp modulations to a difference in the height of the two symmetry-independent long-chain molecules due to the complexation with Cu²⁺ ions. The modulations of about the same frequency but of a lower amplitude are present for a simplified model which only involves the hydrocarbon chains with a 2.5 Å shift in height (Fig. 3C, ii). As expected, the modulations vanish when the two hydrocarbon chains are positioned at the same level ($\Delta z = 0$) as depicted in Fig. 3C,iii. Therefore we interpret the strong reflections (1,1), (1,̄1) and (0,2) as arising primarily²⁰ from the hydrocarbon chains in a subcell $a_s=a=6.10\text{ \AA}$, $b_s=(a+b)/2=4.97\text{ \AA}$, $\gamma_s=54.1^\circ$, $A_s=24.6\text{ \AA}^2$ (fig. 3A, insert). The tilt of the hydrocarbon chains was calculated from the q_z positions of the maxima of the (1,1), (1,̄1) and (0,2) Bragg rods. The aliphatic chains, in the film of 19.6 Å thickness, are tilted at an angle of 34° from the normal to the *ab* plane which corresponds to a chain length of about $19.6/\cos 34^\circ=24\text{ \AA}$, a value consistent with the length of a C₁₆H₃₃- chain. The direction of the tilted chain projected onto the *ab* plane is shown in Fig. 3A (inset); the cross-sectional area occupied by such a chain is about $A_s * \cos 34^\circ=20.4\text{ \AA}^2$.

On the basis of the above GIXD data we could not conclude whether a spontaneous separation of enantiomers had taken place or not, since the two crystallographically-independent molecules in the unit cell might be of the same or of opposite handedness. This question was resolved by making use of optically resolved (*S*)-C₁₆-gly.

The (*S*)-C₁₆-gly spread over copper acetate solution displayed a GIXD pattern (Fig. 4A) which is different from that of (*R,S*)-C₁₆-gly, indicating that the latter film is not phase-separated into domains of opposite handedness but rather heterochiral. All the twelve observed Bragg peaks of (*S*)-C₁₆-gly (Fig. 4A) were indexed according to an oblique unit cell of dimension $a=15.65\text{ \AA}$, $b=14.63\text{ \AA}$, $\gamma=104.7^\circ$, $A=221.54\text{ \AA}^2$. The Bragg rods of the strong (3,1) and coinciding (0,3) and (3,̄2) reflections (Fig. 4B), have FWHM(q_z) = 0.33 Å⁻¹, corresponding to a monolayer ~19 Å thick, as in the racemic system. These three reflections (Fig. 4A) correspond to a subcell of hydrocarbon chain packing $a_s=a/3=5.22\text{ \AA}$, $b_s=(2a/3+b)/3=5.22\text{ \AA}$, $\gamma_s=64.7^\circ$, $A_s=24.6\text{ \AA}^2$, A: $A_s=9:1$. The relationship between the subcell (a_s, b_s) and the unit cell (a, b) is given in Fig. 4A (inset). The intensity maxima of the (3,1), and partially resolved (0,3) and (3,̄2) Bragg rod profiles yielded a chain tilt of 37°, and a resulting cross-sectional area of $A_s * \cos 37^\circ=20.6\text{ \AA}^2$. The chains are tilted in a direction almost perpendicular to the diagonal ($a+b$) as shown in Fig. 4A (inset). The Bragg rod of the weak (0,1) reflection is modulated (Fig. 4C) similar to the (0,1) and (1,0) Bragg rods of the (*R,S*)-C₁₆-gly-Cu diffraction pattern (Fig. 3B)²¹.

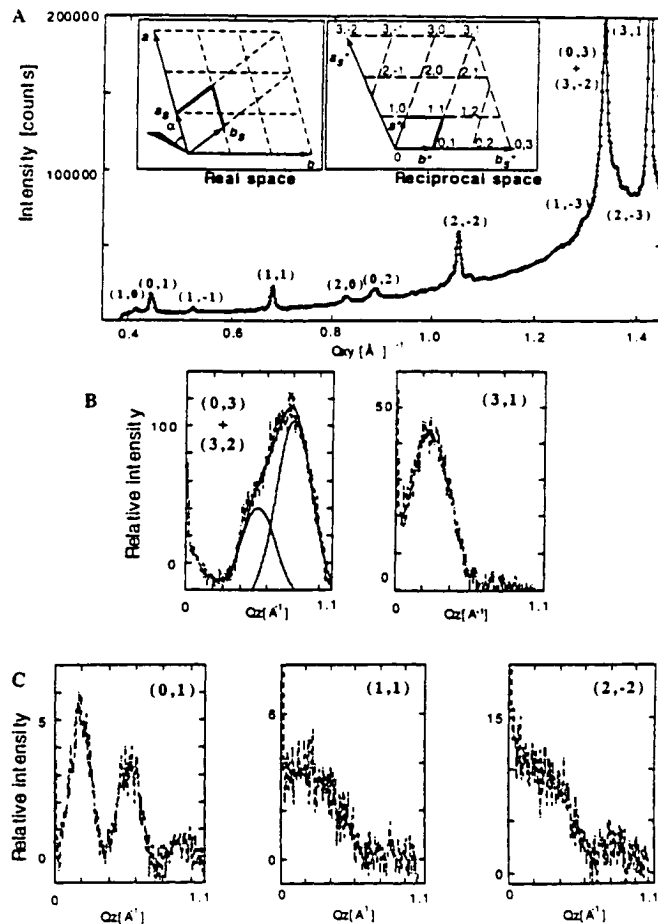


Fig. 4 Grazing incidence diffraction pattern of chiral-resolved C₁₆-gly spread over copper acetate solution:

A - Bragg peaks with the assigned (h,k) indices. Inset shows the two-dimensional unit cell, and the subcell corresponding to the hydrocarbon chain packing, in real and reciprocal space. The angle between the projection of the tilted chain (indicated as a wedge) onto the ab plane and the a axis is $\alpha = 50^\circ$.

B - Bragg rods of those reflections with a major contribution from the hydrocarbon chains;

C - Bragg rods of those reflections with a major contribution from the head groups.

The width of Bragg rod modulation of the (0,3), (3,2) and (3,1) reflections corresponding to the hydrocarbon chain packing unambiguously indicate that (*S*)-C₁₆-gly forms a crystalline monolayer film on the Cu(Ac)₂ subphase. However, the low surface area per molecule obtained by isotherm measurements as well as the results of SFM experiments suggest partial multilayer formation. We assume that in these systems multilayers formed at the air-liquid interface are not crystalline and do not contribute to the diffraction pattern.

α-Amino acid amphiphile bearing an amide group in the chain. As discussed above, we made use of an amide group in the hydrocarbon chain in order to achieve a spontaneous separation of enantiomers in Langmuir monolayer of the *α*-amino acids on pure water¹³.

The isotherms of chiral-resolved and racemic C₁₅-lys on aqueous solution of copper acetate ($c=10^{-3}M$) (Fig. 5A,B, curve 2) are more expanded than on pure water (Fig. 5A,B curve 1), indicating that the Cu ions from the subphase interact with the head groups of the amphiphile. Neither dilution of the copper acetate solution down to $10^{-5}M$, nor variation of the subphase temperature from 5° to 28°C caused any noticeable change in the isotherm behavior.

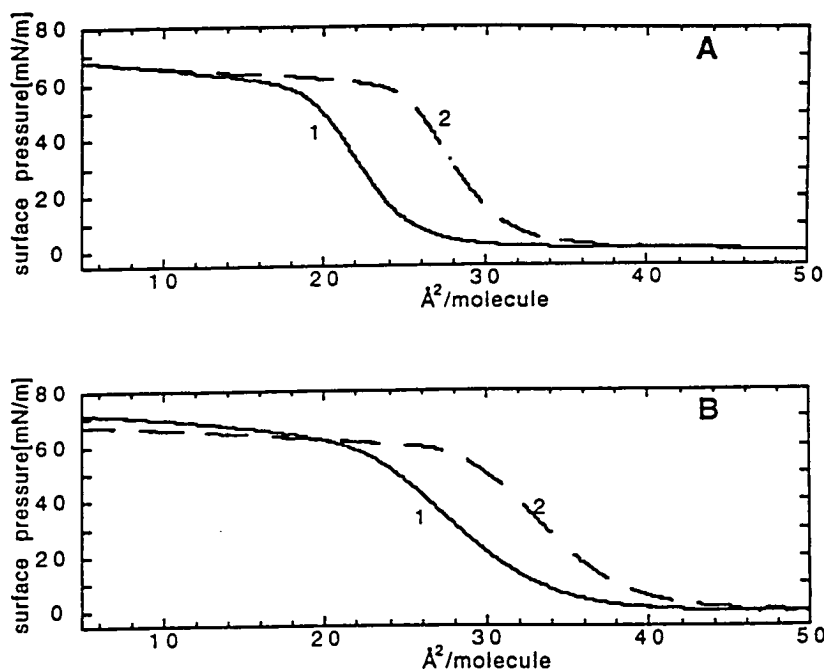


Fig. 5 Surface pressure-area isotherms of chiral resolved (A) and racemic (B) C₁₅-lys on water (solid line) and on copper acetate (broken line) solutions.

The interaction between the monolayer and copper ions was also confirmed by the substantial differences in the GIXD patterns of (*S*)-C₁₅-lys on copper acetate solution (Fig. 6A) and on pure water¹³.

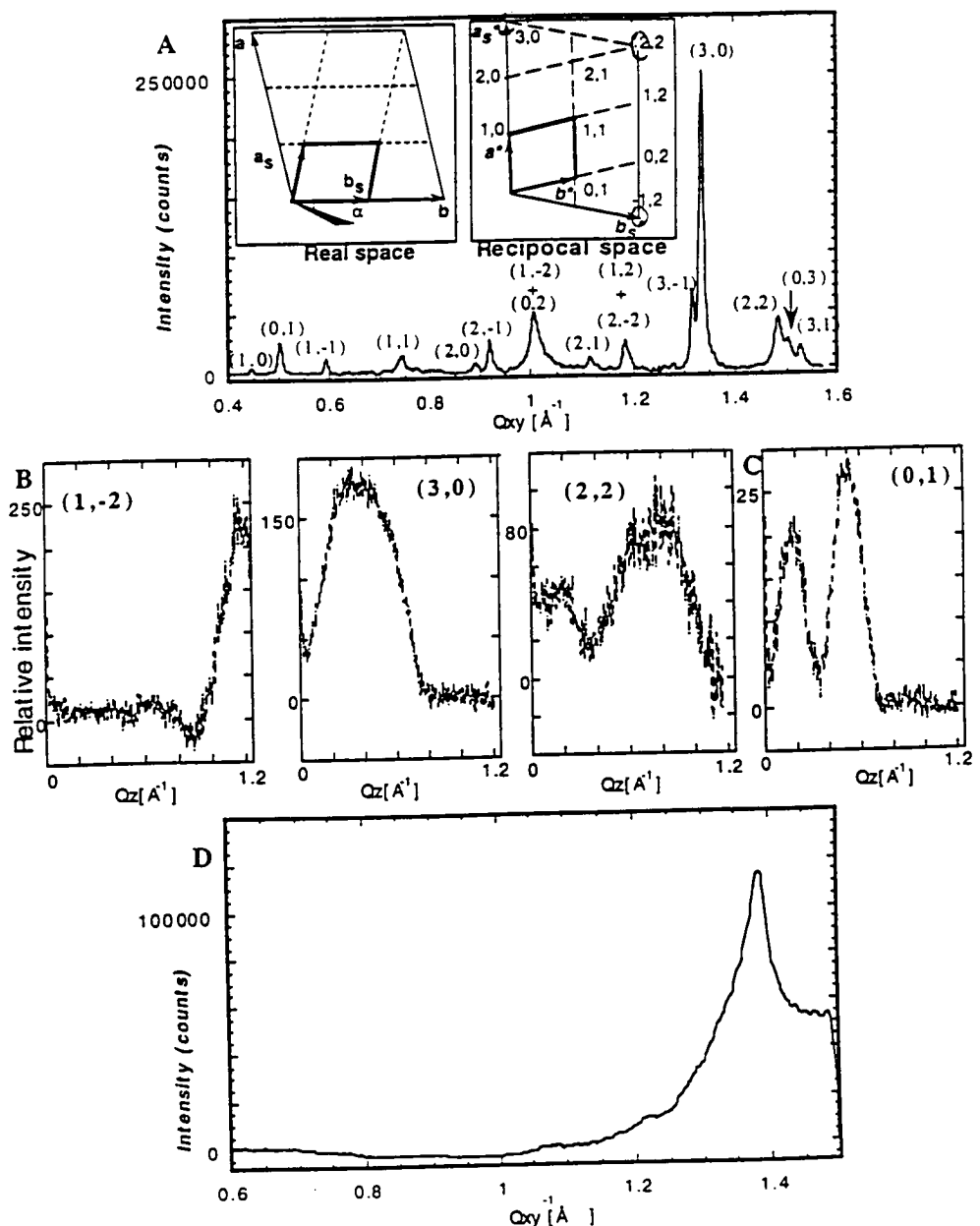


Fig. 6 Grazing incidence diffraction pattern of chiral-resolved C₁₅-lys spread over copper acetate solution:

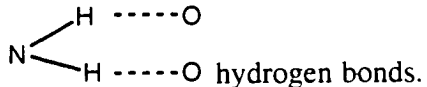
- A - Bragg peaks with the assigned (h,k) indices. Inset shows the two-dimensional unit cell, and the subcell corresponding to the hydrocarbon chain packing, in real and reciprocal space. Angle $\alpha = 12^\circ$ is between the projection of the tilted chain (indicated as a wedge) onto the ab plane and the b axis;
- B - Bragg rods of those reflections with a major contribution from the hydrocarbon chains;
- C - Intensity modulations along the Bragg rod of the $(0,1)$ reflection shown in A;
- D - Bragg peak of (R,S) -C₁₅-lys.

The GIXD patterns of the film on copper acetate solution remain unchanged upon compression from 36 to 25 $\text{\AA}^2/\text{molecule}$. All the measured Bragg peaks of (S) -C₁₅-lys on copper acetate solution were indexed in terms of a large oblique unit cell of dimensions $a = 14.40 \text{\AA}$, $b = 12.77 \text{\AA}$, $\gamma = 103.0^\circ$, $A = 179.2 \text{\AA}^2$. The three strong

reflections $(1,\bar{2})$, $(3,0)$, $(2,2)$ correspond to a subcell of hydrocarbon chain packing $a_S = (a+b)/3 = 4.80\text{\AA}$, $b_S = b/2 = 6.39\text{\AA}$, $\gamma_S = 77.4^\circ$, $A_S = 29.9\text{\AA}^2$ ($A:A_S=6:1$) indicating that the supercell (a,b) , as shown in Fig. 6A (inset), contains six amphiphilic molecules. The hydrocarbon chains are tilted by 50° from the layer normal in the direction of the b_S-a_S vector (see Fig. 6A, inset), as calculated from positions of the intensity profile maxima of $(1,\bar{2})$, $(3,0)$ and $(2,2)$ Bragg rods. The cross-sectional area per chain is $A_S * \cos 50^\circ = 19\text{\AA}^2$. The average FWHM of the Bragg rod intensity profiles of $(3,0)$ and $(2,2)$ reflections $= 0.45\text{\AA}^{-1}$, corresponds to a film thickness of $\sim 14\text{\AA}$. We rationalize the observed intensity modulations of the low order reflections, such as $(0,1)$ reflection (Fig. 6C), as arising from the contribution of symmetry-independent molecules with different z -coordinates.

The GIXD pattern of (R,S) -C₁₅-lys on Cu(Ac)₂ solution (Fig. 6D) does not contain superlattice reflections. Only one very broad strong Bragg peak arising from the hydrocarbon chain packing was observed, indicating that the racemic monolayer is poorly ordered. We may conclude that the enantiomers in the racemic film do not separate into islands of opposite handedness, as it was observed for such molecules on pure water¹³.

We conclude that at the air-copper acetate solution interface the films of racemic α -amino acids containing either a regular hydrocarbon chain or one with an amide linkage do not separate into domains of opposite handedness, and are less crystalline than their chiral-resolved counterparts. The lack of chiral segregation may be explained in terms the constraints imposed by the effect of copper complexation on the conformation of the head group, which precludes formation of a two-dimensional net of



Chiral discrimination of C₁₅-lys on Copper Solutions of Water Soluble α -Amino Acids. Here we examine the diastereomeric interactions between the monolayers of chiral-resolved (S) -C₁₅-lys on copper acetate solutions with optically pure (R' or S') alanine, serine or valine injected into the subphase. The possibility of artifacts caused by impurities was ruled out by cross-check experiments involving the use of amphiphilic and water-soluble α -amino acids of both handedness.

Injection of the water-soluble component with an absolute configuration the same (i.e. S') as that of the amphiphile (i.e. S) led to a more expanded pressure-area isotherm than for the two chiral components of opposite handedness (i.e. S,R'). (Fig. 7). Injection of valine led to more expanded isotherms than the use of either serine or alanine (cf. Fig. 7 C and A,B).

Injection of either (R') or (S') serine into the copper acetate subphase under the enantiomeric (S) -C₁₅-lys monolayer induced a change in the GIXD pattern (cf. Fig. 6

and 8). The supercell reflections arising from the contribution of the copper ions disappeared. Three distinct reflections were observed for each of the two diastereomeric systems (*S,S'*) and (*S,R'*) (Fig. 8 A,B). Each diffraction pattern was indexed in terms of an oblique unit cell of dimensions $a = 4.93\text{\AA}$, $b = 5.01\text{\AA}$, $\gamma = 98.5^\circ$, $A = 24.4\text{\AA}^2$ for (*S,R'*) and $a = 4.80\text{\AA}$, $b = 5.09\text{\AA}$, $\gamma = 99.0^\circ$, $A_S = 24.2\text{\AA}^2$ for (*S,S'*) monolayers. In the diffraction pattern of the (*S,S'*) monolayer one weak reflection observed at $q_{xy} = 1.44\text{\AA}^{-1}$ (labeled *) could not be indexed. It arise from a minor crystalline phase that we cannot account for.

Noticeable differences in the diffraction patterns of the (*S,S'*) and (*S,R'*) films indicate somewhat dissimilar molecular packing arrangements of the two diastereomeric systems. These GIXD results are compatible with ordered binding of the water-soluble α -amino acids to the headgroups of the amphiphiles *via* copper ion complexation. These measurements, however, cannot explain the observed variation of the surface pressure-area isotherms (Fig. 7).

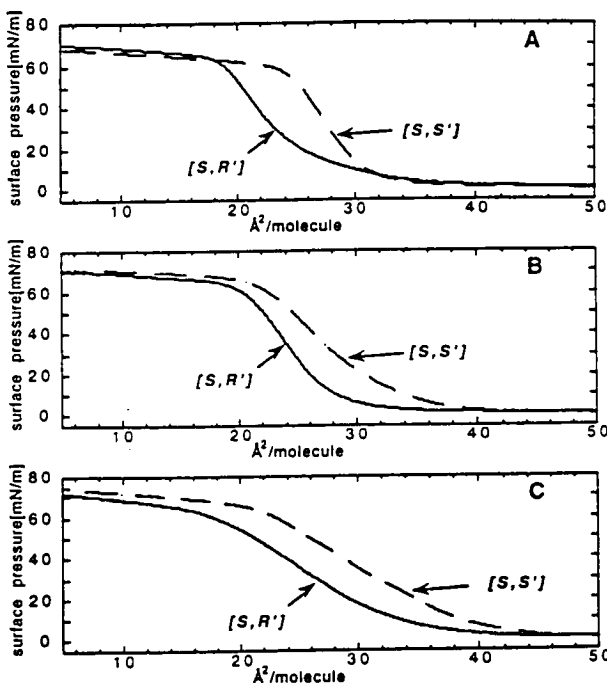


Fig. 7 The effect on the surface pressure-area isotherms of (*S*)-C15-lys of injecting of (A) serine, (B) alanine and (C) valine into the copper acetate solution .

[*S,S'*], [*S,R'*] refer to isotherm of the (*S*) amphiphile on the subphase containing the injected (*S'*) or (*R'*) water-soluble α -amino acid respectively.

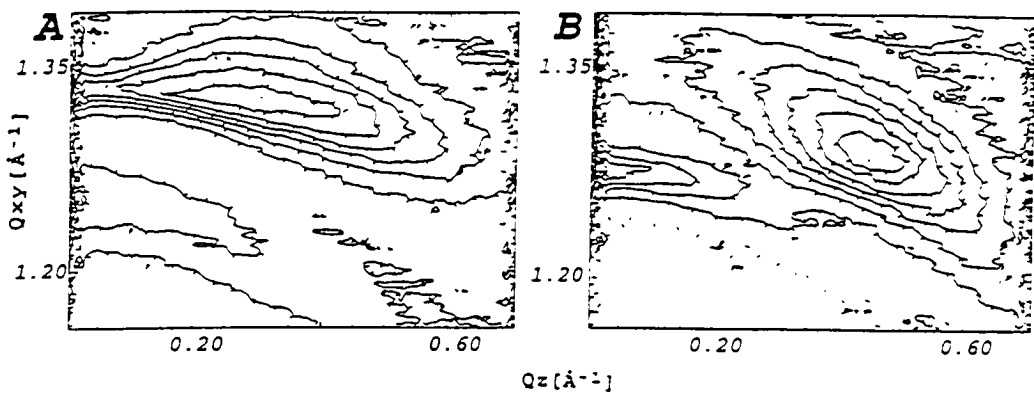
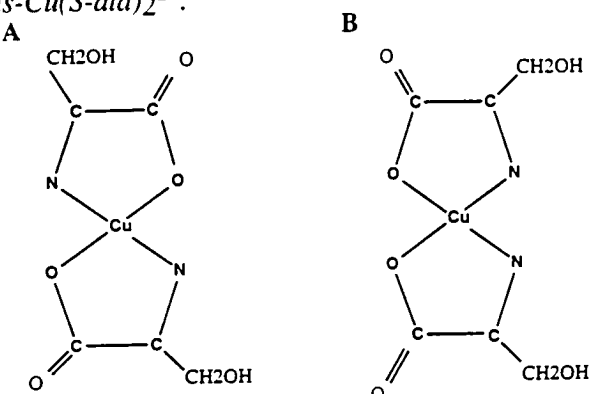


Fig. 8 Grazing incidence diffraction pattern of (*S*)-C15-lys spread over a copper acetate solution followed by injection of *S*-serine and *R*-serine. Bragg peaks (upper part) and two-dimensional intensity contour plots $I(Q_{xy}, Q_z)$ (lower part). The Bragg rods of the $(1, -1)$ and $(1, -1)'$ reflections was not measured.

Some of the copper complexes of the optically pure α -amino acids ($CuS'2$) adopt in bulk crystals a *cis*-configuration (Scheme 1B), whereas their racemic analogs ($CuS'R'$) are usually in the *trans*- form.^{17, 18, 22-25} Thus the racemic complex of serine¹⁷ in the crystal is centrosymmetric and has a *trans* configuration (Scheme 1A), while the $Cu(S'\text{-ser})_2$ complex¹⁸ (Scheme 1B) exhibits a local two-fold symmetry about the Cu atom, with a *cis*-arrangement of the two serine residues and one water molecule as an apical ligand. In the XPS measurements of these complexes, the binding energy line of $Cu(2p)$ of the *trans*-copper complex of racemic serine is 0.23(5) eV higher than that of the *cis*-copper complex of the chiral resolved serine. The variation of the position of the Cu^{2+} binding energy line due to either the water molecule in an apical position or the diastereomeric composition of the complexes was found to be negligible by independent measurements of the crystals of *trans*- $Cu(S\text{-ala})(R\text{-ala})\cdot H_2O$, *trans*- $Cu(S\text{-ala})(R\text{-ala})$ ²⁶ and *trans*- $Cu(S\text{-ala})_2$ ²⁷.



Scheme 1

Comparative XPS measurements of 3-D crystals of copper complexes and 2-D films of *S*-Cu-*S'* and *S*-Cu-*R'* throw light on the variation of the head group structure

of the two amphiphilic complexes. The relative atomic concentration of [Cu] to [N] deduced from the XPS measurements is in agreement with formation of both *S*-Cu-*S'* and *S*-Cu-*R'* complexes. The binding energies of the light elements *C* and *N* constituting the chain of the two diastereomeric complexes are essentially identical, whereas distinct differences in binding energies for the Cu ions were observed (Table 1). The binding energy line of Cu(2p) for the *S*-Cu-*R'* complex is approximately 0.24(1) eV higher than that of the *S*-Cu-*S'* (or *R*-Cu-*R'*) complex, which is significant as compared with the precision (~ 0.025 eV) of the energy scan²⁸. The correlation between the relative shifts of the binding energy lines of Cu(2p) allows us to propose the structural similarity between complexes of Cu(*S'*-ser)₂ and Cu(*S'*-ser)(*R'*-ser) in the bulk crystals and amphiphilic *S*-Cu-*S'* and *S*-Cu-*R'* complexes in thin films correspondingly²⁹. Therefore we propose that the α -amino acid groups in the two amphiphilic diastereomeric complexes may be arranged in a different way around the Cu²⁺ ion: amphiphilic complex *S*-Cu-*S'* appears in the *cis*- form, whereas the complex *S*-Cu-*R'* appears in the *trans*- form (Scheme 1).

Table 1 Chemical shift of the elements of the film deposited on a glass support.

System	Copper	Carbon from the hydrocarbon chain	Nitrogen from the amide group of the hydrocarbon chain	Oxygen from the amide group of the hydrocarbon chain
<i>S</i> -Cu- <i>R'</i>	934.95 \pm 0.02	285.98 \pm 0.02	399.89 \pm 0.01	531.46 \pm 0.01
<i>S</i> -Cu- <i>S'</i>	934.70 \pm 0.02	285.99 \pm 0.02	399.88 \pm 0.01	531.45 \pm 0.02
<i>R</i> -Cu- <i>R'</i>	934.72 \pm 0.02	284.98 \pm 0.02	399.89 \pm 0.01	531.45 \pm 0.02

We conclude from an analysis of the GIXD data that racemic mixtures of palmitoyl-lysine on copper acetate solution do not separate into 2-D crystallites of opposite handedness, unlike on pure water¹³. We rationalize the differences in the isotherm behavior of *S*-Cu-*S'* and *R*-Cu-*R'* complexes in terms of the following proposed packing arrangements of the monolayer of the two diastereomeric amphiphilic complexes shown in Fig. 9. Each molecule participates in three hydrogen bonds; one linking amide groups and the other two involving two amino acid residues of the complex. Gillard *et al*³⁰ suggested that in solution the optically pure (*S'*-Cu-*S'* or *R'*-Cu-*R'*) α -amino acid complexes coexist in their *cis*- and *trans*- forms close to conditions of equilibrium. The formation of crystals where all the molecules assume

one of these configurations is driven by kinetic rather than by thermodynamic factors. We propose that the homochiral water-soluble S' -Cu- S' (or R' -Cu- R') complex existing in the solution subphase should be attached to the periphery of the S -Cu- S' (or R -Cu- R') crystalline monolayer islands (Scheme 2) more strongly than to the islands of R -Cu- S' (or S -Cu- R'). These interactions should occur by virtue of a molecular fit between the peripheries of the amphiphilic clusters and the water-soluble molecules via strong hydrogen bonds³¹. A similar type of interactions between 2-D crystallites with water-soluble molecules, but not of an enantioselective nature, were deduced by observation that glycine in the aqueous subphase inhibited the growth of 2-D crystalline domains of perfluorododecyl-asparate and that β -alanine in the solution induced a reduction and indeed disappearance of the 2-D crystals of the amphiphile.³²

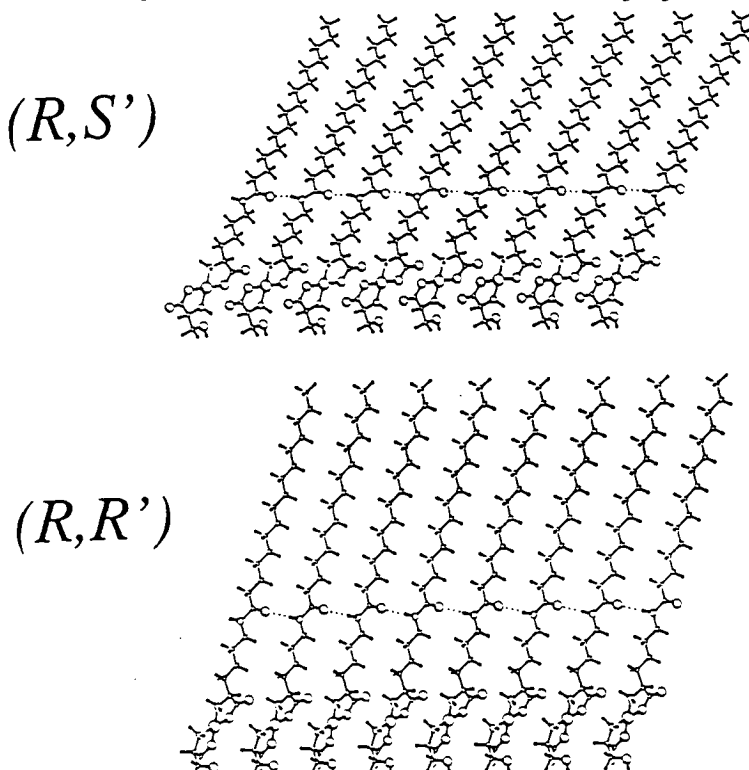


Fig. 9 Plausible monolayer packing arrangements of the two amphiphilic diastereomeric copper complexes: the amphiphilic ligand is (R)-C₁₅-lys; the water-soluble α -amino acid is (top) (S')- serine, (bottom) (R')- serine.

Consequently, upon compression of the S -Cu- S' or R -Cu- R' films, the bond short-chain complexes (S' -Cu- S' or R' -Cu- R' respectively) have to be expelled from the interface, leading to more expanded isotherm. On the other hand, much weaker interactions will occur between the R -Cu- S' (or R -Cu- S') head groups of the amphiphile and the S' -Cu- S' (or R -Cu- R') water-soluble molecules either in their *cis*- or *trans*- configuration leading to less-expanded isotherms in agreement with observed (Fig. 7). The additional expansion of the isotherms in the presence of valine (Fig. 7C)

can be rationalized by assuming a higher concentration of water-soluble species of hydrophobic $Cu(valine)_2$ at the solution surface.

The present observations provide insight on the stereospecific interactions between small clusters and molecules of the environment, and their resulting structure. This process of diastereoselective attachment of water-soluble copper complexes should be akin to the attachment of 'tailor-made' auxiliary molecules to the surfaces of growing three-dimensional nuclei or crystals^{11,33}. In order to provide more understanding at the molecular level on the nature of these interactions within supersaturated solutions it will be imperative in future studies to design new analytical tools for probing such interactions.

Acknowledgments

We thank S.Mathlis for the SFM measurements. We acknowledge financial support from the German Israeli Foundation, GIF and the Dansyne program of the Danish Foundation for Natural Sciences and the E.U.'s TMR program, and we thank HASYLAB, Desy, Hamburg, for synchrotron beam time.

References and Notes

- 1 Weissbuch I., Addadi L., Leiserowitz L., Lahav M. *Science* **1991** *253*, 637.
- 2 Weissbuch I., Zbaida D., Addadi L., Leiserowitz L., Lahav M. *J. Am. Chem. Soc.* **1987** *109*, 1869.
- 3 Weissbuch I., Leiserowitz L., Lahav M. *Adv. Mater.* **1994** *6*, 952.
- 4 Staab E., Addadi L., Leiserowitz L., Lahav M. *Adv. Mater.* **1990** *2*, 40.
- 5 Weissbuch I., Kuzmenko I., Vaida M., Zait S., Leiserowitz L., Lahav M. *Chem.Mater.* **1994** *6*, 1258.
- 6 Berfeld M., Zbaida D., Leiserowitz L., Lahav M. *Advanced Mater.* **1999** *in press*.
- 7 Addadi L., Weinstein S., Gati E., Weissbuch I., Lahav M. *J.Am.Chem.Soc.* **1982** *104*, 4610.
- 8 Addadi L., Van Mil J., Lahav M. *J. Am. Chem. Soc.* **1982** *104*, 3422.
- 9 Harada K. *Nature* **1965** *205*, 590.
- 10 Addadi L., Van Mil J., Lahav M. *J. Am. Chem. Soc.* **1981** *103*, 1249.
- 11 Addadi L., Berkovitch-Yellin Z., Weissbuch I., van Mil J., Shimon L.J.W., Lahav M., Leiserowitz L. *Angew. Chem. Int. Ed. Engl.*, **1985** *24*, 466.
- 12 Weissbuch I., Addadi L., Berkovitch-Yellin Z., Gati E., Lahav M., Leiserowitz L. *Nature* **1984** *310*, 161.

- 13 Weissbuch I., Berfeld M., Bowman W., Kjaer K., Als-Nielsen J., Lahav M., Leiserowitz L. *J. Am. Chem. Soc.* **1997** *119*, 933.
- 14 Gillard R.D, Laurie S.H, in *Amino acids, Peptides, Proteins. Special Periodical Reports*, Yong G.T., Eds. The Chemical Society,, London, , vol. 3, pp. 323 (1970).
- 15 Paquet A. *Can. J. Chem.* **1976** *54*, 733.
- 16 D'yakon I.A., Donu S.V., Chapurina L.F., Kairyak L.N. *Sov.Phys.Crystallogr.* **1992** *37*, 751.
- 17 Van Der Helm D., Franks W.A. *Acta Cryst* **1969** *B25*, 451.
- 18 *GIXD experiments were performed on the liquid-surface diffractometer at beam line BW1 at HASYLAB, DESY, Hamburg. The dimensions of the footprint of incoming X-ray beam on the liquid surface were approximately 5 x 50 mm². The scattered intensity was collected by means of a vertical position-sensitive detector (PSD), which intercepts photons over the range 0 ≤ q_z ≤ 0.9 Å⁻¹ (q_z is the vertical component of the X-ray scattering vector). Measurements were performed by scanning the horizontal component of the scattering vector, q_{xy}, and simultaneously resolving q_z with the PSD. Diffraction data are represented in three ways: as contour plots I(q_{xy}, q_z); the grazing-incidence diffraction pattern shows the Bragg peak intensity profiles I(q_{xy}) obtained by integrating the whole q_z intensity for any q_{xy} along the measured range. Bragg rod profiles show the scattered intensity I(q_z) in channels along the PSD, integrated over the whole range in q_{xy} for a Bragg peak. The q_{xy} positions of the Bragg peaks yield the lattice repeat distance d = 2π/q_{xy}, which may be indexed by the two Miller indices h, k to yield the unit cell. The full width at half-maximum (FWHM) of the Bragg peaks in q_{xy} units yield the 2-D crystalline coherence length associated with the h,k reflection. The width Δq_z of the Bragg rod profile along q_z gives a measure of the thickness of the crystalline film, T ≈ 0.9(2π)/Δq_z. More detailed descriptions of the GIXD method used for monolayer structure determination are given in: J. Als-Nielsen, Kjaer K., in *Proceedings of the NATO Advanced Study Institute, Phase Transitions in Soft Condensed Matter*, Riste T., Sherrington D., Eds. Plenum Press, New York., Geilo, Norway, pp. 113 (1989) J. Als-Nielsen, D. Jacquemain, Kjaer K., F. Leveiller, M. Lahav, L. Leiserowitz *Physics Reports*, **1994** *246*, 251 and Weissbuch I., Popowitz-Biro R., Lahav M., Leiserowitz L., Kjaer K., Als-Nielsen J., in *Advances in Chemical Physics*, Prigogine I., Rice S.A., Eds. John Wiley & Sons, NY, , vol. 102, pp. 39 (1997).*
- 19 *In terms of the monolayer model involving hydrocarbon chains at different heights we may discard an alternative interpretation of the GIXD pattern incorporating a coexistence of mono and multilayer.*

- 20 We cannot account for the FWHM of the (1,1) and (2,-2) reflections which are as broad as 0.65\AA^{-1} .
- 21 Herlinger A.W., Wenhold S.L., L. T.V. *J. of Am. Chem. Soc.* **1970** 92, 6474.
- 22 Steren C.A., Calvo R., Castellano E.E., Fabiane M.S., Piro O.E. *Physica B* **1990** 164, 323.
- 23 Weeks C.M., Coopre A., Norton D.A. *Acta Cryst.* **1969** B25, 443.
- 24 Goodman B.A., McPhail B., Powell H.K.J. *J.Chem.Soc., Dalton Trans.*, **1981** , 822.
- 25 Mirceva A. *Acta Cryst.* **1989** C45, 1141.
- 26 Dijkstra A. *Acta Cryst.* **1966** 20, 588.
- 27 *For nitrogen constituting the complex head groups the shift of the binding energy line was at most 0.1 eV in the direction opposite to that for copper ions.*
- 28 The effect of the cis-trans isomerisation of the ligands around metal ion in the coordinating compounds of the platinum on the XPS signal was described in the review: Srivastava S. *Applied Spectroscopy Reviews*, **1986** 22, 401.
- 29 Gillard R.D., Mason R., Payne N.C., Robertson G.B. *J.Chem.Soc.(A)*, **1969**, 1864.
- 30 Ariga K., Kunitake T. *Acc. Chem. Res.* **1998** 31, 371.
- 31 Jacquemain D., Thesis for the Degree of Doctor of Philosophy, Weizmann Institute of Science, Rehovot, Israel (1992).
- 32 Weissbuch I., Popovitz-Biro R., Lahav M., Leiserowitz L. *Acta Cryst.* **1995** B51, 115.

3. Overall summary and conclusions

*In the first part of the thesis (Section 2.1) we have provided information on the structure of nuclei formed at very early stages of the crystallization process. The unusual shape of the enantiomorphous twins of {R,S}-alanine induced by the chiral α -amino acid additives is *prima facie* evidence that the clusters, at very early stages of their formation, assume structures akin to their mature crystalline phases. In systems where more than one crystalline phase can be formed, additive molecules designed on the structural basis of the mature crystal, can be targeted stereospecifically to nuclei of a particular phase resulting in a prevention of their growth into macroscopic crystals. Our results demonstrate that the "tailor-made" additive is a far more efficient inhibitor during the stage of crystal nucleation than during the later stage of crystal growth. But once the nuclei of the phase unaffected by the additive reached a certain size, it acted as a template for the epitaxial crystallization of the thermodynamically more stable form, leading to unusual twinning of the crystal of {R,S}-alanine. The "tailor-made" auxiliary can reduce the speed of growth of the faces it interacts with and modify the morphology of the crystal, but can hardly prevent the crystal formation. The X-ray intensity diffraction pattern of a twinned crystal of {R,S}-alanine grown from 40:60 R:S alanine solutions indicated symmetry lowering as a result of enantiomeric disorder.*

This work also has bearing on theoretical aspects of crystal nucleation. The existence of structured clusters in supersaturated solutions prior to crystal nucleation invokes again the central role played by the anisotropy of intermolecular forces in the organization of molecules and raises the question of whether the importance of interfacial effects have not been overstated in the classical theories of crystal nucleation.

Recent studies had shown that amphiphilic and bolaamphiphilic molecules self-organise at air-solution interfaces forming crystalline monolayers and multilayers three to five layers thick. The ability to observe their structure and follow their dynamics as affected by "tailor-made" additives by modern methods such as grazing incidence X-ray diffraction, complemented by atomic force microscopy and cryo-transmission electron microscopy, should provide a more direct entry in the understanding of the mechanism of growth, dissolution and micro-twinning of clusters at the early stages of crystal nucleation.

We have in general examined the problem of spontaneous separation of enantiomers in two- and three-dimensional crystals (Section 2.3). We stress that although the process is driven by the same thermodynamic and kinetic factors both in two- and in three-dimensional systems the amphiphilic crystalline monolayers at an interface cannot possess a center of inversion, the most common symmetry element in bulk crystals. This fact should in principle lead to better chances for spontaneous

separation in the Langmuir or Langmuir-Blodgett monomolecular films. On the other hand, the monolayers of most amphiphiles studied to date incorporate long aliphatic chains that have an intrinsic tendency to pack in a herring-bone motif requiring glide plane symmetry, thus creating a bias towards racemate formation. Moreover, 2D crystals supposedly have much higher degree of molecular and therefore enantiomeric disorder than bulk crystals. All these factors necessitate a careful choice of molecules to guarantee enantiomeric separation in two-dimensions. Unambiguous detection of spontaneous resolution in 2D appears to require atomic resolution of molecular packing arrangement, which can in principle be obtained by grazing incidence X-ray diffraction or atomic force microscopy, whereas in bulk solids spontaneous resolution can be easily detected in most cases by various macroscopic methods.

In order to evaluate the extent of chiral disorder that may take place in spontaneously resolving monolayer racemates we have designed and studied a diasteromeric monolayer system containing madelic acid and phenylethylamine moieties each bearing one chiral center (Section 2.4). Diastereomeric interactions were used for the first time to demonstrate clearly two-dimensional chiral separation of long chain molecules at the air/liquid interface. The extent of chiral disorder was assessed from the GIXD pattern analysis and was shown to be low but probably non-zero. *The results show that the oblique lattice symmetry is not a sufficient proof for spontaneous separation of chiral molecules in two dimensions.* One way to ascertain whether such a separation occurred would require a determination of the monolayer crystal structure making use of GIXD Bragg rod data, complemented by lattice energy calculations.

In order to shed light on general packing motifs that take place for the most common Langmuir monolayer types with alkyl chains on liquid surfaces we analysed available grazing incidence X-ray diffraction data (Section 2.2). We show that the increase of order in the condensed phases of Langmuir monolayers of various substances is accompanied by a continuous change from a hexagonal packing motif of orientationally-disordered hydrocarbon chains to one of two closely-packed states. One of them is the commonly assigned as the herringbone motif. The other arrangement, which we designated as the pseudo-herringbone motif, is rarely observed in three-dimensional organic crystals, but occurs regularly in Langmuir monolayers. Both motifs were characterized by lattice-energy calculations. These calculations suggest for Langmuir monolayers with highly tilted hydrocarbon chains the existence of various phases in similar thermodynamic conditions. A gradual drift in lattice spacings going from crystalline phases to mesophases indicates minor changes in local packing of the molecules in the corresponding phase transitions.

We made use of known molecular interactions for the purpose of supramolecular design at the air-liquid interface (Sections 2.5 and 2.6). Interdigitated films composed of long-chain water-insoluble chiral acid molecule (*para*-

pentadecylmandelic acid of absolute configuration *R*) and water-soluble chiral base (phenylethylamine, *R'*) were generated at the air-solution interface. The (*R,R'*) structure was characterized to near atomic resolution by grazing incidence X-ray diffraction (GIXD) and complemented by other techniques such as atomic force microscopy (AFM) and 3D X-ray single crystal diffraction. In this study we have concentrated on two major aspects of using amidinium-carboxylate interactions at the air-water interface. We also used some other systems (for example, involving amidinium-carboxylate interactions) that provided new insights into the process of interdigitated film formation at air-solution interface.

We have also studied in-layer attachment of water soluble species depending on mutual chirality of both water insoluble films and water soluble complexes (Section 2.7). We made use of Langmuir monolayers of the copper complexes *S-Cu-S'* and *S-Cu-R'* [where *S* represents (*S*)-palmitoyl-lysine, and *S'* and *R'* represent chiral(*S*) and (*R*) forms of alanine, serine or valine], that were generated *in situ* at the air-solution interface. These studies provided some evidence on the stereospecific interactions between small clusters and molecules of the environment, and their resulting structure. The process of diastereoselective attachment of water-soluble copper complexes is akin to the attachment of 'tailor-made' auxiliary molecules to the surfaces of growing three-dimensional crystals, as, for example, in the case of {*R,S*}-alanine crystals grown in presence of chiral tailor-made additives.

Appendix

Surface Sensitive X-ray Methods

The intensity measured in a conventional X-ray scattering experiment is proportional to the number of scatterers, *i.e.*, the irradiated sample volume. This, in turn, is proportional to the penetration depth of the radiation in a sample. For X-rays of about 1 Å wavelength, this penetration ranges from a few micrometers for very highly absorbing material to a few millimeters for low absorbing materials. In contrast, the depth to which the surface effects persist rarely extends beyond 100 Å. Consequently, scattering from the surface region is so weak compared to that from the bulk that it is completely overwhelmed by it. A method restricting the penetration depth to the surface region is therefore a prerequisite for all surface diffraction/scattering experiments. This can be achieved by using grazing angles of incidence and employing the phenomenon of total external reflection from the surface.

The refractive index n of matter for X-rays in the 1 Å wavelength range is given by equation (i).

$$n = 1 - \delta - i\beta \quad (i)$$

$\delta = 2\pi\rho r_0/k^2$ where $k = 2\pi/\lambda$ is the X-ray wavenumber and λ is the wavelength. ρ is the electron density and $r_0 = 2.82 \times 10^{-13}$ cm is the classical electron radius. Typically δ is of the order of 10^{-5} . The term β is equal to $-\mu/(2k)$ where μ is the linear absorption coefficient. For X-rays of wavelength $\lambda \approx 1$ Å, absorption is small and $\beta \ll \delta$.

Consider now a plane wave with wavevector \mathbf{k}_i incident at an angle α_i on a planar interface separating a homogeneous medium from the vacuum, as shown in Figure 1.

The wave will be partially reflected into the vacuum in the direction given by $\alpha_r = \alpha_i$, and partially refracted into the lower medium in the direction given by α'_r . Snell's law for this case yields equation (ii).

$$n \cos \alpha'_r = \cos \alpha_i \quad (ii)$$

As $n < 1$, for angles of incidence α_i less than or equal to an angle α_c which is defined as $\alpha_c = \cos^{-1}(n) = (2\delta)^{1/2}$, the well known phenomenon of total reflection occurs: the incident wave is totally reflected, while the refracted wave becomes evanescent travelling along the surface. The amplitude of the evanescent wave decays exponentially with depth. Figure 2 shows the penetration depth Λ of the X-rays in water

versus angle of incidence α_i . For $\alpha_i < 0.5 \alpha_c$, the penetration depth is 46 Å independent of the X-ray wavelength. The evanescent wave may therefore be diffracted by crystalline material in a surface layer of that thickness and provide information on its *in plane* structure. Such diffraction is called grazing incidence diffraction (GIXD).

$$|q| = |\mathbf{k}_r - \mathbf{k}_i| = (4\pi / \lambda) \sin \alpha_r$$

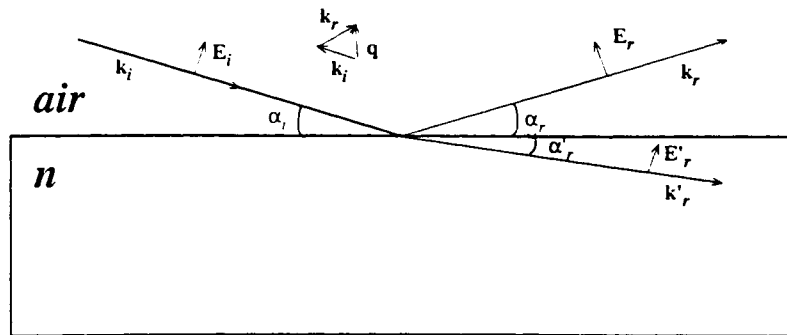


Figure 1. Refracted (E'_r) and reflected (E_r) waves resulting from an incident plane wave with amplitude $|E_i|$ upon an interface between air and a material of refraction index n . Electric fields E are illustrated for one polarization only. The symbol q is the scattering vector, with k_i and k_r the incident and reflected wave vectors of magnitude $2\pi/\lambda$, where λ is the wavelength. Note that as n becomes slightly smaller than 1, $\alpha'_r < \alpha_i = \alpha_r$. This provides for total reflection at angles $\alpha_r < \alpha_c$, where α_c is the critical angle for total external reflection.

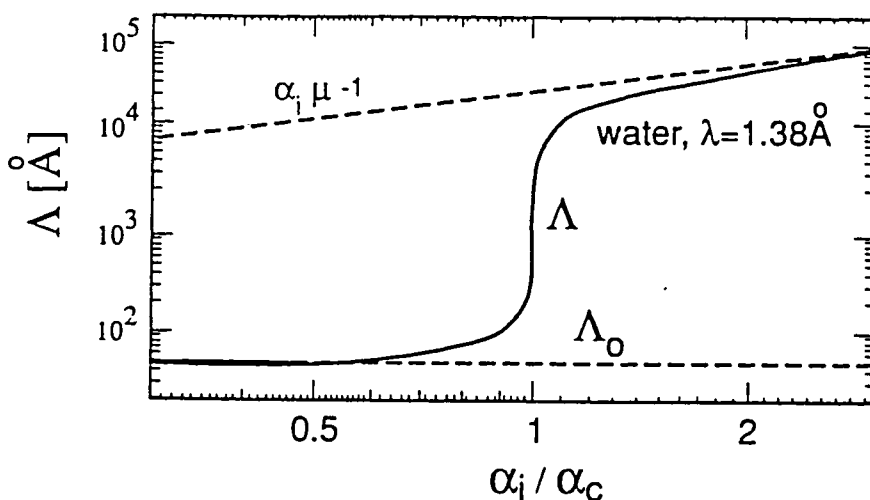


Figure 2. X-ray beam penetration depth Λ in water at $\lambda = 1.38 \text{ \AA}$ versus incidence angle α_i / α_c , α_c being the critical angle for total external reflection. The limiting value Λ_0 of the penetration depth for $\alpha_i / \alpha_c \ll 1$ is a characteristic materials constant, $\Lambda_0 = (\pi \rho \sigma)^{-1/2} / 4$.

independent of the X-ray wavelength λ . For $\alpha_i/\alpha_c \gg 1$ the penetration depth is $\alpha_i \mu^{-1}$ where the linear absorption coefficient μ does depend on λ .

In 3-D crystals, diffraction from a set of crystal planes with an inter-planar spacing d occurs only when the Bragg law is obeyed; namely when, firstly, the scattering vector length $|\mathbf{q}|$ given by $|\mathbf{k}_f - \mathbf{k}_i| = 4\pi \sin \theta / \lambda$ is equal to $2\pi d^*$, where d^* is the reciprocal of the interplanar spacing d and secondly, the normal to the planes bisects the angle between the incident and outgoing beam.

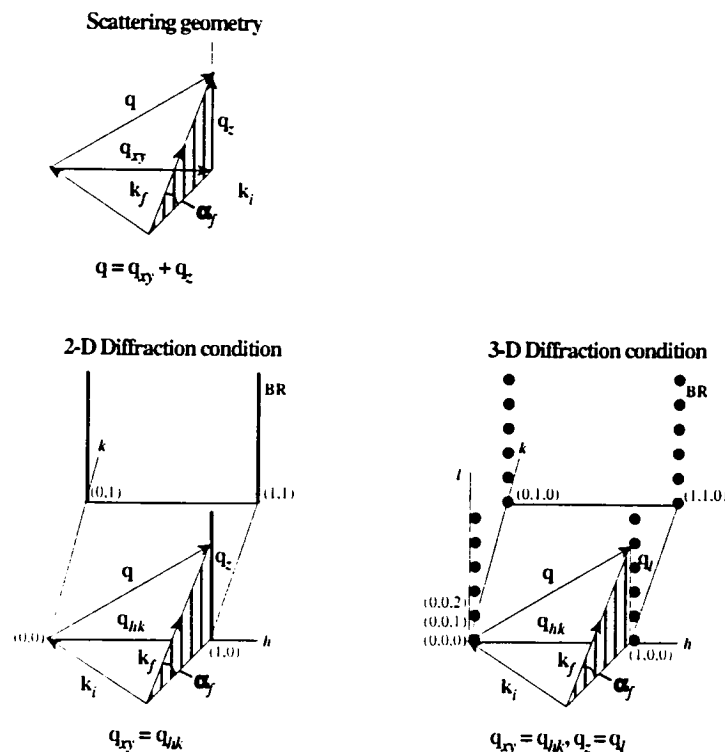


Figure 3. - Top - The general scattering geometry. \mathbf{k}_i and \mathbf{k}_f are the wave-vectors of the incident and diffracted beams respectively. The scattering vector $\mathbf{q} = \mathbf{k}_f - \mathbf{k}_i$ has components \mathbf{q}_{xy} parallel to the monolayer plane and \mathbf{q}_z perpendicular to it. - **Bottom -** The scattering from a 3-D crystal (right) in a given orientation lies in reciprocal or \mathbf{q} space at the reciprocal lattice points (h,k,l) . Diffraction is taking place when \mathbf{q} coincides with a specific reciprocal lattice point, $(1,0,3)$ in this particular case. The scattering from a 2-D crystalline material (left) in reciprocal space extends in rods (Bragg Rods BR) in the \mathbf{q}_z direction, perpendicular to the plane of the monolayer and of its reciprocal 2-D net. Bragg rod diffraction occurs when the scattering vector \mathbf{q} ends on an (h,k) Bragg rod, $(1,0)$ in this particular case.

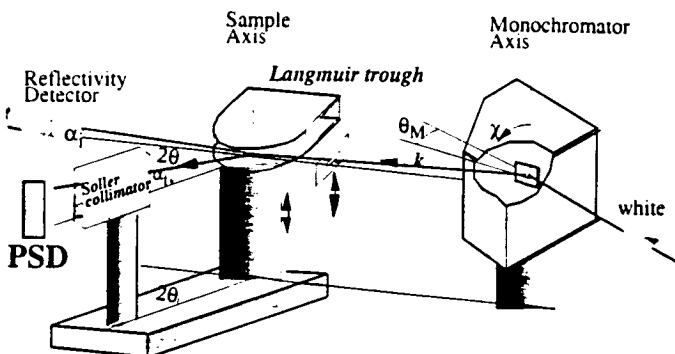
This condition may be mathematically expressed in terms of the reciprocal lattice vectors $\mathbf{d}^* = h\mathbf{a}^* + k\mathbf{b}^* + l\mathbf{c}^*$ where \mathbf{a}^* , \mathbf{b}^* , \mathbf{c}^* are the reciprocal vectors of the unit

cell vectors \mathbf{a} , \mathbf{b} , \mathbf{c} and h, k, l are integers that represent the Miller indices of planes with a spacing d_{hkl} . Diffraction therefore only takes place in 3-D crystals when the scattering vector \mathbf{q} coincides with (h,k,l) points of the reciprocal 3-D lattice (Figure 3).

For a 2-D crystal lying in the xy plane, the diffraction condition is that the component of the scattering vector in the horizontal plane, labelled \mathbf{q}_{xy} must coincide with a reciprocal lattice vector \mathbf{q}_{hk} , where $\mathbf{q}_{hk} = 2\pi\mathbf{d}^* = 2\pi(h \mathbf{a}^* + k \mathbf{b}^*)$. There is no similar selection rule or restriction on the scattering vector component \mathbf{q}_z along the film normal. The magnitude of q_z is $(2\pi/\lambda)\sin \alpha_f$, where α_f is the angle between the diffracted beam and the water surface, shown in Figure 3. Thus, the Bragg scattering from a 2-D crystal extends as continuous rods (Bragg rods) parallel to \mathbf{q}_z through the 2-D reciprocal lattice points (Bottom part of Figure 3, *left*). The finite thickness of the 2-D crystal causes the Bragg rod to extend over finite q_z intervals. The intensity distribution along these intervals is determined by the vertical electron distribution in the molecules and is expressed as the Fourier transform of the resulting electron density along the film normal. This intensity modulation can now be analysed to obtain information, for example, on the direction and magnitude of the molecular tilt in the crystalline part of the amphiphilic film. In addition, detailed information on the electron density distribution in the vertical direction, laterally averaged over both the *ordered* and *disordered* parts of the film can be obtained from the deviation of the measured X-ray reflectivity from the Fresnel law. By combining the methods of grazing incidence X-ray diffraction and X-ray specular reflectivity, the structure of 2-D crystals of amphiphilic molecules at air-water interfaces can be accurately characterized. We now discuss these methods in some detail.

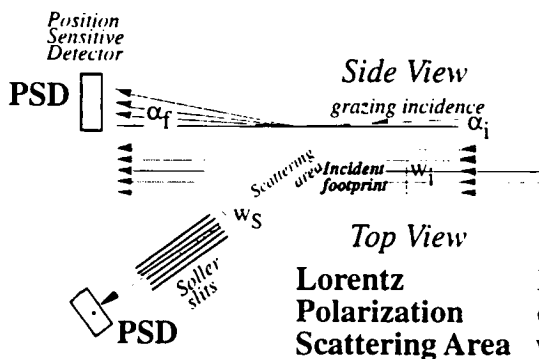
Grazing Incidence X-ray Diffraction

For all the diffraction patterns measured so far, the films of amphiphilic molecules were found to be composed of crystallites randomly oriented on the water surface, namely a 2-D "powder". Thus, the collection of the diffracted radiation was made in two ways using a position sensitive detector (PSD, Figure 4), mounted vertically behind a horizontally collimating Soller slit, which intercepted photons over a given q_z -range. The scattered intensity measured by scanning different values of q_{xy} and integrating over the whole q_z -window of the PSD, yields *Bragg peaks*. Simultaneously, the scattered intensity recorded in channels along the PSD, but integrated over q_{xy} across a peak produces q_z -resolved scans called *Bragg rod* profiles.



Physical variable Diffraction variable

$$\begin{aligned} \theta_M & \quad \lambda = 2\pi / k \\ \chi & \quad \left. \alpha_i \right\} k \\ 2\theta & \quad q_{xy} = 2k \sin\theta \\ \alpha_f & \quad q_z = k \sin\alpha_f \end{aligned}$$



$$\begin{aligned} \text{Lorentz} & \quad 1/\sin 2\theta \\ \text{Polarization} & \quad \cos 2\theta \\ \text{Scattering Area} & \quad w_i w_s / \sin 2\theta \end{aligned}$$

Figure 4. (top) Experimental setup of the liquid surface diffractometer at beamline BW1 (X-ray synchrotron source at Hasylab, DESY, Hamburg). The white X-ray beam is monochromated and deflected down towards the sample by tilting the Be monocrrometer crystal in Laue geometry. The incident and specular reflected beam intensities are monitored by the NaI Beam Monitor and NaI XR detector, respectively. The diffraction beam is detected with a position-sensitive detector (PSD). (bottom) Side and top views of the grazing incidence diffraction (GIXD) geometry. The footprint of the grazing incidence beam is indicated. The position sensitive detector (PSD) has its axis along the vertical direction z. Only the area ABCD contributes to the measured scattering. \mathbf{k}_i and \mathbf{k}_f are the incident and outgoing wave-vectors. The scattering vector \mathbf{q} is given by $\mathbf{k}_f - \mathbf{k}_i$.

Bragg peaks. The analysis of the Bragg peaks is similar to that of a conventional 3-D powder pattern; the reflections can be indexed by two Miller indices, hk . Their angular positions $2\theta_{hk}$, corresponding to $q_{hk} = (4\pi/\lambda)\sin\theta_{hk}$, yield the repeat distances $d_{hk} = 2\pi/q_{hk}$ for the 2-D lattice structure. The full width at half-maximum of the Bragg peak, FWHM in q_{xy} units, corrected by the resolution of the Soller

collimator, Δ in q_{xy} units, yields the 2-D crystalline coherence length L , associated with the hk reflection, through the Scherrer formula, given in equation (iii).

$$L \approx 0.90 \times 2\pi/[FWHM^2 - \Delta^2]^{1/2} \quad (\text{iii})$$

L is the average length, in the direction of the reciprocal lattice vector \mathbf{q}_{hk} , of all diffracting crystallites over which "perfect" crystallinity extends. The integrated intensity in the peak is determined by the square of the molecular structure factor $|F_{hk}|^2$ integrated along the Bragg rod over the window of q_z seen by the detector. The structure factor F_{hk} is given by equation (iv).

$$F_{hk}(q_z) = \sum_j f_j \exp i(\mathbf{q}_{hk} \cdot \mathbf{r}_j + q_z z_j) \quad (\text{iv})$$

f_j is the scattering factor of the atom j , $\mathbf{r}_j = x_j \mathbf{a} + y_j \mathbf{b}$ is the vector specifying the (x,y) position of the atom j in the unit cell of dimensions a, b and z_j is the atomic coordinate in Ångstroms along the vertical direction.

Bragg rod profiles. The variation of the intensity I_{hk} as a function of q_z is given by equation (v) and defines the profile of the Bragg rod.

$$I_{hk}(q_z) = V(q_z) \times |F_{hk}(q_z)|^2 \times D W_{hk}(q_z) \quad (\text{v})$$

The grazing geometry factor $V(q_z)$ describes the interference of rays diffracted upwards with rays diffracted down and subsequently reflected back up by the interface. $V(q_z)$ differs from unity only in the vicinity of $q_z = 1/2 q_c$, where it contributes a sharp peak. Explicitely, $V(x) = 2x$ for $0 < x \leq 1$ and $2x / [x + (x^2 - 1)^{1/2}]$ for $x > 1$ where $x \equiv 2q_z/q_c$ and $q_c = (4\pi/\lambda)\sin \alpha_c = 0.021764 \text{ \AA}^{-1}$.

In equation (v), the most important variation is due to the molecular structure factor $F_{hk}(q_z)$ that was defined by equation (iv). For the simple linear surfactant molecules considered here, the square of the molecular structure factor $|F(\mathbf{q})|^2$ is a bell-shaped function which reaches its maximum when the scattering vector $\mathbf{q} = (\mathbf{q}_{hk}, q_z)$ is orthogonal to the molecular axis. Thus, when the molecules are vertical or tilted in a plane perpendicular to \mathbf{q}_{hk} , the maximum intensity along the Bragg rod will occur at the horizon, for $q_z = 0 \text{ \AA}^{-1}$. For molecules tilted otherwise, we expect the Bragg rod maximum at a finite q_z , dependent upon both the magnitude and direction of the tilt relative to the in-plane scattering vector \mathbf{q}_{hk} . Assuming that the molecules are uniformly and rigidly tilted in the 2-D crystal, the angle τ between the molecular axis and the surface normal is given by equation (vi).

$$\cos \chi_{hk} \tan t = q_z^\circ / |\mathbf{q}_{hk}| \quad (vi)$$

q_z° is the position of the maximum along the Bragg rod and χ_{hk} is the azimuthal angle between the tilt direction projected on the xy plane and the reciprocal lattice vector \mathbf{q}_{hk} . Finally, the width of the bell-shaped Bragg rod profile is inversely proportional to the length of the molecule.

The Debye-Waller factor $DW_{hk}(q_z) = \exp - (q^2 U)$ in equation (v), where U is the mean-square displacement, accounts for the internal thermal motion of the atoms in the molecule, as well as for possible ripples on the water surface, which lead to roughness of the interface. In general, molecular thermal vibrations in crystals are anisotropic, which leads to a dependence of the corresponding temperature factor on the direction of the scattering vector. For a 2-D crystal lying in the xy plane, the extent of the GIXD data can, in cases where high order reflections have been observed, allow the temperature factor U to be decomposed into an in-plane, U_{xy} , and an out-of-plane, U_z , component. Then, the exponential term $DW_{hk}(q_z)$ in equation (v) can be written: $\exp - (q^2 U) = \exp - (q_{hk}^2 U_{xy} + q_z^2 U_z)$, where $\mathbf{q} = \mathbf{q}_{hk} + \mathbf{q}_z$. If all the observed reflections for the 2-D crystal are in the same q_{xy} range, as in most of the cases we studied, the exponential term $\exp - (q_{hk}^2 U_{xy})$ is approximately the same for all (h, k) reflections and plays the role of a scaling factor. The exponential factor can then be approximated by $\exp - (q_z^2 U_z)$ in equation (v).

Integrated intensity. The integrated intensity i_{hk} of the (h, k) reflection is given by equation (vii).

$$i_{hk} = \frac{1}{\sin 2\theta} \frac{\cos^2 2\theta}{\sin 2\theta} \frac{1}{A_c^2} \int I_{hk}(q_z) dq_z \quad (vii)$$

I_{hk} is calculated from equation (v) and integrated over the finite q_z range corresponding to the measuring window of the PSD (Figure 4). The factor $1/\sin 2\theta$ corrects the intensity for the area contributing to the scattering (ABCD, in Figure 4). $\cos^2 2\theta / \sin 2\theta$ is the Lorentz-Polarization factor. A_c is the unit cell area in the crystallites. Since the sample consists of a 2-D "powder", the observed intensity i for a given q_{hk} (or $2\theta_{hk}$) position contains contribution from both the (h, k) and (\bar{h}, \bar{k}) reflections, with possibly several h, k integer values, which yields equation (viii).

$$i(q_{hk}) = \sum_{h \bar{k}} (i_{hk} + i_{\bar{h}\bar{k}}) \quad (viii)$$

The observed integrated intensity, $i_{ob}(q_{hk})$, is proportional to $i(q_{hk})$, and is given by equation (ix).

$$i_{ob}(q_{hk}) = K i(q_{hk}) \quad (\text{ix})$$

The factor K scales the measured, $i_{ob}(q_{hk})$, and the calculated, $i(q_{hk})$, integrated intensities. It is calculated as the ratio of all observed intensities of the GIXD pattern to that of all calculated intensities.

The diffraction patterns for simple cases. It is useful at this stage to describe how the unit cell dimensions and molecular orientation may be determined from the GIXD data for simple cases. We consider the molecule as a freely rotating alkane chain. *i.e.* it has cylindrical symmetry. These molecules pack in three different cells: hexagonal ($a = b$, $\gamma = 120^\circ$), distorted hexagonal ($a = b$, $\gamma \neq 120^\circ$) which may be more properly described as centered rectangular ($a' = |a+b|$, $b' = |a-b|$) and oblique ($a \neq b \neq |a+b|$). They are shown in Figure 5. The molecules in a hexagonal cell are aligned vertically, in the distorted hexagonal cell the molecules are tilted along a symmetry direction and in the oblique cell the molecules are tilted along an arbitrary direction. As mentioned earlier, all Langmuir monolayers studied to date by GIXD consist of "powders" of randomly ordered 2-D crystallites on the water surface so that the GIXD measurements are not made on single crystals. Thus, the diffraction spectra consist of coinciding Bragg rods of reflections (h,k,q_z) and (\bar{h},\bar{k},q_z) ; the notation $\{h,k,q_z\}$ designating both reflections. In general, the intensity distribution along their two coinciding Bragg rods will be different unless the monolayer structure has a two-fold symmetry along the vertical axis.

The hexagonal cell has three equivalent lattice spacings d_{hk} : d_{10} , d_{01} and $d_{1\bar{1}}$. The GIXD spectrum from these three reflections will appear as a single peak with all corresponding Bragg rods peaking at $q_z = 0 \text{ \AA}^{-1}$ (Figure 5, top row). The corresponding GIXD spectrum for the distorted hexagonal cell will comprise two peaks; one a superimposed doublet arising from the coinciding $\{1,0\}$ and $\{0,1\}$ reflections, and the remaining $\{1,\bar{1}\}$ peak (Figure 5, middle row). The separation between the two peaks depends upon the deviation of the angle γ from 120° . In the oblique cell the degree to which the three peaks $\{1,0\}$, $\{0,1\}$ and $\{1,\bar{1}\}$ are resolved (Figure 5, bottom row), depends upon the deviation from centered rectangular (*i.e.*, distorted hexagonal) cell symmetry.

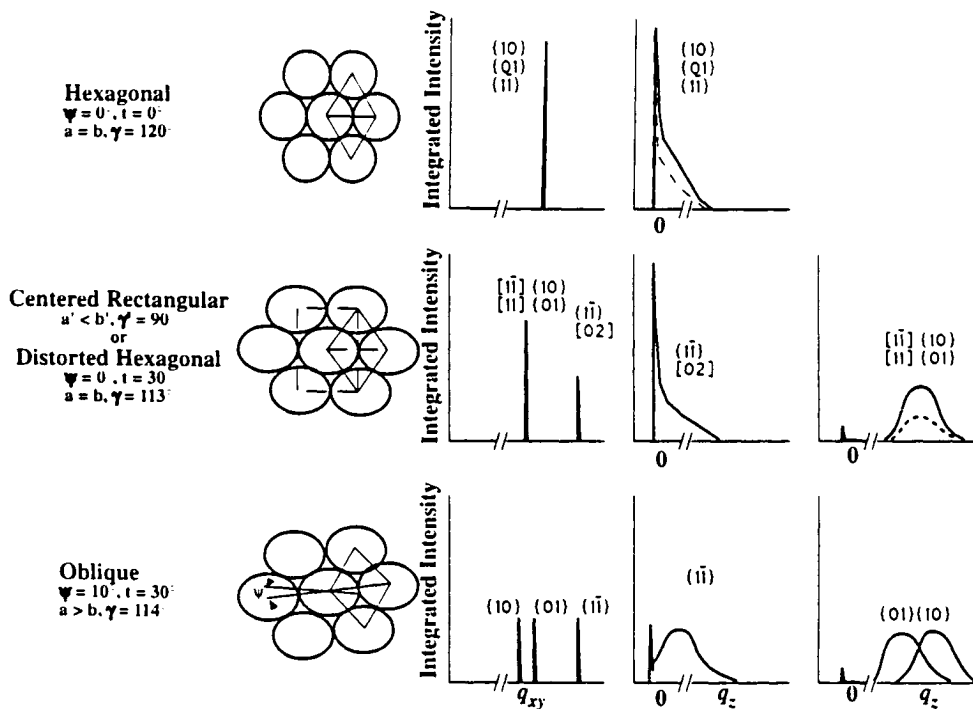


Figure 5. Three possible structures and diffraction from a monolayer of close-packed, freely rotating alkyl chains. The left column shows schematic top views of the molecular packing in hexagonal, distorted hexagonal and oblique unit cells. The second column shows the Bragg peaks and the last two columns the Bragg rods for the three structures. When more than one reflection coincides, the dashed lines represent the intensity from individual reflections as indicated by the Miller indices. The solid line represents the intensity from a 2-D powder sample; that is, the sum of the intensities indicated by dashed lines. When the molecular axis is perpendicular to the water surface the lattice is hexagonal (top row), and the $\{1,0\}$, $\{0,1\}$ and $\{1,\bar{1}\}$ reflections are degenerate. The Bragg rod obtained from the single in-plane diffraction peak has its maximum at $q_z = 0 \text{ \AA}^{-1}$. When the molecular axis is tilted towards nearest neighbours (middle row), the hexagonal structure is distorted to a centered rectangular structure (rectangular notation at the top, distorted hexagonal notation at the bottom). The degeneracy of the three reflections is partially lifted resulting in two peaks. The Bragg rod of the two degenerate reflections $\{1,0\}$ and $\{0,1\}$ ($[1,1]$, $[1,\bar{1}]$ in the rectangular notation) is centered at $q_z \geq 0 \text{ \AA}^{-1}$. The Bragg rod of the $\{1,\bar{1}\}$ reflection ($[0,2]$ in the rectangular notation) is still centered around $q_z = 0 \text{ \AA}^{-1}$. Finally, when the molecular axis is tilted in a non-symmetry direction, the intersection between the close-packed circular chains and the water surface forms an oblique 2-D lattice (bottom row). The degeneracy is completely lifted and the peak positions of the three Bragg rods determine the tilt angle as well as the azimuthal angle ψ unambiguously.

4. Statement of collaboration

This multidisciplinary project involved collaboration with people from several groups. The liquid surface diffractometer was built and maintained by Kristian Kjær (Dept. of Solid State Physics and Chemistry, Risø National Laboratory, Roskilde, Denmark) and Jens Als-Nielsen (Niels Bohr Institute, H.C. Ørsted Laboratory, Copenhagen, Denmark). Their contribution to the GIXD measurements and to the analysis of the diffractions data was indispensable.

The analysis of packing modes of long hydrocarbon chains (Section 2.2) involved a great deal of collaboration with V.M. Kaganer (Institute of Crystallography, Russian Academy of Sciences, Moscow, Russia) whose initiative and energy in large part carried the work through. I have had a fruitful collaboration with Hanna Rapaport on structural studies of ionophores and cholesterol at air-liquid interface (this part of work was not included in the thesis), with Ronith Buller on chiral interdigitated films (2.5), with Maria Berfeld on in-plane attachment of chiral water-soluble complexes (Section 2.7), with Isabelle Weissbuch on structural characterization of twinned (*R,S*)-alanine crystals (Section 2.1) and with Maik Kindermann on the design and characterization of non-chiral interdigitated films (Section 2.6). Ronith Buller, Edna Shavit and especially Maik Kindermann synthesized various amphiphilic and water-soluble compounds to be studied at air-liquid interface. AFM studies were performed by S. Matlis and S. Cohen.

The computer programs for the analysis of GIXD diffraction data were developed or modified by F. Leveiller, D. Jacquemain, W. Bouwman and R. Edgar. Some other important and frequently used programs involved Cerius² and SHELXTL.